

THE NATURE AND ORIGIN OF FINE-SCALE SEA-FLOOR RELIEF

by

JOHN SHAI-FU SHIH

B.S., Stanford University  
(1974)

M.S., Stanford University  
(1974)

SUBMITTED IN PARTIAL FULFILLMENT  
OF THE REQUIREMENTS FOR THE  
DEGREE OF

DOCTOR OF PHILOSOPHY

at the

MASSACHUSETTS INSTITUTE OF TECHNOLOGY

and the

WOODS HOLE OCEANOGRAPHIC INSTITUTION

(December 1979)

*(i.e. February, 1980)*

Signature of Author.....  
Joint Program in Oceanography, Massachusetts Institute of  
Technology/Woods Hole Oceanographic Institution, and the  
Department of Earth and Planetary Sciences, Massachusetts  
Institute of Technology, December 1979.

Certified by *S*  
Thesis Supervisor /

Accepted by.....  
Joint Oceanographic Committee in the Earth Sciences,  
Massachusetts Institute of Technology/Woods Hole Oceanographic  
Institution

**WITHDRAWN**  
ASSOCIATED INSTITUTE  
OF TECHNOLOGY  
DE **FROM** 1980  
**MIT LIBRARIES**



Room 14-0551  
77 Massachusetts Avenue  
Cambridge, MA 02139  
Ph: 617.253.5668 Fax: 617.253.1690  
Email: docs@mit.edu  
<http://libraries.mit.edu/docs>

## **DISCLAIMER OF QUALITY**

Due to the condition of the original material, there are unavoidable flaws in this reproduction. We have made every effort possible to provide you with the best copy available. If you are dissatisfied with this product and find it unusable, please contact Document Services as soon as possible.

Thank you.

**Certain pages in the original document contain graphics that are illegible. This is the best copy available**

# THE NATURE AND ORIGIN OF FINE-SCALE SEA-FLOOR RELIEF

by

JOHN SHAI-FU SHIH

Submitted to the Department of Earth and Planetary Sciences  
Massachusetts Institute of Technology

and

the Department of Geology and Geophysics  
Woods Hole Oceanographic Institution

on December 14, 1979 in partial fulfillment of the requirements  
for the Degree of Doctor of Philosophy

## ABSTRACT

Bathymetric profiles of mid-ocean ridges show that the morphology of ridge crests and the roughness of sea-floor relief created there is commonly related to the spreading rate. To study the creation of fine-scale sea-floor relief at mid-ocean ridges, detailed bathymetric profiles of mid-ocean ridges collected with the deep tow instrument package were compiled. Tectonic features were identified in order to provide an estimate of the zone over which tectonic relief is created. The results suggest the age of sea-floor to which tectonism is active is considerably greater at the slow spreading Mid-Atlantic Ridge though not noticeably variable among faster spreading centers. The roughness of sea-floor relief was measured using longer deep tow profiles. Surprisingly, the sea-floor relief created at slow spreading centers is not noticeably rougher than that created at faster spreading centers, contrary to the often noted inverse relationship between sea-floor roughness and spreading rate. It is postulated that the apparent smooth sea-floor relief created at fast spreading centers is due to the inability of typical surface ship profiling systems to resolve the small amplitude/short wavelength relief created there.

Surface ship bathymetric profiles of mid-ocean ridges were also compiled to better define the relationships between the dimensions of median rifts or central highs at spreading centers and the roughness of sea-floor relief as seen by surface ship profiling systems with spreading rate. The measurement of ridge crest dimensions shows that though the slow spreading Mid-Atlantic Ridge commonly does have median rifts and the fast spreading East Pacific Rise has central highs, when ridge crest dimensions are plotted versus spreading rate, no clear correlation can be seen in the individual oceans. The roughness of sea-floor relief was measured using the compiled surface ship profiles. A good

inverse correlation between roughness and spreading rate can be seen in the Atlantic but not in the Pacific.

The hypothesis that the roughness of sea-floor relief created at spreading centers is related to the ability of the lithosphere to support relief within the zone of relief formation was considered. The strength of the lithosphere at spreading centers was estimated from measured strengths of rocks and theoretical thermal models of the lithosphere near spreading axes. The load imposed of the lithosphere by sea-floor relief was estimated using deep tow bathymetric profiles. The calculations show the lithosphere should achieve much higher strengths within the zone of relief formation at slow spreading centers compared to fast spreading centers. Furthermore, the calculated lithospheric strengths within the zone of relief formation increase exponentially for spreading centers of lower spreading rates. This can explain why an inverse correlation between sea-floor roughness and spreading rate could be seen along the slow spreading Mid-Atlantic Ridge but not along the fast spreading East Pacific Rise. Finally, the extent of tectonism, or the width of the zone of relief formation, at spreading centers is suggested to be controlled by the width of magma chambers at faster spreading centers and the extent of viscous forces at deeply rifted slow spreading centers.

Name of Title of Thesis Supervisor: Tanya Atwater, Associate  
Professor of Marine Geophysics



## ACKNOWLEDGEMENTS

I am grateful to many people who have helped me in the course of this work. Most of all, I would like to thank Tanya Atwater and Ken Macdonald, who have acted as my thesis advisors. They have always given me encouragement and support as well as advice. As my academic advisors, Peter Molnar and Dave Johnson have also provided much needed guidance. I have had the fortunate opportunity to work with the deep tow group at the Scripps Institution of Oceanography. In particular, I would like to thank F.N. Spiess, Peter Lonsdale, and John Mudie for making the deep tow data available to me and Steve Miller and Kathy Poole for their help in processing the data. I greatly appreciate the comments on earlier versions of the thesis from my committee members: Tanya Atwater, Henry Dick, Kim Klitgord, Ken Macdonald, and Dick von Herzen, as well as discussions with Hans Schouten and Peter Molnar. My work was funded by the Woods Hole Oceanographic Institution Research Fellowship, the Navy/Office of Naval Research Contract N00014-75-C-0291, and NSF Grant Number OCE77-20224.

TABLE OF CONTENTS

	Page
Abstract	2
Acknowledgements	4
Table of Contents	5
List of Tables	7
List of Figures	7
Chapter I: Morphology of Ridge Crests and Sea-floor as Seen by the Deep Tow Instrument Package	
1.1 Introduction	10
1.2 Data and the Deep Tow Instrument Package	11
1.3 General Morphology of the Spreading Centers	39
1.4 Volcanic and Tectonic Relief at Spreading Centers	47
1.5 Plate Boundary Widths	51
1.6 Reverse Faulting	64
1.7 Elimination of Median Rift and Central Horst Relief	70
1.8 Roughness of Sea-Floor Relief	72
1.9 Power Spectra of Deep Tow Profiles	86
1.10 Summary	92
Chapter II: Morphology of Ridge Crests and Sea-floor as Seen By Surface Ship Profiling Systems	
2.1 Introduction	95
2.2 Data Base	96
2.3 Definition of Median Rift and Central High Dimensions	124
2.4 Dimension of Median Rifts Defined Relative to the Adjacent Rift Mountain Peaks	127

	Page	
2.5	Dimensions of Median Rifts and Central Highs Relative to the Best Fitting Depth Versus Square Root of Age Curves	132
2.6	Source of Variability in Ridge Crest Dimensions	140
2.7	Roughness of Sea-Floor Relief	162
2.8	Summary	168
Chapter III:	The Formation of Fine-Scale Sea-Floor Relief at Mid-Ocean Ridges	
3.1	Introduction	171
3.2	The Strength of the Lithosphere Near Spreading Centers	173
3.3	Estimates of the Buoyancy Forces	177
3.4	Relationships Between the Calculated Lithospheric Strengths and Buoyancy Forces	181
3.5	Relationships Between Spreading Rate and the Roughness of Sea-Floor Relief	194
3.6	Extent of Tectonism at Spreading Centers	195
3.7	Summary	197
Chapter IV:	Summary and Conclusions	
4.1	Deep Tow Results	200
4.2	Surface Ship Results	201
4.3	Formation of Fine-Scale Sea-Floor Relief at Mid-Ocean Ridges	204
References		206
Appendix I:	Location of Surface Ship Profiles Compiled for This Study	214
Biographical Note		222

## LIST OF TABLES

	Page
Table I: Deep tow surveys used in this study	16
II: Statistics for rift depths and volumes defined relative to the adjacent rift mountain peaks	131
III: Statistics for median rift and central high dimensions defined relative to the best fitting depth versus square root of age curves	144
IV: Statistics of the best fitting depth versus square root of age curves between 20° and 30° N along the MAR	151
V: Roughness of sea-floor relief and its relationship with spreading rate	167

## LIST OF FIGURES

Figure 1: Location of deep tow ridge crest surveys used in this study	14
2: Fence diagrams of EPR 21°N and EPR 3°S : bathymetric data with side-scan targets	19
3: Projected deep tow profiles of ridge crests	22
4: Longer deep tow profiles	30
5: Deep tow profiling and side-scan records	34
6: Definition of terms used to describe sea-floor tectonic features	41
7: Fault throws across fault zones versus distance to spreading axes for the MAR and Gorda Rise	49
8: Fault throws versus distance to spreading axes for the longer deep tow profiles	52
9: Width of the central low relief zones	59
10: Estimates of the plate boundary half-widths	65

	Page
Figure 11: Plate boundary half-width estimates expressed in terms of the age of sea-floor to which tectonism is active	67
12: Cumulative vertical sea-floor relief versus distance to spreading axes	74
13: Five kilometer averages of sea-floor roughness	79
14: Roughness of sea-floor relief versus spreading rate	83
15: Power spectra of deep tow profiles	89
16: Surface ship profiles of ridge crests	98
17: Definition of median rift and central high dimensions	125
18: Depth of median rifts defined relative to the adjacent rift mountain peaks	129
19: MAR rift volumes defined relative to the adjacent rift mountain peaks	133
20: The slope and intercept depth of the best fitting depth versus square root of age curves	137
21: Rift depths and volumes and central high heights and volumes defined relative to the best fitting depth versus square root of age curves	141
22: Location of bathymetric profiles digitized from Navy bathymetric contour maps of the North Atlantic	147
23: Slope and intercept depth of best fitting depth versus square root of age curves determined from profiles of the MAR between 20° and 30°N	149
24: Location of profiles from detailed surveys of the MAR	153
25: Ridge crest profiles digitized from Navy bathymetric contour maps	157

	Page
Figure 26: Ridge crest profiles from detailed surveys of the MAR	159
27: Roughness of sea-floor relief versus spreading rate	164
28: Strength of the lithosphere near spreading centers	178
29: Sea-floor relief used to calculate the buoyancy forces	182
30: Buoyancy force attributable to sea-floor relief created at different spreading rates	187

# Chapter I: Morphology of Ridge Crests and Sea-Floor as Seen by the Deep Tow Instrument Package

## 1.1 Introduction

At divergent plate boundaries, asthenospheric material upwells, cools, and becomes part of spreading lithospheric plates. The very large scale topography of the sea-floor reflects the conductive cooling of the resulting lithosphere (e.g. Sclater and Francheteau, 1970; Sclater et al, 1971; Parker and Oldenburg, 1974; Parsons and Sclater, 1977).

Superimposed on the large scale thermal relief of the sea-floor are second order topographic features which simple conductive cooling models of the lithosphere cannot explain.

Two essential features of the finer scale relief are:

- 1) the presence of median rifts at most slow (less than 20 mm/yr half rate) and intermediate rate (20-40 mm/yr half rate) spreading centers, and 2) the greater roughness of relief for sea-floor created at slower spreading rates as seen in surface ship profiling records.

Detailed surveys of mid-ocean ridges show the sea-floor to be created initially by volcanic extrusion with little relief. Most of the sea-floor relief is tectonic in origin and is added on the flanks of the extrusive zone by faulting, tilting, and warping of the sea-floor (Larson, 1971; Atwater and Mudie, 1973; Klitgord and Mudie, 1974; Normark, 1976; Ballard and van Andel, 1977; Macdonald and Luyendyk, 1977;

Lonsdale, 1977a; Lonsdale and Spiess, 1979). Thus, it is necessary to study the tectonic evolution of the sea-floor as it migrates away from spreading centers in order to understand the relief formation process and its relationship to spreading rate. Typical surface ship profiling systems are not able to resolve the important small scale tectonic features of the sea-floor. Bathymetric profiles collected with the deep tow instrument package of the Marine Physical Laboratory of the Scripps Institution of Oceanography are the only widely available high resolution data. The deep tow data allow the identification of fault scarps, the basic tectonic expression of the sea-floor. Deep tow side-scan records make possible the mapping of the fault scarps. In this first chapter, the morphology of the sea-floor and mid-ocean ridges as seen by deep tow surveys will be presented. Attempts will be made to quantify the variations in the nature of relief at ridge crests in terms of spreading rate.

## 1.2 Data and the Deep Tow Instrument Package

### The Deep Tow Instrument Package

The deep tow instrument package is comprised of a number of geophysical and geological instruments designed to be towed close to the sea-floor. The instruments include up and down looking sonars, side-scan sonars, 4 kHz sonar for sediment penetration, magnetometer, water temperature sensors, and photographic and television cameras (Spiess and Tyce,



1973). At various times a number of other devices have been deployed with the package. In most deep tow surveys, the location of the instrument package is determined by ranging to a number of moored acoustic transponders positioned before the surveys. But for long profiles of ridge crests, the deep tow package is often out of the range of the transponder net. In these cases, the location of the instrument relative to the ship often has been calculated using TOAD, a computer program designed to simulate the dynamics of a long cable towed through water (Ivers and Mudie, 1973). The precision of the navigation relative to the ship using TOAD has been estimated to be 400-600 m (Ivers and Mudie, 1973). The location of the instrument package relative to the ship can also be determined by matching topographic features recorded by the instrument package with those recorded by the ship. The location of the ship is in turn typically determined from satellite fixes.

Between the first deep tow survey of a mid-ocean ridge in 1967 and the most recent, numerous improvements have been made to the instrument package. Of particular interest here is the addition of an improved narrow beam down looking sonar in 1975 which resulted in substantial improvement of the resolution of steep slopes. The data from the East Pacific Rise (EPR) at 9°N, 3°S, and some from 21°N and the Galapagos Spreading Center (GSC) used in this study were collected with the improved down looking system.

### Deep Tow Surveys

Up to 1978, the deep tow "Fish" has been used to survey mid-ocean ridges at 10 sites. Several sites have been surveyed more than once and three additional transform fault surveys have coverage of adjacent spreading centers (Crane, 1976; Lonsdale and Shor, 1979; Macdonald et al, 1979b). The mid-ocean ridges surveyed have spreading rates ranging from 10 to 76 mm/yr half rate. Figure 1 shows the locations of the sites. Most of the surveys have been reported elsewhere. Table I lists the sites, the nature of the surveys, and the papers in which they have been described. A number of these surveys were detailed studies of ridge crests (Gorda Rise, EPR at 21°N, 9°N, and 3°S, the GSC, the Mid-Atlantic Ridge (MAR) at 37°N, and the Reykjanes Ridge). Others were isolated long profiles collected for the measurement of the near-bottom magnetic field (EPR 21°N-Oconostotow, Costa Rica Rift (CRR), and the Pacific-Antarctic Ridge (PAR) at 51°S).

### Labelling of the Profiles

In the figures and tables of this paper, the profiles from the Gorda Rise have been labelled in the manner of Atwater and Mudie (1973). The GSC profiles are labelled as in Klitgord and Mudie (1974) and Crane (1978). Primes have been added to the labels from Crane (1978) and lower case letters used for profiles not previously published. The data shown from Klitgord and Mudie (1974) and Crane (1978) have

Figure 1: Location of deep tow surveys of mid-ocean ridges compiled for this study.

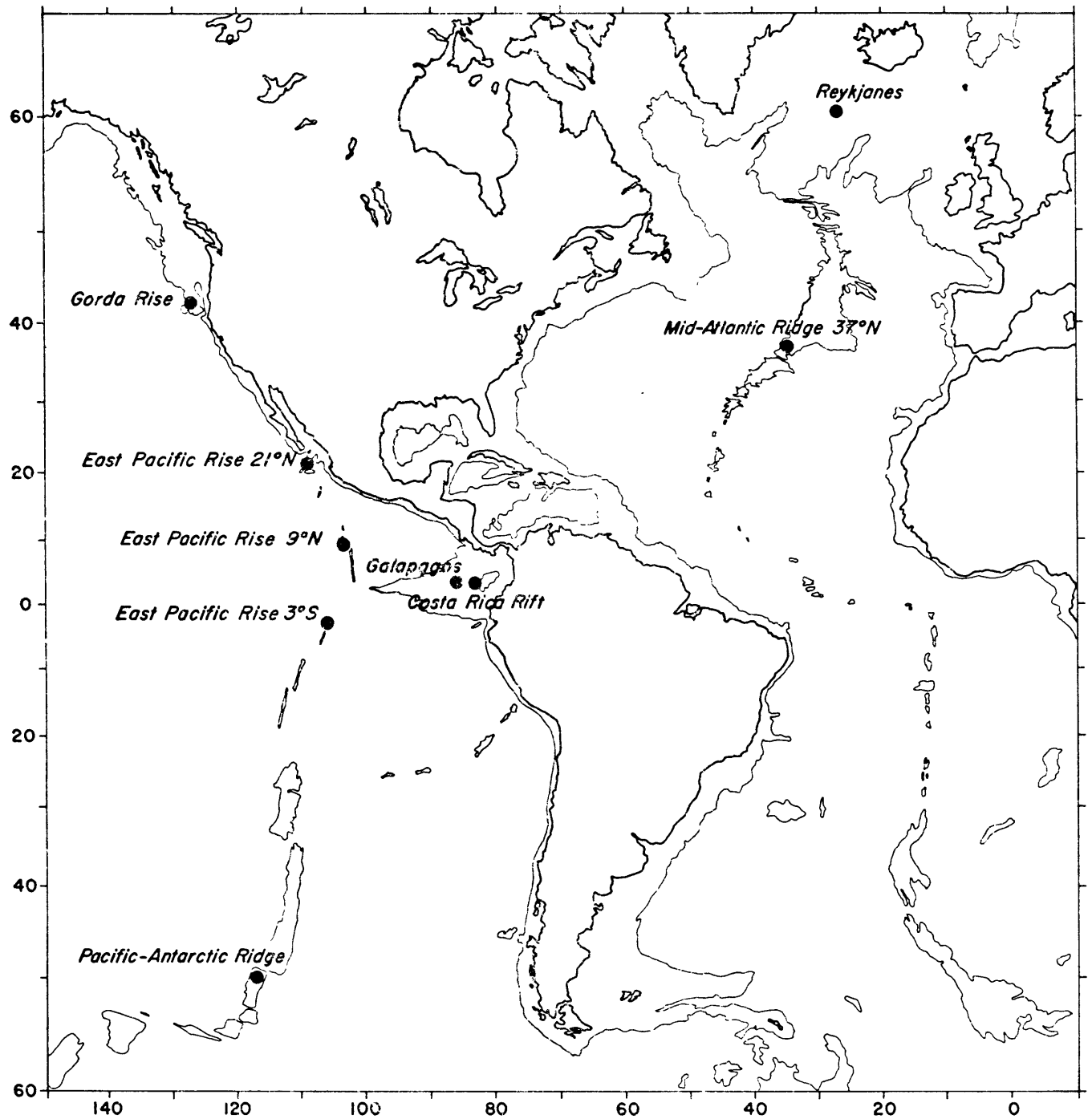


Table I: Deep Tow Surveys Used in This Study

Site	Spreading Half-Rate	Type of Survey	References
1. East Pacific Rise 3°S (EPR 3°S)	76 mm/yr	Detailed	Lonsdale, 1977a
2. East Pacific Rise 9°N (EPR 9°N)	58	Detailed	Lonsdale & Spiess, 1979
3. Pacific-Antarctic Ridge 51°s (PAR)	48	Longlines	Mudie et al, 1972 Klitgord et al, 1975
4. Costa Rica Rift (CRR)	38	Longline	Klitgord et al, 1975
5. Galapagos Spreading Center 86°W (GSC)	35	Detailed	Klitgord & Mudie, 1974 Klitgord et al, 1975 Crane, 1978
6. East Pacific Rise 21°N (EPR 21°N)	30/38	Detailed	Larson, 1971 Klitgord et al, 1975 Normark, 1976 Crane & Normark, 1977
7. Gorda Rise	12/41	Detailed	Atwater & Mudie, 1973 Klitgord et al, 1975
8. Mid-Atlantic Ridge 37°N (MAR)	13/11	Detailed	Macdonald & Luyendyk, 1977 Luyendyk & Macdonald, 1977
9. Reykjanes Ridge	10	Longlines	Shih et al, 1978

been fitted together by matching topographic features. The EPR 3°S profiles shown by Lonsdale (1977a) are composites. They are shown as collected in this paper with different labels. The two profiles from EPR 9°N are portions of two long crossings of the ridge crest shown in Figure 14 of Lonsdale and Spiess (1979). During expedition SOUTHTOW, three long profiles of the west flank and one of the east flank of PAR were collected (Mudie et al, 1972). The three western profiles are labelled as north, central, and south, and the eastern profile as east. The north and east profiles are two halves of a single traverse shown in Klitgord et al (1975). The profiles from EPR 21°N were collected during expeditions TIPTOW, COCOTOW, and FRANCIS DRAKE (Larson, 1971; Normark, 1976; Crane and Normark, 1977; Macdonald et al, 1979a). A long profile was collected near EPR 21°N during expedition OCONOSTOTOW. The detailed ridge crest surveys at EPR 21°N were fitted together by matching topographic features. A new labelling convention is used here. The profiles of the Reykjanes Ridge are from Shih et al (1978) and they have been projected onto the N90°E direction here. The MAR profiles have been labelled in the manner of Macdonald and Luyendyk (1977).

### Magnetic Data

The near-bottom magnetic field was measured with the bathymetry in all of these surveys and has been interpreted to give spreading rates and the location of the spreading

axes, the location where the age of the sea-floor is effectively zero, at most locations (Atwater and Mudie, 1973; Larson, 1971; Klitgord and Mudie, 1974; Klitgord et al, 1975; Shih et al, 1978; Macdonald, 1977; Macdonald et al, 1979a). The surveys at  $3^{\circ}\text{S}$  and  $9^{\circ}\text{N}$  did not include any magnetic anomaly reversals and the spreading rates were determined from surface ship magnetic data (Lonsdale, 1977a; Lonsdale and Spiess, 1979).

#### Digitization of the Bathymetric Data

Deep tow bathymetric data are usually digitized for analysis. Depending on which survey, the records have been digitized at either inflection points such that when straight lines are connected between them, the resulting time series is within four meters of the original, or the records were digitized at even 30 sec or one minute intervals. The average digitization interval using the inflection point method is one per minute. Using a typical towing speed of about two km/hr, one data point per minute gives a digitization interval of one per 33 m of distance covered. Samples of the bathymetric data have been plotted in the form of fence diagrams and projected profiles in Figures 2,3, and 4. For detailed locations of the profiles, see the references listed in Table I.

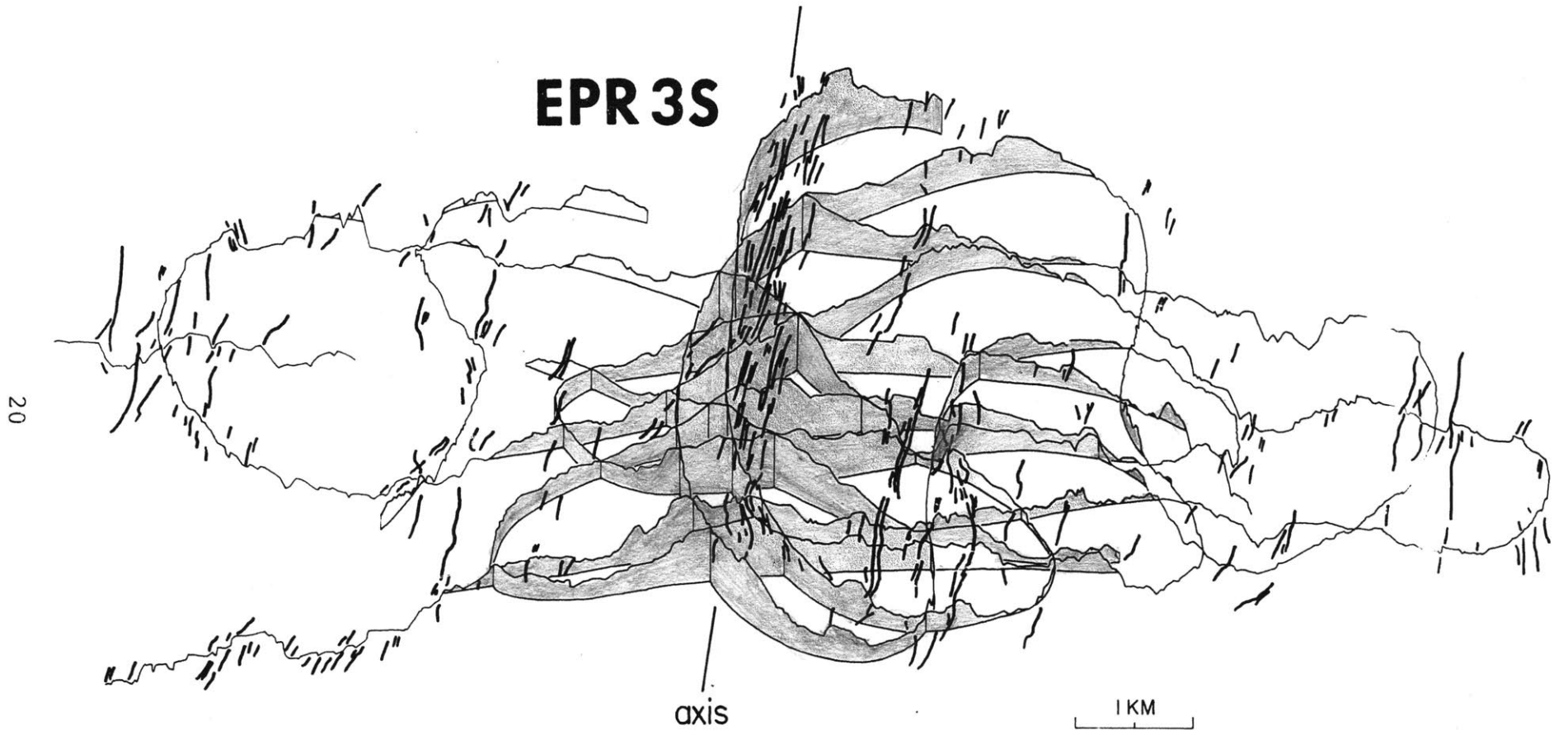
#### Identification of Fault Scarps

The deep tow profiling system, in combination with the side-scan sonars, is particularly suited to the mapping of

Figure 2: Fence diagrams of detailed ridge crest surveys from EPR 3°S and EPR 21°N. Side-scan data show the lineated nature of fault scarps. Side-scan targets were assumed to have the same depth as the sea-floor where the deep tow instrument track crosses the targets. Vertical exaggeration is 4X for EPR 3°S and 2X for EPR 21°N. EPR 21°N side-scan data courtesy of Bill Normark.



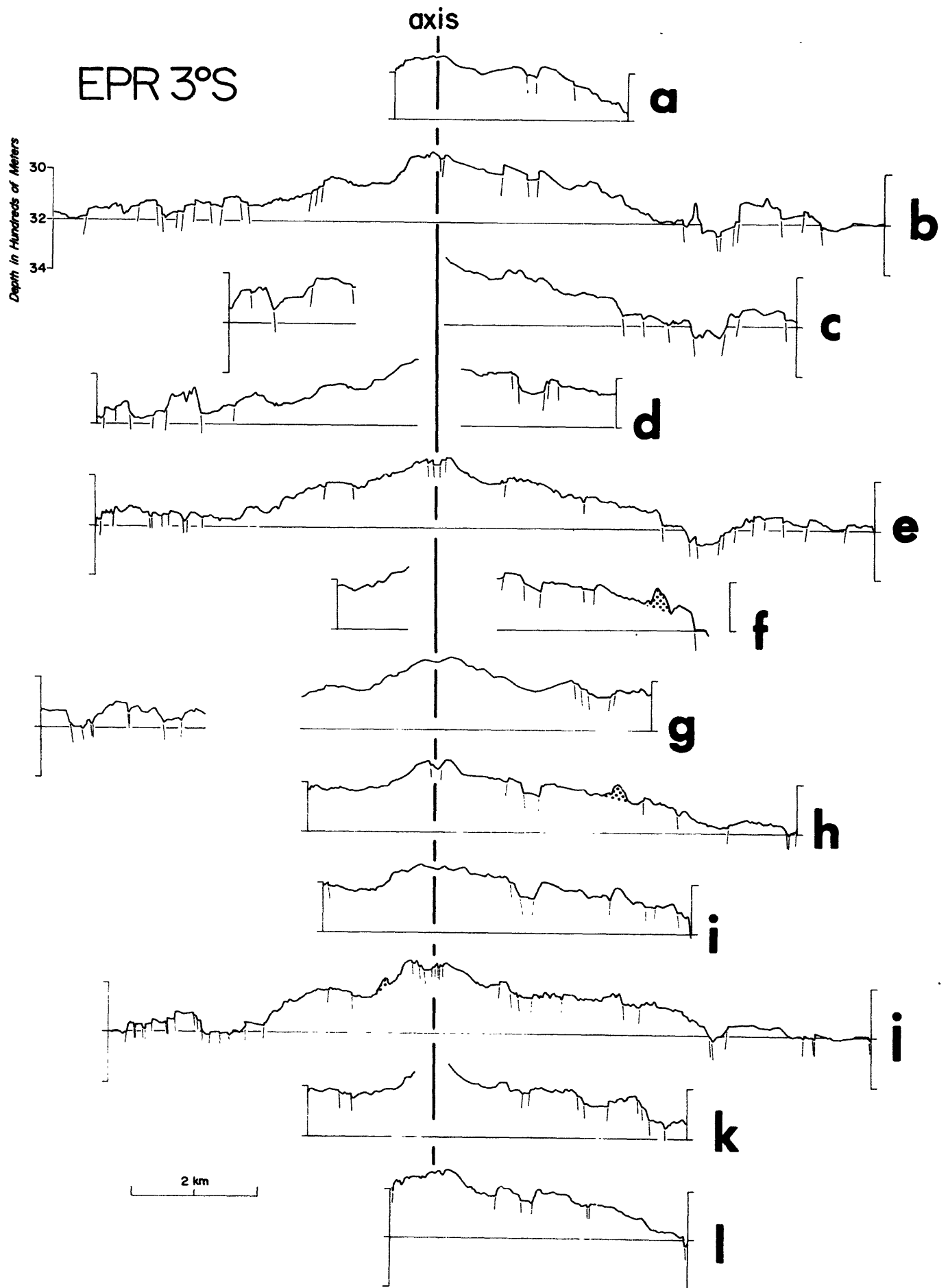
# EPR 3S

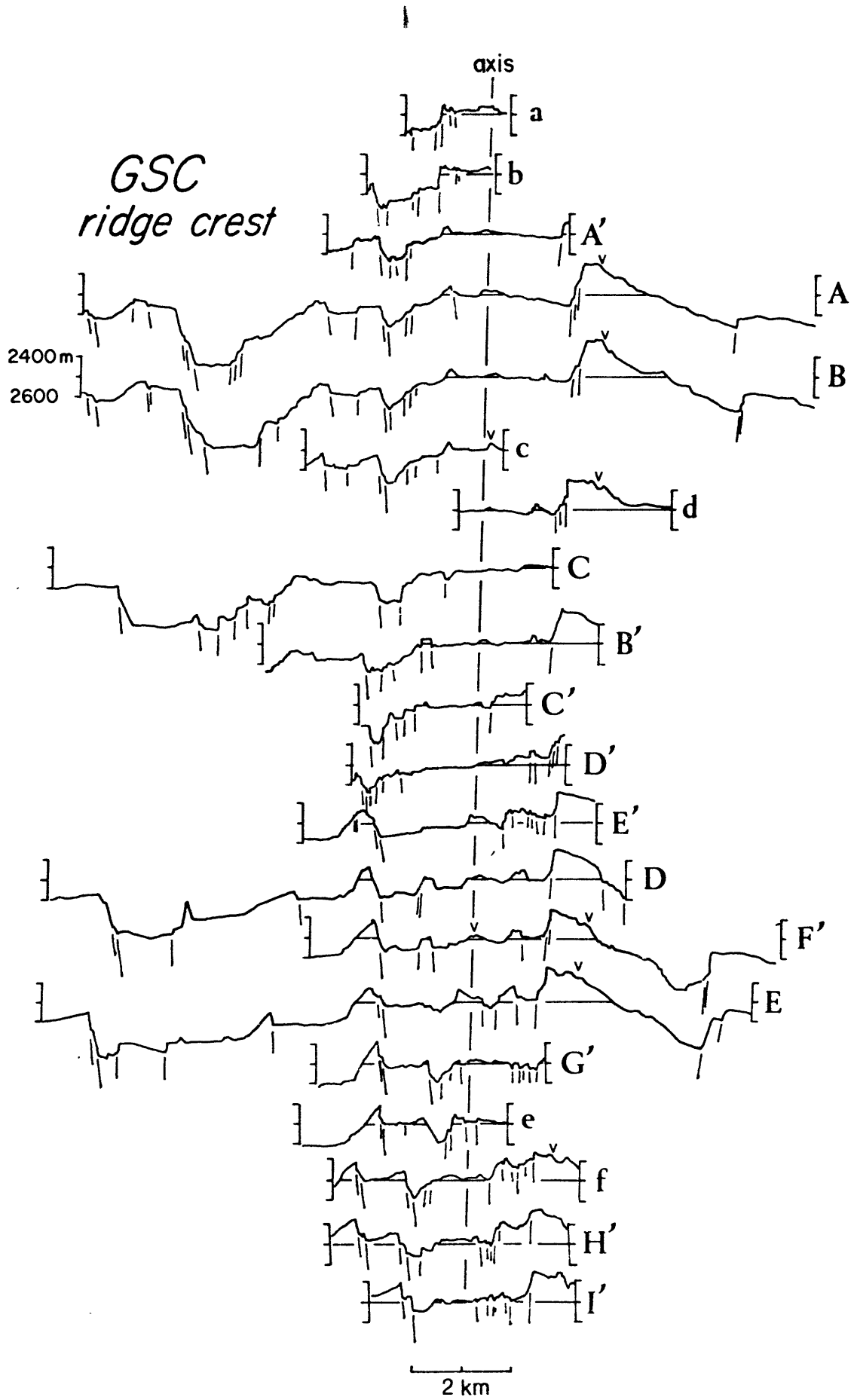


# EPR 21°N

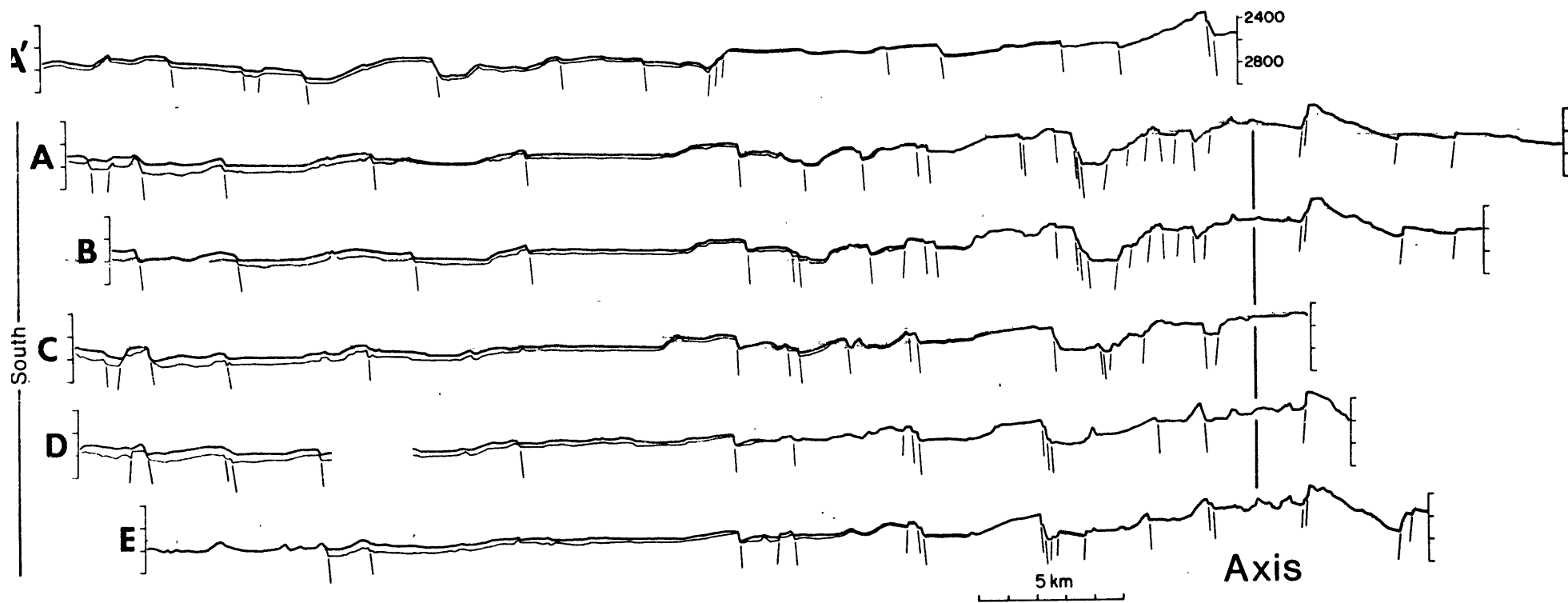


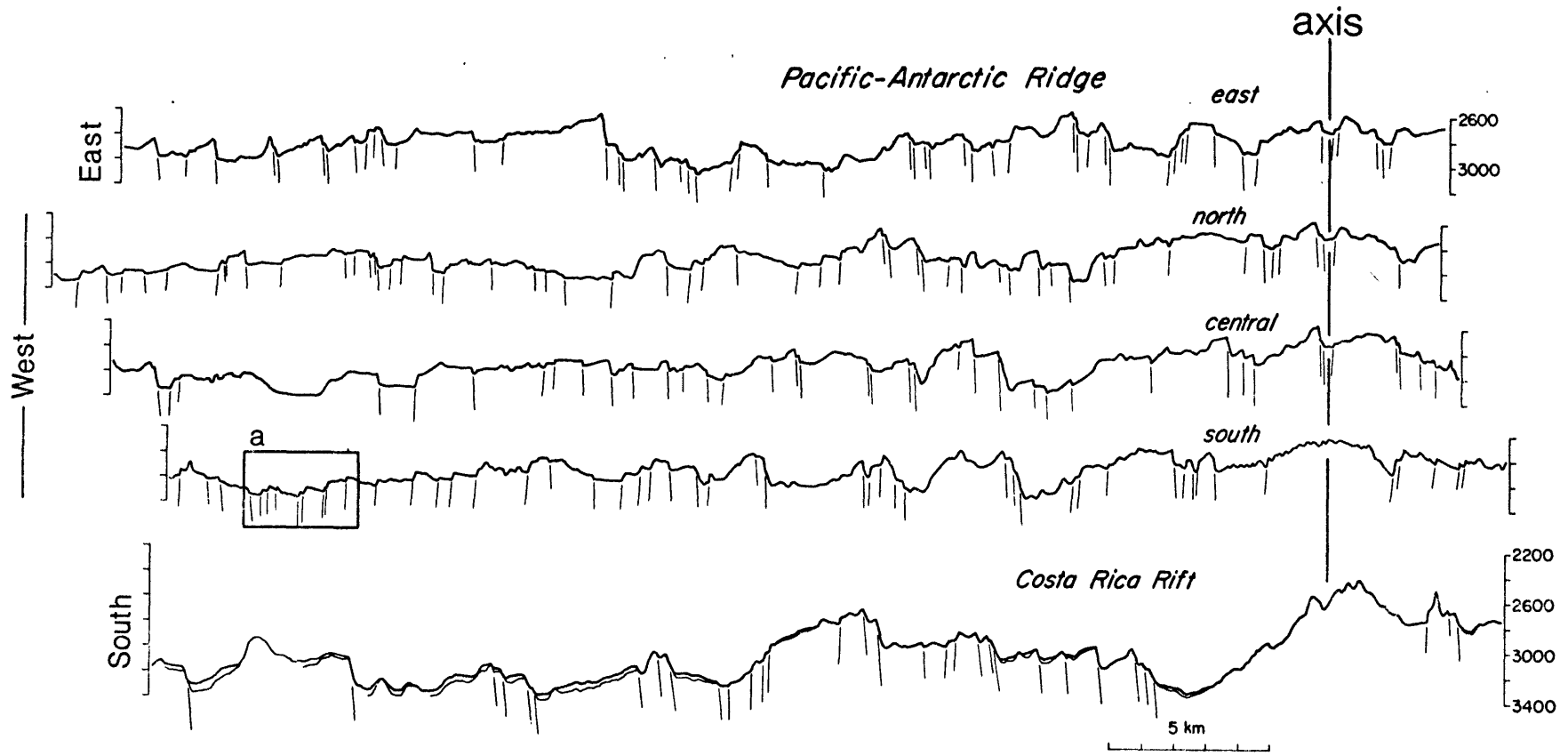
Figure 3: Projected profiles of ridge crests from detailed surveys. Stippled areas or "v" s show features interpreted to be volcanic constructions. Few volcanic features were identified outside of the central low relief zone, probably due to the dominance of tectonic relief outside of the central low relief zone. Vertical exaggeration is 4X. Box a shows the location of deep tow record presented in Figure 5b.





# *Galapagos Spreading Center*





West

East

South

*Pacific-Antarctic Ridge*

*Costa Rica Rift*

axis

*east*

*north*

*central*

*south*

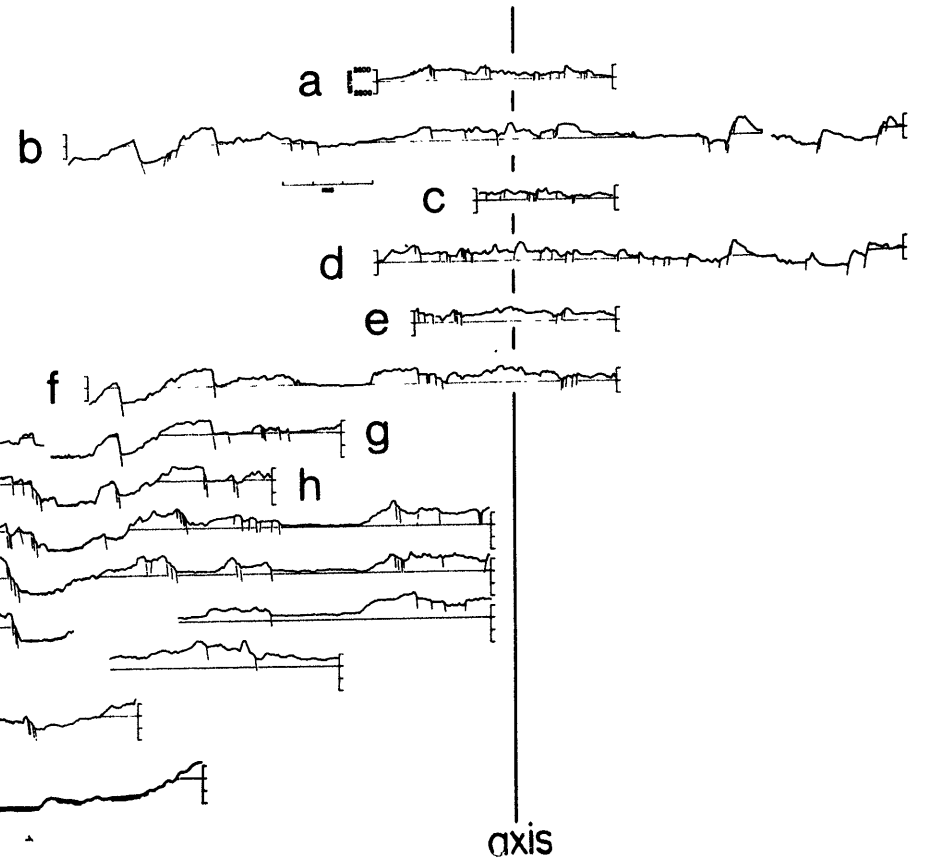
a

5 km

2600  
3000

2200  
2600  
3000  
3400

# EPR 21°N longer profiles

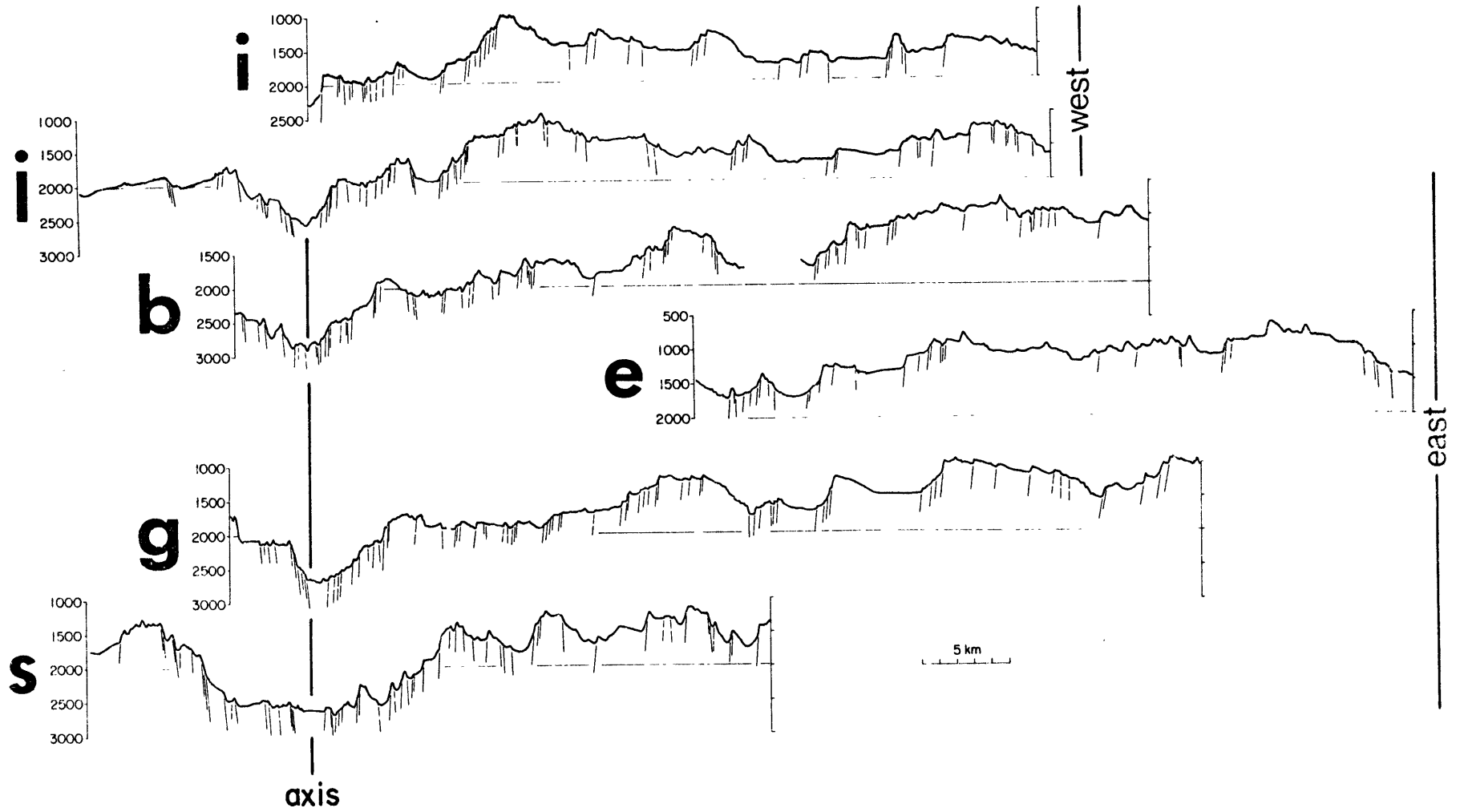


27





# MAR



# Gorda

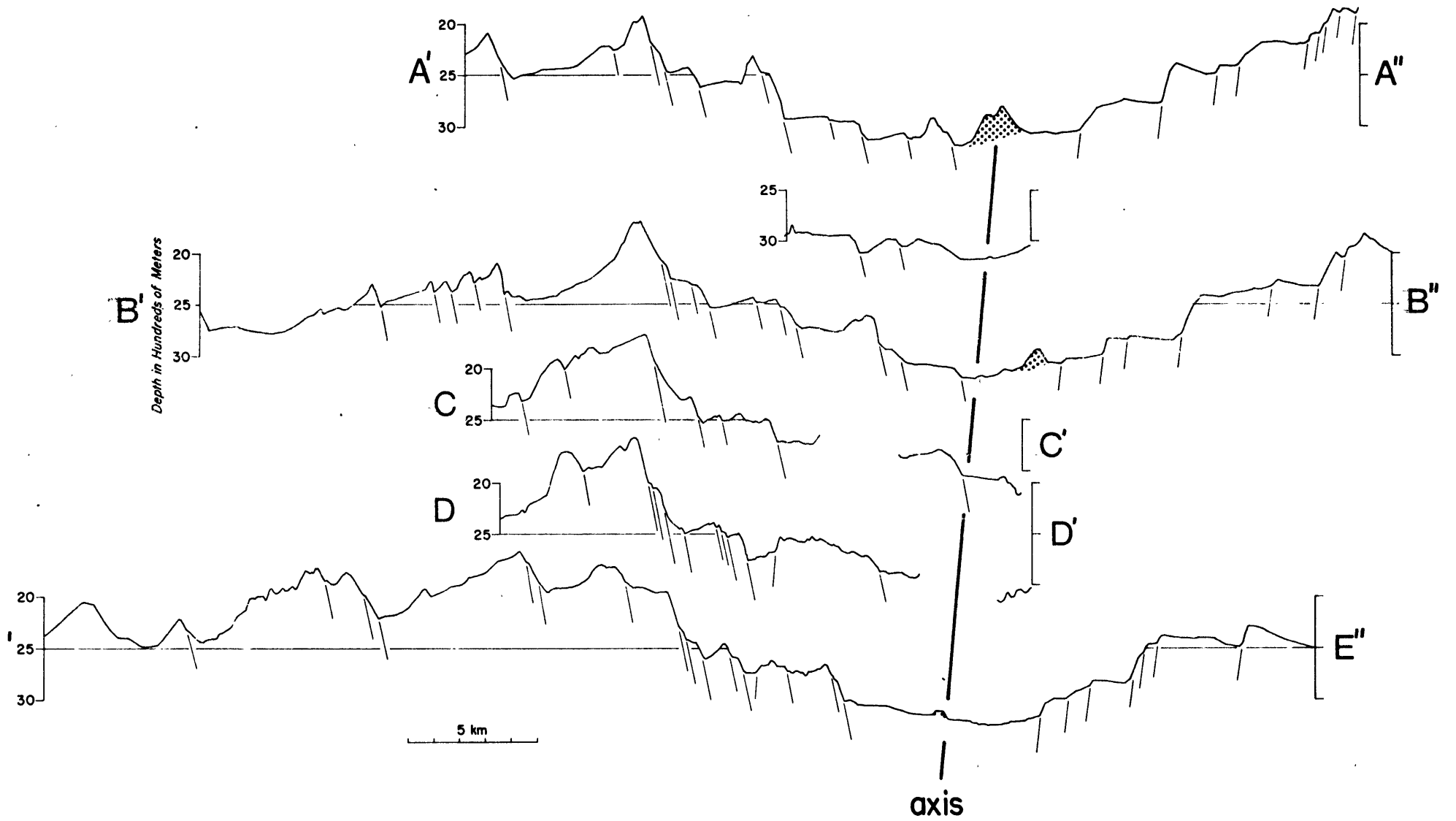


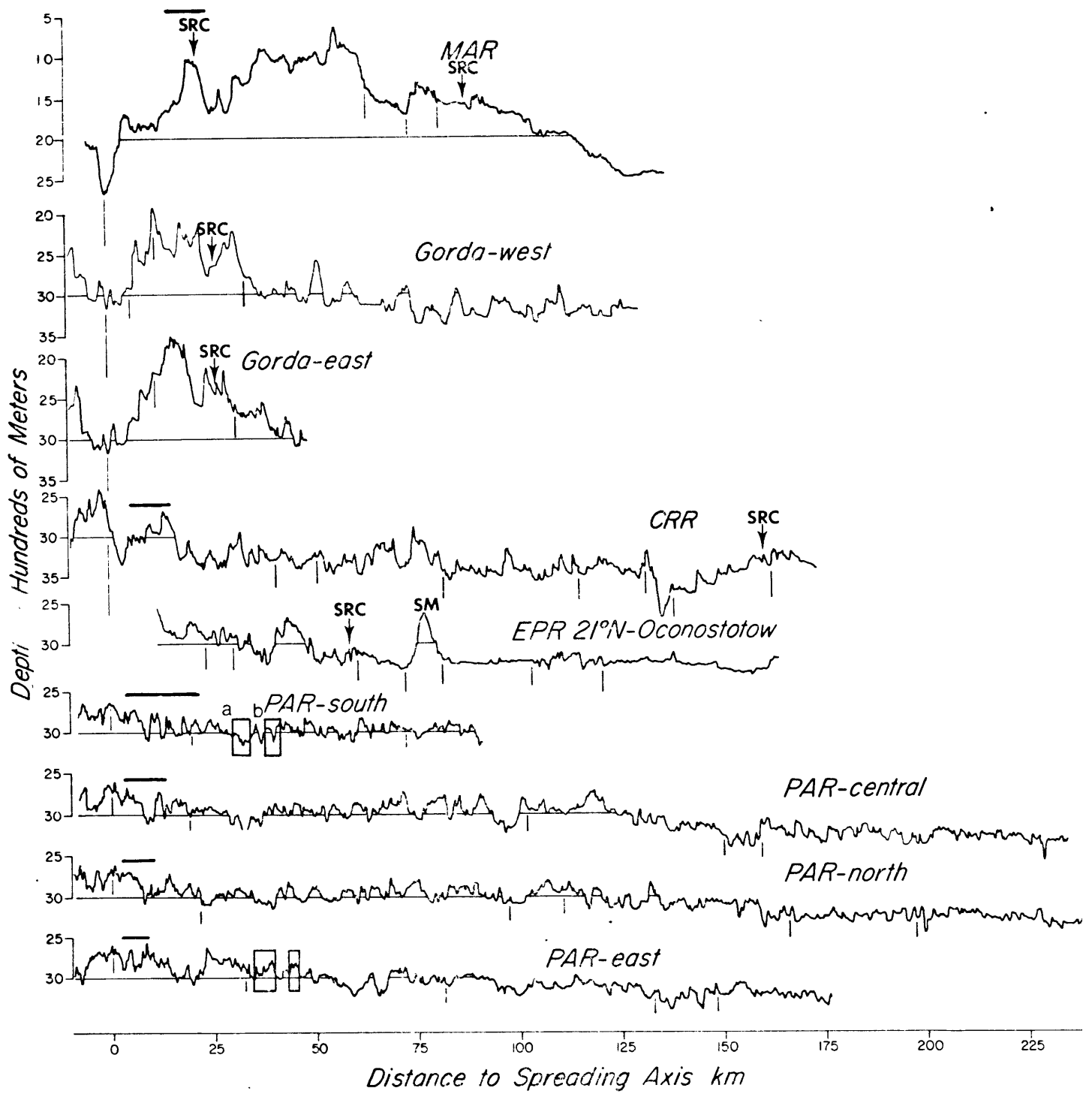
Figure 4: Longer deep tow profiles. Bars over the profiles show the estimated plate boundary half-widths as discussed in Section 1.5. Vertical bars under the profiles show the locations of changes in the roughness of sea-floor relief. They correspond with the vertical bars under the cumulative vertical relief curves shown in Figure 14. SRC=location of spreading rate change, SM=seamount. Vertical exaggeration is 20X. Boxes indicate the location of deep tow records shown in Figure 5.

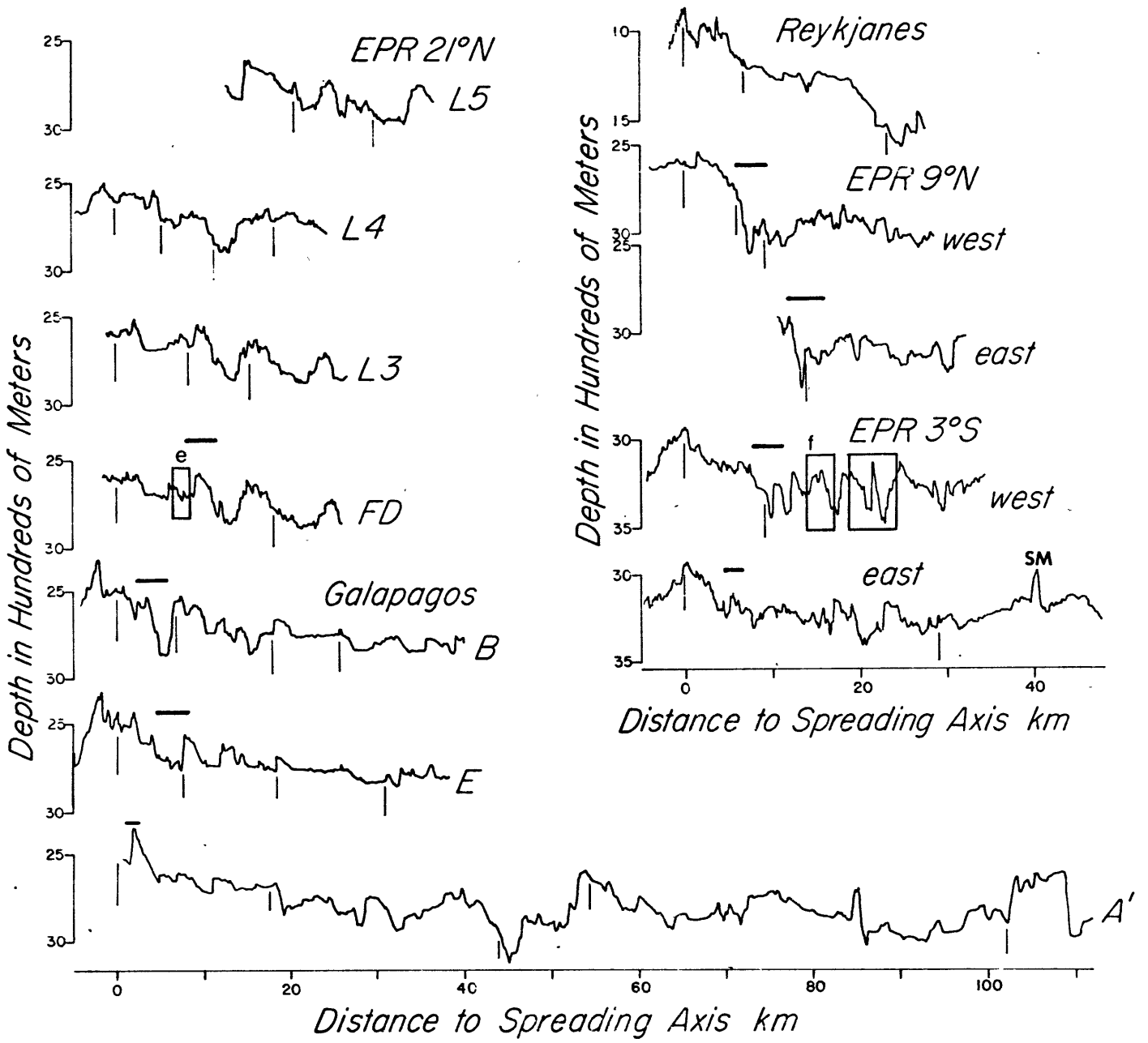
Box a- Figure 5b

Box b- Figure 5c

Box e- Figure 5d

Box f- Figure 5a



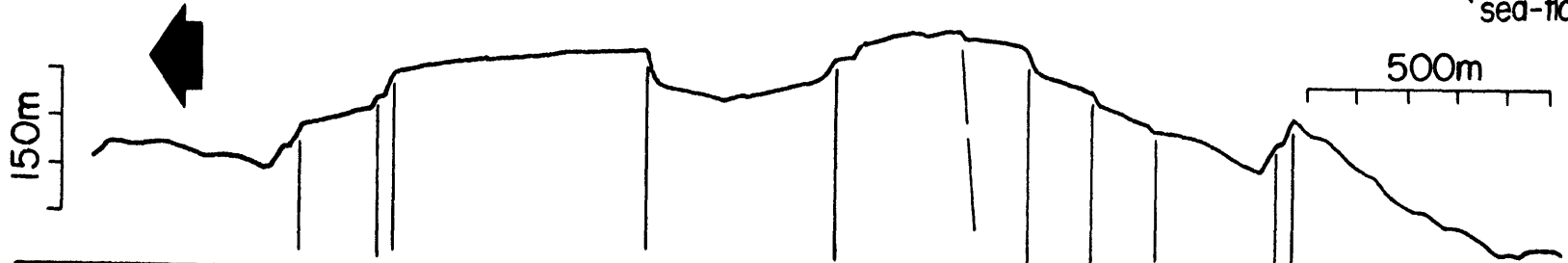
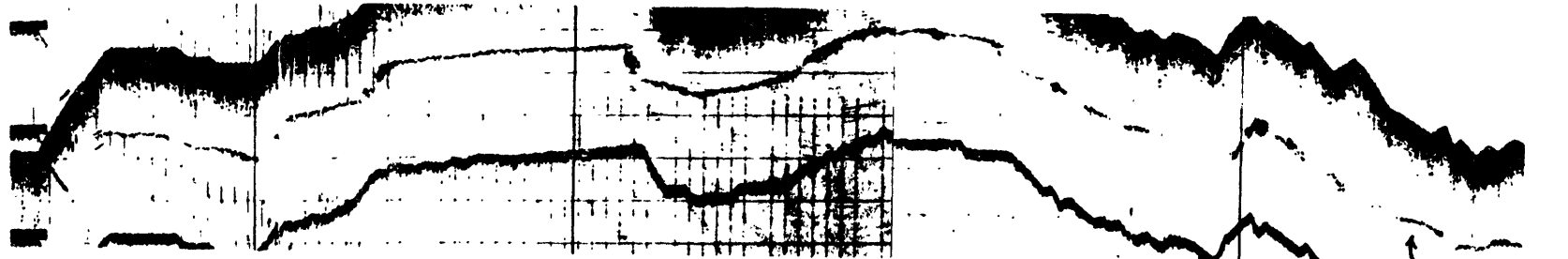


fault scarps and volcanoes. Fault scarps show up as abrupt breaks in the bathymetric records. They usually have very steep slopes, often beyond the resolution of the profiling system, and in cross-section form rectangular to triangularly shaped fault blocks. The sharp breaks in slope are often marked by side-echoes or zones of extra thick return trace in the records. Fault scarps and fissures show up in side-scan records as sharp linear reflectors, often traceable between adjacent profiles. Fault scarps can be differentiated from steep volcanic flow fronts by the more sinuous and discontinuous side-scan signature of the latter features. Side-scan data also show volcanoes as isolated features and fault scarps as lineated features which sometimes can be traced between profiles. The inclusion of side-scan targets in fence diagrams shows conclusively the lineated nature of fault scarps and fissures (Figure 2).

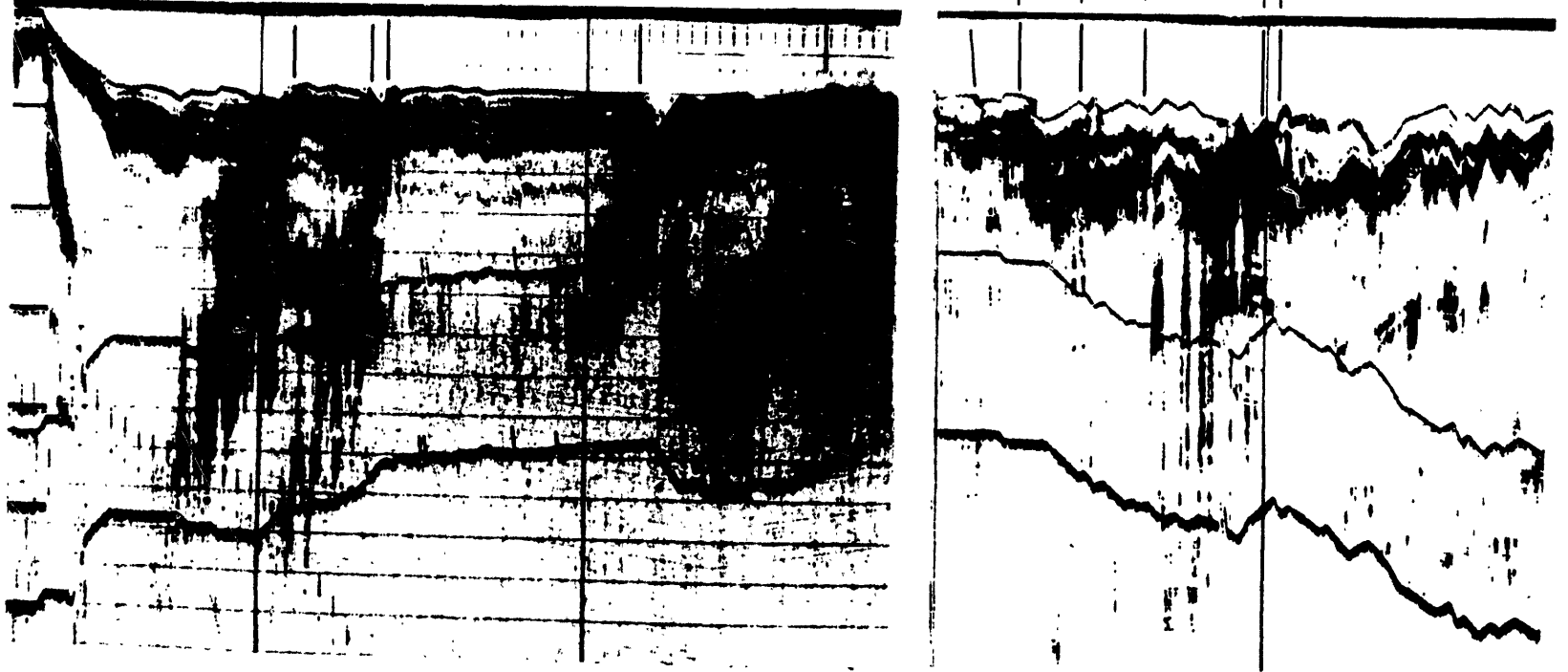
Examples of deep tow records are shown in Figure 5. In records collected with the older profiling system, fault scarps are often marked by parabolic side-echoes above breaks in the bottom trace. The sea-floor often decreases in slope below the steepest parts of the fault scarps. These probably are talus aprons, possibly covering fault slivers. Bottom photographs and submersible observations show talus slopes often obscure large portions of fault scarps (e.g. Ballard and van Andel, 1977). The superior resolution of the newer profiling system as well as submersible surveys show that

Figure 5: Deep tow profiling and side-scan records.  
Horizontal scales=500m, vertical scales=150m.  
Vertical lines indicate locations of interpreted  
fault scarps and their corresponding side-scan  
signatures. Arrows point toward the spreading  
axes. EPR profiles were collected with the  
new profiling system while the PAR profiles were  
collected with the old profiling system.  
Locations of the figures:  
5a- EPR 3<sup>0</sup>S, see Figure 4, Box f.  
5b&c- PAR, see Figures 3 and 4, Boxes a and b.  
5d- EPR 21<sup>0</sup>N, see Figure 4, Box e.

5a EPR 3°S

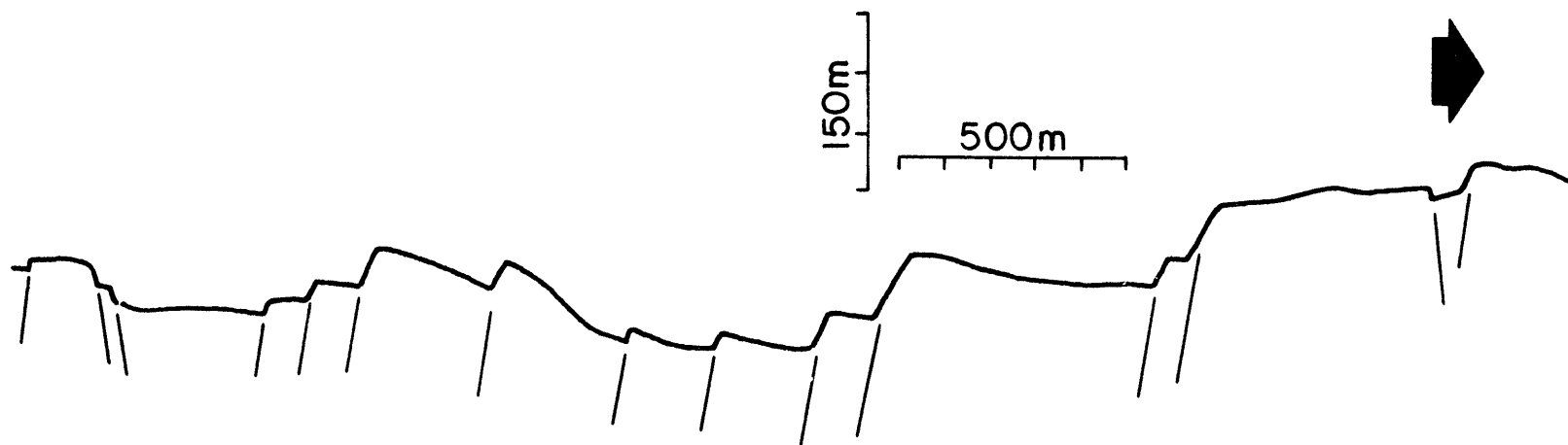
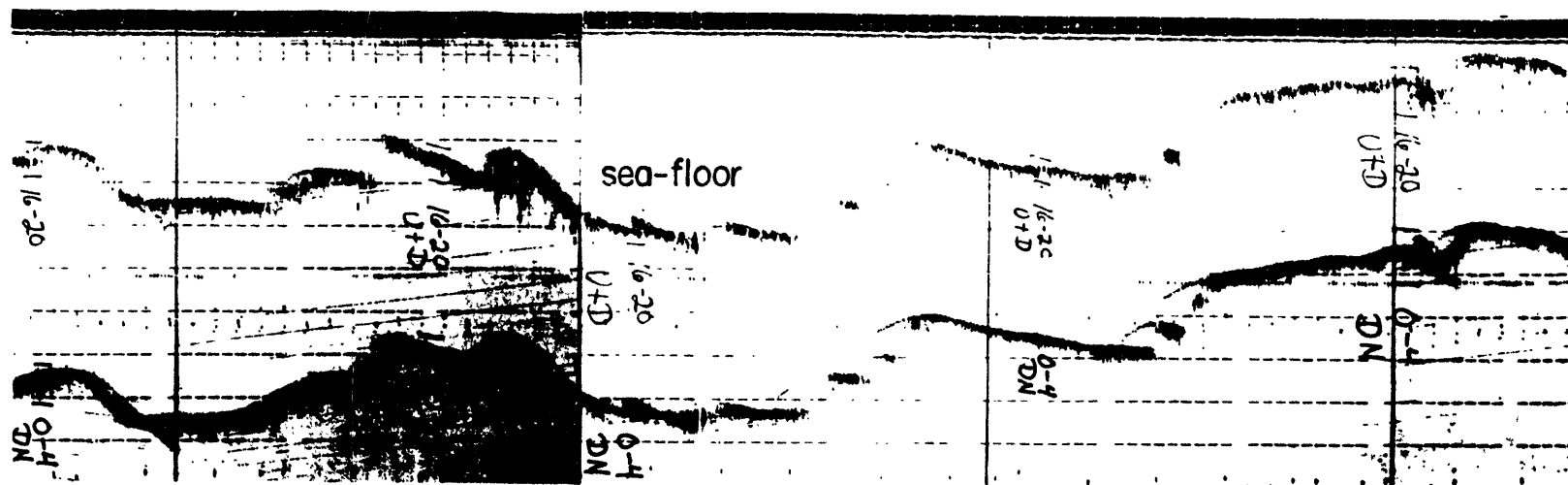


right side-scan

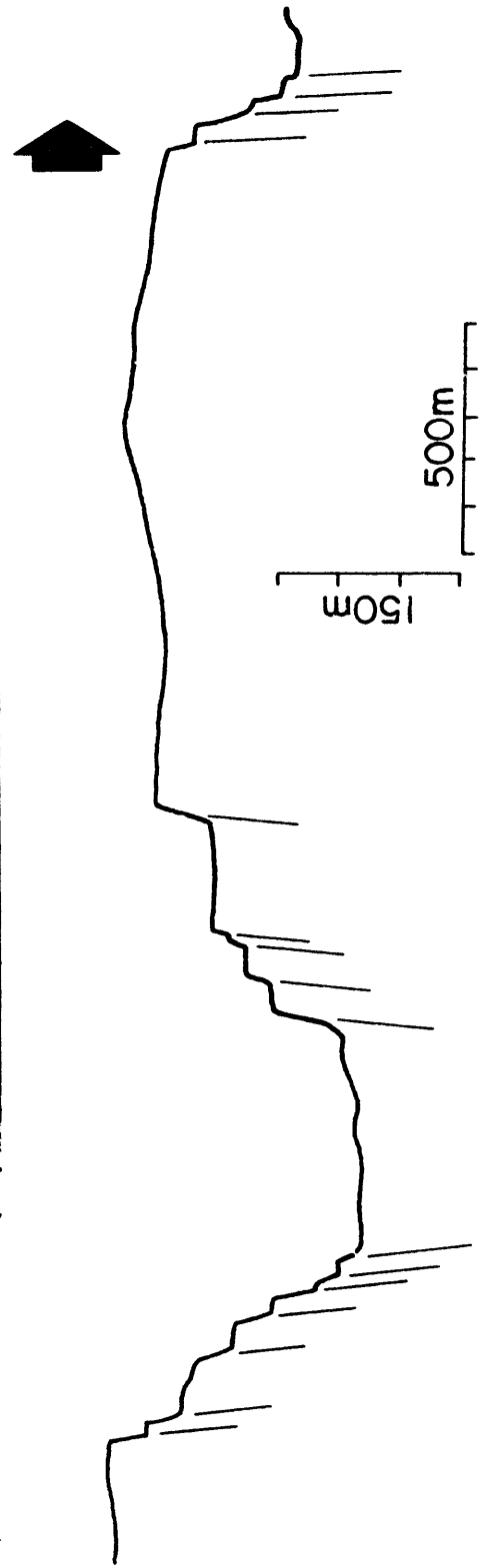




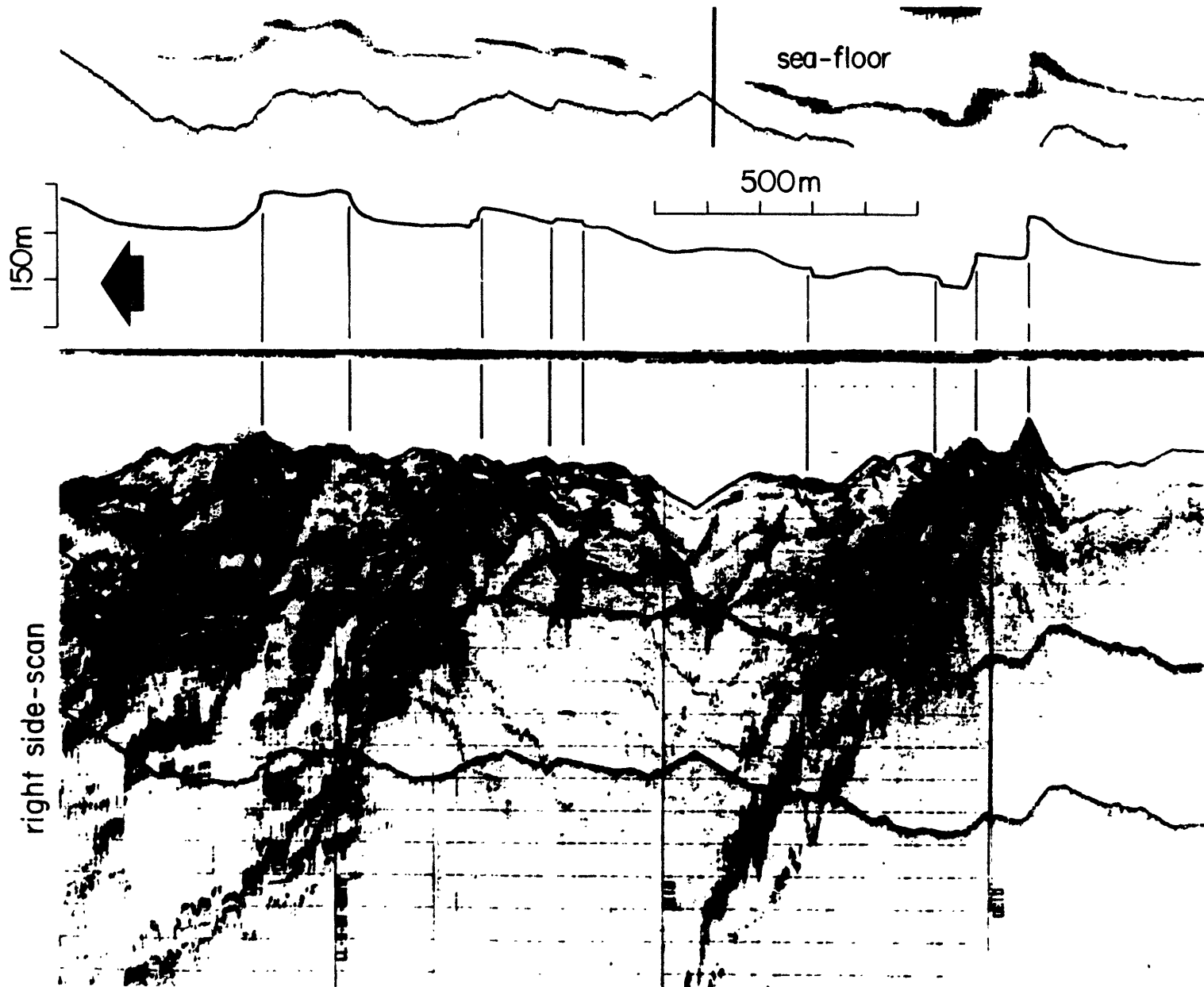
# 5b PAR



5c PAR



5d EPR 21°N



fault scarps identified in older deep tow records are often actually fault zones with several individual fault slivers. This difference tends to make estimates of fault throws on individual faults from older deep tow records be greater though the total measured throw across fault zones would be the same. Original deep tow profiling, side-scan, and sediment penetration records were always used in the identification of fault scarps in this study. As many of the examples in Figure 5 show, fault scarps are distinctive in many ways which are often lost in the digitization process. Any simple criterion, such as the slope of the sea-floor, is insufficient to characterize fault scarps. This is especially true for fault dips as they often are not resolved by the profiling system and the digitized fault dips are highly dependent on the digitization method.

### 1.3 General Morphology of the Spreading Centers

#### Typical Features of Mid-Ocean Ridges

In general, spreading axes are easily identifiable in bathymetric profiles without the aid of magnetic data. Mid-ocean ridges typically are the shallowest features in the oceans and their flanks deepen systematically away from the ridge crests. At the spreading axes, either a central high or a median rift is commonly present. The rift or central high usually is very prominent and it is also typically the highest high or the lowest low in the vicinity. In deep

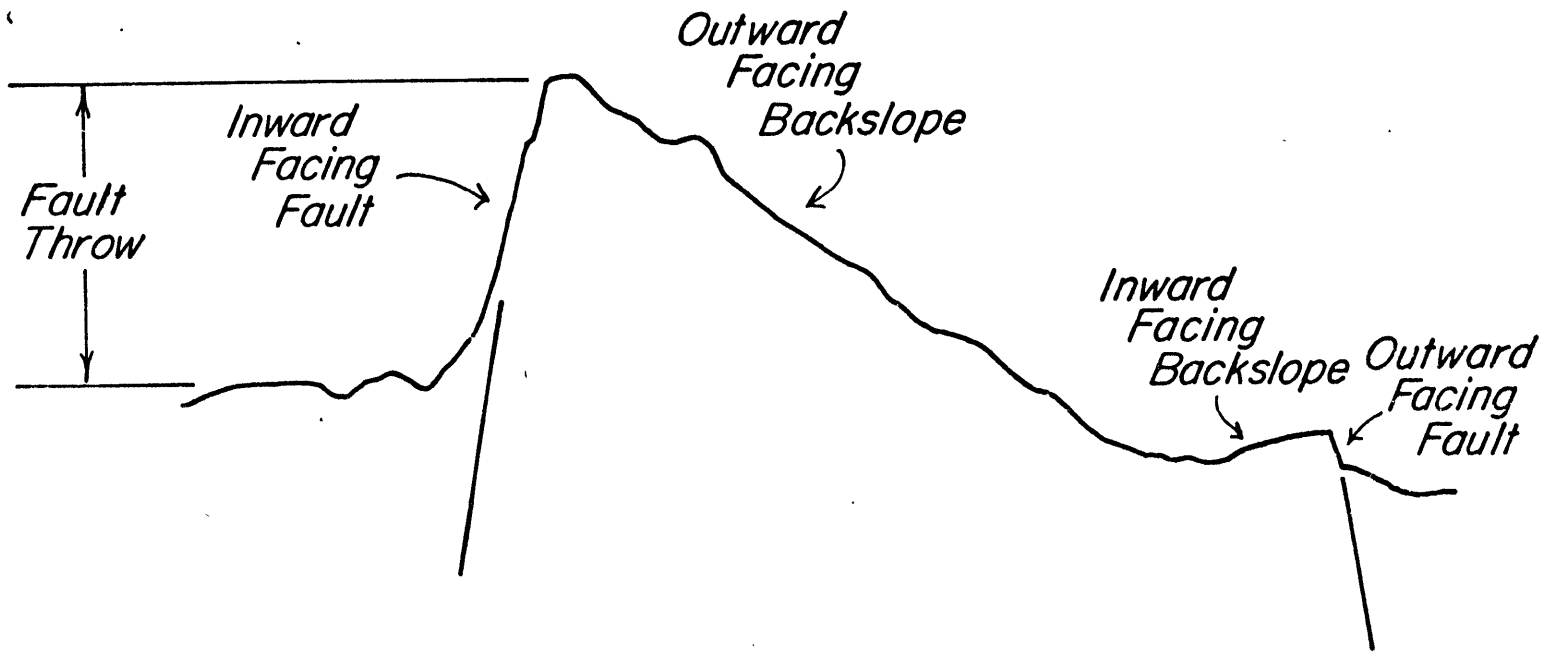
tow profiles, the spreading axes are also usually quite easy to locate. Most fault scarps face toward the axes and fault block back-slopes dip away from the spreading axes (Figure 6 defines the terms that will be used to describe the tectonic relief). Whether a ridge crest is rifted or has a central high, its spreading axis is always characterized by a zone of low tectonic relief.

Based on the deep tow surveys, the spreading centers can be divided into three morphological zones: 1) Astride the spreading axes are zones of low relief. Fault throws are small and fault scarps are few. Perhaps due to the lack of large tectonic relief, volcanoes often are prominent in this zone. 2) Bracketing the central low relief zones are areas of increasing tectonic relief. Fault scarps increase in throw, often very suddenly. At rifted mid-ocean ridges, the transition between the low relief central zone and the tectonic zone is defined by the large inward facing faults that form the median valley walls. 3) Outside of the zone of increasing tectonic relief are the abyssal hills. Here there are few signs of additional tectonic activity. The relief has been frozen into the lithosphere and is passively carried away by sea-floor spreading.

Beyond these general features, mid-ocean ridge crest morphology can be quite variable and distinct in detail. To a large part, ridge crest morphology can be correlated with spreading rate (Menard, 1967; Cann, 1968; Anderson and

Figure 6: Definition of terms used to describe sea-floor tectonic features. Inward facing faults and back-slopes dip toward spreading axes while outward facing faults and back-slopes dip away from spreading axes.

← *Spreading Axis*



Noltimier, 1973). The spreading centers surveyed by deep tow can be divided into four groups by spreading rate. The Gorda Rise and the MAR have deep median rifts and slow spreading rates. EPR 21°N, GSC, and CRR have shallow rifts and intermediate spreading rates. EPR 3°S, EPR 9°N, and PAR have central highs and fast spreading rates. The Reykjanes Ridge is unique in having a central high yet with a low spreading rate.

#### Slow Spreading Centers: MAR and Gorda Rise

Of the slow spreading centers, the Gorda Rise has a broader and shallower median rift. The inner rift in the southern FAMOUS area (profile s in Figure 3) comes close to the width of the Gorda, however. The median valley walls essentially rise directly into the rift mountains at the Gorda Rise. The rift mountains appear to be formed of large outward tilted fault blocks. Note the spreading rate slowed only recently from 41 mm/yr to 12 mm/yr at 2.2 mybp (Atwater and Mudie, 1973; Klitgard et al, 1975). The sea-floor created at the time of the spreading rate change is now only 26 km from the spreading axis.

In contrast to the Gorda Rise, the MAR at 37°N has a very narrow inner rift valley in places. The rift walls do not rise straight into the rift mountains. Instead, there are a number of terraces (Macdonald and Luyendyk, 1977). Asymmetric spreading and minor spreading rate changes have occurred within the deep tow survey area (Macdonald, 1977). However,



the rate changes are quite small compared to that at Gorda.

Intermediate Rate Spreading Centers:  $EPR 21^{\circ}N$ , GSC, CRR

The most prominent features of the intermediate rate spreading centers are the tilted fault blocks which are 200 to 300 m high and face inward toward the spreading axes. At the GSC, the inner rift valley defined by the large fault blocks is only 3-4 km wide. The valley walls are not symmetrical and in places on the southern flank the valley is bound by grabens rather than uplifted fault blocks. The relief decreases dramatically away from the spreading axis toward the south. However, the relief increases again south of the surveyed area. Notably, there is not a similar pattern to the north of the spreading axis (profile A', Figures 3 and 4). The graben at 110 km from the spreading axis in the GSC-A' profile in Figure 4 may be the abandoned spreading axis of a spreading center jump which occurred between anomaly 2' and 3 time (Anderson et al, 1976; Sclater et al, 1974; Hey et al, 1977). Following the analysis of Anderson et al (1976), sea-floor between about 70 and 120 km from the spreading axis on the north flank of the GSC was actually created south of the spreading axis and subsequently attached to the Cocos plate by the jump.

At  $EPR 21^{\circ}N$ , the first 200 to 300 m high fault blocks are 8 to 12 km from the spreading axis. Within the valley defined by these faults is a rifted central high 7 to 8 km wide and 100 to 150 m high (Normark, 1976). The spreading

rate and direction changed at EPR 21°N at about 2.7 mybp (Larson, 1972; Klitgord et al, 1975). The site of the changes is about 60 km from the spreading axis in the EPR 21°N-Oconostotow profiles in Figure 4. Unfortunately, the site of the spreading change is also close to a seamount, which may have affected the relief formation process.

The morphology of CRR is rather ambiguous. There appears to be a median rift with inward facing fault scarps on the southern flank of the rift valley. However, the magnetic anomaly identifications place the spreading axis up on what appears to be the northern median valley wall (Klitgord et al, 1975). The northern valley wall does not appear to be composed of fault scarps typical of rift walls. Instead, the northern wall appears to be constructed of volcanics. The CRR deep tow profile is located close to the CRR/Panama Fracture Zone intersection. The ambiguous morphology may be due to the proximity of the transform fault. The deep tow profile is at 83°W, between the Panama FZ at 82.5°W and the Ecuador FZ at 84.5°W. Surface ship profiles at 83.2° show a median rift while profiles between 83.7° and 84.4°W do not (Grim, 1970). Perhaps the median rift deepens as the Panama FZ is approached, analogous to the EPR near the Tamayo FZ (Macdonald et al, 1979b). This phenomenon has been attributed to the enhancement of viscous head loss near ridge crest/transform fault intersections (Sleep and Biehler, 1970). The spreading rate increased from 26 to 38.5 mm/yr at 4.2 mybp (Klitgord

et al, 1975). The site of the rate increase is now 160 km from the spreading axis, close to the southern end of the deep tow profile.

Fast Spreading Centers: PAR, EPR 9°N, EPR 3°S

Of the fast spreading centers surveyed by deep tow, PAR is the most poorly surveyed. Two of the three deep tow crossings of the PAR crest show shallow central rifts about one-half km wide and 100 m deep atop narrow central highs. The third profile (profile south) is of very poor quality and only shows numerous side-echoes at the ridge crest. However, the records do show that a central rift similar to those in the other crossing is not present. Relief increases very quickly going away from the spreading axis. The fault blocks are more symmetrical than at the intermediate rate spreading centers.

The ridge axis at EPR 3°S is in the form of a central shield volcano flanked by horst and graben style topography (Lonsdale, 1977a). The spreading center stands distinctively higher than the surrounding sea-floor in contrast to the intermediate rate and slow spreading centers. Fault throws clearly increase going away from the spreading axis.

EPR 9°N has a distinctively more rectangular cross sectional shape when compared to EPR 3°S. The shoulders of the central high are composed of large outward facing faults (Lonsdale and Spiess, 1979). Compared to most of the EPR, EPR at 9°N is atypical for its more rectangularly shaped

central high.

### The Reykjanes Ridge

The Reykjanes Ridge is atypical for its oblique spreading and the lack of a median rift given its spreading rate. The ridge crest morphology changes from being flat topped to a peaked ridge crest to the more typical rifted ridge crest going southward away from Iceland (Laughton et al, 1979). The Reykjanes Ridge is related to the Iceland hotspot nearby and not typical of mid-ocean ridges. The Reykjanes Ridge will not be considered in detail here.

## 1.4 Volcanic and Tectonic Relief at Spreading Centers

### Volcanic Relief

Qualitatively, it is quite clear from the bathymetric data that the spreading axes are coincident with zones of low relief and the tectonic relief increases with distance from the spreading axes. To see if there are patterns in the scale of volcanic relief between spreading centers and if the increase in tectonic relief away from spreading axes can be documented, major volcanoes and fault scarps have been identified and their heights measured from the profiles shown in Figure 3.

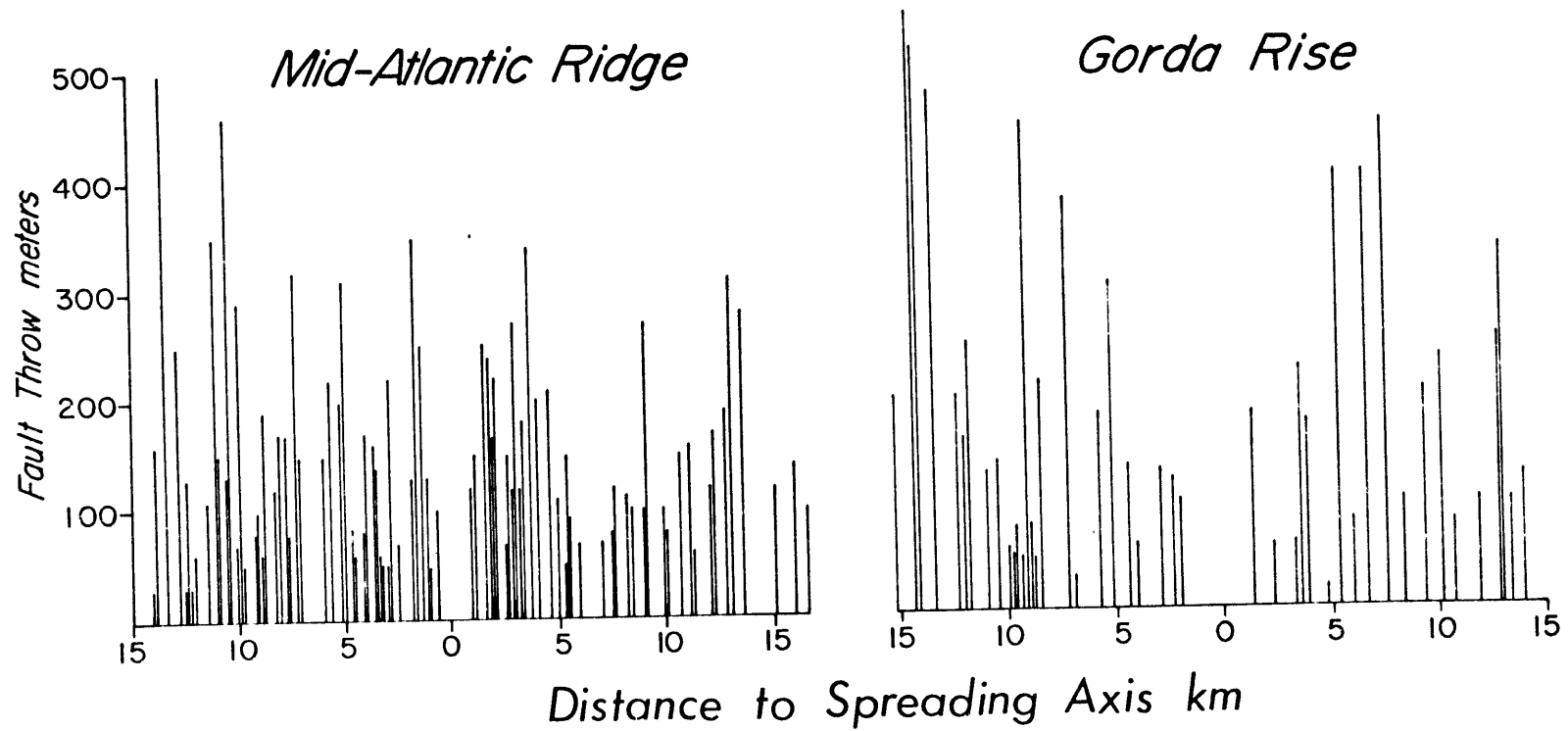
Volcanoes are prominent within the central low relief zone at the slow spreading MAR and Gorda Rise. The volcanoes at the MAR rise up to about 200 m above the surrounding median valley floor. There are three volcanic features in the

median valley of the Gorda Rise. The largest stands about 300 m high. Volcanoes are hard to identify at the intermediate rate GSC, but there are some volcanic features up to 50 m high within the median valley as well as on the back-slopes of some of the tilted fault blocks bounding the median valley. EPR 21°N shows a number of well developed volcanoes. Within 10 km of the spreading axis, the largest volcanoes are about 80 m high and numerous smaller ones can be identified in the profiles shown in Figure 3. At EPR 9°N and 3°S, volcanoes up to 80 m high have been mapped by Lonsdale (1977a) and Lonsdale and Spiess (1979). A large volcano 200 m high is present at 40 km from the spreading axis on the east flank of EPR 3°S (Figure 4). From the anomalously thin sediment cover, Lonsdale (1977a) has interpreted the area to be a site of extinct off-axis volcanism. Volcanoes with sizes similar to those found within the central low relief zones are not typically prominent outside of the central low relief zones. This is probably because the increasing tectonic relief overwhelms the volcanic relief. However, volcanoes have been identified in a detailed survey outside of the central low relief zone at EPR 21°N (Macdonald et al, 1979a).

### Tectonic Relief

The throws of fault scarps from the slow spreading MAR and Gorda Rise have been plotted against the distance to the spreading axes to define the distribution of tectonic relief at the spreading centers (Figure 7). Closely spaced faults

Figure 7: Offset across fault zones versus distance to spreading axes. Fault zones with offsets of less than about 20 m were not tabulated.



forming single large offsets were considered single fault scarps. Fault throws have also been measured in 14 of the longer deep tow profiles (Figure 4 and 8). The throws were measured across individual fault scarps whenever they can be identified. Thus, the magnitude of individual throws are not comparable between profiles due to the differences in the resolution of the old and new profiling systems.

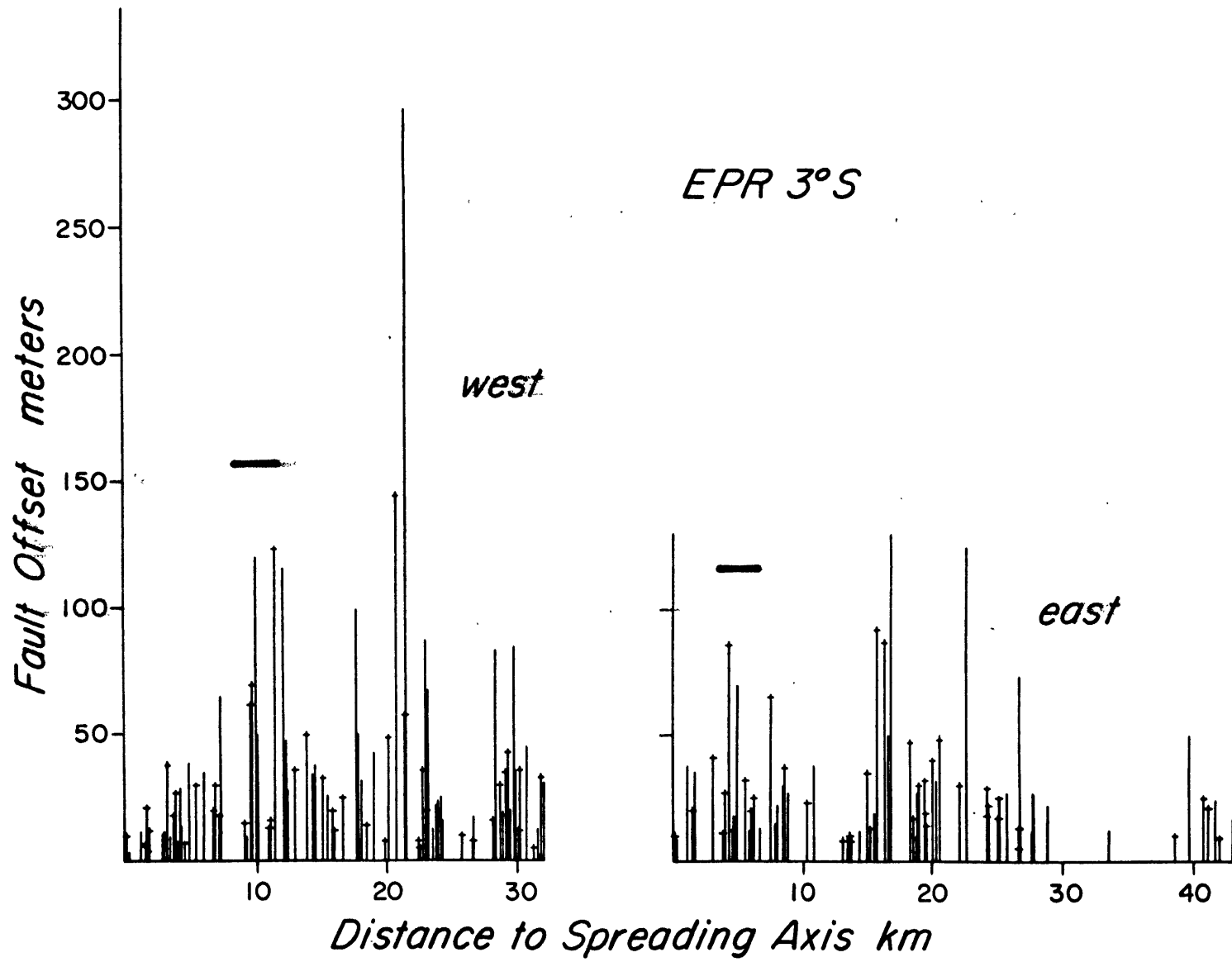
## 1.5 Plate Boundary Widths

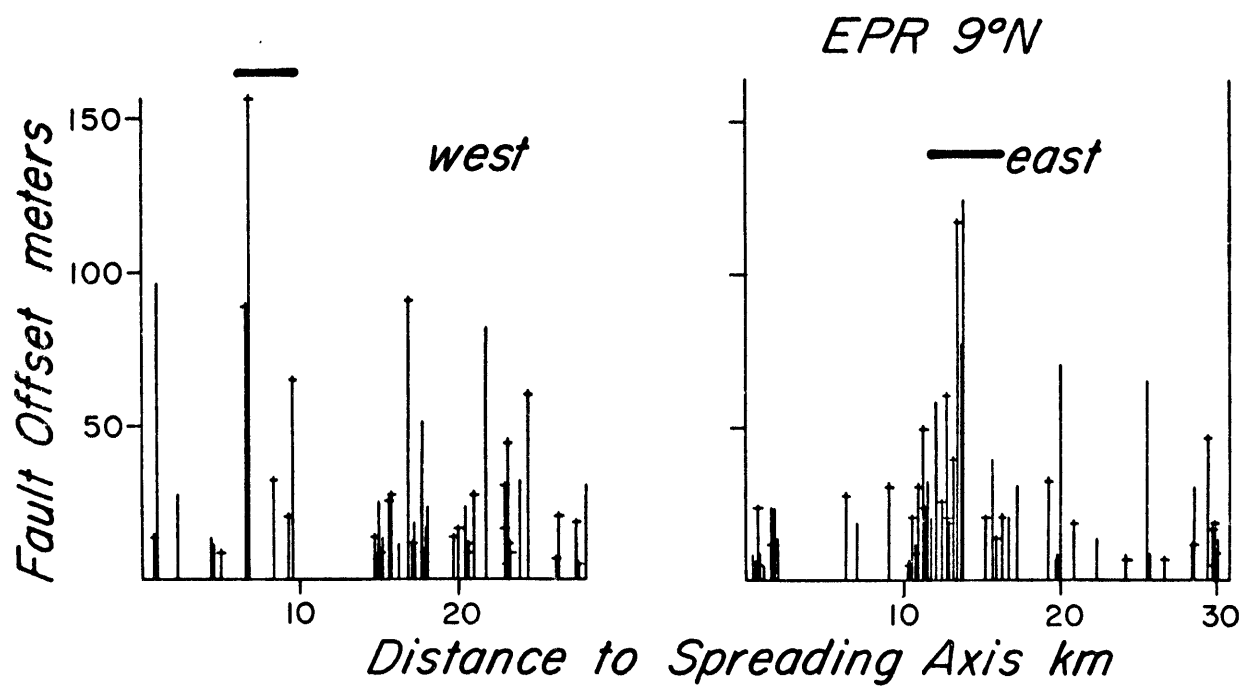
### Distribution of Tectonic Relief

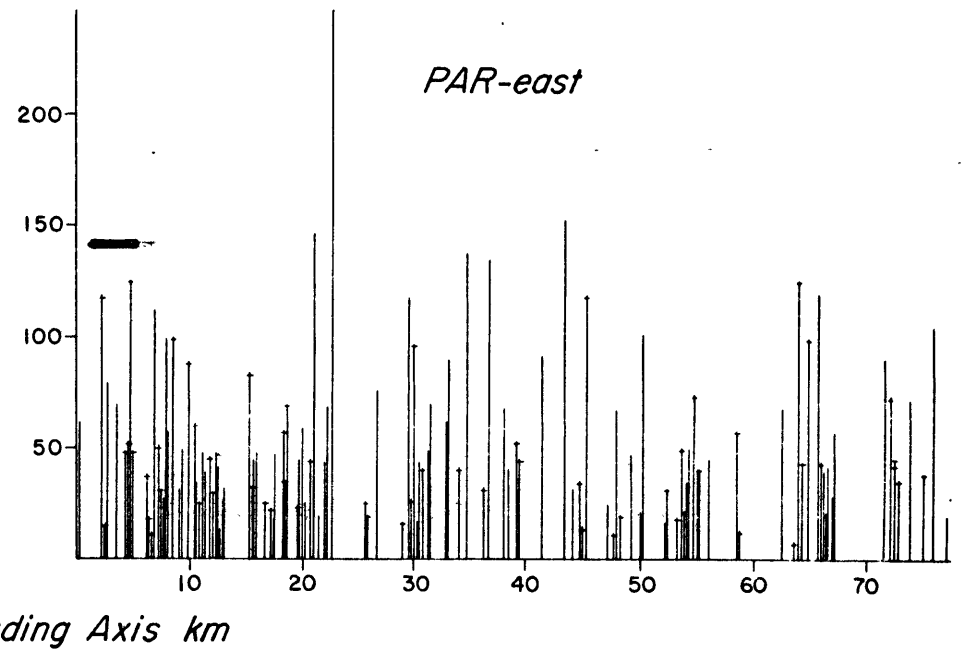
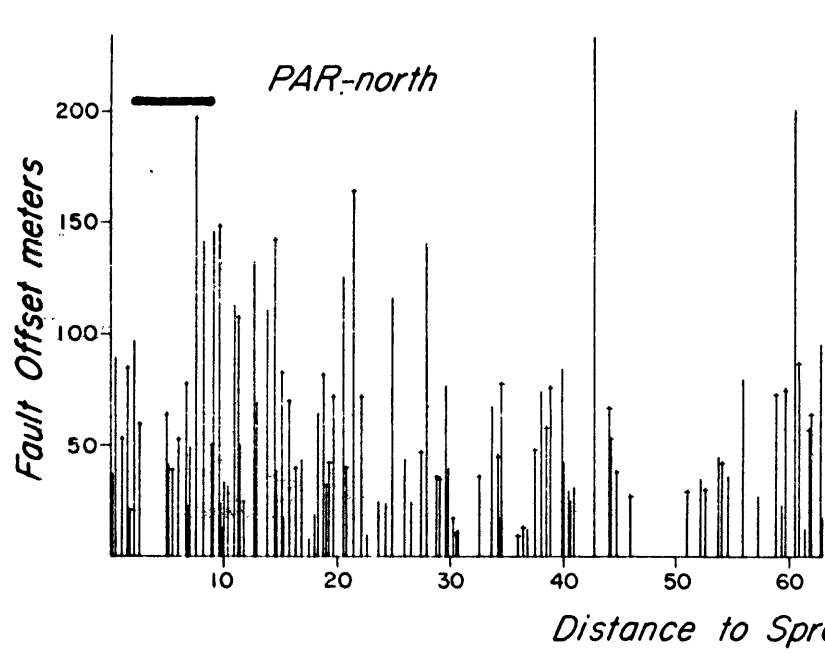
New ocean floor created within the central volcanic zones has little relief. Most of the mature sea-floor relief is acquired tectonically as the sea-floor migrates away from the spreading axes. The tabulation of fault throws and the examination of deep tow profiles show tectonic relief increases on the flank of the central low relief zones. The increase in the tectonic relief is commonly quite abrupt such as at the edge of the median valley floors at the slow and intermediate rate spreading centers. Large horst and graben relief also appears dramatically at the base of the central highs at the fast spreading EPR 9°N and 3°S. The width of the central low relief zone has been postulated to equal the width of the underlying magma chamber (Bryan and Moore, 1977; Lonsdale, 1977a). To see if this width is a function of spreading rate, the range of values for each spreading center is shown in Figure 9.

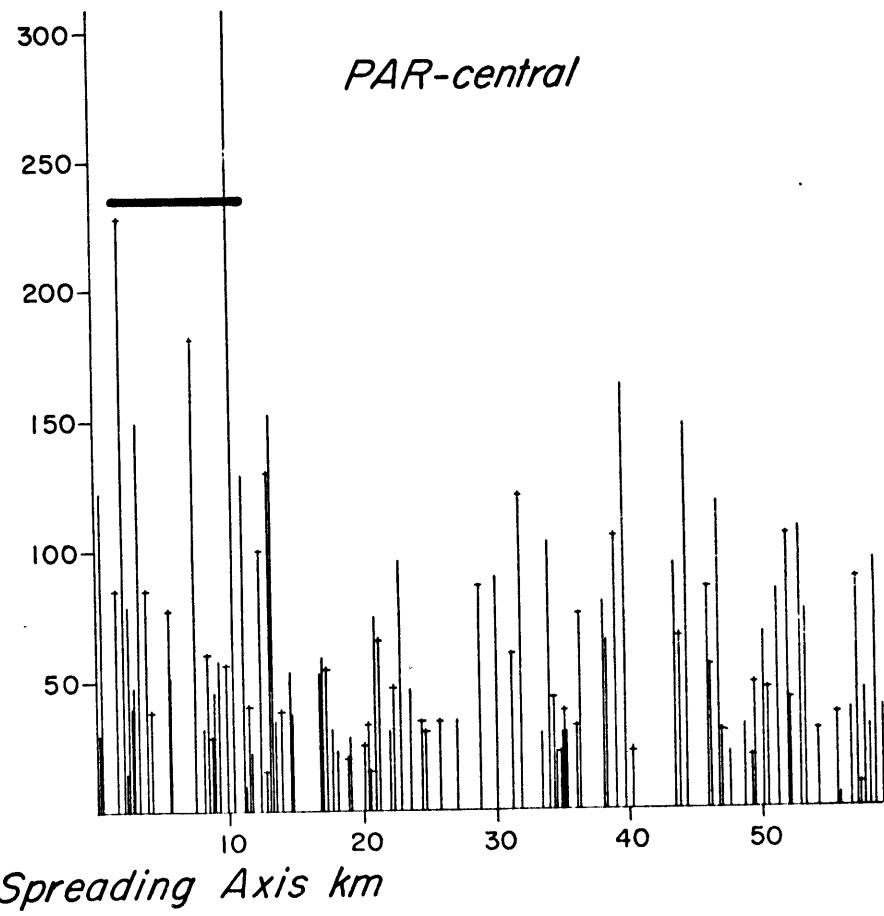
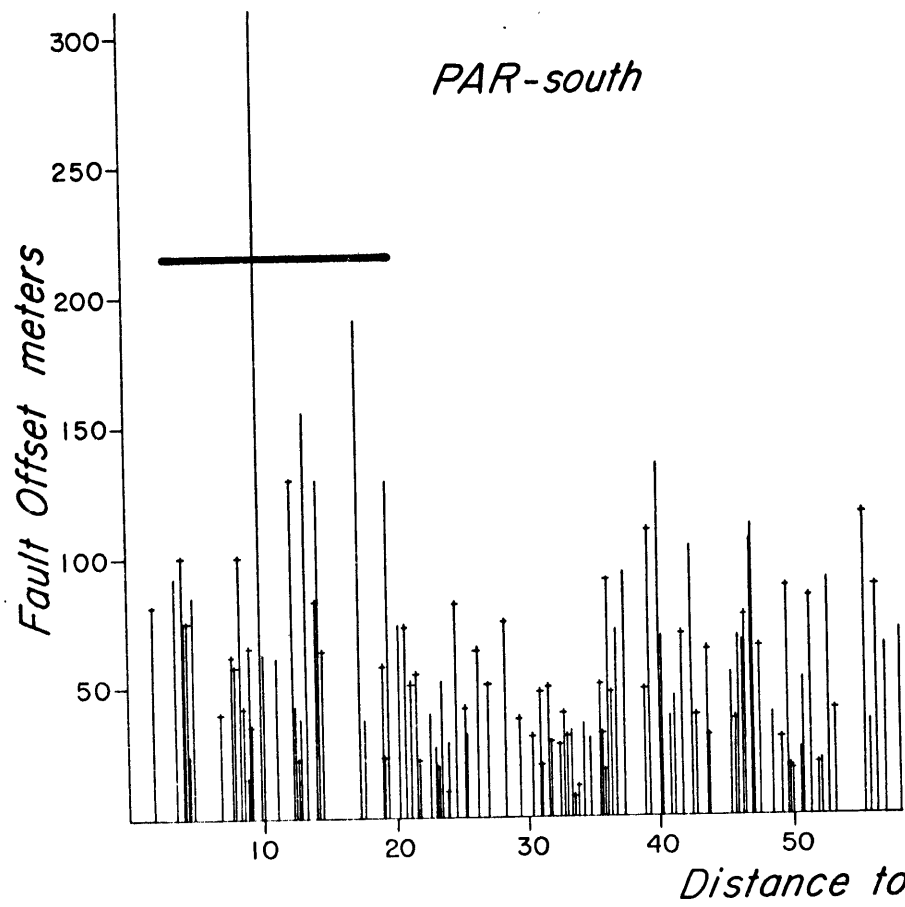


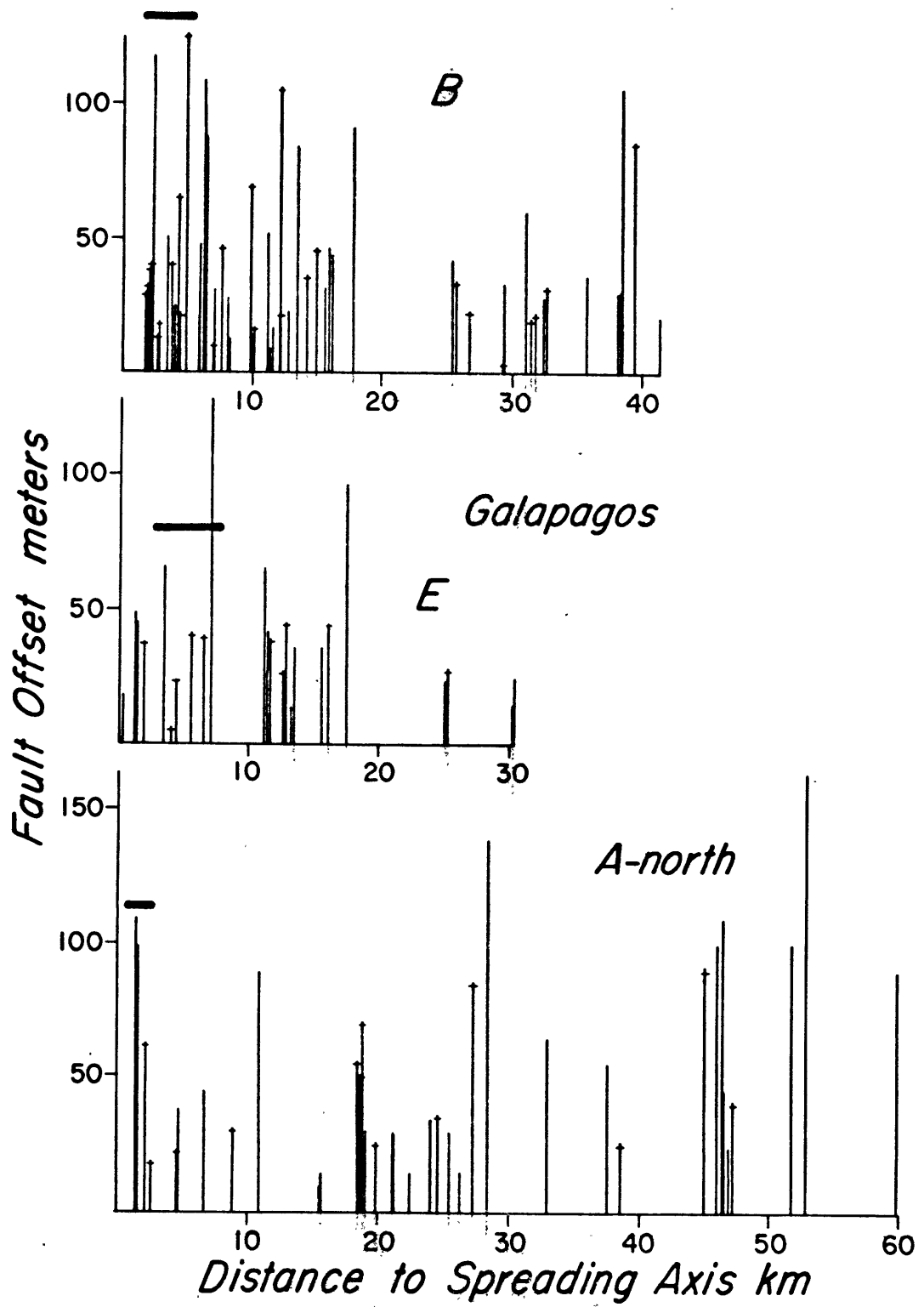
Figure 8: Fault throws across individual fault scarps versus distance to spreading axes. Crosses indicate outward facing faults. Bars show estimates of the plate boundary half-widths based on the increase in fault throws going away from the spreading axes. The plate boundary half-widths are also shown by the horizontal bars above the bathymetric profiles in Figure 4.











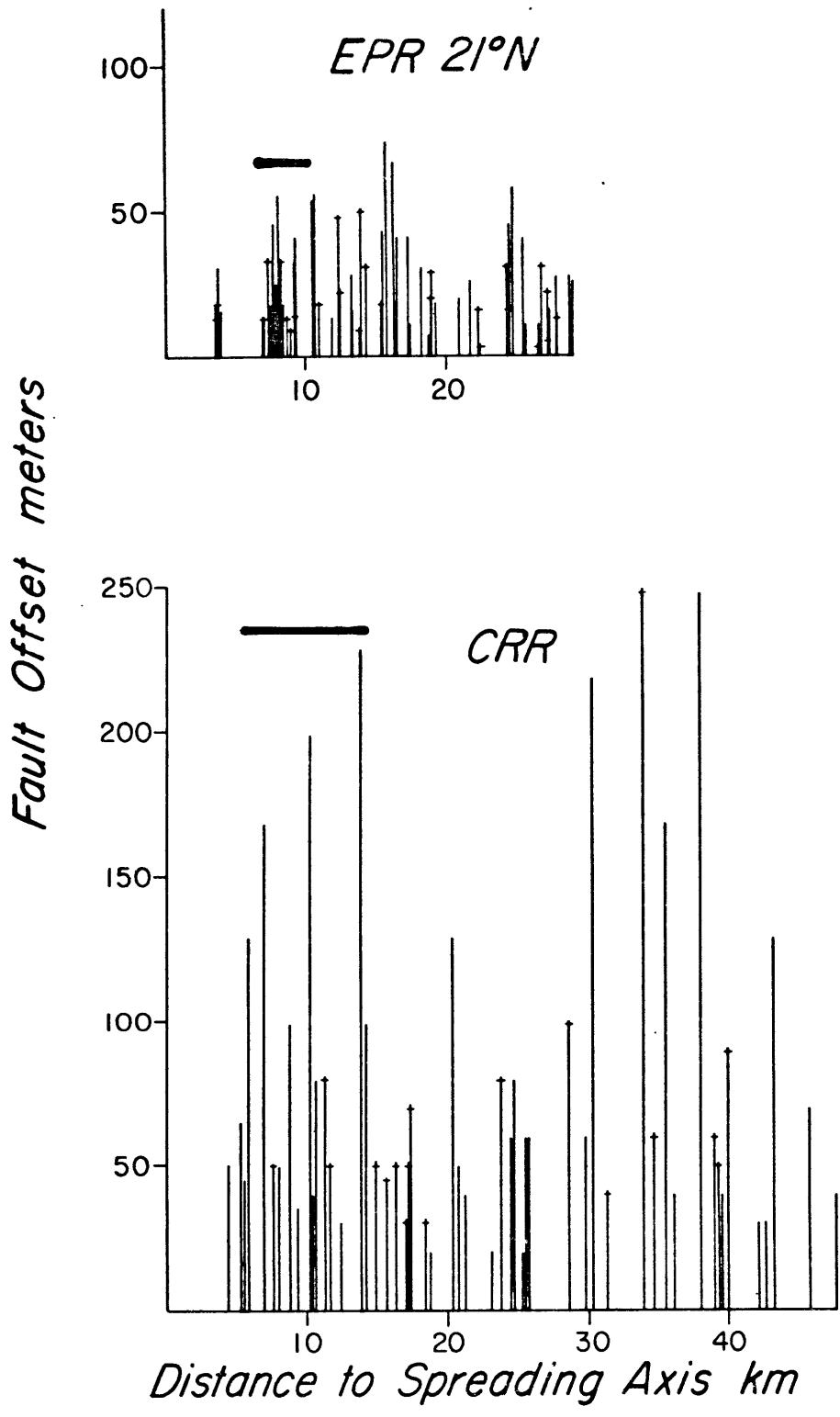
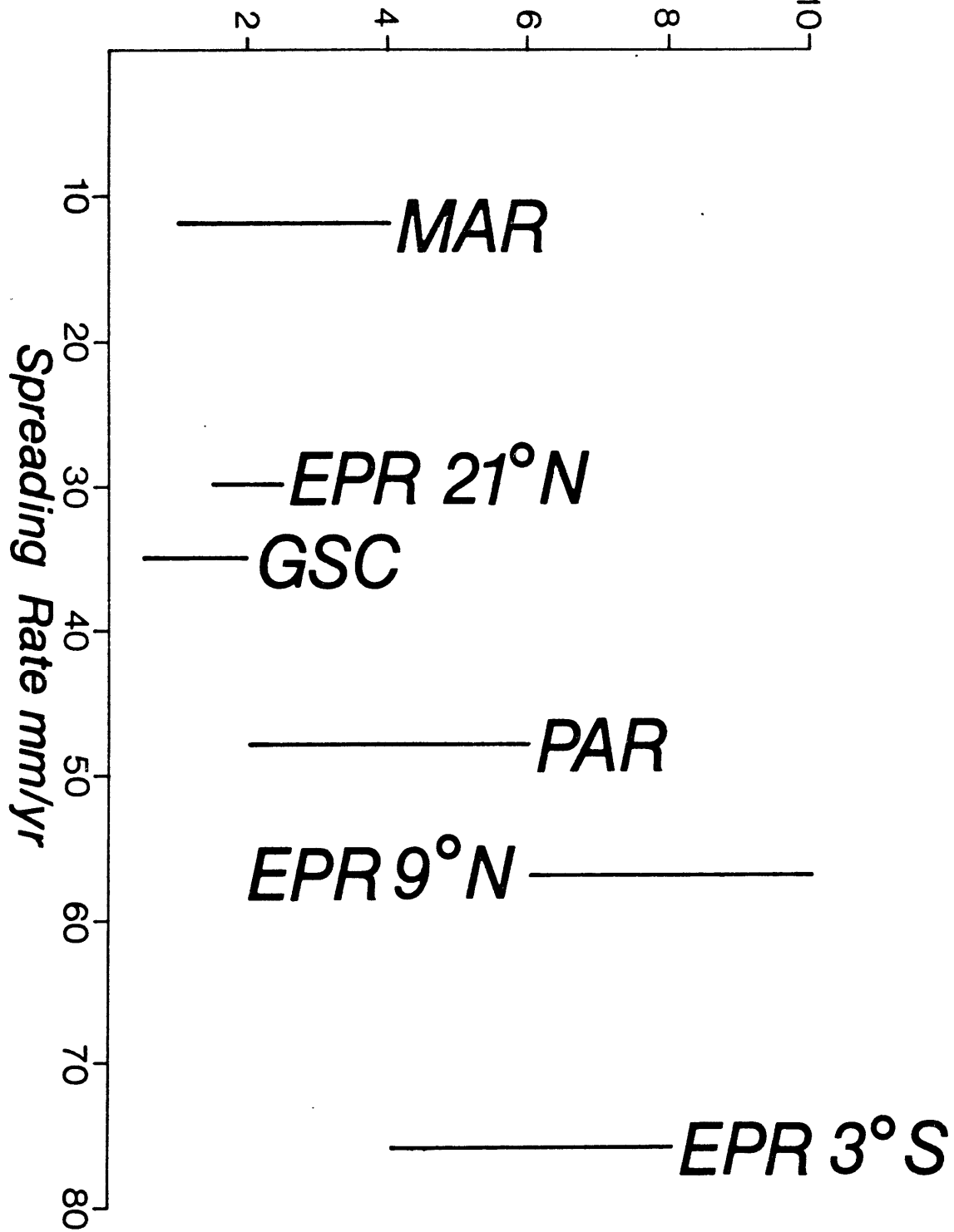


Figure 9: Half-widths of the central low relief zone  
versus spreading rate.



Half-Width of Central Low-Relief Zone km



Luyendyk and Macdonald (1976) have termed the zone of active tectonism at divergent plate boundaries as the plate boundary zone. The width of the central low relief zone thus must be a minimum estimate of the plate boundary zone. The tabulation of fault throws shows that the tectonic relief does not continue to grow indefinitely. The fault throws reach some ambient value fluctuating about some mean. In some of the profiles, the fault throws seem to decrease with distance from the spreading axes. Some of this decrease is accountable by the increasing sediment cover in older sea-floor. While it is clear where tectonic relief formation first becomes important, it is not clear where tectonic relief formation ceases. The concentration of earthquakes close to the plate boundaries in the ocean basins and the preservation of magnetic anomalies suggest little tectonic deformation occurs in oceanic plate interiors.

One possible estimate of the width of the plate boundary zone is the distance from the spreading axis at which the fault throws reach the ambient size. At this distance, the relief of mature sea-floor is reached and there is no reason to postulate continued tectonic relief formation. It is difficult to determine precisely where sea-floor relief reaches the mature roughness due to the many fluctuations in the size of relief even in mature sea-floor. It is quite likely that the plate boundary zone is variable to some extent in time and space. However, a rough estimate of where the fault

growth ceases is possible by examining the throw of faults versus distance from the spreading axes as well as considering the deep tow profiles themselves. The horizontal bars in Figure 8 and the bars above the profiles in Figure 4 show the estimates of the plate boundary half-widths determined in this way.

#### Maintenance of Median Rift Relief

As exemplified by the Gorda Rise and the MAR at  $37^{\circ}\text{N}$ , most slow spreading centers have deep median rifts. For their median rifts to be steady state features, there must be some process by which the upward climbing staircase topography of the rift walls is eliminated as sea-floor migrates out of the median rifts. Though there is some debate as to the mechanism by which the rift valley relief is removed in the rift mountains, there needs to be some form of tectonic deformation in the rift mountains regardless of the mechanism (Osmaston, 1970; Harrison, 1974; Harrison and Stieltjes, 1977; Macdonald and Atwater, 1978). Therefore, the plate boundary zone should be approximated by the distance to the rift mountains at deeply rifted mid-ocean ridges.

Contour maps of the MAR in the FAMOUS area show the peak to peak distance between the rift mountain tops is quite variable from 25-80 km (Ramberg et al, 1977). Figure 4 shows the shallowest point in the rift mountains to be about 60 km from the spreading axis on the east flank of MAR but only about 15 km on the west flank. If the rift relief is constant

over time, then the local plate boundary half-widths are between 15 and 60 km. The very large distance to the rift mountain top on the east flank gives a plate boundary width which is much greater than the other estimates. The nearly universal presence of rift valleys at slow spreading centers suggests they are steady state features, but it seems clear that the shorter wavelength topography is not and constitute a sort of superimposed "noise" for the half-width estimates. It is likely that the rift mountains on the east flank of the MAR in the FAMOUS area are not steady state features. The location where the sea-floor topography first stops climbing upwards and the first large outward facing relief is present on the east flank is at 24 km from the spreading axis (Figure 4, MAR profile). The more likely plate boundary half-width there is thus 24 km.

Comparison of topography due to inward facing faults and the total topography using long range side-scan sonar data from the MAR near 40°N shows that most of the bathymetry can be explained by inward facing faults created at the inner median valley walls out to 15 to 20 km from the spreading axis (Searle and Laughton, 1977). Beyond 15 to 20 km, some other relief modifying process is required because the bathymetry contains more relief than attributable to the inward facing faults. Thus, tectonic activity must be present at 15 to 20 km from the spreading axis. At the Gorda Rise, the ocean floor created at the last spreading rate change is only now

in the rift mountain tops. It may be that the rift valley will continue to widen and a plate boundary width estimated from the present median rift configuration is not representative of the present spreading rate. Figure 10 shows estimates of the plate boundary half-widths based on the distribution of tectonic relief at spreading centers and the distance to the rift mountains from deep tow profiles. The plate boundary half-widths can also be expressed in terms of the age of the lithosphere to which tectonism is active (Figure 11).

#### Other Estimates of the Plate Boundary Width

The plate boundary widths determined here can be compared with those by other workers. Lonsdale (1977a) and Lonsdale and Spiess (1979) estimated the plate boundary half-widths to be at least 20 km at EPR 3°S, 6 to 10 km at EPR 9°N, and at least 25 km at the MAR. Lonsdale (1977a) estimated the half-widths to be only 2 to 3 km at GSC but Klitgord and Mudie (1974) favor the collapse of faults and estimated the half-width to be 5 to 11 km. At EPR 21°N, Normark (1976) noted that fault scarps comparable to that of typical abyssal hills are found only at distances of 10 km or more from the spreading axis. Thus, the plate boundary half-width must be at least 10 km.

### 1.6 Reverse Faulting

#### Bathymetric Data

The increase in tectonic relief away from spreading axes

Figure 10: Estimated plate boundary zone half-widths  
versus spreading rate.

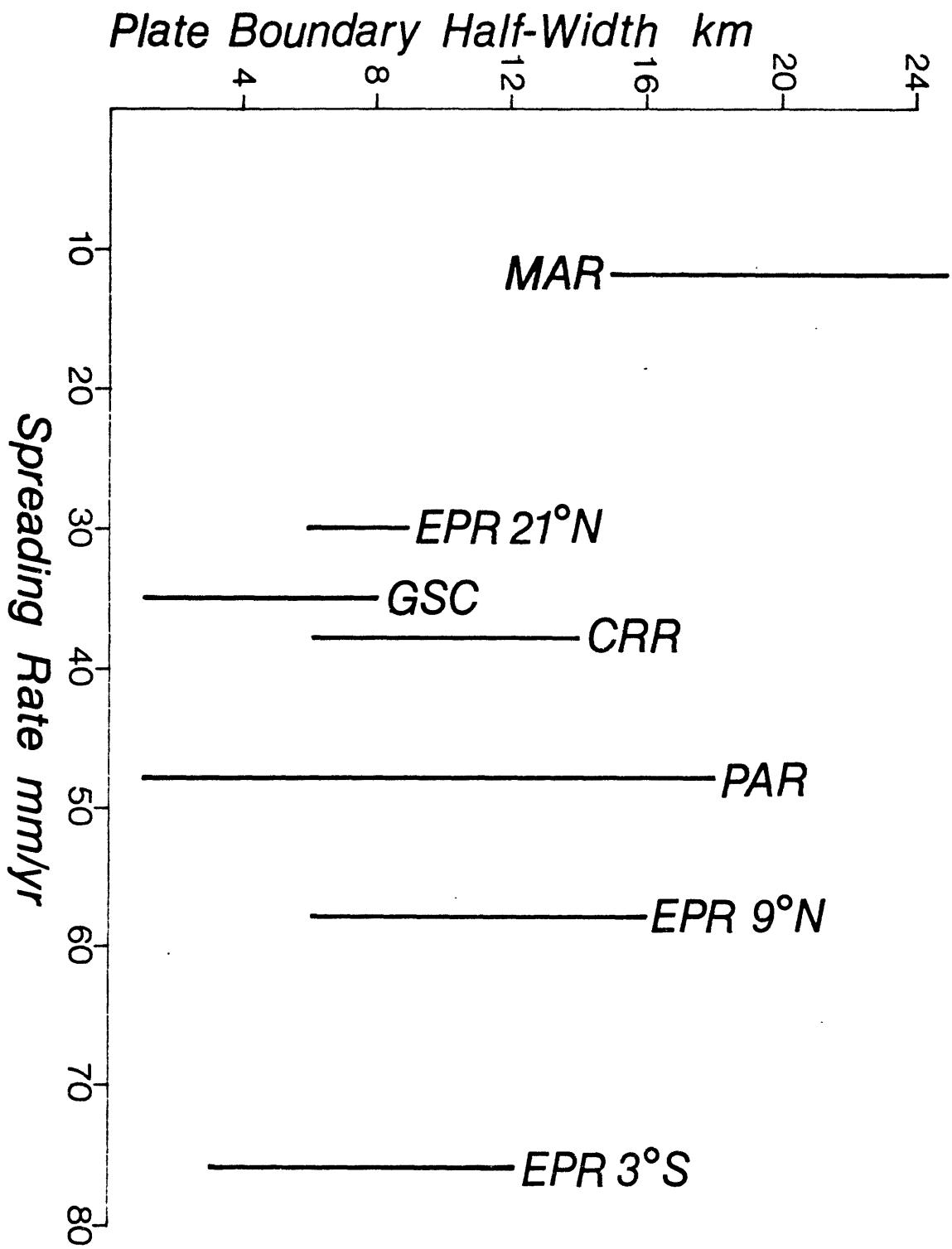
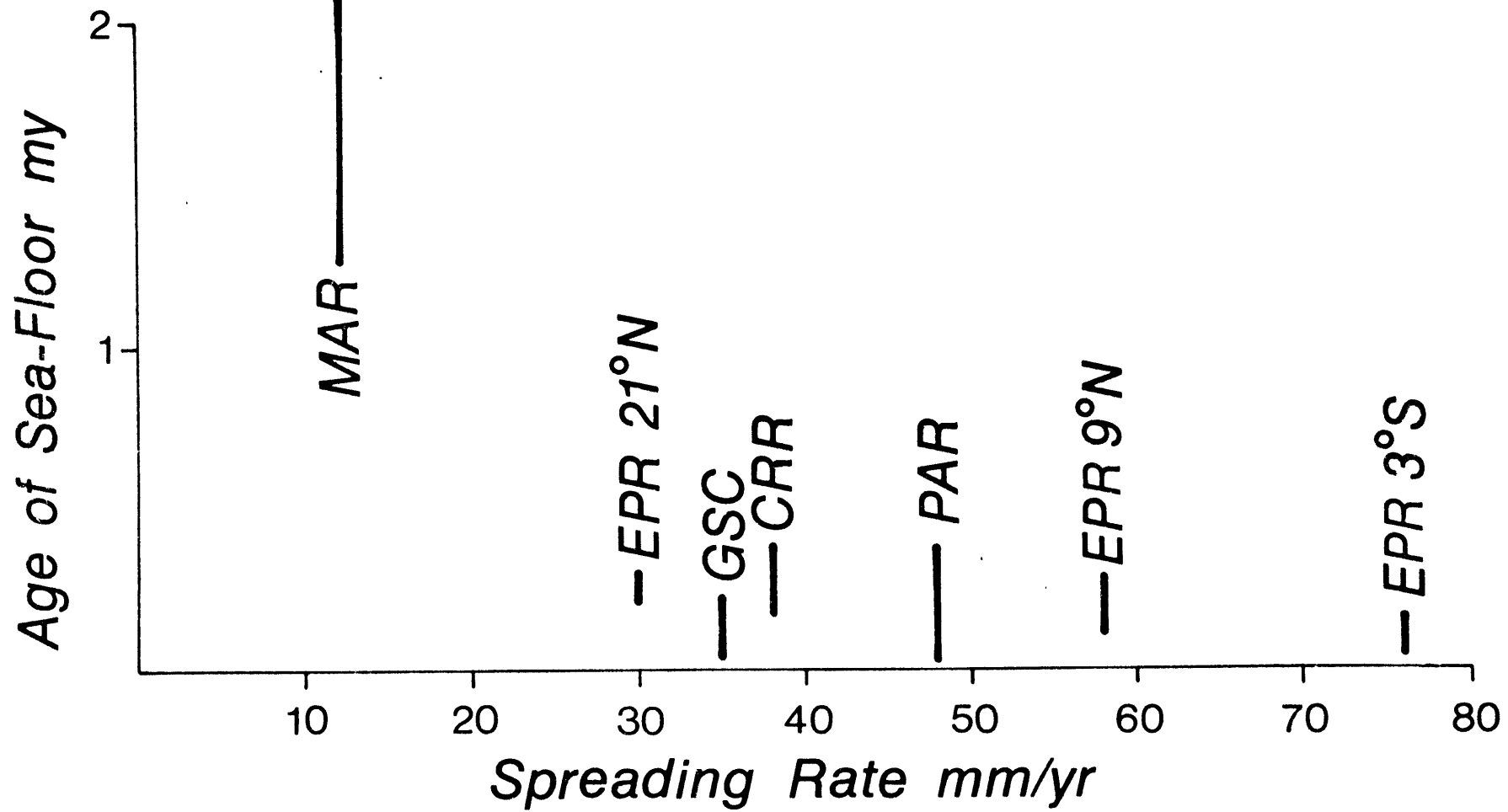


Figure 11: Estimated plate boundary half-widths in terms of the age of the sea-floor to which tectonism is active.





shows tectonism must be active at spreading centers. The width of the zone over which tectonism is active was estimated by looking for the distance at which the tectonic relief reaches the density similar to that of mature ocean floor well away from spreading axes. However, there is the possibility that significant tectonic activity in the form of reverse faulting may occur outside of the zone of increasing tectonic relief. Because reverse faulting can reduce relief, the zone over which tectonism is important may be significantly wider than the zone of increasing tectonic relief.

In contrast to normal faulting and tilting of the sea-floor, reverse faulting (and reverse tilting) can leave no evidence of its activity in bathymetric profiles since it can cancel offset on previously existing normal faults. Earthquake fault plane solutions or visual observation of geological cross sections that cut across fault traces may unambiguously document the occurrence of reverse faults. However, bathymetric profiles can only confirm the occurrence of positive relief creation processes. Reverse faults that have positive relief could easily be eroded to resemble normal faults. Thus, some other constraint is needed to determine the importance of reverse faulting. Macdonald and Atwater (1978) pointed out that of the available evidence, 1) the many normal fault plane solutions of mid-ocean ridge earthquakes, 2) the pervasive fissuring of the sea-floor, 3) the confirmed normal faults from detailed surveys, and

4) the active volcanic extrusion, all suggest extensional stresses at spreading centers. This is contrary to the compressive stresses that are associated with reverse faults.

The bathymetric data alone cannot prove or disprove the occurrence of reverse faults. Though there are good reasons why evidence for reverse faults may be difficult to find, the available evidence only suggest tensional stresses at spreading centers. The circumstantial evidence suggests that if reverse faulting occurs, it occurs only rarely close to spreading axes. Therefore, the distance at which the sea-floor first achieves the relief typical of mature sea-floor at large distances from the spreading axes is a reasonable measure of the plate boundary width.

#### 1.7 Elimination of Median Rift and Central Horst Relief Median Rifts as Steady State Features

At intermediate rate and fast spreading centers the relief formation process through faulting can be easily visualized. Horizontal extension on the flanks of the central high forms horst and graben relief at the fast spreading centers, perhaps in the manner described in detail by Lonsdale (1977a). Increasing offset along pre-existing fissures grows to form the walls of grabens and horsts. At intermediate rate spreading centers, fault scarp growth coincident with the tilting or warping of fault blocks can produce the characteristic tilted fault block relief.

In contrast, the relief formation process is more complex at deeply rifted spreading centers because of the necessity of maintaining the median rift relief.

#### Elimination of Median Rift Relief

There is some argument as to whether it is the addition of outward facing faults, the tilting or warping of fault blocks, or the addition of reverse faults that eliminates the rift relief in the rift mountains. The alternatives have been discussed in detail by Harrison and Stieltjes (1977) and Macdonald and Atwater (1978). Recent non-transponder navigated submersible surveys along the back-slopes of two fault blocks in the rift mountains in the FAMOUS area found the back-slopes to be steeply dipping slopes rather than outward facing fault scarps (Atwater et al, 1978).

Reinterpretation of the MAR deep tow profiles shown in Figure 3 suggests that though some of the large outward facing slopes are fault scarps (e.g. box g in profile e, the fault block at about 22 km from the spreading axis in profile b of Figure 3), most of the large outward facing slopes are tilted or warped back-slopes of fault blocks. The deep tow profiles of the Gorda Rise suggest the rift mountains are composed of tilted fault blocks. However, whether the morphology of the Gorda Rise has reached a steady state configuration is not known. The tentative conclusion is that tilting and warping of fault blocks play the dominant part in the elimination of rift relief at the MAR though the addition of outward facing

faults is also important. Reverse faulting may occur, but no definitive evidence is available.

#### Elimination of Median Horst Relief

EPR 9°N is similar to deeply rifted mid-ocean ridges in that its central high has greater relief than the surrounding mature sea-floor (Lonsdale and Spiess, 1979). In contrast to the central high at EPR 3°S which is a shield volcano, the central high at EPR 9°N has large outward facing faults composing its shoulders. For the central horst to be a steady state feature, the horst relief must be removed at the base of the large outward facing faults as the sea-floor migrates away from the spreading axis. This can be accomplished by reverse faulting or inward tilting of the sea-floor at the base of the large outward facing faults. Lonsdale and Spiess (1979) have discussed the necessity of intense reverse faulting involving shear slices perhaps only hundreds of meters wide at the base of the shoulders if the central horst is a steady state feature. The alternative of a non-steady state central horst at EPR 9°N without the necessity of large scale reverse faulting and intense shearing of the crust appears to be more plausible.

### 1.8 Roughness of the Sea-Floor Relief

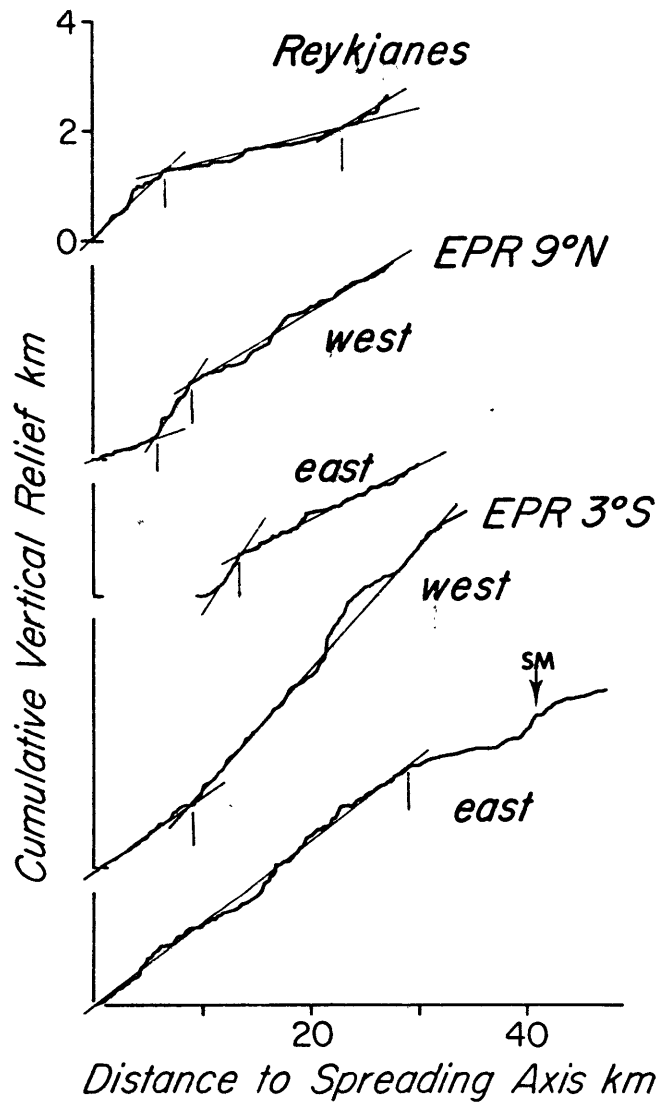
#### Quantitative Measure of Roughness

The roughness of sea-floor relief has been noted to be related to the spreading rate at which the sea-floor is

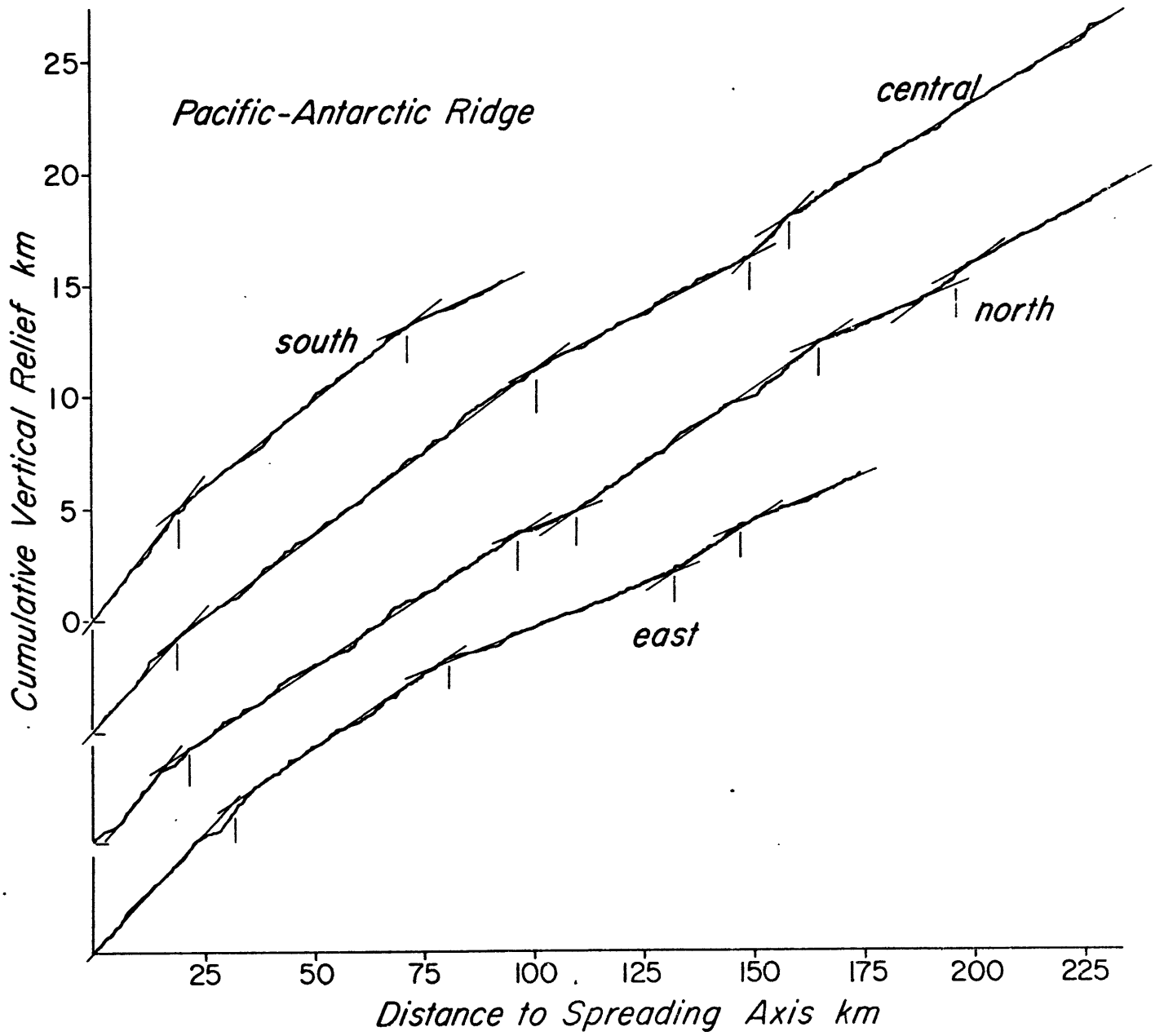
created (Menard, 1967; Anderson and Noltimier, 1973; Molnar et al, 1975). But in order to compare the relief of the sea-floor at different mid-ocean ridges, some quantitative measure of the roughness of sea-floor relief needs to be defined. The roughness of sea-floor relief can be defined as the amount of vertical change in depth per unit of horizontal distance in profiles projected onto the spreading direction. The roughness so defined is also the absolute value of the first derivative of the bathymetry or the slope of the sea-floor.

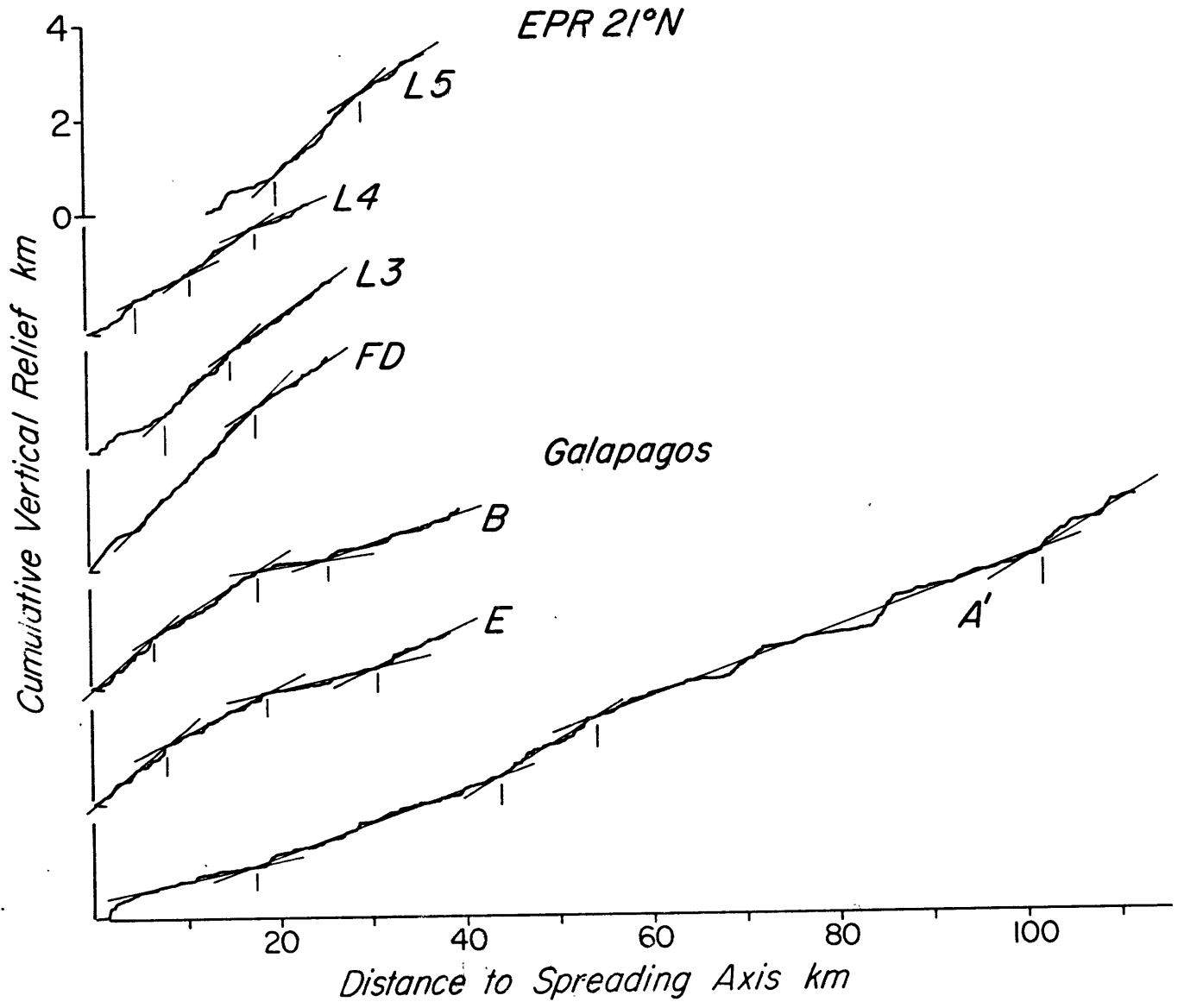
The cumulative vertical relief for 21 of the longer deep tow profiles shown in Figure 4 was calculated to look for the relationship between roughness of sea-floor relief and spreading rate. The cumulative vertical relief was calculated by summing the absolute value of the difference in depth between successive interpolated depth points. The depth points were interpolated at even 50 m intervals on profiles that have been projected onto the spreading directions. The interpolation was carried out to minimize the effect of the difference in resolution between the old and new profiling systems. The slope of the cumulative relief curves is the roughness as defined (Figure 12). The cumulative vertical relief curves were divided into 5 km segments and the slope for each segment measured. The roughness calculated from the 5 km segments is shown in Figure 13. These 5 km values were averaged and plotted

Figure 12: Cumulative vertical relief plotted as a function of distance to spreading axes. Straight lines superimposed on the cumulative vertical relief curves show zones of similar roughness. Vertical bars under the curves show the location of changes in the slopes of the fitted lines. The vertical bars match those in Figure 4. These curves have the best fitting depth versus square root of age subsidence rates removed. However, the general shape of the curves are the same without the removal of the subsidence curves. The curves are labelled as in Figure 4.









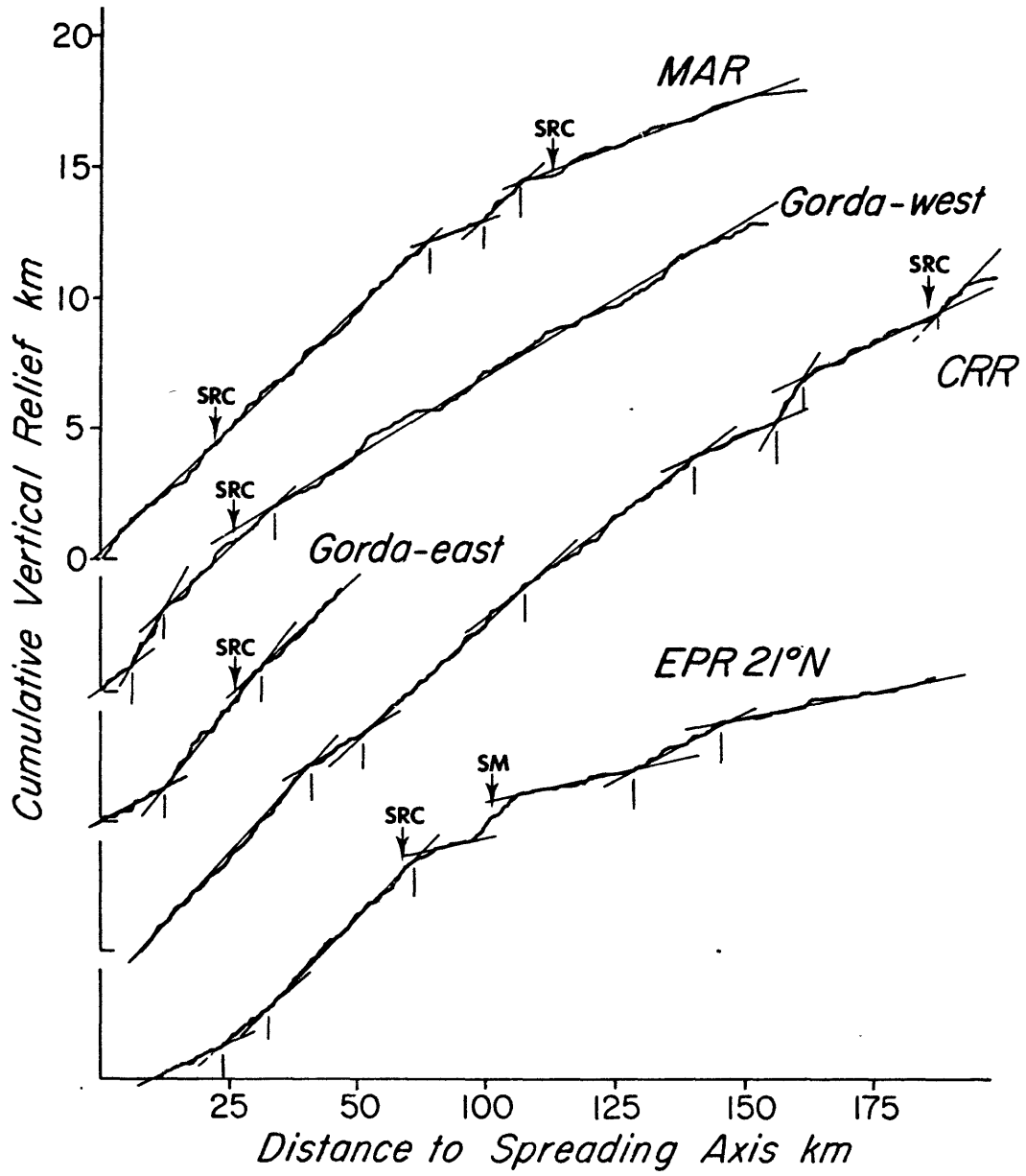
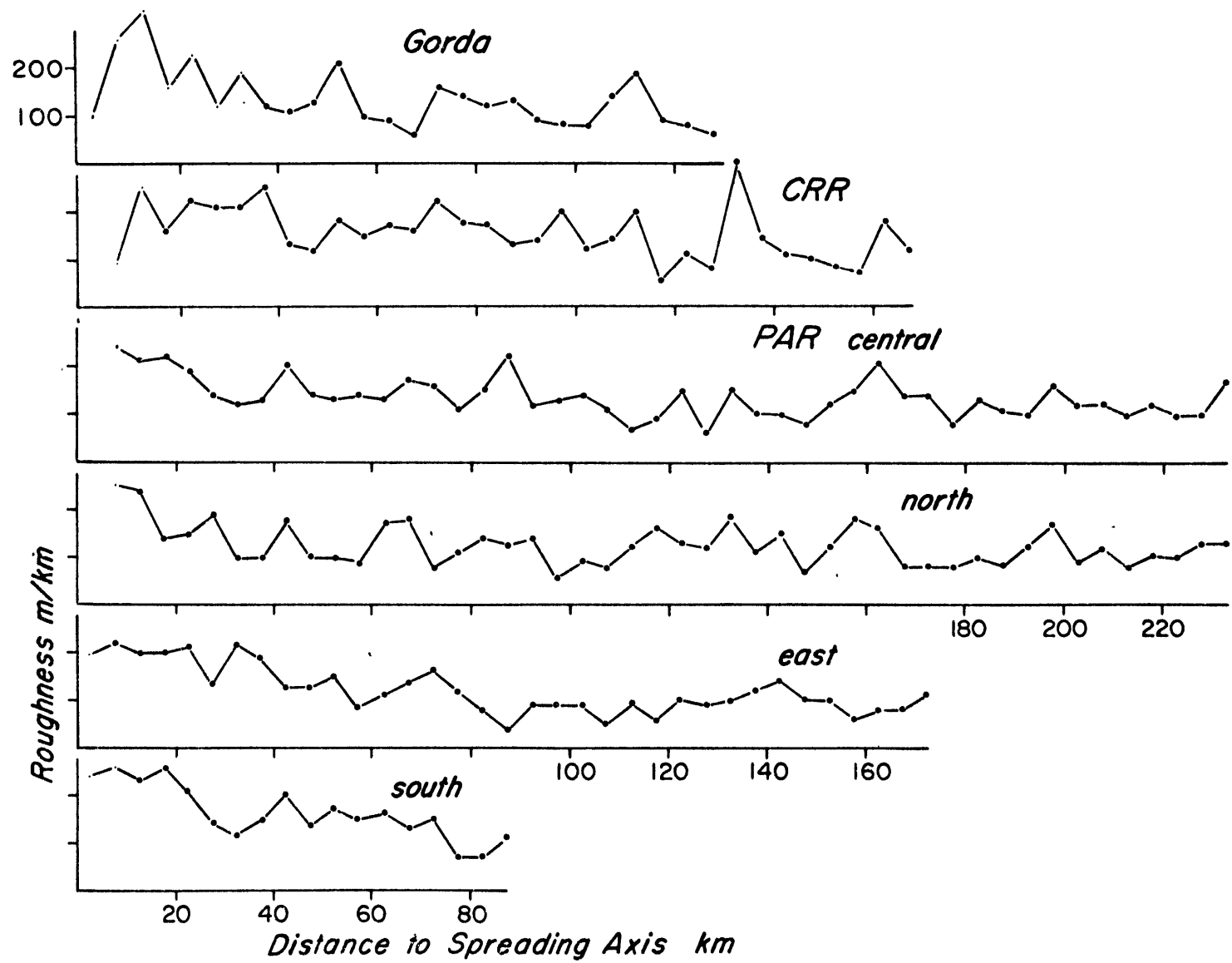
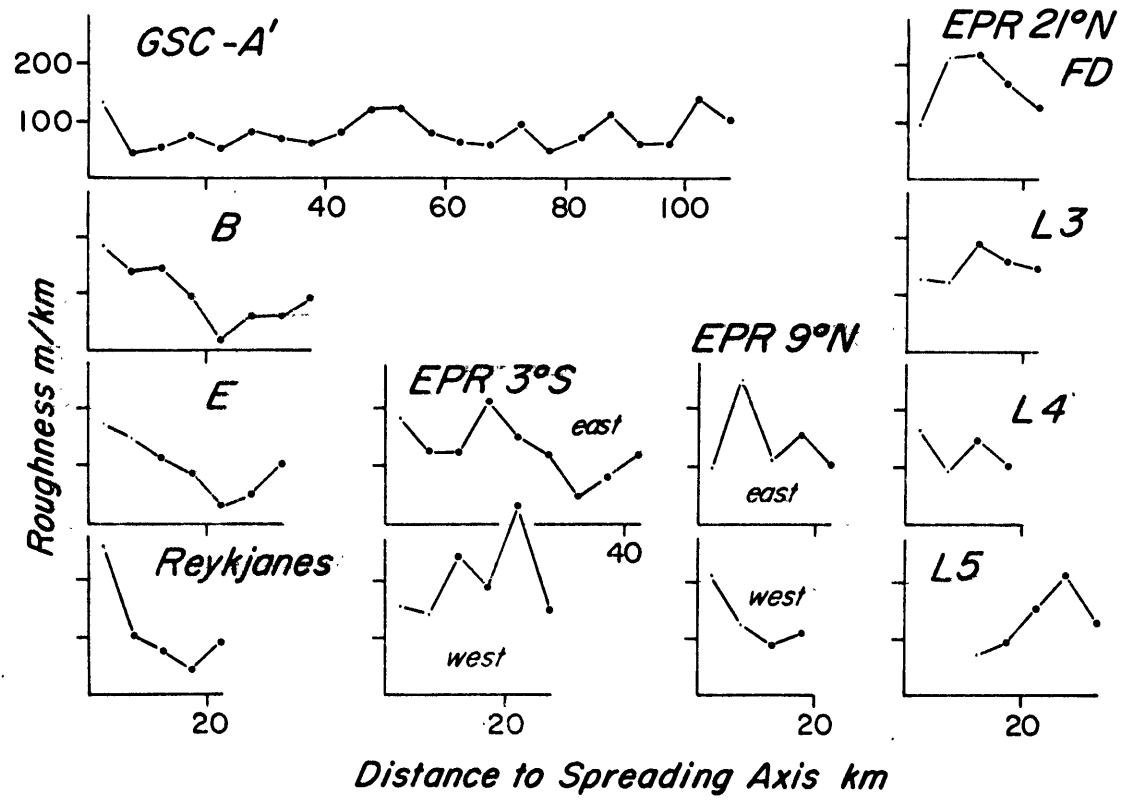


Figure 13: Five kilometer averages of the roughness of relief measured from the cumulative vertical relief curves. The larger dots show the values from areas outside of the plate boundary zones.





against spreading rate in Figure 14. The vertical bars in Figure 14 span one standard deviation on either side of the 5 km means.

#### Relief Reduction Due to Sedimentation

There is a definite trend of decreasing roughness with increasing distance from the spreading axes in the PAR, CRR, and Gorda profiles. The gradual decrease in roughness can be attributed to increasing sediment cover with distance from the spreading axes. Even where the 4 kHz sediment penetration sonar data were used, the lower resolution of the penetration system versus the profiling system will yield lower roughness estimates with increasing sediment thickness. To estimate the relief reduction due to sedimentation, straight lines were fitted to the roughness versus distance curves for the PAR, CRR, and Gorda profiles (Figure 13). The fitted lines give rates of relief reduction between 10 and 85 m/km/my. These rates lower the average roughness of the profiles by 52, 52, and 58 m/km respectively. Close to the spreading axes, the sea-floor may still be undergoing relief modification by tectonism. This is especially troublesome for short profiles where a significant percentage of the profiles is within the tectonically active zone. Better estimates of the sea-floor roughness can be calculated by taking into account the effect of sedimentation and excluding the plate boundary zone whose widths were estimated earlier. The corrected sea-floor roughness estimates are shown by stars in

Figure 14: Roughness of sea-floor relief plotted against spreading rate. The circles show the values calculated using the deep tow profiles shown in Figure 4. The stars show the results when the portions of the profiles within the plate boundary zones are excluded and relief reduction due to sedimentation is accounted for. The vertical bars span one standard deviation on either sides of the means of the unedited data. The values for MAR were calculated using profiles i,j,b,g, and e shown in Figure 3. Horizontal line shows the linear least square fit between roughness calculated using the edited data versus spreading rate.



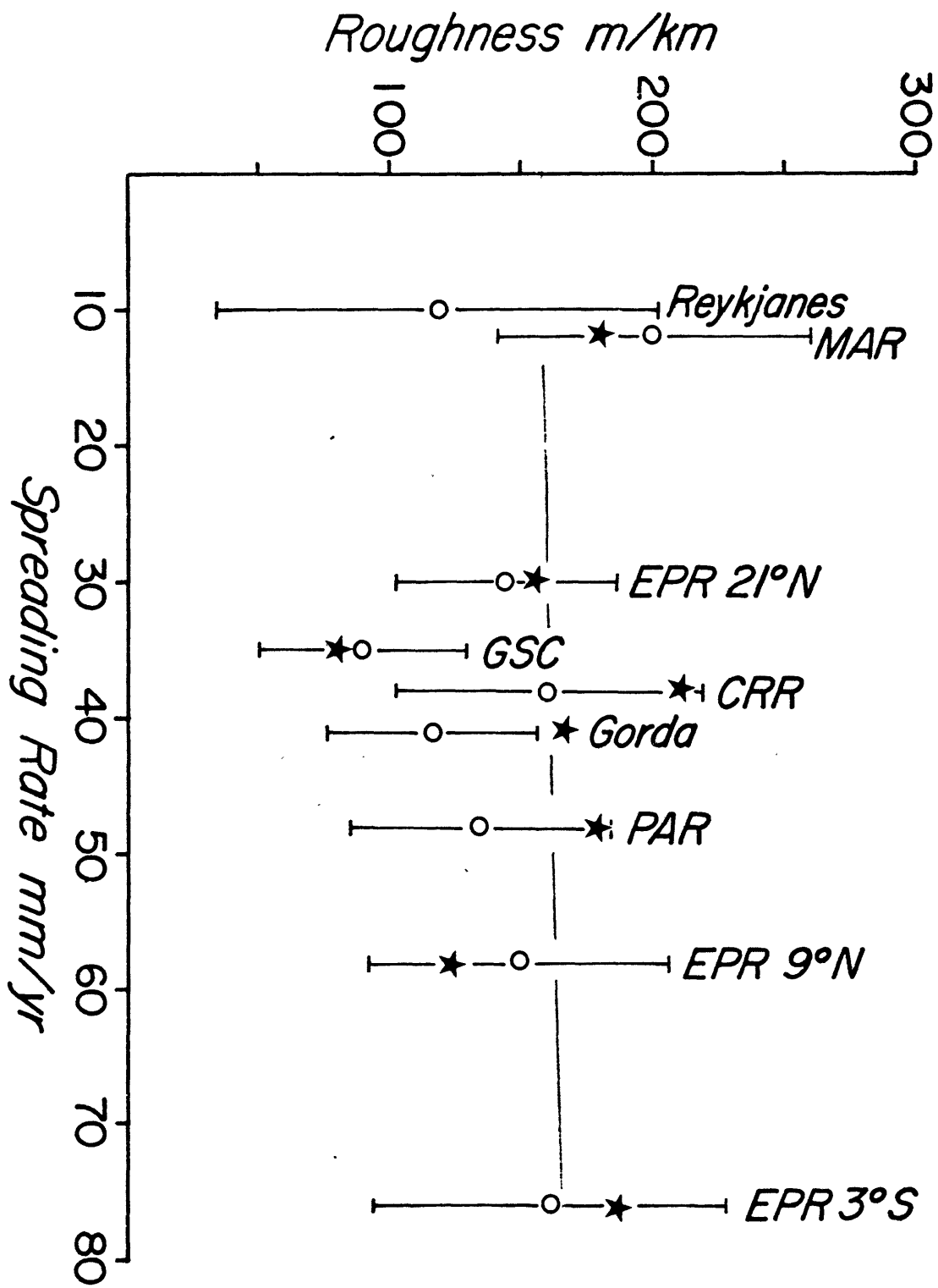


Figure 14.

Wavelength and Amplitude of Relief

Only three ridge crests that have been associated with hotspots, the Reykjanes, the GSC, and possibly the EPR at 9°N (Vogt, 1971; 1974; Anderson et al, 1975) stand out in having lower roughness than the others in Figure 14. With the exception of these three spreading centers, the roughness of sea-floor relief appears to be quite independent of the spreading rate at which the relief is created. The best fit linear relationship between sea-floor roughness and spreading rate has a slope of only 0.11 m/km/mm/yr. The expected range in roughness is less than 10 m/km for spreading rates from 0 mm/yr to 80 mm/yr. These results contradict the common observation based on surface ship profiling records that the roughness of sea-floor relief is inversely related to the spreading rate (Menard, 1967; Anderson and Noltimier, 1973).

A possible explanation of this contradiction is that fast spreading centers create more short wavelength/small amplitude relief compared to slow spreading centers. Typical surface ship profiling systems cannot resolve the short wavelength/small amplitude relief resulting in the apparent lower relief for sea-floor created at faster spreading rates. Typical surface ship profiling systems have a beam width of about 30° and insonify an area 1.3 km in diameter in water 2.5 km deep. The newer deep tow profiling system has a 6° beam width (Lonsdale, 1977a) and the instrument package is

typically towed at less than 100 m above the sea-floor.

The area the deep tow profiling system insonifies is less than 10 m in diameter.

To test the possibility that small amplitude/short wavelength relief resolution is the reason sea-floor created at fast spreading centers has apparent lower relief, the relief that would be seen by a surface ship profiling system with a  $30^\circ$  beam width was calculated using the MAR, EPR  $21^\circ\text{N}$ , GSC, PAR-east, PAR-north, and EPR  $3^\circ\text{S}$  deep tow profiles. The closest point on the sea-floor to an imaginary ship with a  $30^\circ$  wide downward looking sonar was taken to be the apparent depth recorded by the profiling system. The cumulative vertical relief was calculated using a sampling interval of 3.66 km, equivalent to digitizing a profiling record at 10 min intervals for a ship travelling at 12 knots. The results show the roughness of relief would be attenuated by a factor of 8.5 for the EPR  $3^\circ\text{S}$  profile, 5.5 for PAR, 3.0 for GSC, but only 2.9 for the MAR profile. It is thus quite plausible that the lower roughness seen by surface ship profiling systems at fast spreading centers is a function of resolving power.

## 1.9 Power Spectra of Deep Tow Profiles

### Estimates of Power Spectra

The power spectra of selected deep tow profiles were calculated to investigate possible variations in the

wavelength of relief with spreading rate. The digitized profiles were projected onto the spreading directions and sampled at even 50 m intervals. Due to the limited length of the profiles available, the spectral analysis was limited to wavelengths up to 20 km. For spreading centers where longer profiles are available, the longer profiles were broken into 20 km segments and the spectrum for each segment separately evaluated and then averaged. Trends for each 20 km segment were removed by least squares. The profiles were tapered and the number of points in the resulting time series were padded to a power of two before the spectra were calculated. The averaged spectra were smoothed using a 27 point triangular filter.

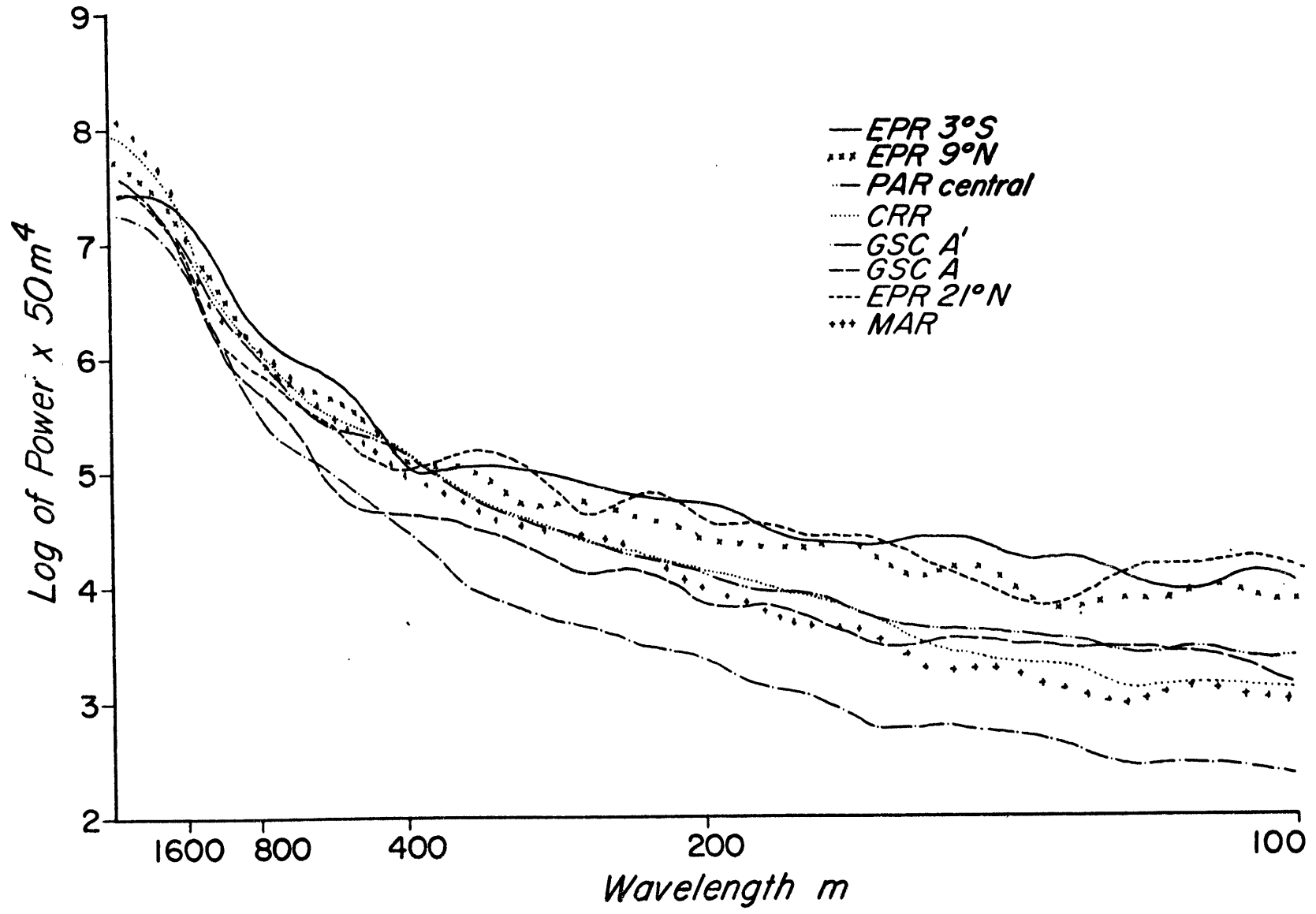
A large part of the EPR 3<sup>0</sup>S profiles shown in Figure 4 contains the central low relief zone and the off-axis volcanic zone on the east flank. These portions of the profiles are atypical of mature sea-floor created at the spreading center. Thus, the power spectrum for EPR 3<sup>0</sup>S was calculated using only the western profile from 15 to 35 km from the spreading axis. Similar reasoning led to the use of two 20 km segments outside of the axial horst in the EPR 9<sup>0</sup>N profiles. The spreading axes in the EPR 21<sup>0</sup>N and CRR profiles were also omitted. The long profile from MAR shown in Figure 4 was used to calculate the power spectrum. The inner rift valley was not used but the rift terraces and rift mountains were included in the profile used. It is

questionable whether the resulting spectrum is representative of mature sea-floor created at MAR. However, the wavelength of the median valley is much longer than 20 km and thus the calculated spectrum may be valid for relief with wavelengths up to 20 km.

#### Differences in the Spectra of the Spreading Centers

The power spectra of the deep tow profiles have the typical "red" spectrum of sea-floor topography (Bell, 1975; 1979). At the short wavelengths, the spectra can be divided into three groups (Figure 15). The spectra for EPR 21°N, 9°N, and 3°S have the most short wavelength power, those for PAR, GSC-A, and CRR have less, and GSC-A' has the least. The EPR 21°N, 9°N, and 3°S profiles were collected with the new profiling system and all were digitized at inflection points rather than at even time intervals. These three profiles are also the shortest, covering sea-floor of young age and with the least amount of sediment cover. These factors result in profiles with more sharp corners and thus more short wavelength power. At the long wavelengths, the MAR and CRR have the most power. These are also the two spreading centers with the largest median rifts excluding the modern Gorda Rise. The GSC-A' profile stands out in having little power at all wavelengths. It is a longer profile than GSC-A and thus contains a large percentage of older and better sedimented sea-floor. This may in part be the reason why it has less power at shorter wavelengths. The two GSC profiles both,

Figure 15: Power spectra of deep tow profiles.



however, have the least power for wavelengths longer than about 200 m. The GSC appears to be unique in that it creates less relief at the longer wavelengths than the other mid-ocean ridges surveyed by deep tow.

#### Wavelength of Fault Blocks.

The nature of the spectral estimates does not allow easy physical interpretation of the results. In part this is because the basic unit of sea-floor relief, the fault block, contains power at a wide range of wavelengths — wavelengths not equivalent to the width of fault blocks. Furthermore, fault blocks often contain smaller units or occur in groups that make up larger units where each larger unit may be interpreted to be a fault block. The result is that it is very difficult to define individual fault blocks. The ambiguity can be illustrated by Figure 5c. It is not possible to decide how many fault blocks of what widths are present. Krause and Menard (1965) tried to determine the width and amplitude of abyssal hills and they were confronted with a similar dilemma. They decided there are abyssal hills superimposed on other abyssal hills. The red spectrum of bathymetric profiles reflects the fact that sea-floor relief has a full range of wavelengths. It is safe to say that the spectral estimates do seem to confirm the contention that MAR has relief with more long wavelength components than other spreading centers. However, no interpretation can be made on the specific dimensions of fault blocks.



## 1.10 Summary

### Formation of Tectonic Relief

Analysis of detailed bathymetric profiles of mid-ocean ridges of various spreading rates found their morphology to be quite similar in many ways. Spreading axes are always coincident with zones of low tectonic relief. The relief increases in magnitude away from the spreading axes by the addition of fault scarps and the tilting or warping of the sea-floor. At some distance from the spreading axes, the relief reaches some ambient density where tectonic activity is interpreted to become negligible and the relief is frozen into the lithosphere.

### Width of the Plate Boundary Zone

The width of the zone over which tectonism is active at divergent plate boundaries, the plate boundary zone, was estimated by looking for the distance from the spreading axes where mature sea-floor relief is first achieved. At faster spreading centers, the variation in the size of fault scarps versus distance from the spreading axes was used to gauge the maturity of the sea-floor relief. At deeply rifted mid-ocean ridges, mature relief is achieved at the point where the rift valley relief is eliminated. The plate boundary widths turn out to be quite similar for intermediate rate and fast spreading centers. The plate boundary width is noticeably wider for the slow spreading MAR. If the plate boundary widths are interpreted in terms of the age of the

sea-floor to which tectonism is active, then the age is much greater at the slow spreading MAR. No clear trend is evident for the intermediate rate and fast spreading centers.

#### Reverse Faulting

If reverse faulting occurs, tectonic activity may be occurring at distances from the spreading axes greater than the estimated plate boundary zones. Reverse faulting can reduce the throws on pre-existing normal faults, which would go undetected in the analyses of fault scarp throws. Because reverse faults can be easily eroded to resemble normal faults, their existence cannot be proved or disproved by the examination of bathymetric data. However, no available evidence indicates the occurrence of reverse faults near spreading axes and the dominance of tensional tectonic features at spreading centers suggests reverse faulting rarely occurs there.

#### Maintenance of Median Rift Relief

The median rift valley relief at deeply rifted mid-ocean ridges can be eliminated by the addition of outward facing faults, tilting or warping of the sea-floor, or reverse faulting. Analysis of MAR profiles suggests outward tilting or warping of the sea-floor is the dominant mechanism though the addition of outward facing faults is also important.

#### Roughness of Sea-Floor Relief

The roughness of sea-floor relief was defined to be the cumulative vertical relief per unit of horizontal distance.

Estimates of the sea-floor roughness using deep tow profiles projected onto the spreading direction and sampled at even 50 m intervals showed little correlation with spreading rate. These results are contrary to the often noted inverse relationship seen in surface ship profiles. The apparent contradiction may be due to the inability of typical surface ship profiling systems to resolve much of the small amplitude/short wavelength relief created at fast spreading centers. Calculation of the relief that would be seen by a surface ship wide beam sonar system using deep tow data suggests this is true. Spectral estimates using deep tow profiles also suggest there is more long wavelength relief in sea-floor created along the slow spreading MAR compared to that created along faster spreading centers. However, the spectral analyses cannot be interpreted to determine if there are differences in the size of fault blocks for sea-floor created at different spreading rate.

## Chapter II: Morphology of Ridge Crests and the Sea-Floor as Seen by Surface Ship Profiling Systems

### 2.1 Introduction

The relationships that slow spreading centers have rifted ridge crests and create rough sea-floor relief while fast spreading centers have non-rifted ridge crests and create smooth relief have been widely noted. However, the validity of these generalizations have not been tested by any systematic study of ridge crest morphology and sea-floor relief. These generalizations suggest the roughness of sea-floor relief, the dimension of median rifts at slow spreading centers, and the dimension of central highs at fast spreading centers all vary consistently with spreading rate. Dynamic models of ridge crest and sea-floor relief formation have emphasized these spreading rate dependent relationships (Lachenbruch, 1973; 1976; Sleep and Rosendahl, 1979). Therefore, it is important to establish to what extent these relationships between ridge crest, sea-floor relief, and spreading rate are true.

Deep tow profiles of mid-ocean ridges are too few to answer the problems stated above. Instead, bathymetric profiles of mid-ocean ridges collected with surface ship profiling systems close to the spreading directions and away from fracture zones have been compiled. The dimensions of median rifts can be defined relative to the flanking rift

mountains (Tapponnier and Francheteau, 1978) or to the regional isostatic level (Lachenbruch, 1973). Straight lines were fitted to depth versus square root of age plots of projected surface ship profiles to see if the regional isostatic level can be approximated by the subsidence of the sea-floor attributable to the conductive cooling of the lithosphere. The roughness of the sea-floor relief was measured in terms of meters of vertical relief per km of horizontal distance along projected profiles, similar to the way roughness was measured in the deep tow profiles

## 2.2 Data Base

### Data Base

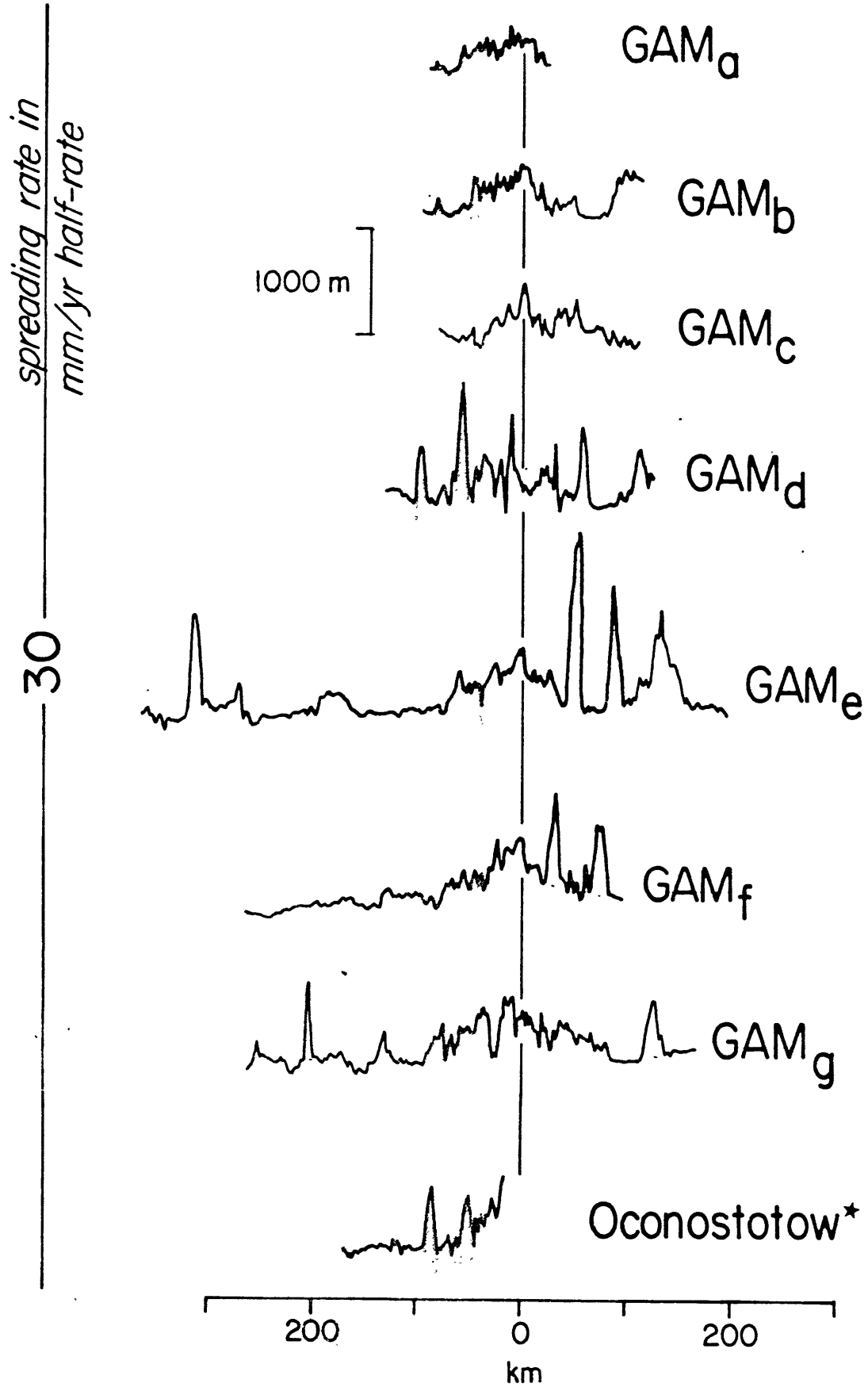
Surface ship bathymetric profiles from the Atlantic, Pacific, and Indian Oceans were compiled for this study. Bathymetric data in digital form were acquired from the Woods Hole Oceanographic Institution (WHOI), the Scripps Institution of Oceanography (SIO), and the National Geophysical and Solar-Terrestrial Data Center (NGSDC). The data acquired through NGSDC originated from the Lamont-Doherty Geological Observatory (LDGO), Oregon State University (OSU), and the National Oceanic and Atmospheric Administration (NOAA). This digital data was used for the fitting of depth versus square root of age curves and the calculation of sea-floor roughness. Profiles published in journals and reports with vertical exaggeration of 100X supplement the digitally

acquired data (Heirtzler et al, 1969; McKenzie and Sclater, 1971; Johnson and Vogt, 1973; Talwani et al, 1974; Johnson et al, 1976; Hayes et al, 1969; 1972; 1975; 1976; 1977; 1978). Appendix I shows the locations and Figure 16 the profiles compiled. The profiles in Figure 16 are arranged from north to south in the Atlantic, Pacific, and Indian Oceans, and east to west in the Southeast Indian Ocean. Profiles acquired in digital form are labelled according to NGSDC and SIO conventions. Profiles traced from publications follow the manner in which they were labelled in the publications.

#### Digitization of Bathymetric Data

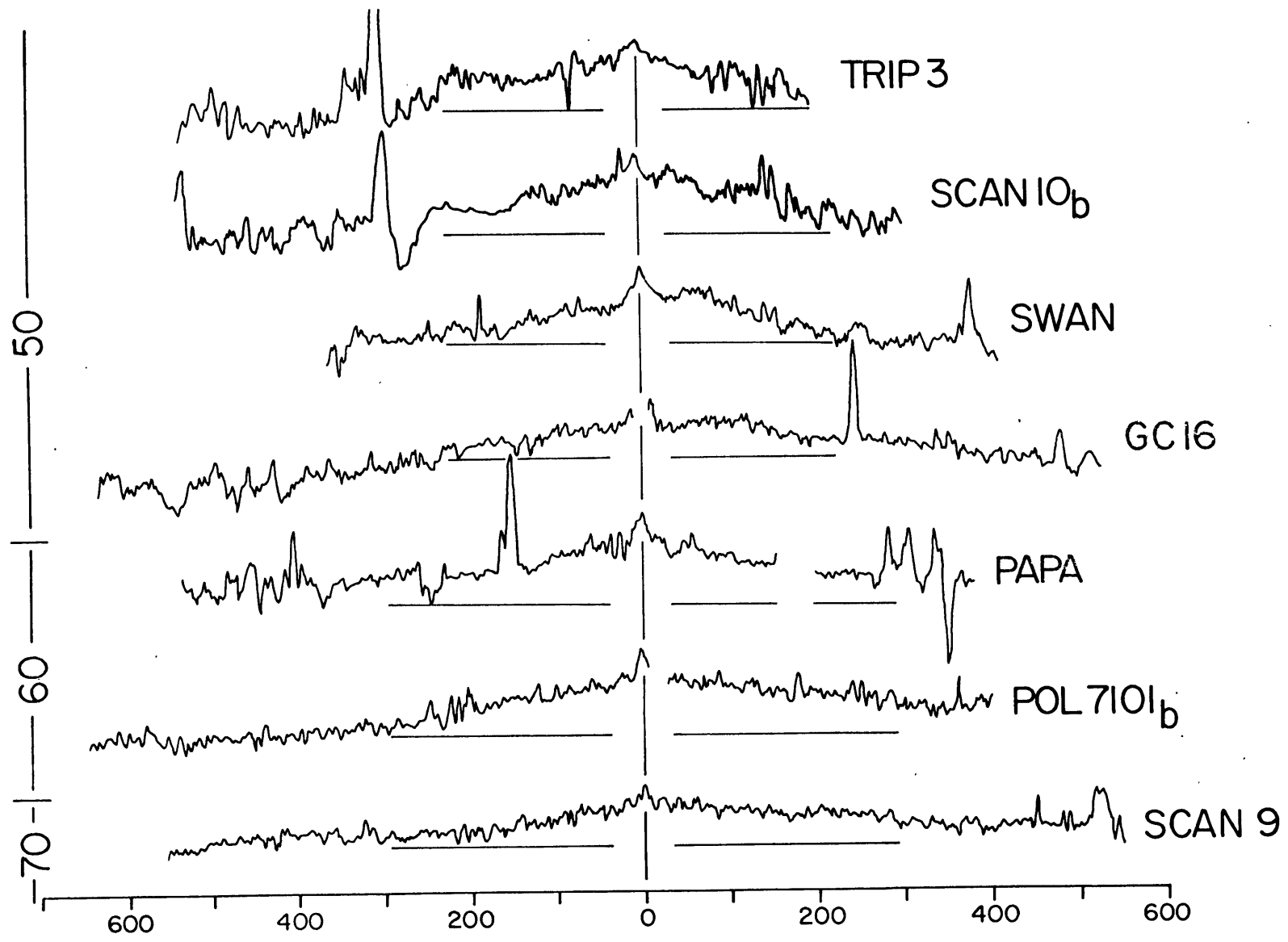
Whether traced from publications or acquired in digital form, the bathymetric data all have been digitized from analog echo sounding records. Thus, the digitization process used determines how accurately the data represent the actual sea-floor relief. The digital data as acquired from the various sources have even and uneven digitization intervals ranging from 2 to 15 minutes. Most of the data from SIO have even three or five minute intervals. Even five minute intervals are typical for OSU data while six minute intervals are common for LDGO data. Much of the NOAA data have uneven digitization interval averaging about one per 10 minutes. To minimize the effect of the wide range of digitization intervals, the digital data have been projected onto the local spreading directions and then sampled at even two nautical mile (3.66 km) intervals. All depths and distances shown in

Figure 16a: Bathymetric profiles from the Pacific and Southwest Indian Oceans. All profiles except those indicated by "\*" have been projected along small circles defined by the relevant plate rotation poles. Oconostotow, EPR 3°S, and the PAR profiles are deep tow profiles. Spreading rates from Minster and Jordan (1978) are truncated to the nearest 10 mm/yr half-rate. Profiles arranged from north to south. Vertical exaggeration is 100X for all profiles in Figure 16. Horizontal lines under the profiles show the sections used to calculate the roughness of sea-floor relief and fitting of the depth versus square root of age curves. Locations of the profiles are shown in Appendix I.

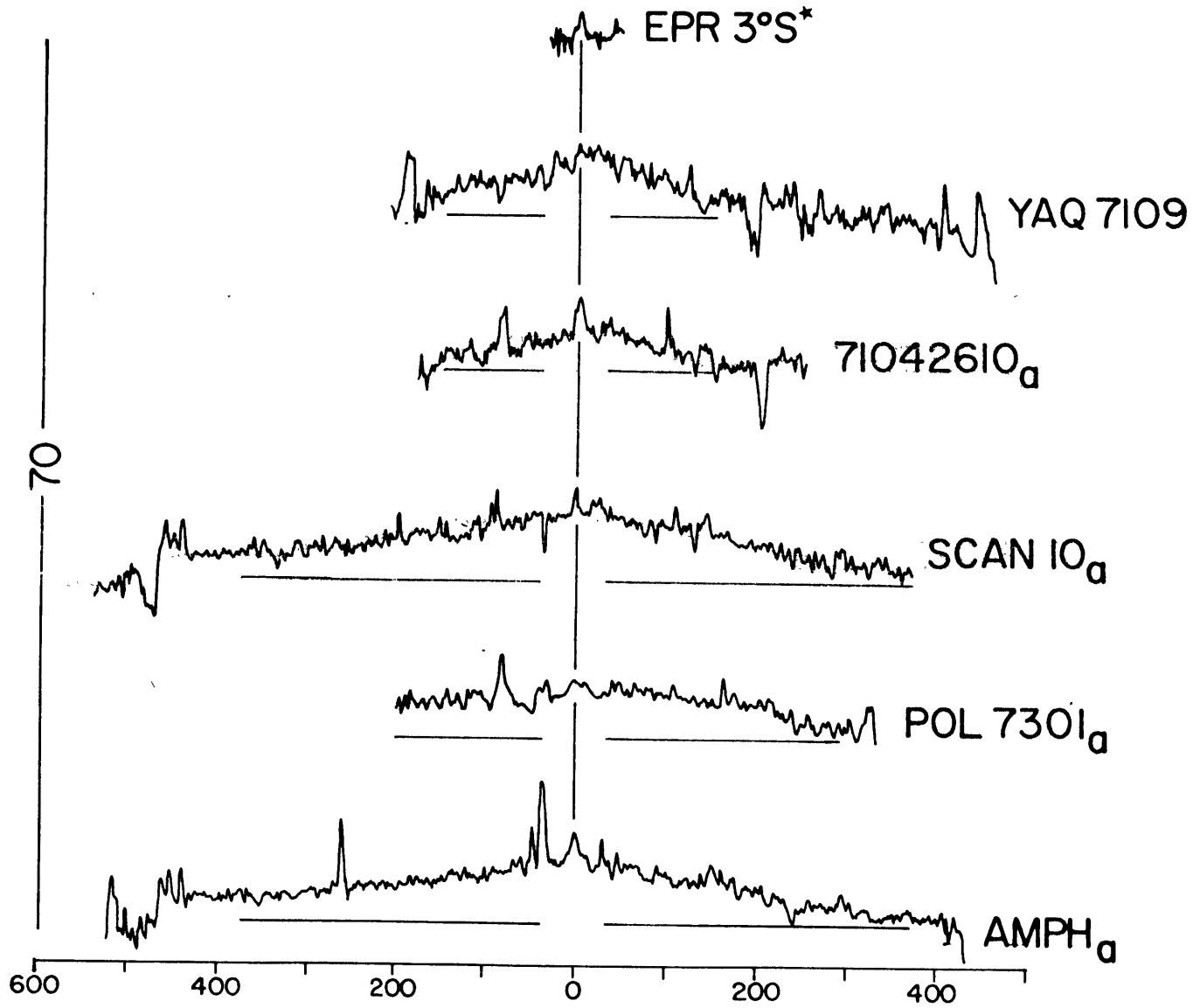


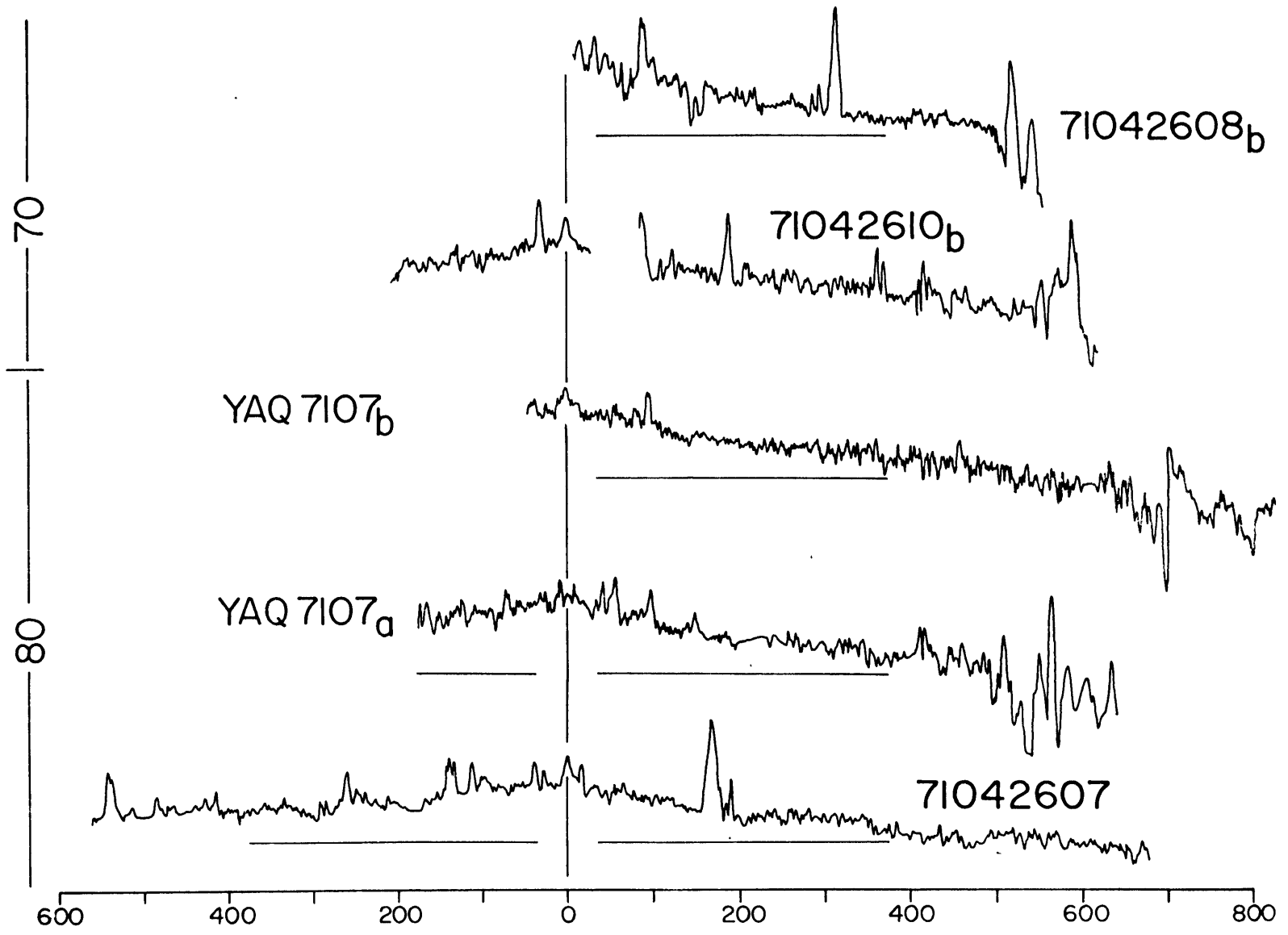


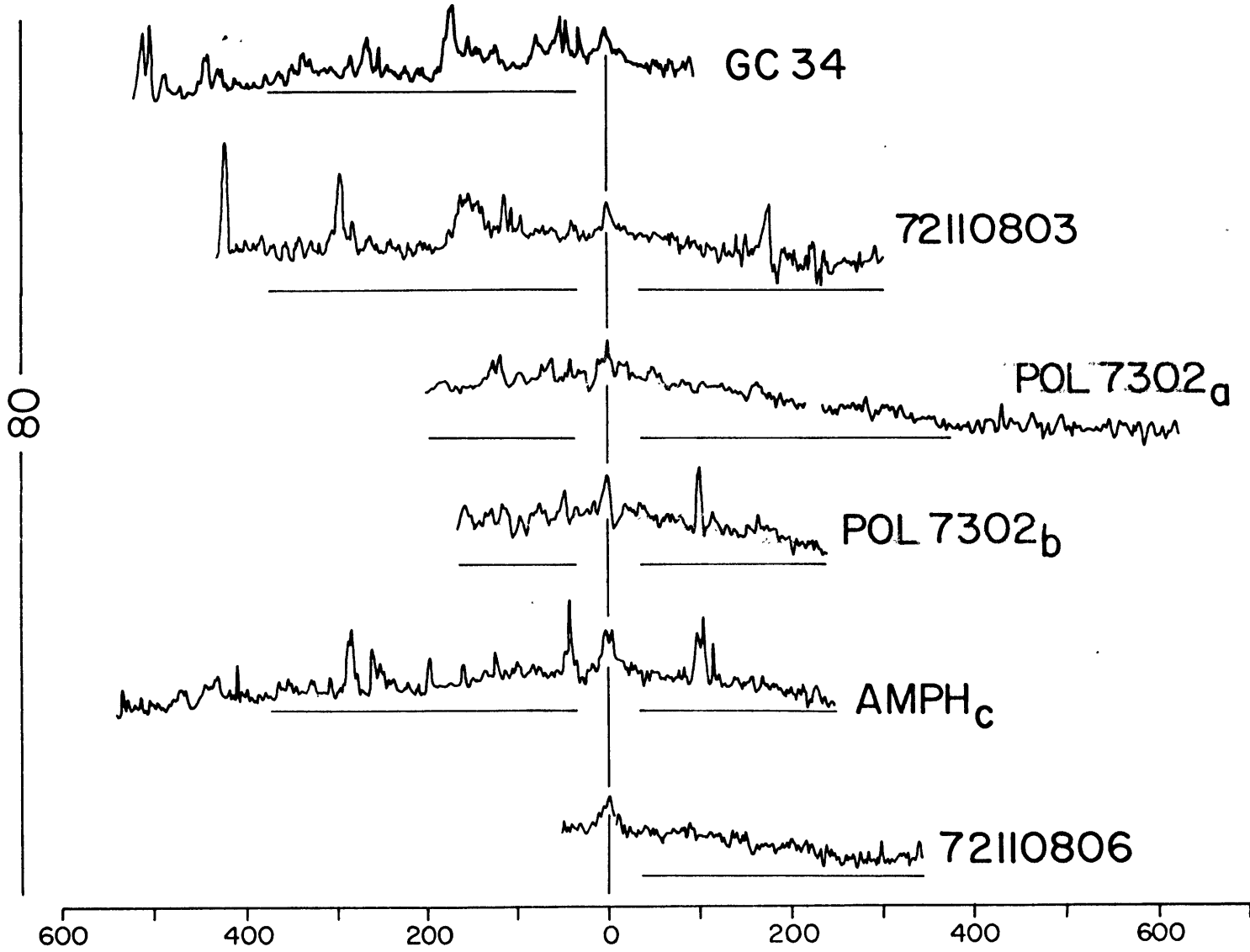
100

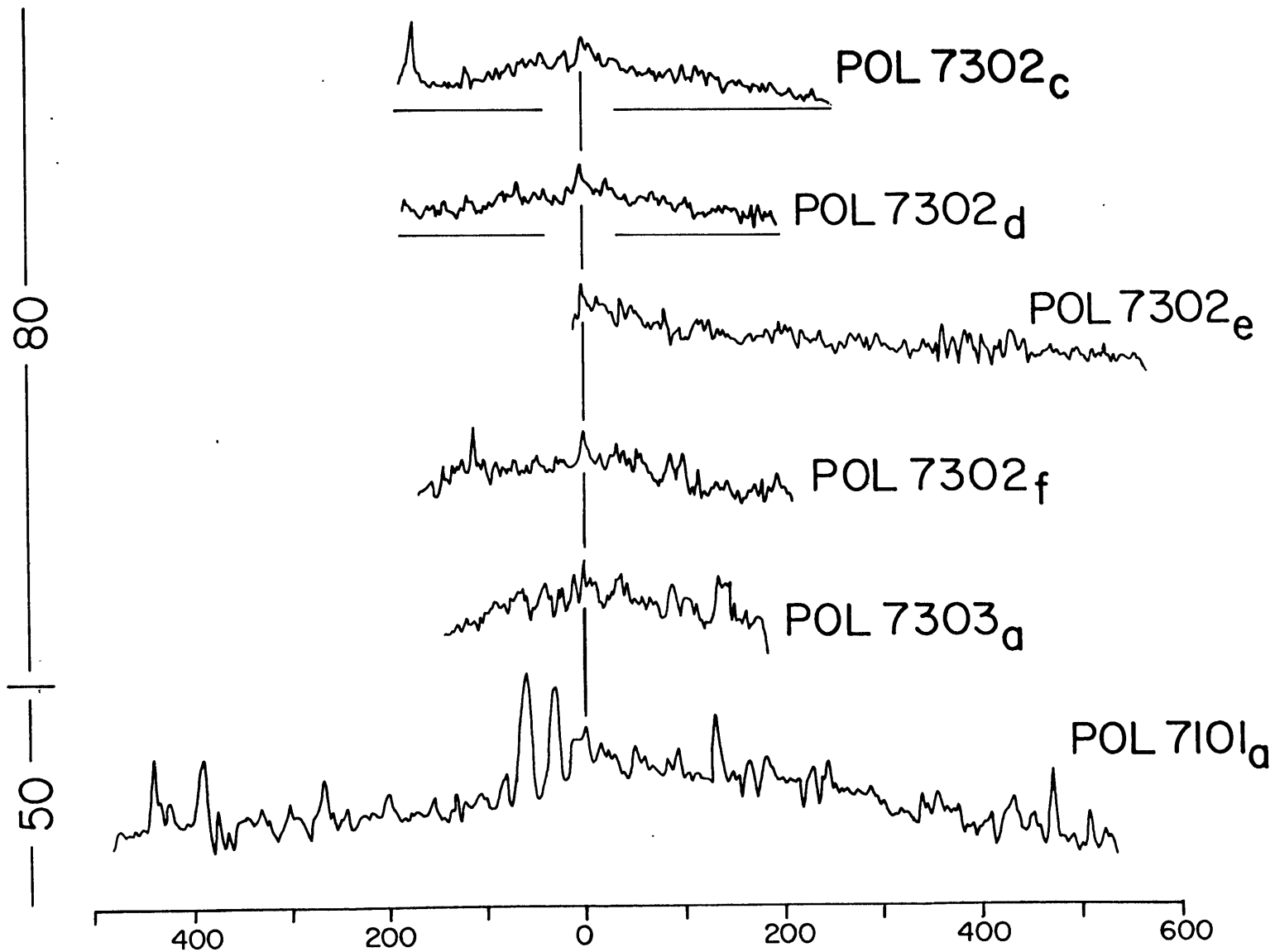


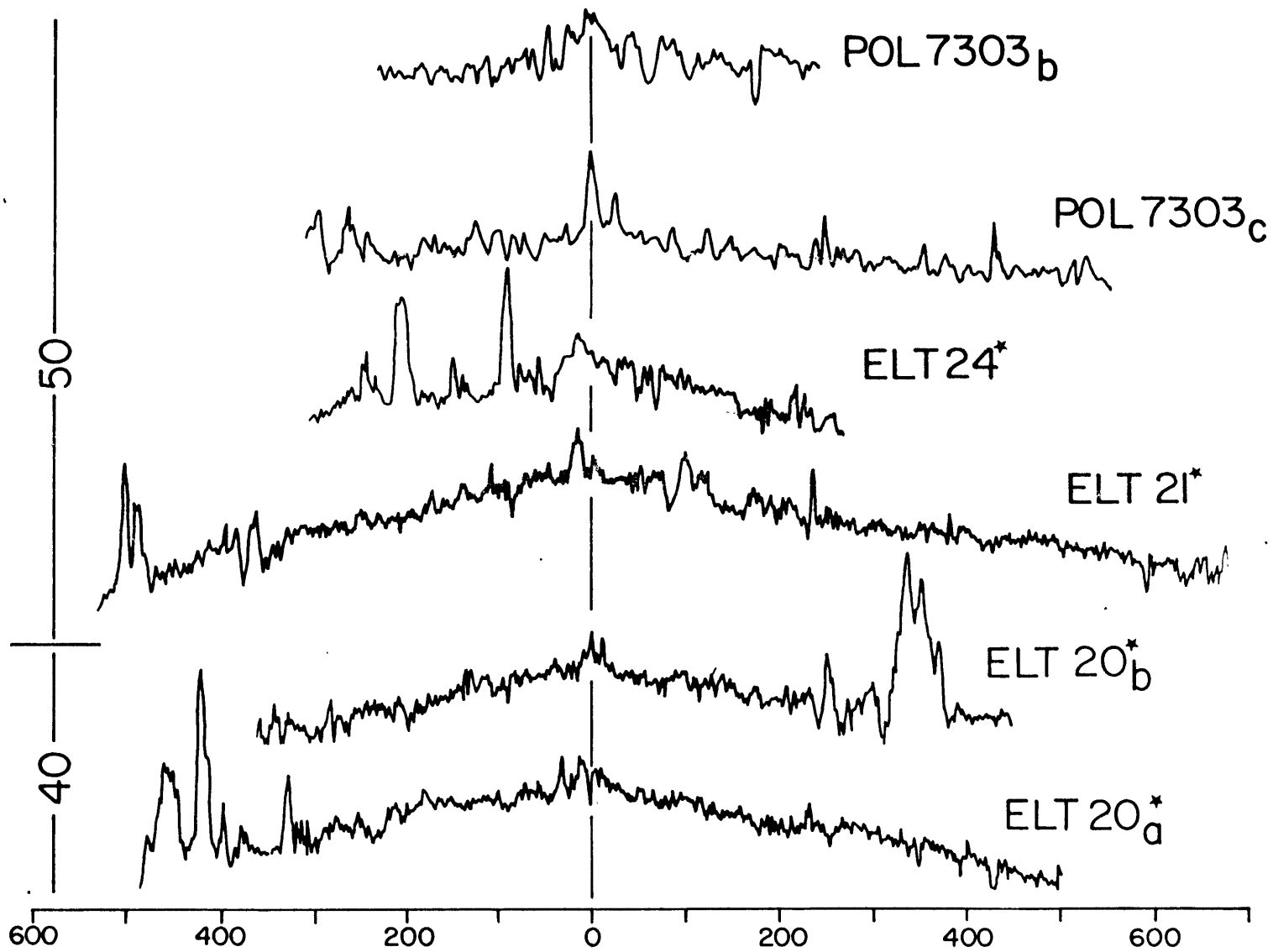
101

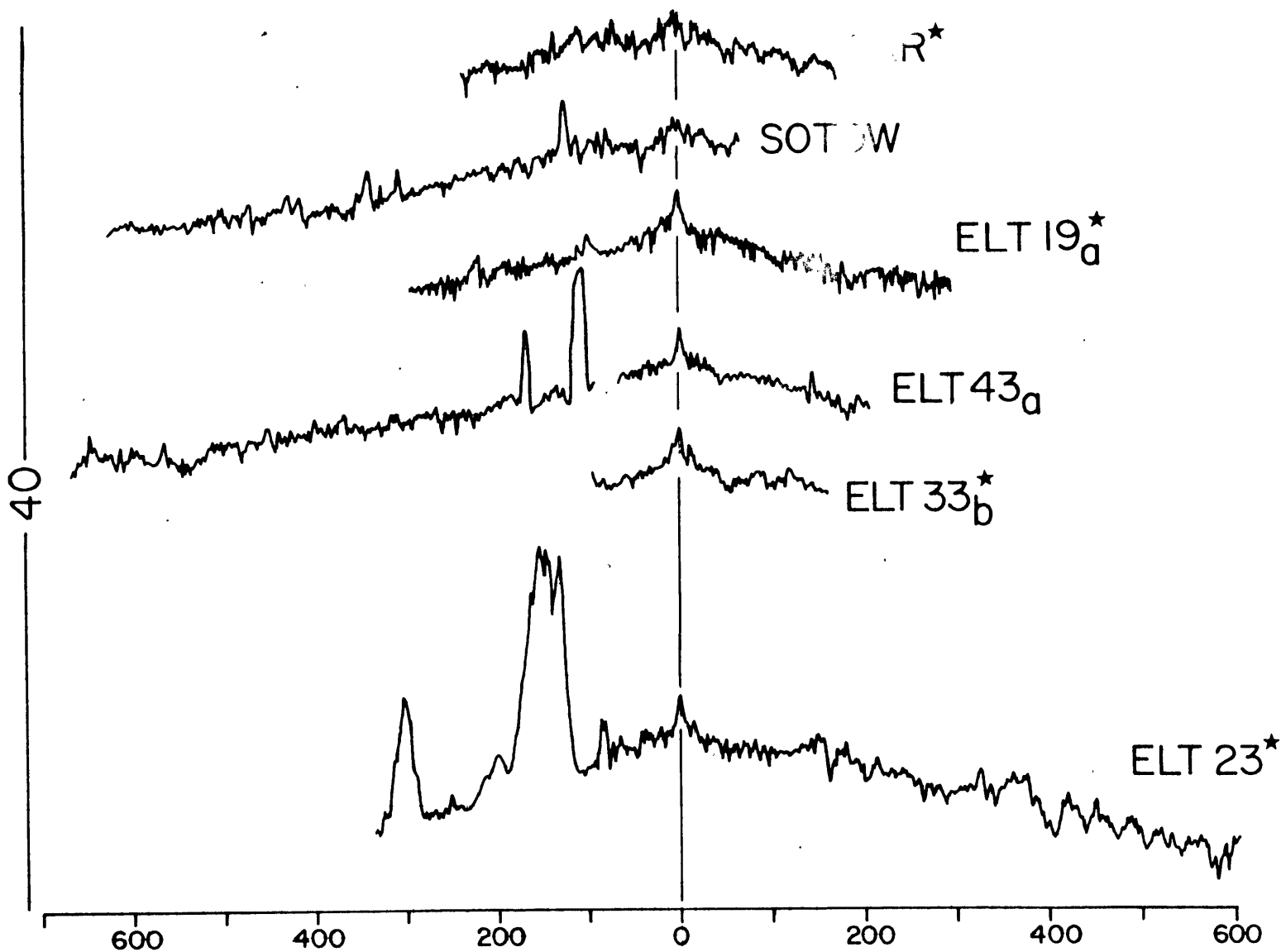


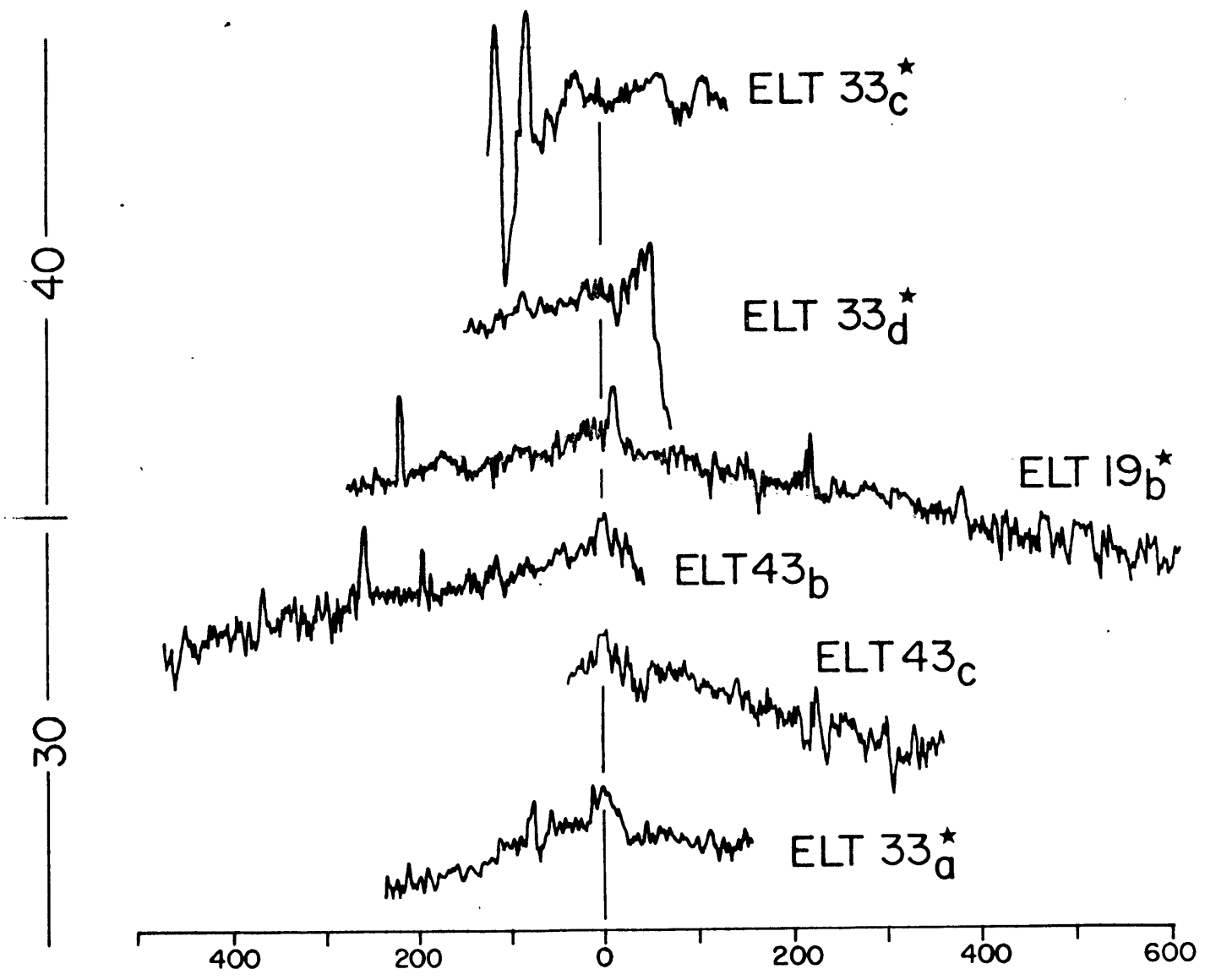




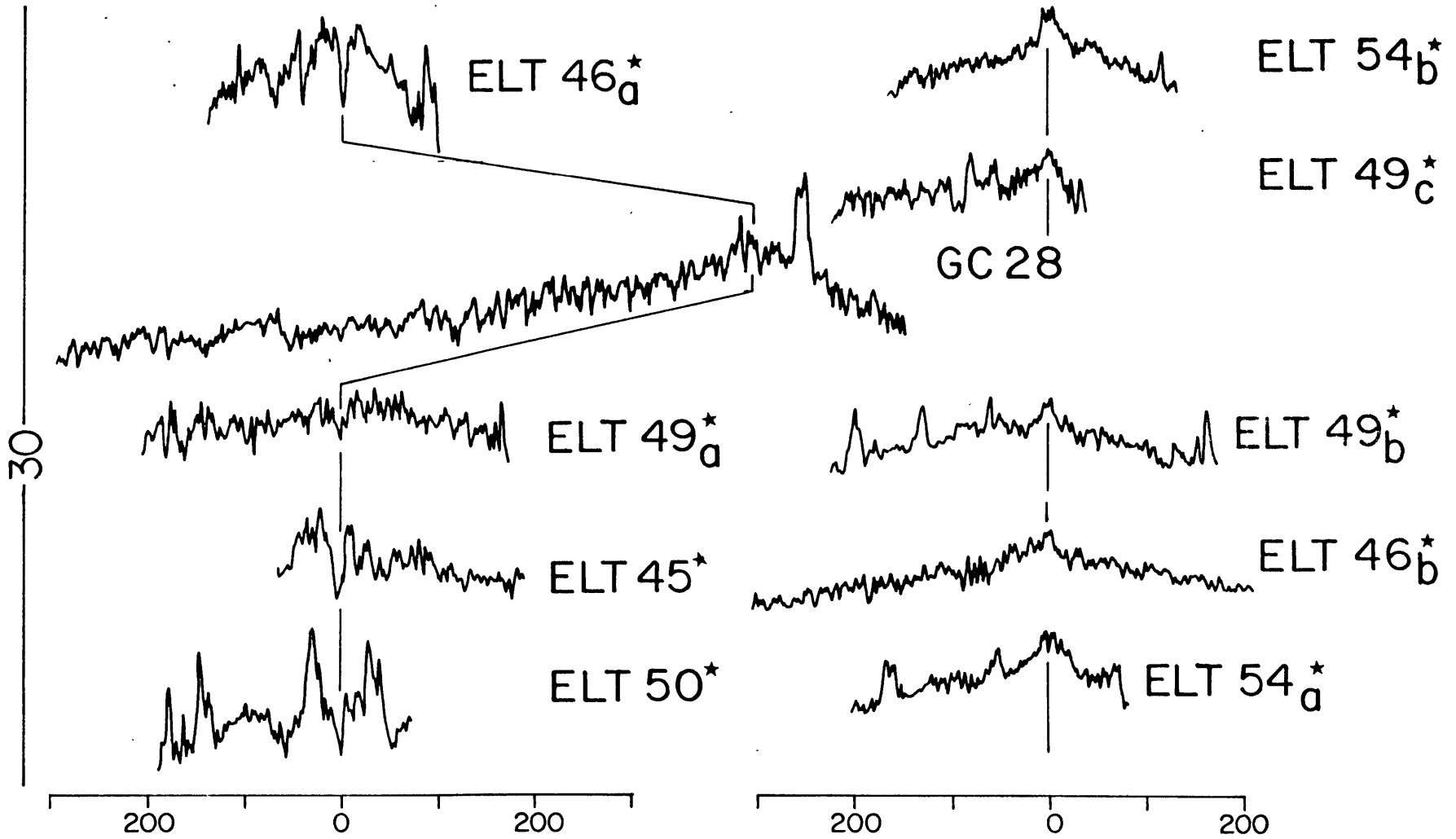












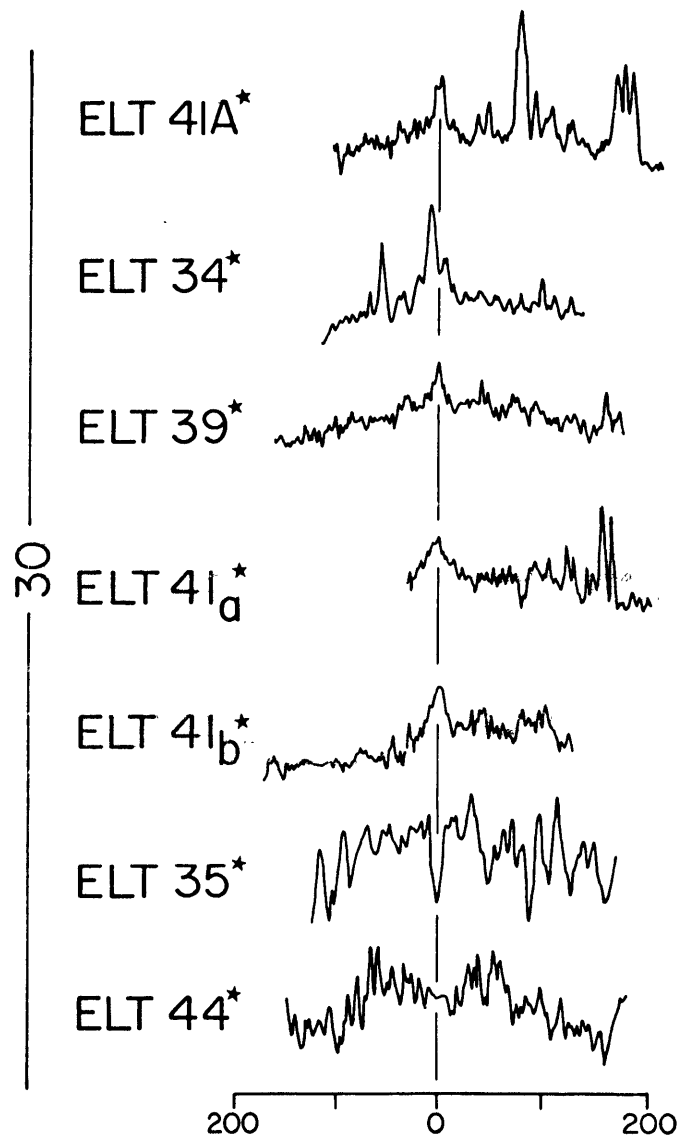
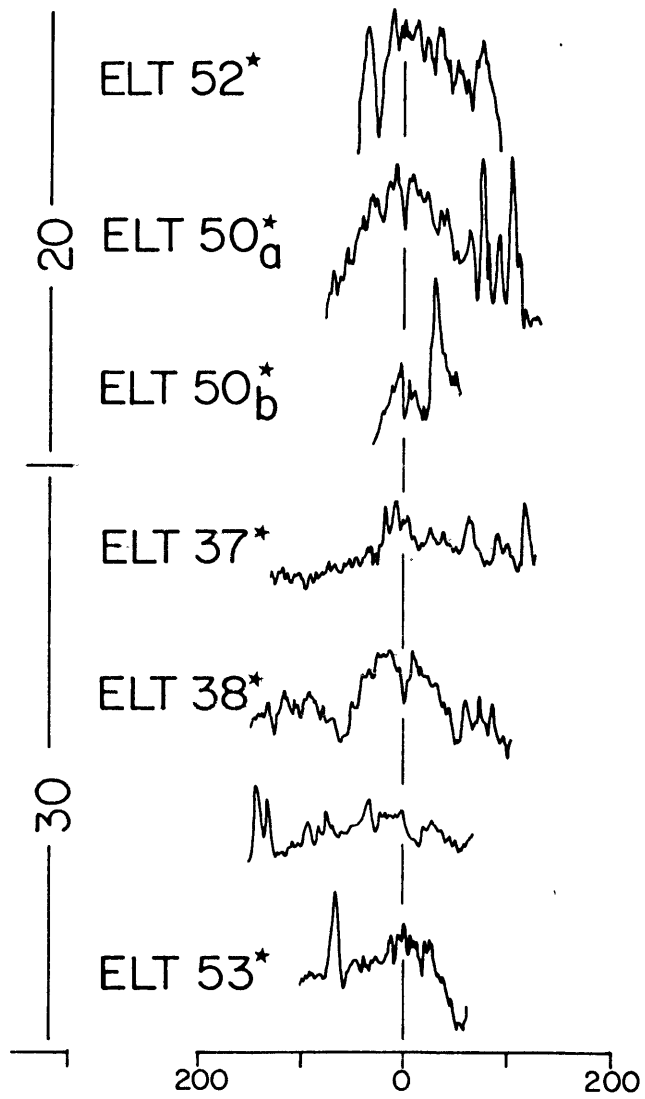
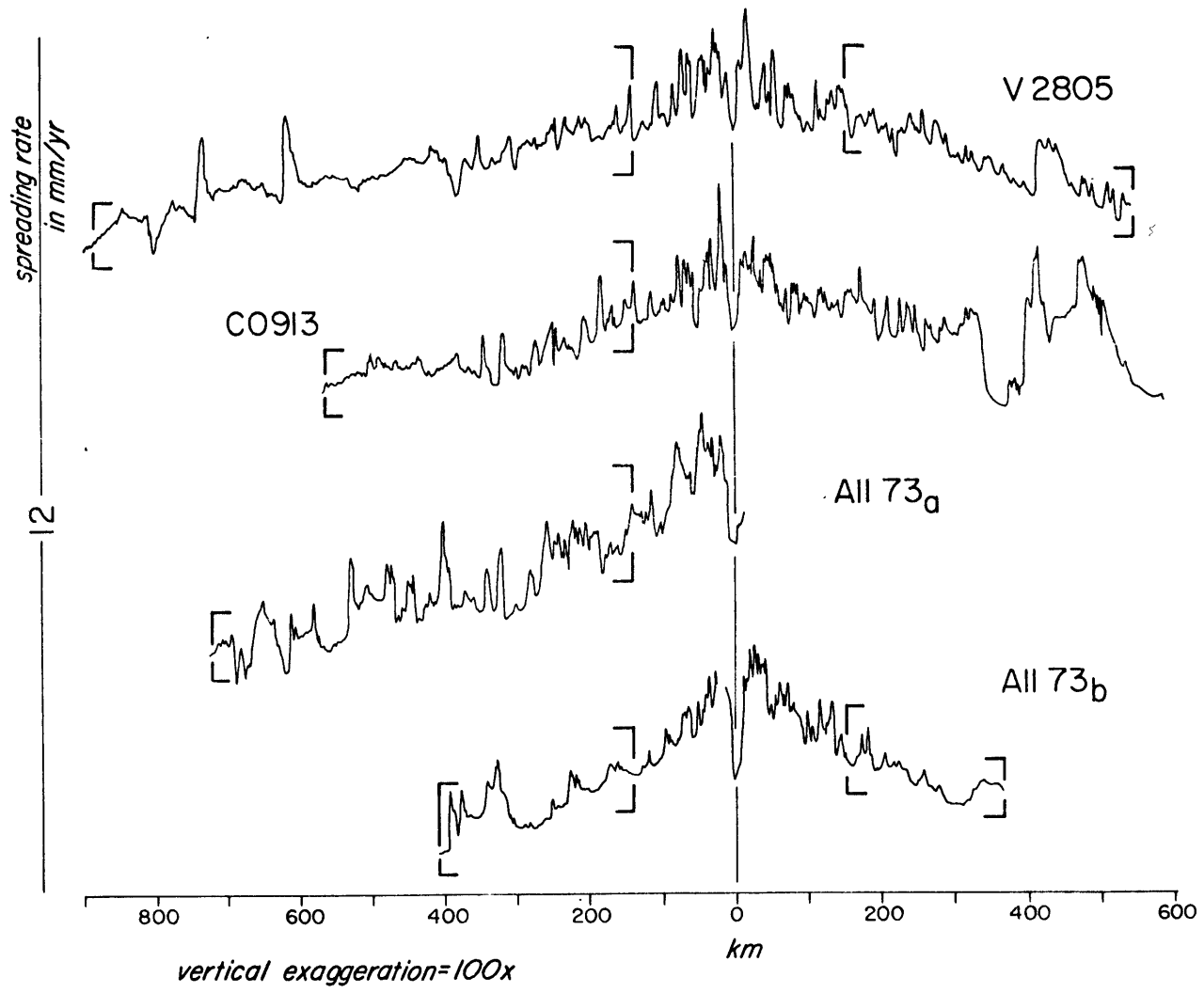
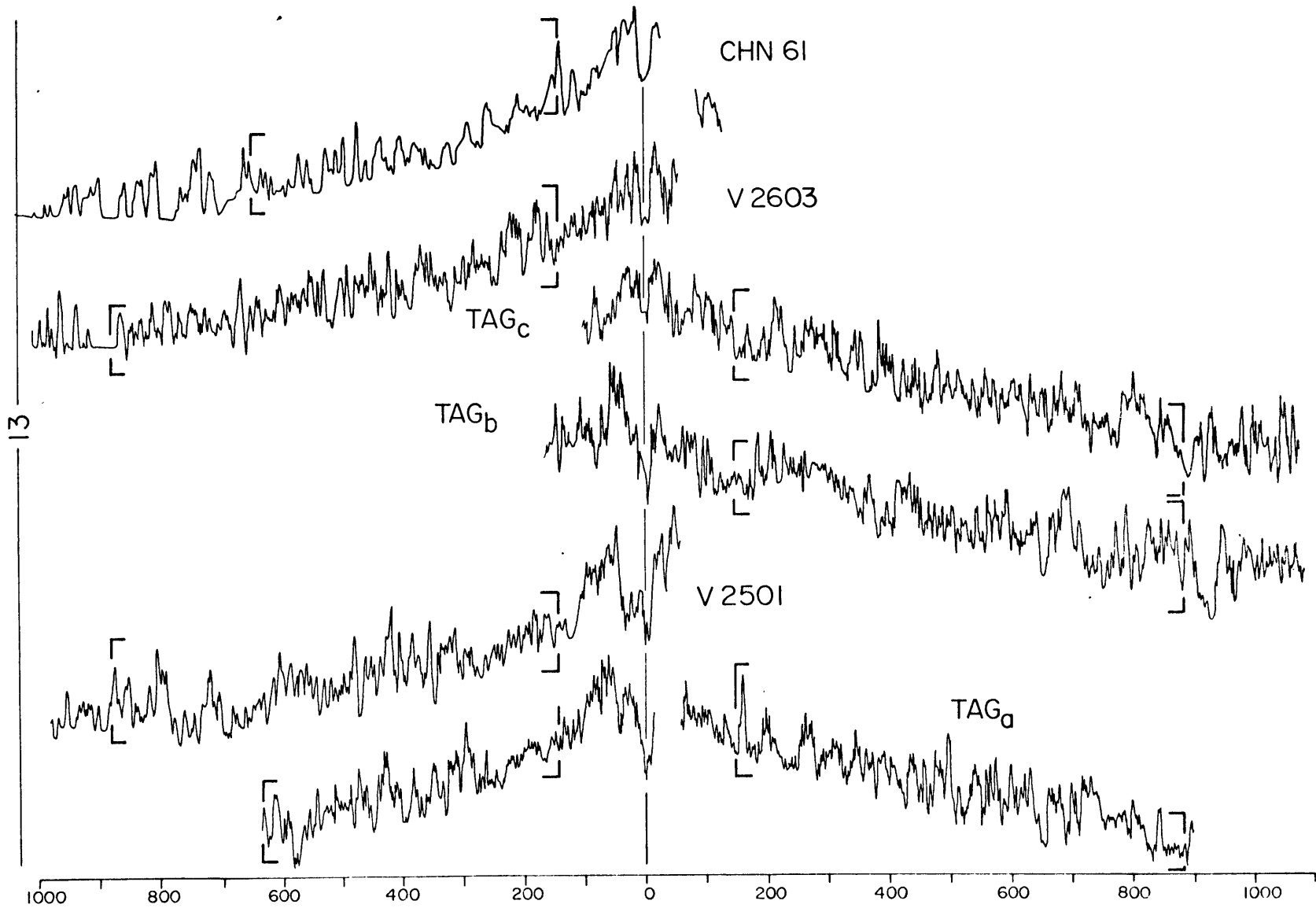
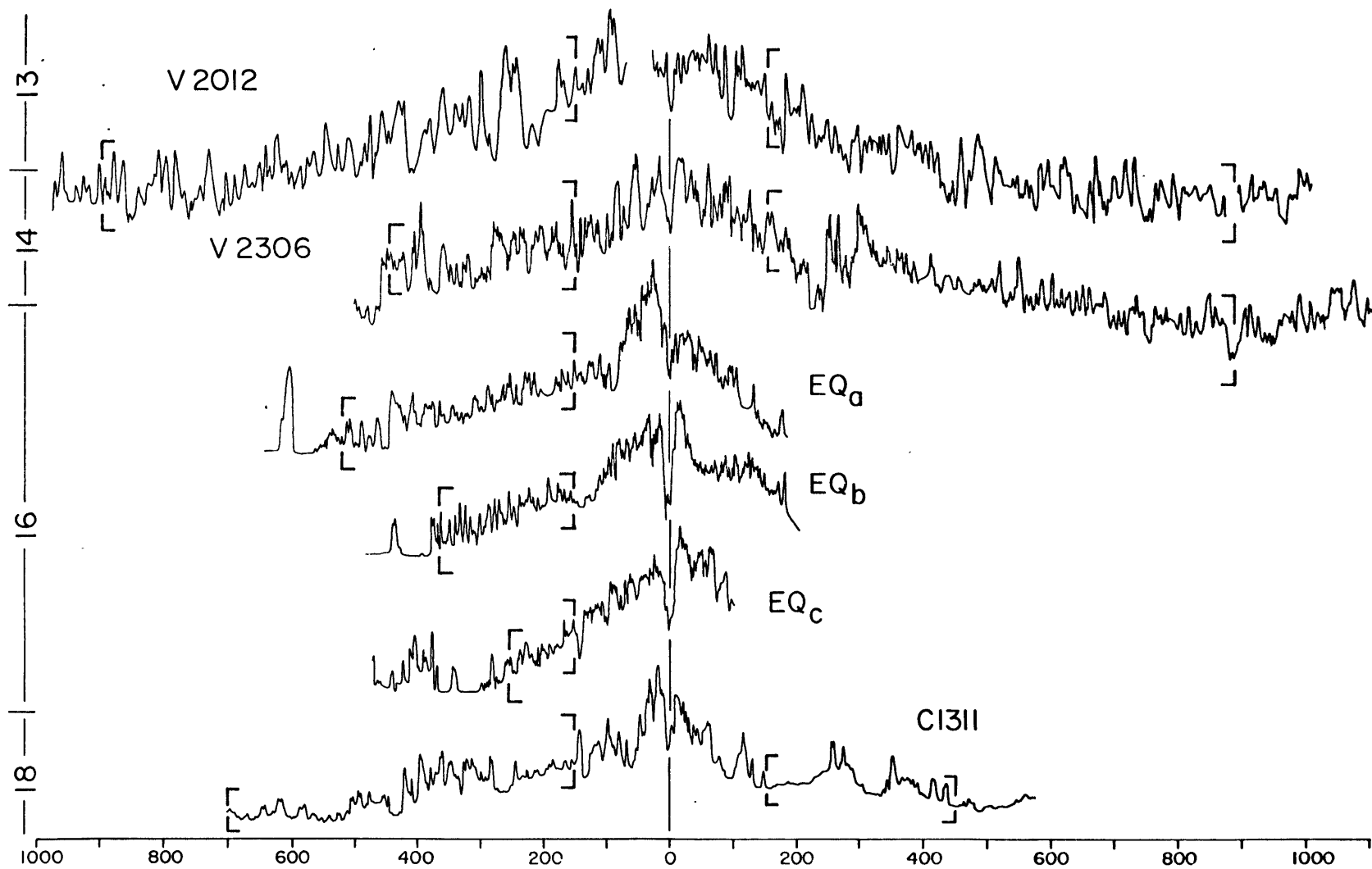
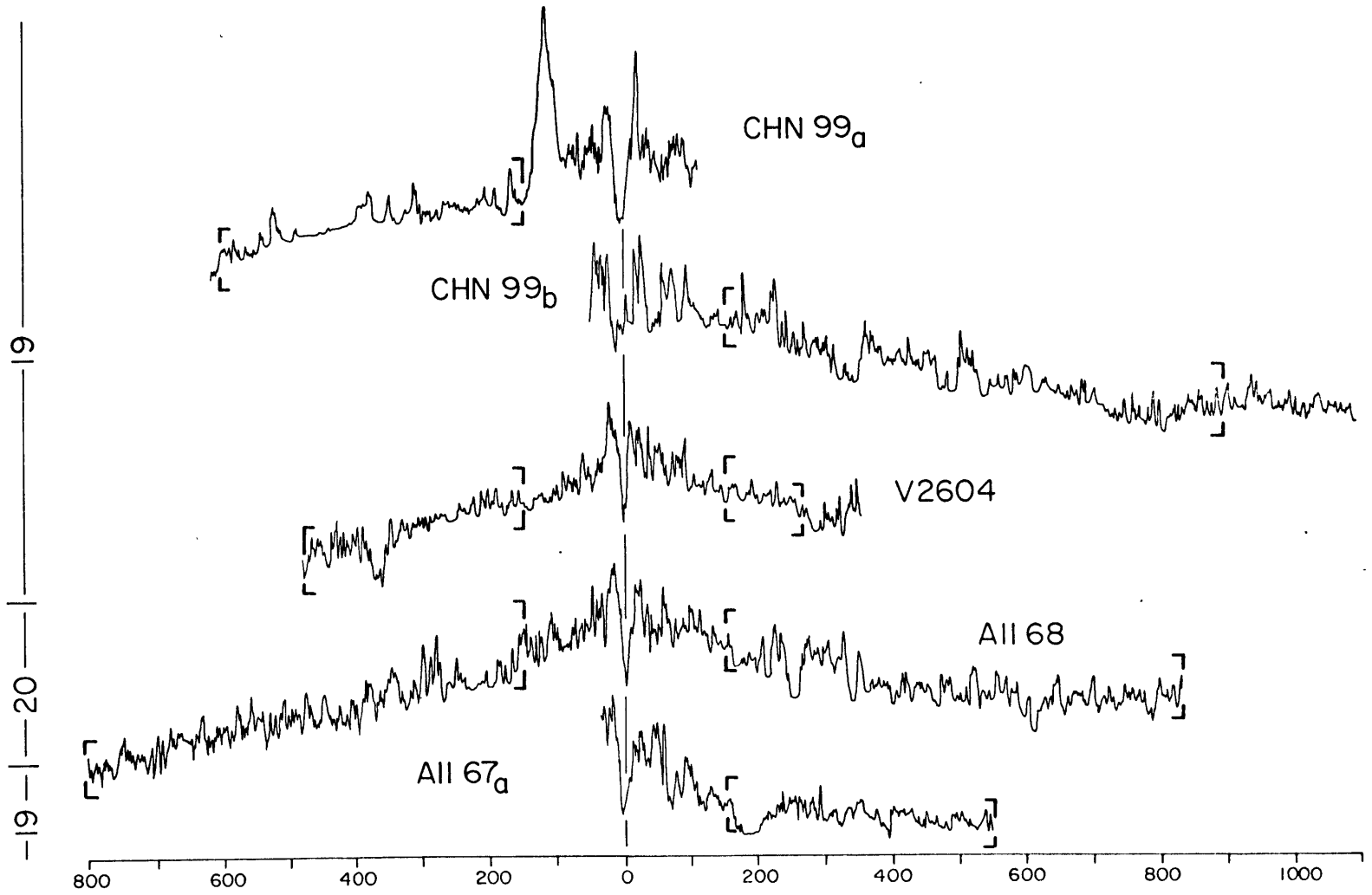


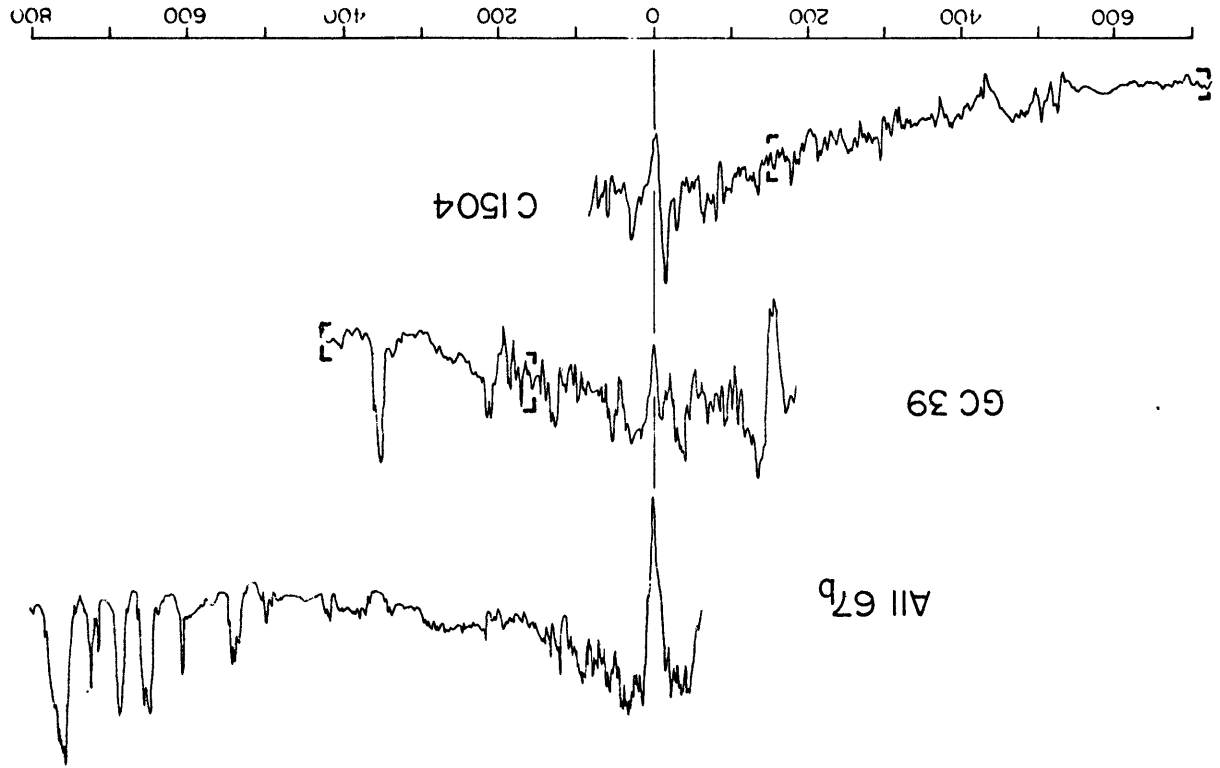
Figure 16b: Projected profiles from the Atlantic Ocean arranged from north to south. Brackets show the sections used to calculate the roughness of sea-floor relief and the fitting of depth versus square root of age curves.







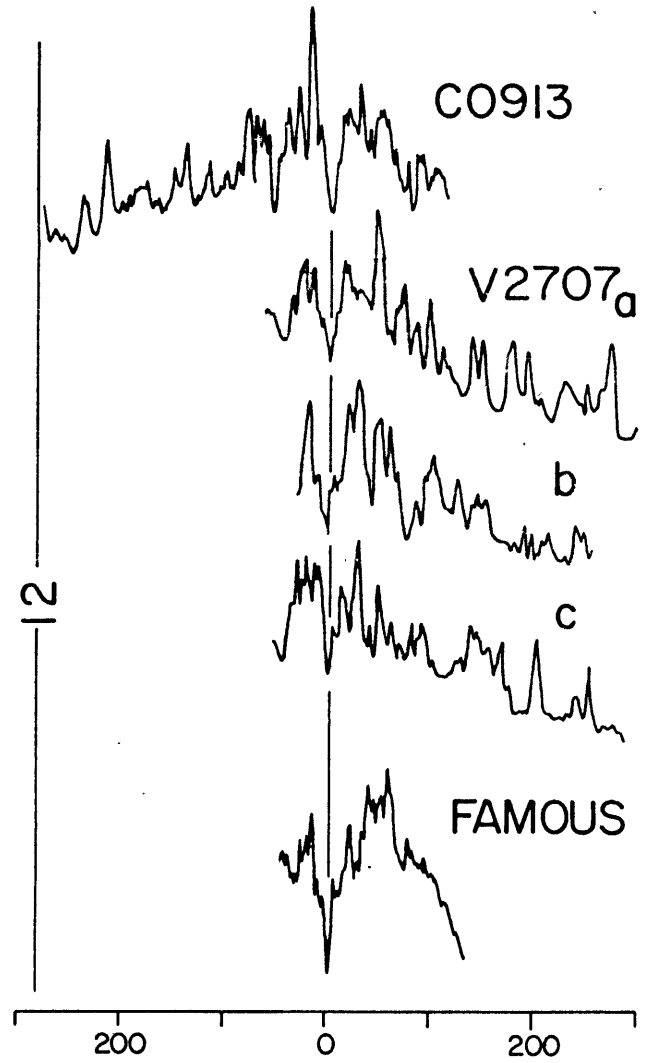
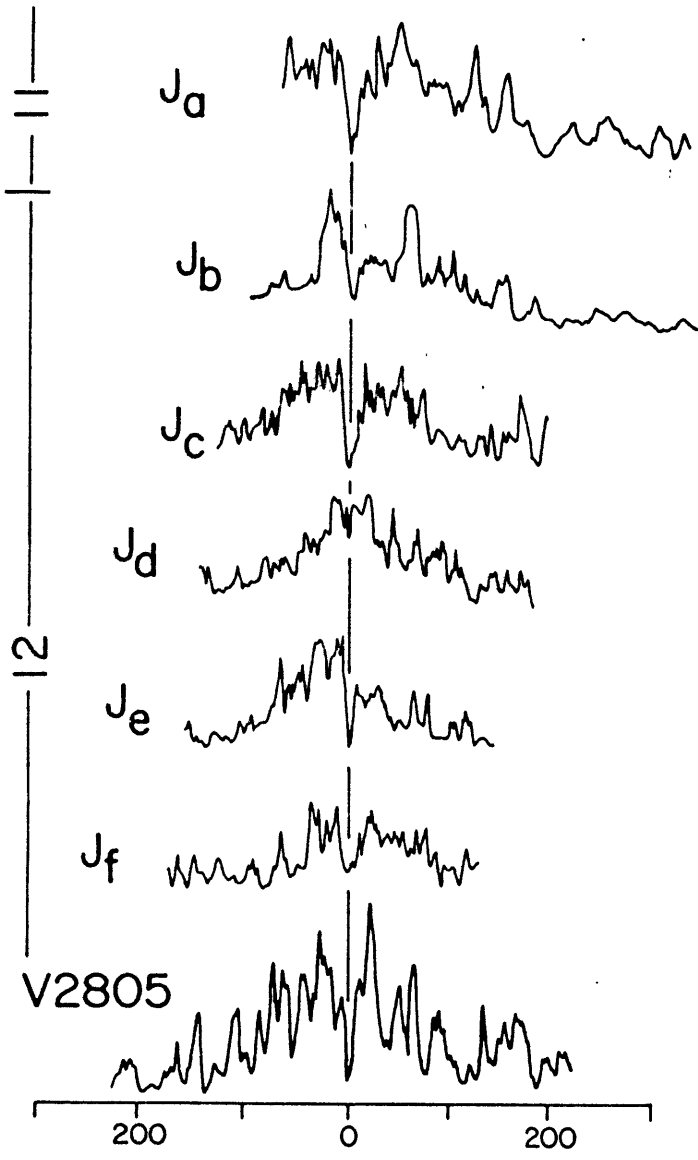


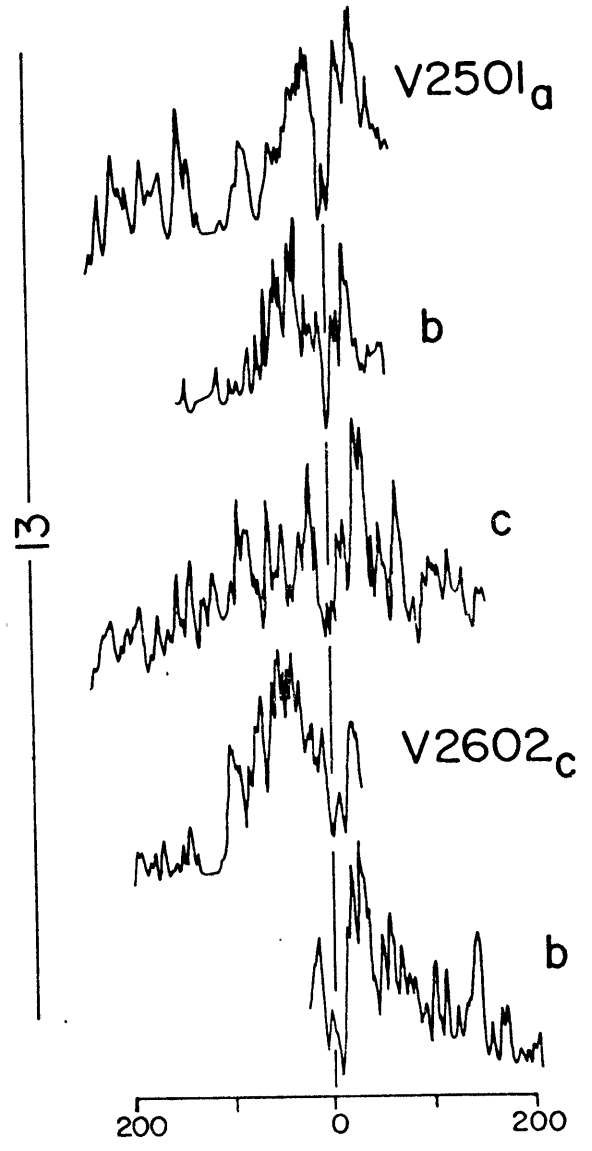
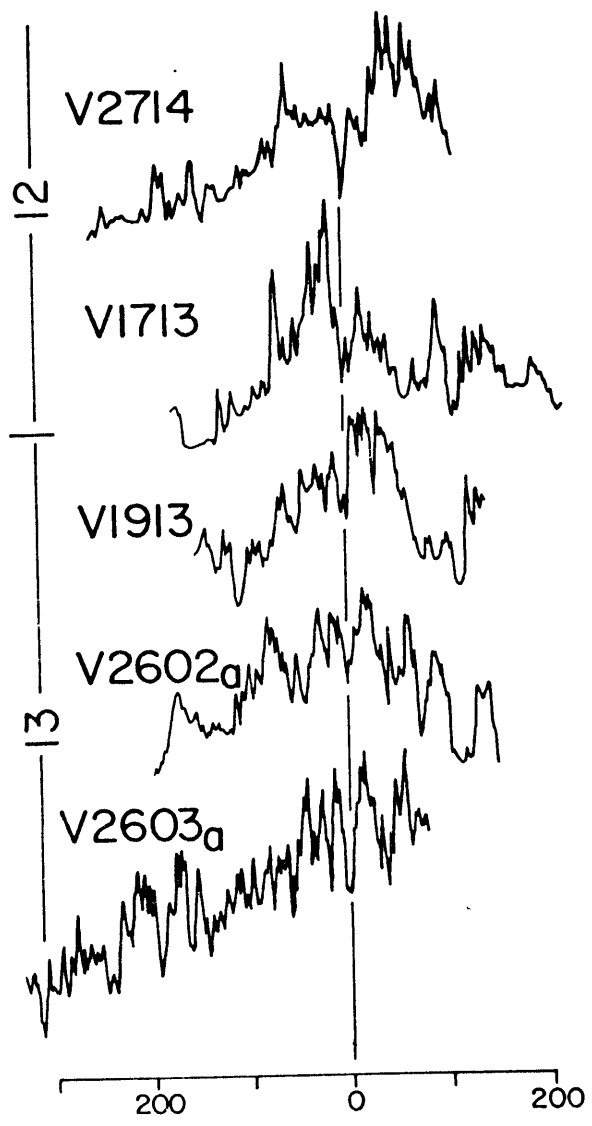


18 | 19



Figure 16c: Non-projected profiles of the MAR. The FAMOUS profile is a deep tow profile. Same scale as Figures 16a, 16b, and 16d.





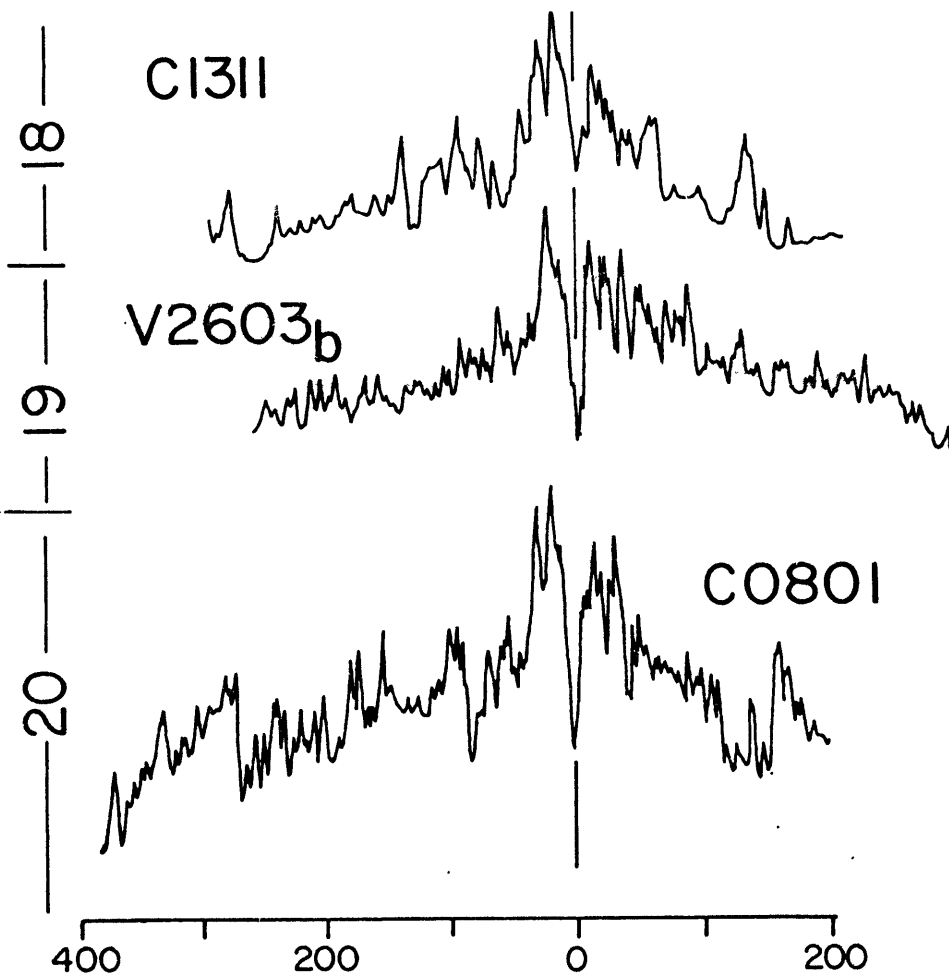
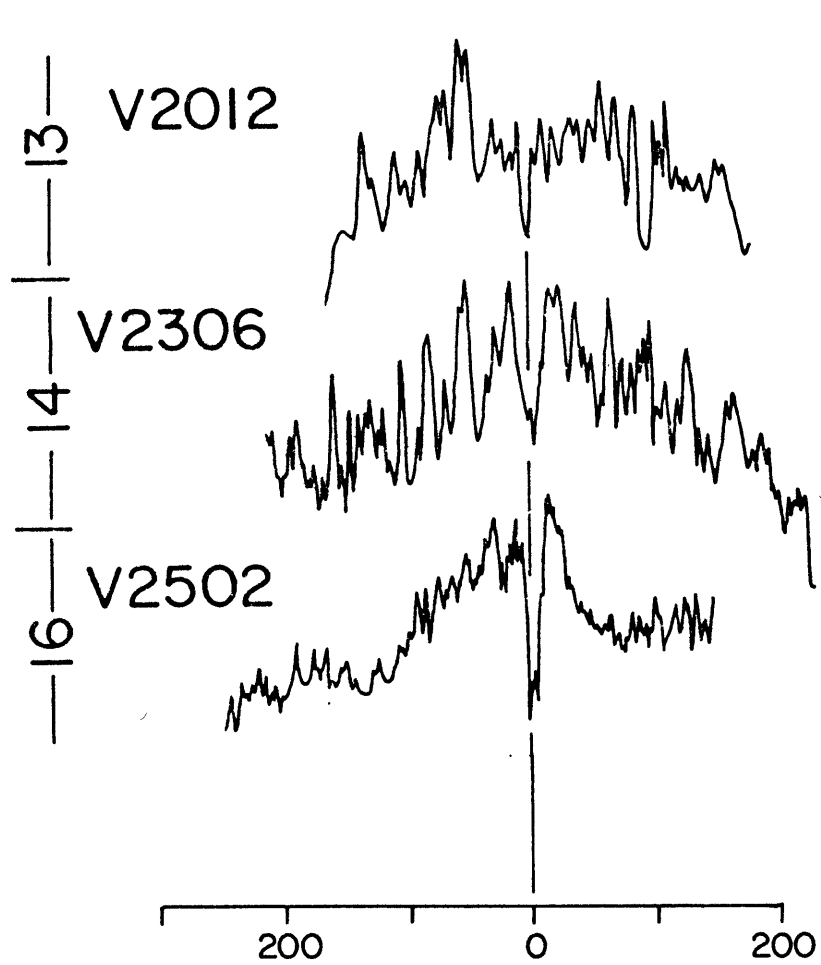
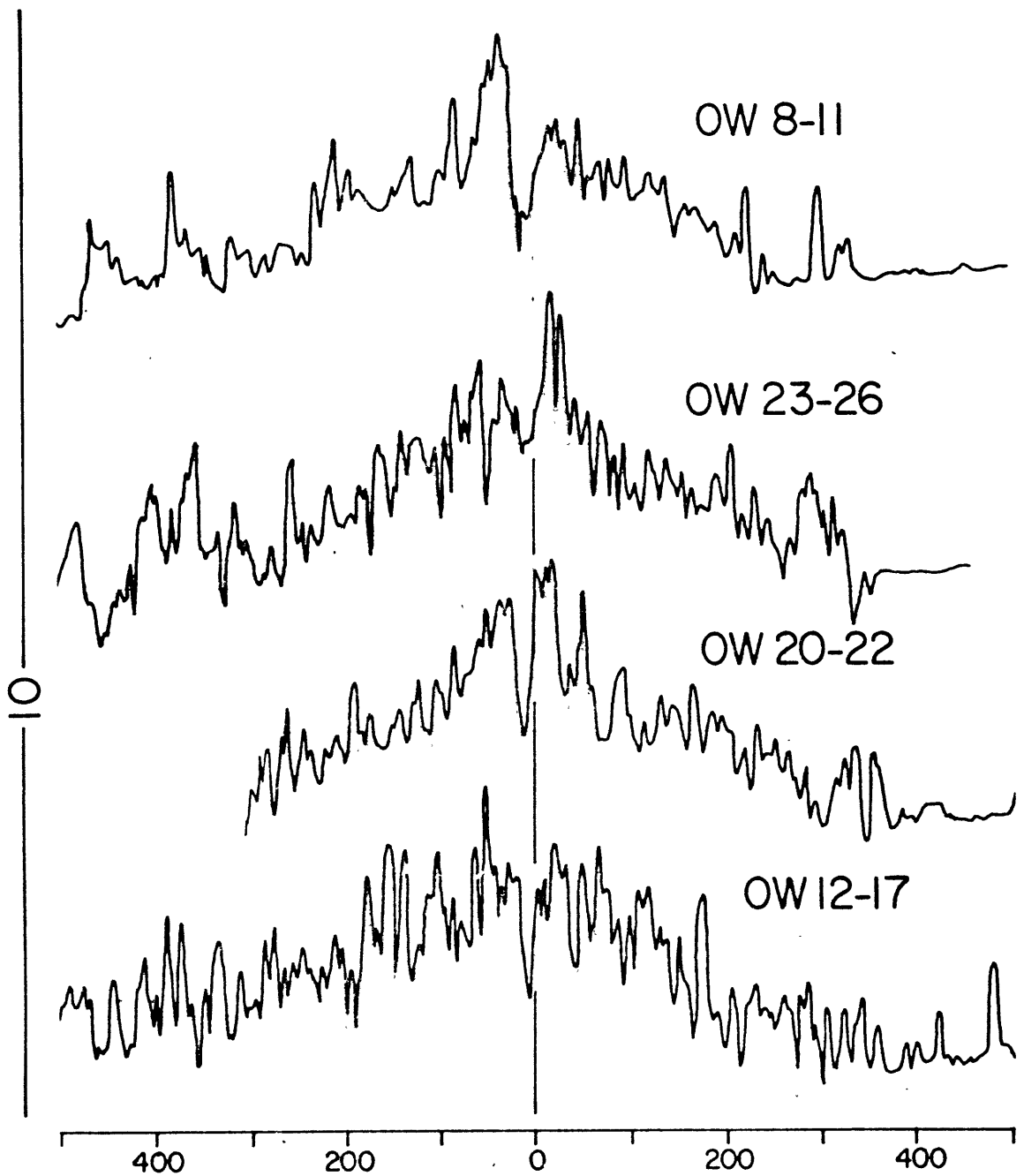
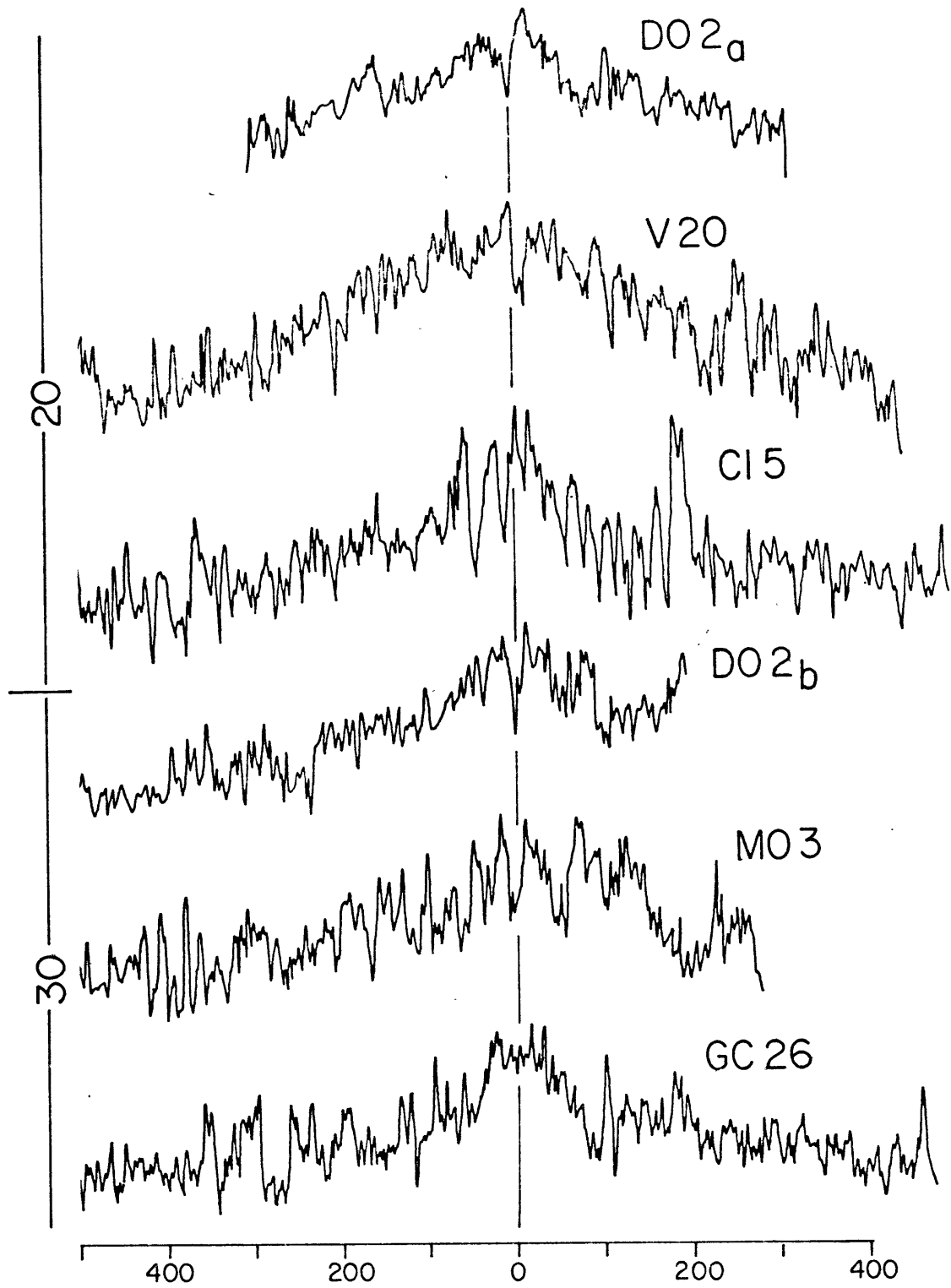
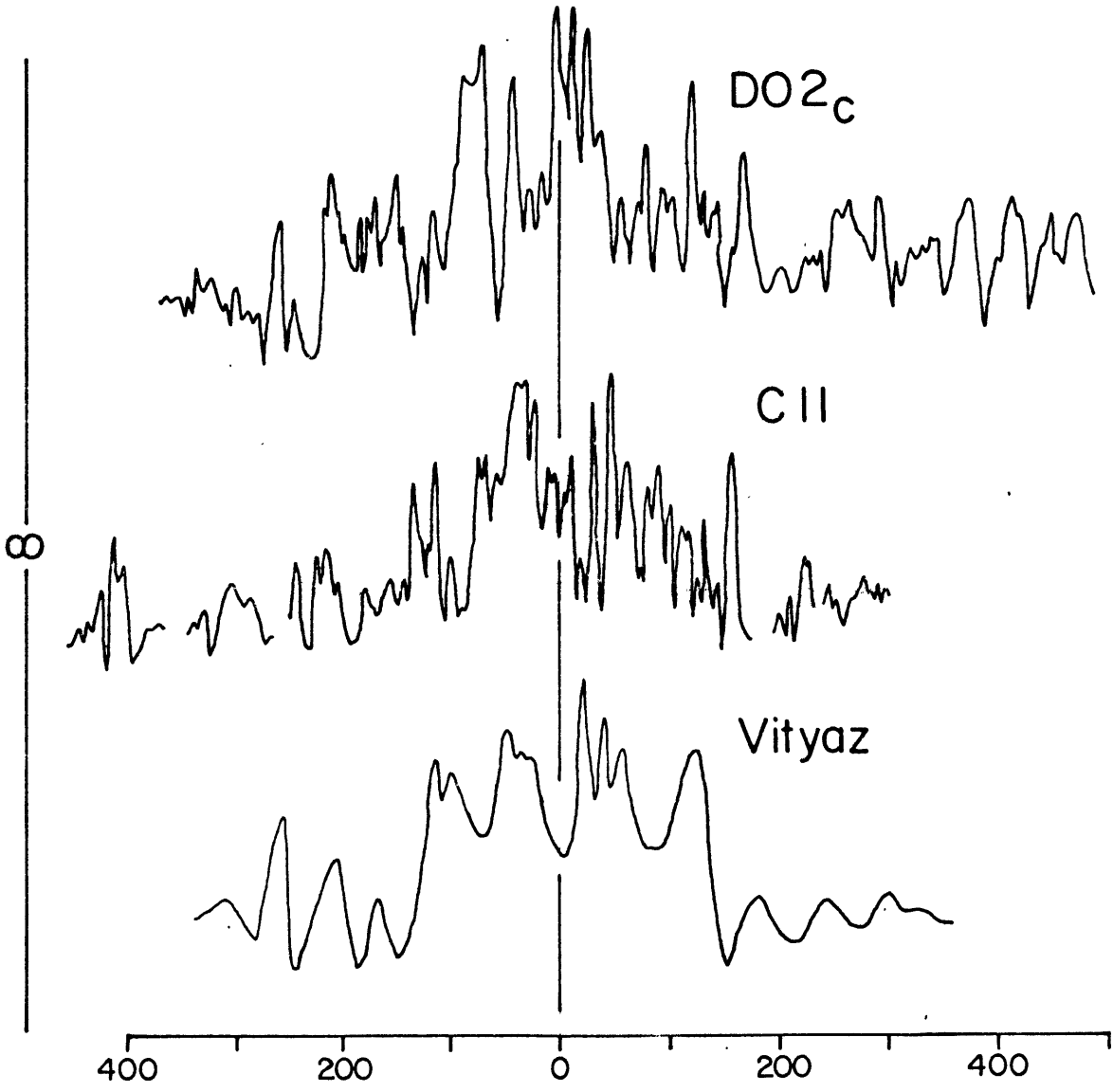


Figure 16d: Profiles from the Western Indian Ocean. Profiles OW8-11 to V20 are from the Central Indian Ridge, profiles CI5 to GC26 are from the Southeast Indian Ridge, and profiles D02<sub>c</sub> to Vityaz are from the Southwest Indian Ridge. Most profiles are from McKenzie and Sclater (1971). Profiles are arranged from north to south.





123





meters and kilometers in the figures have been converted from fathoms and nautical miles using the conversion factor of 1.83.

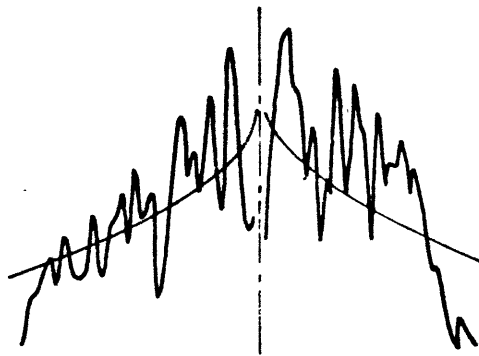
### Projection of the Profiles

Digitally acquired bathymetric data were projected onto the local spreading directions defined by small circles associated with the relevant plate rotation poles as given by Minster et al (1973) in the manner described by Trehu (1975). The projection of the profiles minimizes the possible effects of anisotropy in the sea-floor relief for the estimates of sea-floor roughness. The projection method requires a knowledge of the configuration of the plate boundaries. The plate boundaries in the Atlantic were determined from detailed Navy bathymetric data (J.D. Philips, personal communication). Bathymetric charts by Mammerickx et al (1974) and Molnar et al (1975) were used for the Pacific and maps by McKenzie and Sclater (1971) for the Indian Ocean.

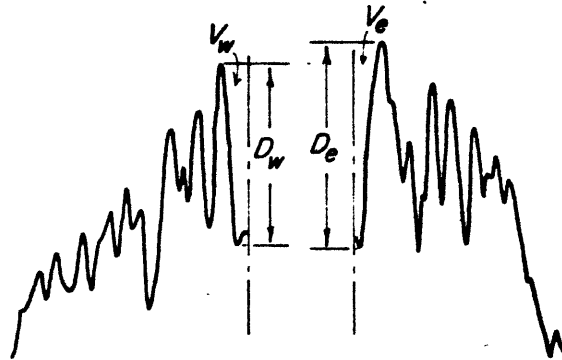
### 2.3 Definition of Median Rift and Central High Dimensions

The dimensions of median rifts and central highs can be measured in a number of ways (Figure 17). For rifted mid-ocean ridges, the most convenient rift dimension to measure is the rift depth defined as the difference in depth between the highest point in the rift mountains and the deepest point in the median rifts. The rift depths defined in this way can be measured in bathymetric profiles that have not been projected onto the local spreading directions so that a wide variety of

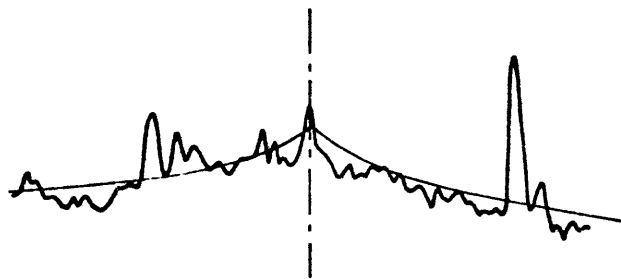
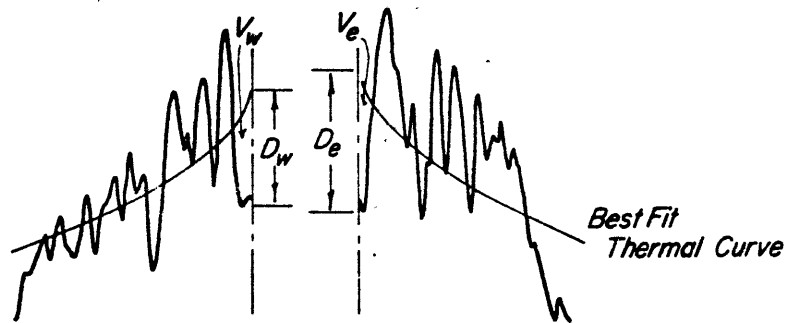
Figure 17: The ways median rift and central high dimensions can be defined. Rift volumes defined relative to the rift mountain peaks are proportional to the buoyancy forces that cause the elimination of rift relief at the rift margins in the model by Tapponnier and Francheteau (1978). Rift and central high dimensions relative to the thermal curves, i.e. the depth versus square root of age curve, should ideally reflect the regional isostatic level.



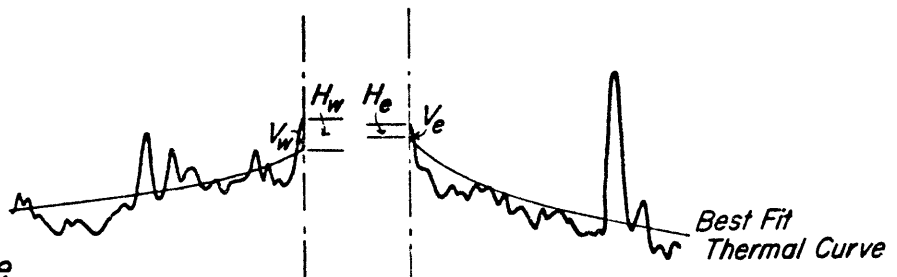
*Rift Dimensions  
Relative to  
Rift Peaks*



*Rift Dimensions  
Relative to  
Thermal Curve*



*Median High  
Dimensions  
Relative to  
Thermal Curve*



*V=Volume, D=Depth, H=Height, e=east, w=west*

data sources can be used. Each ridge crest profile gives two rift depth values; one for each flank of the median rift. The rift volume per unit length of ridge crest can be defined as the cross-sectional area of the rift below the tops of the adjacent rift mountain peaks. The rift volumes need to be measured from projected profiles of ridge crests. Each ridge crest profile also gives two half-rift volumes.

Lachenbruch (1973) has defined rift dimensions relative to the regional isostatic level. The rift depth would be the depth difference between the depth of the median rift and the regional isostatic level. The rift volume per unit length of ridge crest would be the area under the isostatic level from the spreading axis out to where the sea-floor first exceeds this level. For spreading centers with central highs, the height of the central high would be the elevation of the spreading axis above the regional isostatic level and the volume per unit length of ridge crest of the central high the area above the isostatic level from the spreading axis out to where the sea-floor first subsides below the isostatic level.

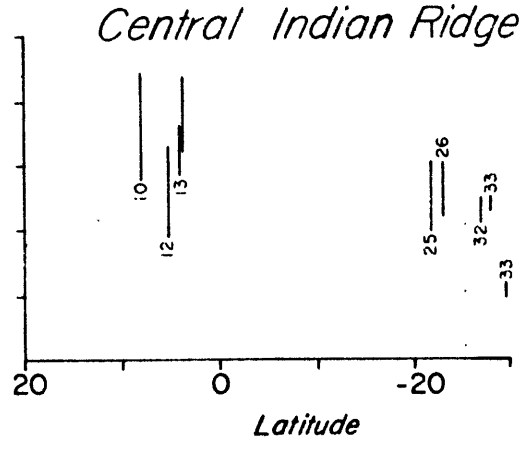
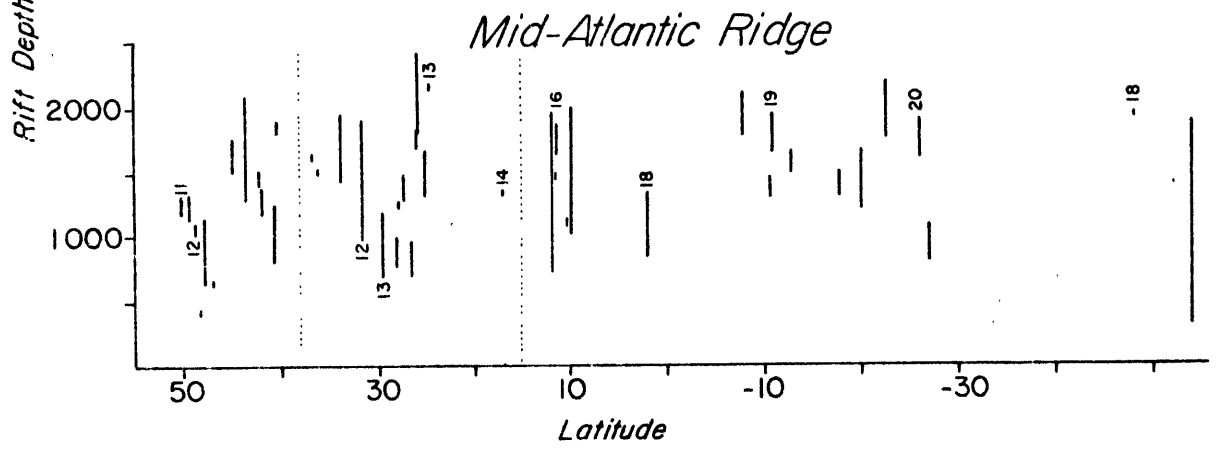
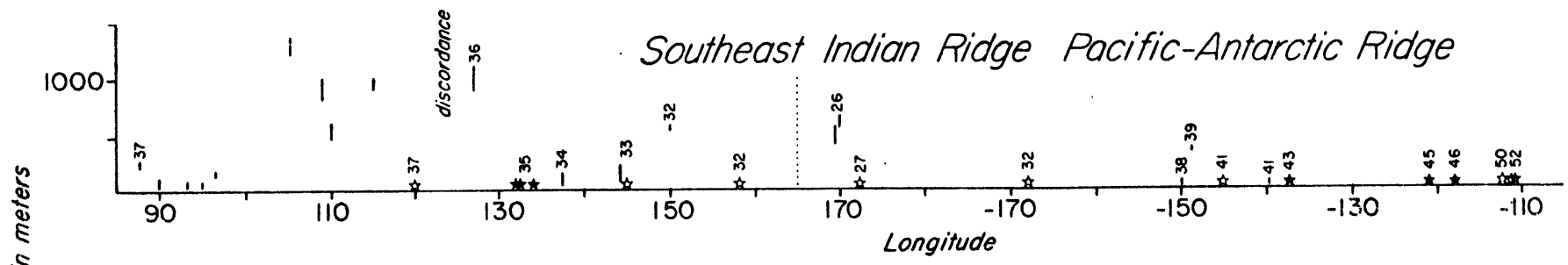
#### 2.4 Dimensions of Median Rifts Defined Relative to the Adjacent Rift Mountain Peaks

The rift depths defined relative to the adjacent rift mountain peaks were measured for profiles from the MAR, the PAR/Southeast Indian Ridge, and the Central Indian/Southeast Indian Ridges based on data from McKenzie and Sclater (1971),

Hayes et al (1969; 1972; 1975; 1976; 1977; 1978), Heirtzler et al (1969), van Andel et al (1971), van Andel and Bowin (1968), Rona et al (1976), Sclater et al (1976), and the profiles compiled for this study in digital form. Figure 18 shows the rift depths and Table II gives the means and standard deviations of the rift depths for data from the Atlantic, eastern and western Indian Oceans separately, and for data from the different oceans together. Best fit relationships between rift depths and spreading rates were calculated by least squares. The coefficient of correlation provides a measure of how well the rift dimensions are linearly related to spreading rate.

Figure 18 and Table II show that the relationship between the depth of median rifts and spreading rate is not simple. Though when the data from the different oceans are considered together a correlation between rift depth and spreading rate is evident, the correlation is sometimes not very clear for data from individual oceans. The data from the MAR actually show a slight positive correlation between spreading rate and rift depth though the coefficient of correlation is very low. The values from the Southeast Indian Ridge south of Australia and PAR also show little relationship between rift depths and spreading rate. There is a good inverse correlation between median rift depths with spreading rate along the Central Indian/Southeast Indian Ridges. It is possible that the rift depths can be correlated with spreading

Figure 18: The depth of median rifts defined as the depth between the rift axes and the adjacent rift mountain peaks. Vertical bars span the difference for the values obtained from opposite flanks of each rift. Dotted lines show the locations of triple junctions. Small numbers are spreading rates in mm/yr half-rate determined from rotation poles and rates given by Minster and Jordan (1978). Closed stars are for ridge crests with well defined central highs and open stars for ridge crests with poorly defined central highs. The "discordance" zone is an area of disturbed sea-floor topography defined by Weissel and Hayes (1974).



★ well defined central highs      ☆ poorly defined central highs

Table II: Rift Depths and Volumes Relative to the Adjacent Rift Mountain Peaks

	Mean	Standard Deviation	Least Square Fit		Coefficient of Correlation
			y-Intercept	Slope	
MAR Rift Depths	1364 m	466 m	933 m	30 m/mm/yr	0.18
Central Indian/ SE Indian Ridge Rift Depths	1274	468	2057	-35	-0.68
SE Indian Ridge/ PAR Rift Depths	487	375	728	-7	-0.10
All Rift Depths	1121	581	1832	-33	-0.62
MAR Rift Volume*	11.4 $\frac{\text{km}^3}{\text{km}}$	7.9 $\frac{\text{km}^3}{\text{km}}$	25.7 $\frac{\text{km}^3}{\text{km}}$	-0.9 $\frac{\text{km}^3/\text{km}}{\text{mm/yr}}$	-0.35

\*Rift volumes expressed in terms of  $\text{km}^3$  per km of ridge axis.



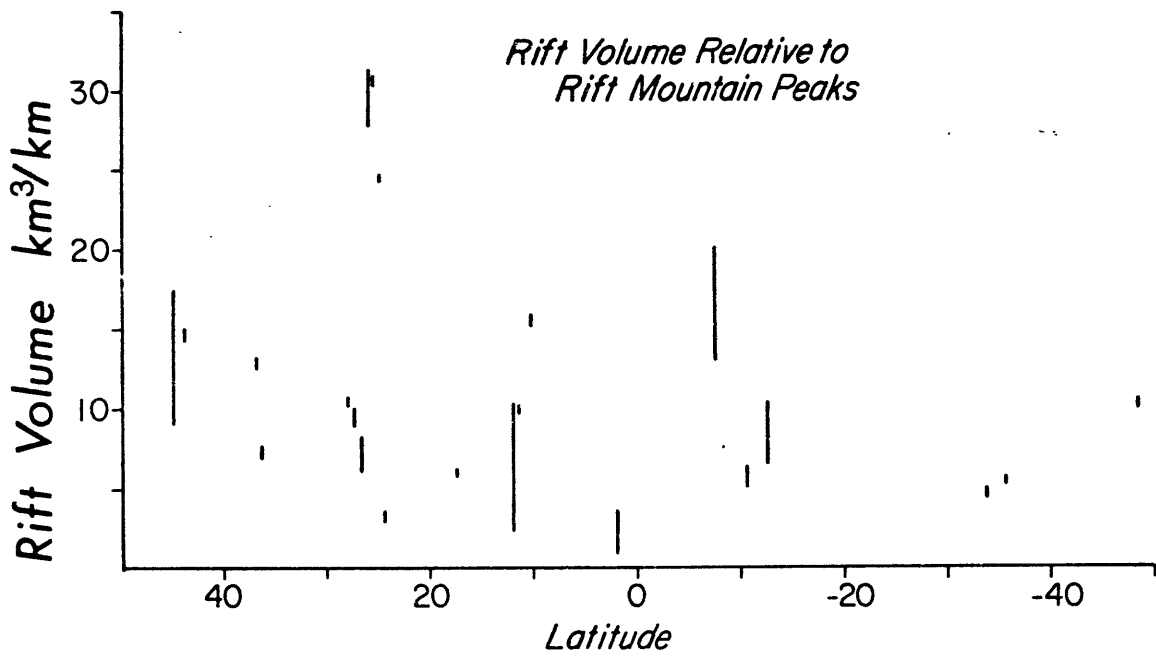
rate in the western Indian Ocean because a greater range of spreading rates is covered there. Also, the data show the rift depth at a particular spreading rate along one rift system is not necessarily comparable to those along other rift systems. For example, the Central Indian Ridge and the Southeast Indian Ridge in the vicinity of the Indian Ocean Triple Junction are spreading at between 25 and 30 mm/yr. However, the median rifts there are significantly deeper than those along the eastern end of the Southeast Indian Ridge and portions of the PAR spreading at similar rates.

The volume of half-rifts per unit length of ridge crest measured relative to the adjacent rift mountain peaks tabulated from projected profiles of the MAR is shown in Figure 19. Table II lists the statistics of the data. The results show there is a trend of smaller rift volumes toward the fast spreading South Atlantic. However, the scatter in the values is quite large and is reflected in the rather low coefficient of correlation.

## 2.5 Dimensions of Median Rifts and Central Highs Relative to the Best Fitting Depth Versus Square Root of Age Curve Establishment of the Regional Isostatic Level

Sclater and Francheteau (1970) showed that the general deepening of the sea-floor away from spreading axes can be explained by the conductive cooling of the lithosphere. As the lithosphere cools, the sea-floor should deepen as a

Figure 19: Median rift half-rift volumes defined relative to the adjacent rift mountain peaks along the MAR.



function of the square root of age (Davis and Lister, 1974). If the oceanic lithosphere is free of other relief modifying processes, then the depth versus square root of age curve would describe the isostatic level of the sea-floor. Though it is known that other processes affect sea-floor relief, including hydrothermal cooling of the lithosphere, formation of fine-scale tectonic relief, and large scale depth anomalies (Sclater and Klitgord, 1973; Crane and Normark, 1977; Cochran and Talwani, 1978; Menard and Dorman, 1977), only the conductive component of sea-floor relief is easily estimable. Therefore, the depth versus square root of age relationship was used as a first order approximation of the isostatic level at ridge crests.

#### Fitting Depth Versus Square Root of Age Curves

Straight lines were fitted to plots of depth versus the square root of age of the sea-floor using data acquired in digital form. The depth points were sampled at even 3.66 km intervals from the projected profiles. In the Pacific, the age of the sampled points was calculated using the spreading rates given by Minster and Jordan (1978) back to anomaly 3 time or about 5 mybp. The analyses were truncated at this age due to major changes in the spreading patterns at that time (Sclater et al, 1971; Molnar et al, 1975; Handschumacher, 1976). Depth points closer than 37 km from the spreading axes were not used in the analyses because ridge crest relief may be significantly affected by processes other than the

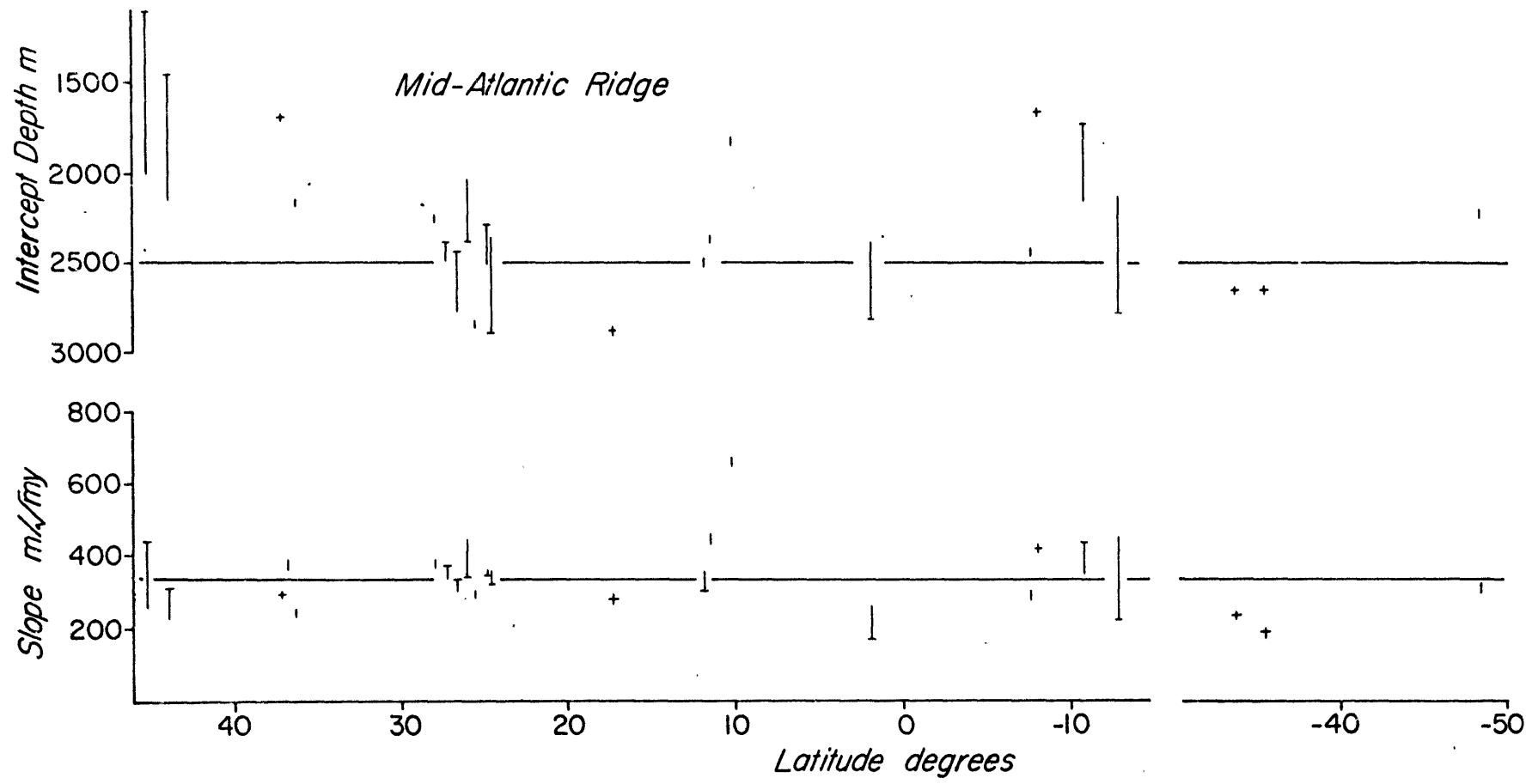
conductive cooling of the lithosphere. In the North Atlantic, the spreading rates given by Laughton et al (1975) and Pitman and Talwani (1972) were used. The analyses were limited to data for sea-floor up to 880 km from the spreading axes and data closer than 146 km from the spreading axes were not used. The present spreading rates given by Minster and Jordan (1978) were assumed out to 880 km from the spreading axes for the South Atlantic. Portions of profiles that contain obvious fracture zones were also not used. Figure 16 shows the portions of the profiles that were used. The parameters of the best fitting depth versus square root of age curves are shown in Figure 20.

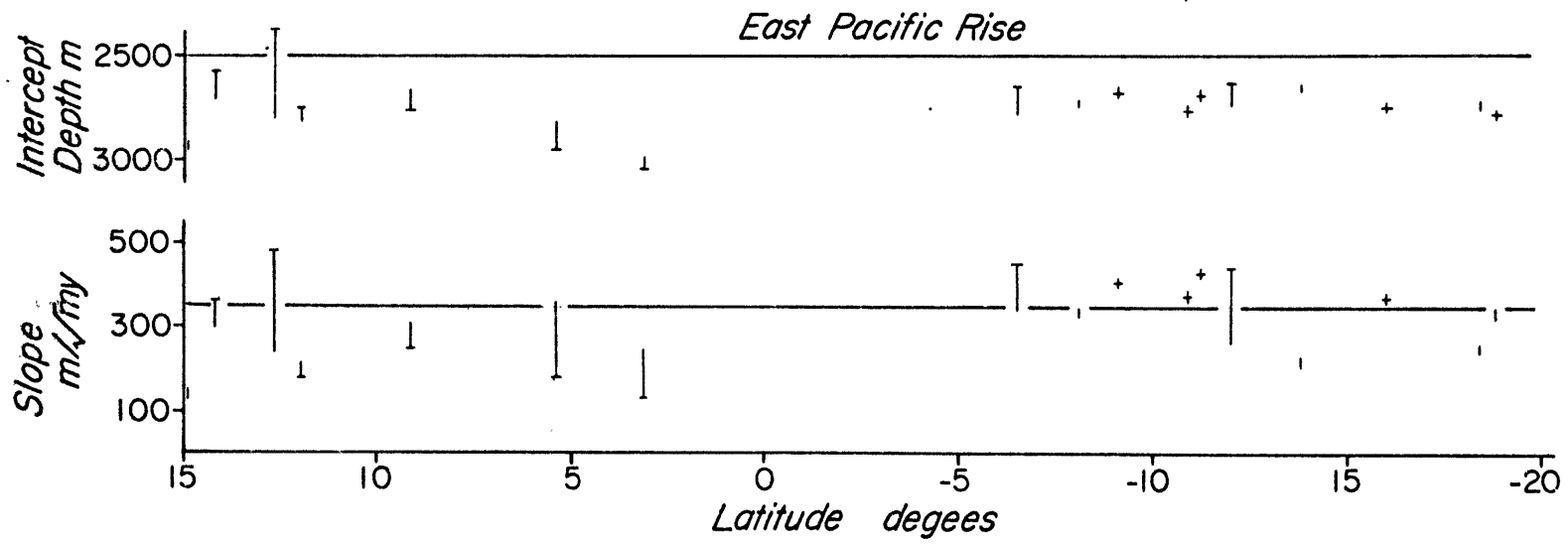
#### Patterns in the Fitted Depth Versus Square Root of Age Curves

The mean for the slopes of the best fitting depth versus square root of age curves is 319 m/sqrt(my) for the MAR and 301 m/sqrt(my) for the EPR. The standard deviations are 72 m/sqrt(my) and 96 m/sqrt(my) for the MAR and EPR respectively. The means for the intercept depths are 2179 m and 2754 m for the Atlantic and Pacific. These values can be compared to the averages of  $342 \pm 65$  m/sqrt(my) for the Atlantic and  $354 \pm 30$  m/sqrt(my) for the Pacific found by Parsons and Sclater (1977). They found the mean intercept depth to be 2500 m for both the Atlantic and Pacific Oceans.

The large standard deviations in the parameters of the depth versus square root of age curves reflect the significant scatter in the results. Figure 20 also shows there can be

Figure 20: The intercept depths and slopes of the best fitting depth versus square root of age curves for profiles from the Atlantic and Pacific. Longer vertical bars span the values from opposite flanks of ridge crests for profiles that cross spreading axes. Short vertical bars and +'s show values where data from only one flank are available. T's and +'s are for values from the eastern flanks. Horizontal lines show whole ocean averages from Parsons and Sclater (1977). Portions of the profiles used to calculate the depth versus square root of age curves are shown in Figure 16.







significant variability even over small areas such as between  $20^{\circ}$  and  $30^{\circ}$ N along the MAR. Such scatter raises the question of whether these fitted curves can successfully approximate the regional isostatic level.

Dimensions of Median Rifts and Central Highs Defined Relative to the Best Fitting Depth Versus Square Root of Age Curves

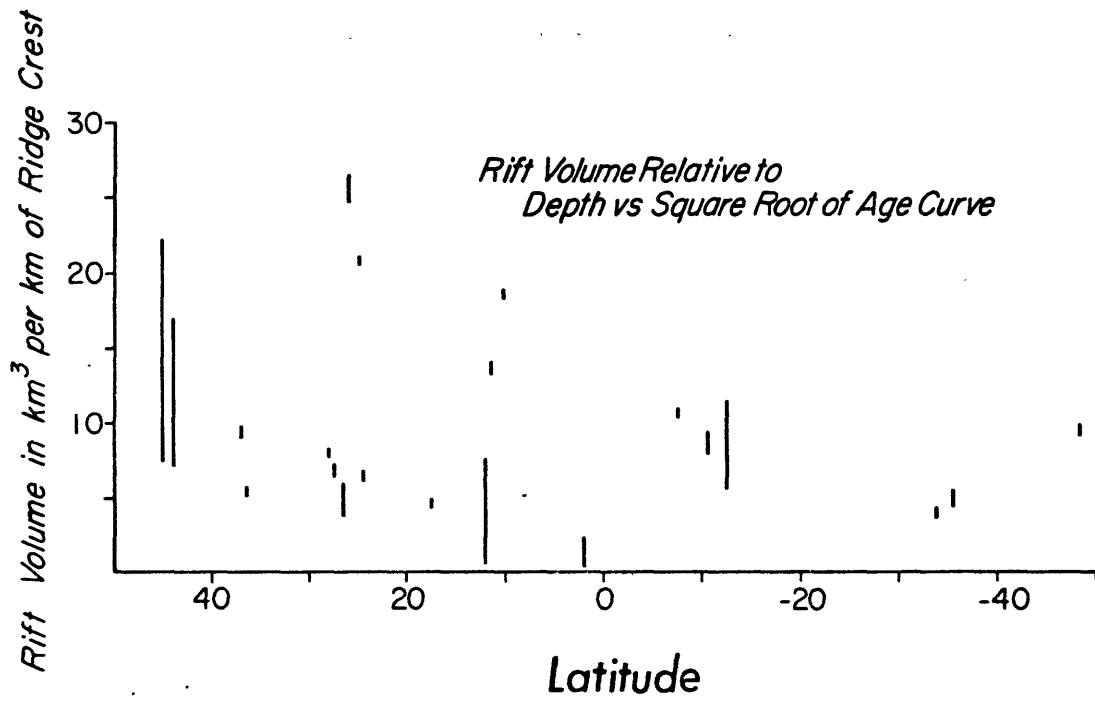
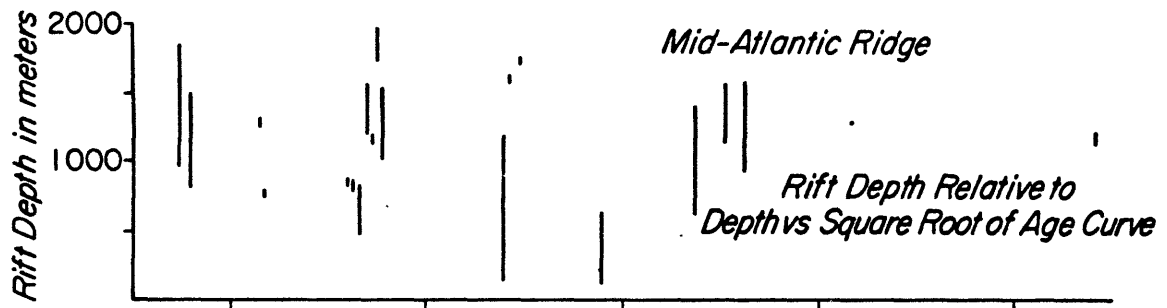
Results from the tabulation of median rift depths and volumes along the MAR and the central high heights and volumes along the EPR relative to the best fitting depth versus square root of age curves are shown in Figure 21 and Table III. The low correlation coefficients show that within the resolution of the data set, there is little relationship between ridge crest dimensions and spreading rate when the MAR and EPR profiles are considered separately. The volume of central highs along the EPR is actually weakly inversely correlated with spreading rate. This is contrary to the expected relationship between the volume of central highs and spreading rate (Lachenbruch, 1973). When the dimensions of median rifts and central highs along the MAR and EPR are considered together, there are better correlations between ridge crest dimensions and spreading rate.

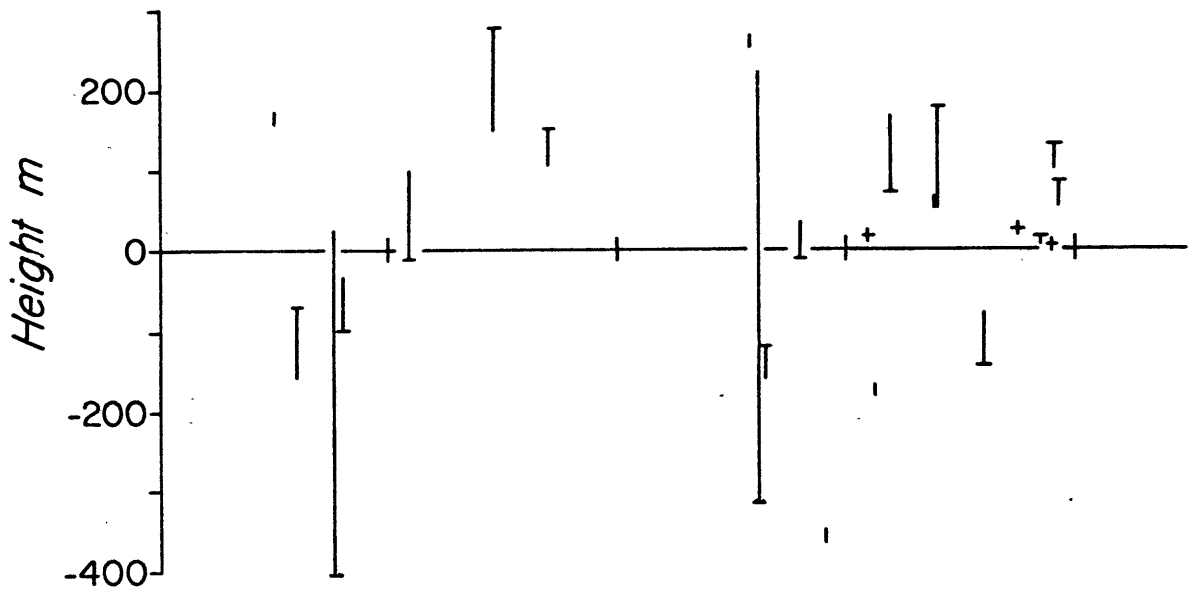
## 2.6 Source of Variability in Ridge Crest Dimensions

Fitting of Depth Versus Square Root of Age Curves Between  $20^{\circ}$  and  $30^{\circ}$ N Along the MAR

Whether median rift dimensions are measured relative to

Figure 21: Rift and central high dimensions relative to the best fitting depth versus square root of age curves based on the projected surface ship profiles shown in Figure 16. For profiles where the best fitting subsidence curve lies above the rift mountain peaks or the central highs, no rift or central high volume is defined. Vertical bars span values obtained from opposite flanks of ridge crests.





*East Pacific Rise*

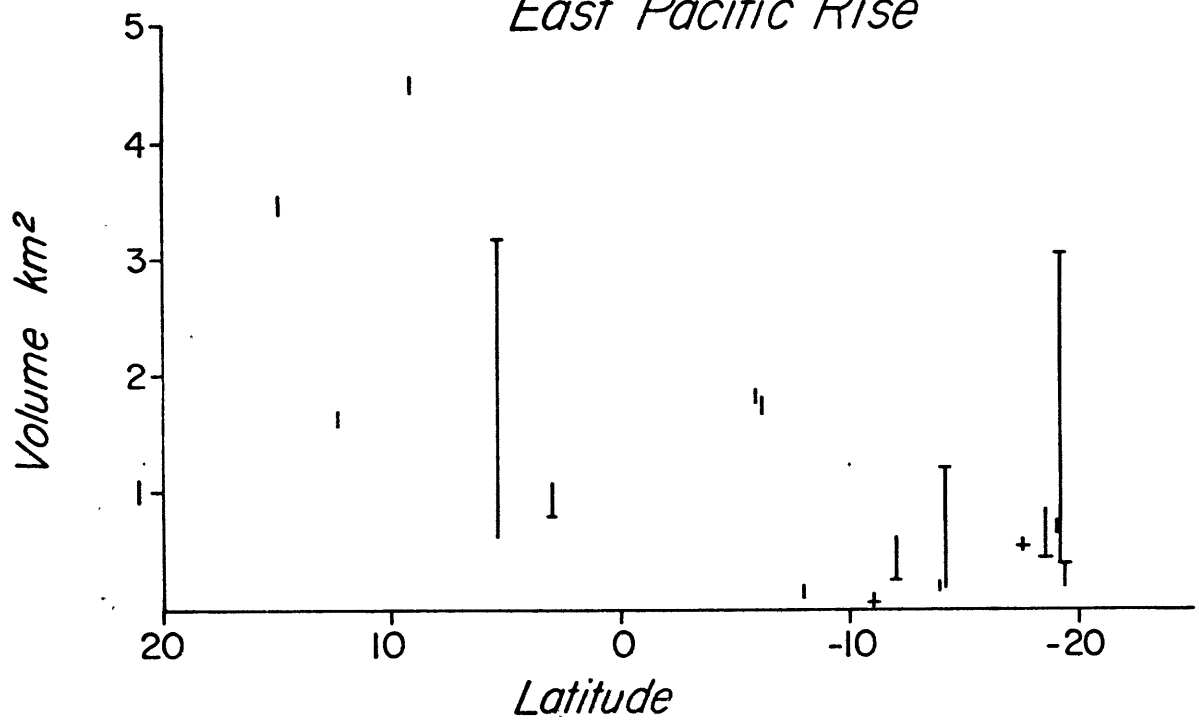


Table III: MAR Rift and EPR Central High Dimensions Defined Relative to the Best Fitting Depth Versus Square Root of Age Curves

	Mean	Standard Deviation	Least Square Fit		Coefficient of Correlation
			y-Intercept	Slope	
MAR Rift Depth*	-1056 m	462 m	-1512 m	30 m/mm/yr	0.20
MAR Rift Volume*	-10.5 km <sup>3</sup> /km	7.0 km <sup>3</sup> /km	-19.5 km <sup>3</sup> /km	.6 $\frac{\text{km}^3/\text{km}}{\text{mm/yr}}$	0.25
EPR Central High Height	15 m	160 m	-167 m	3 m/mm/yr	0.18
EPR Central High Volume	1.1 km <sup>3</sup> /km	1.2 km <sup>3</sup> /km	5.0 km <sup>3</sup> /km	-.05 $\frac{\text{km}^3/\text{km}}{\text{mm/yr}}$	-0.53
MAR & EPR Ridge* Crest Height	-491 m	634 m	-1278 m	17 m/mm/yr	0.83
MAR & EPR Ridge Crest Volume	-5.6 km <sup>3</sup> /km	7.9 km <sup>3</sup> /km	-12.8 km <sup>3</sup> /km	0.2 $\frac{\text{km}^3/\text{km}}{\text{mm/yr}}$	0.71

\* Ridge crest depths and volumes below the best fitting depth versus square root of age curves are negative. Depths and volumes above the best fitting depth versus square root of age curves are positive.

the adjacent rift mountain peaks or the best fitting depth versus square root of age curves, no clear relationship with spreading rate could be established. The same is true of central high dimensions relative to the depth versus square root of age curves. When the depth versus square root of age curves are used as the reference level from which rift and central high dimensions are measured, the resulting values are quite sensitive to the parameters of the subsidence curves. There is the possibility that no clear relationship between ridge crest dimensions and spreading rate could be found because the measured depth versus square root of age curves do not adequately represent the regional isostatic level. For example, the calculated depth versus square root of age rates may be significantly influenced by the numerous small and unidentified fracture zones in the Atlantic. Though the method used to project the profiles before the depth versus square root of age curves were fitted takes into account age discontinuities across identified modern fracture zones, the projection method does not compensate for changes in spreading directions and the formation and elimination of fracture zones.

Detailed bathymetric contour maps of the North Atlantic from the Navy (NAVOCEANO, 1977) show clearly the locations of fracture zones between the equator and about  $30^{\circ}\text{N}$ . The contour maps can be used to construct bathymetric profiles clearly away from fracture zones. A number of profiles between latitudes  $20^{\circ}$  and  $29^{\circ}\text{N}$ , where compiled surface ship

profiles are also plentiful, have been digitized along flow lines between fracture zones from the Navy maps (Figure 22). The bathymetric contours are at even one km and one km plus 600 m depth intervals. The Navy data were processed in the same manner as the surface ship profile data to obtain best fit depth versus square root of age rates. However, the Navy profiles were not projected onto small circles. Figure 23 compares the results from the Navy data with that from the compiled surface ship profile data.

The Navy data show a regional trend of increasing subsidence rates and decreasing intercept depths going from south to north toward the Azores. The mean, standard deviation, and results from fitting straight lines to the parameters of the depth versus square root of age curves as a function of latitude are listed in Table IV. These results show that though the greater Navy data coverage allows the resolution of regional trends, the surface ship data set assembled for this study is too sparse to see such trends. However, it is important to note that the results from the surface ship data are consistent with that of the Navy data. The consistency between the results from the Navy and surface ship profile data suggests the large variability in the parameters of the best fitting depth versus square root of age curves shown in Figure 20 is not due to random errors. Rather, the variability is probably due to regional variations in the subsidence rate of the sea-floor which cannot be resolved by

Figure 22: Location of profiles digitized from Navy bathymetric contour maps of the North Atlantic. Long dashed lines show the location of profiles used to calculate depth versus square root of age curves. Dotted lines show the location of ridge crest profiles shown in Figure 25. Selected depth contours from the Navy maps. Solid circles show the location of the ridge axis.



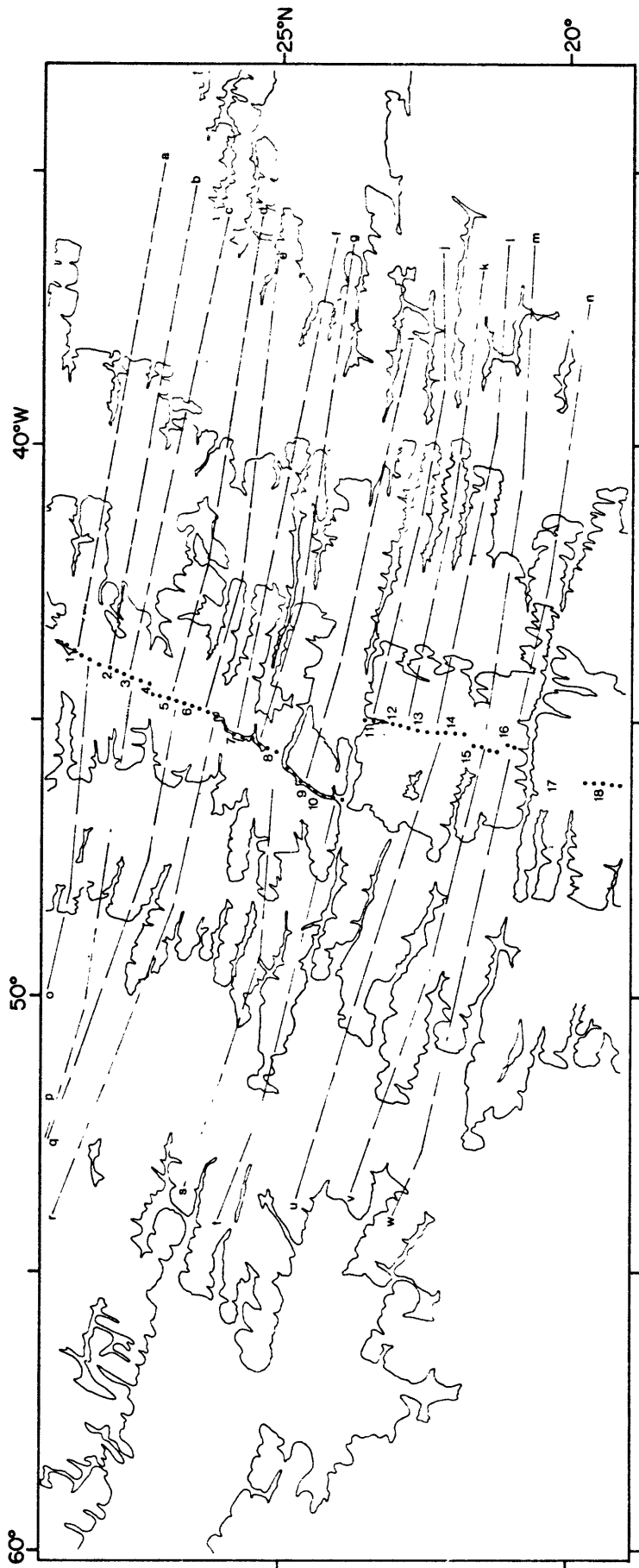


Figure 23: Intercept depths and the slopes of the best fitting depth versus square root of age curves for projected surface ship profiles and profiles digitized from Navy bathymetric maps between  $20^{\circ}$  and  $29^{\circ}$ N in the Atlantic. Circles show the values from the Navy data, squares for results from the projected surface ship profiles. Closed circles and squares are for data from the eastern flank of the Mid-Atlantic Ridge

150

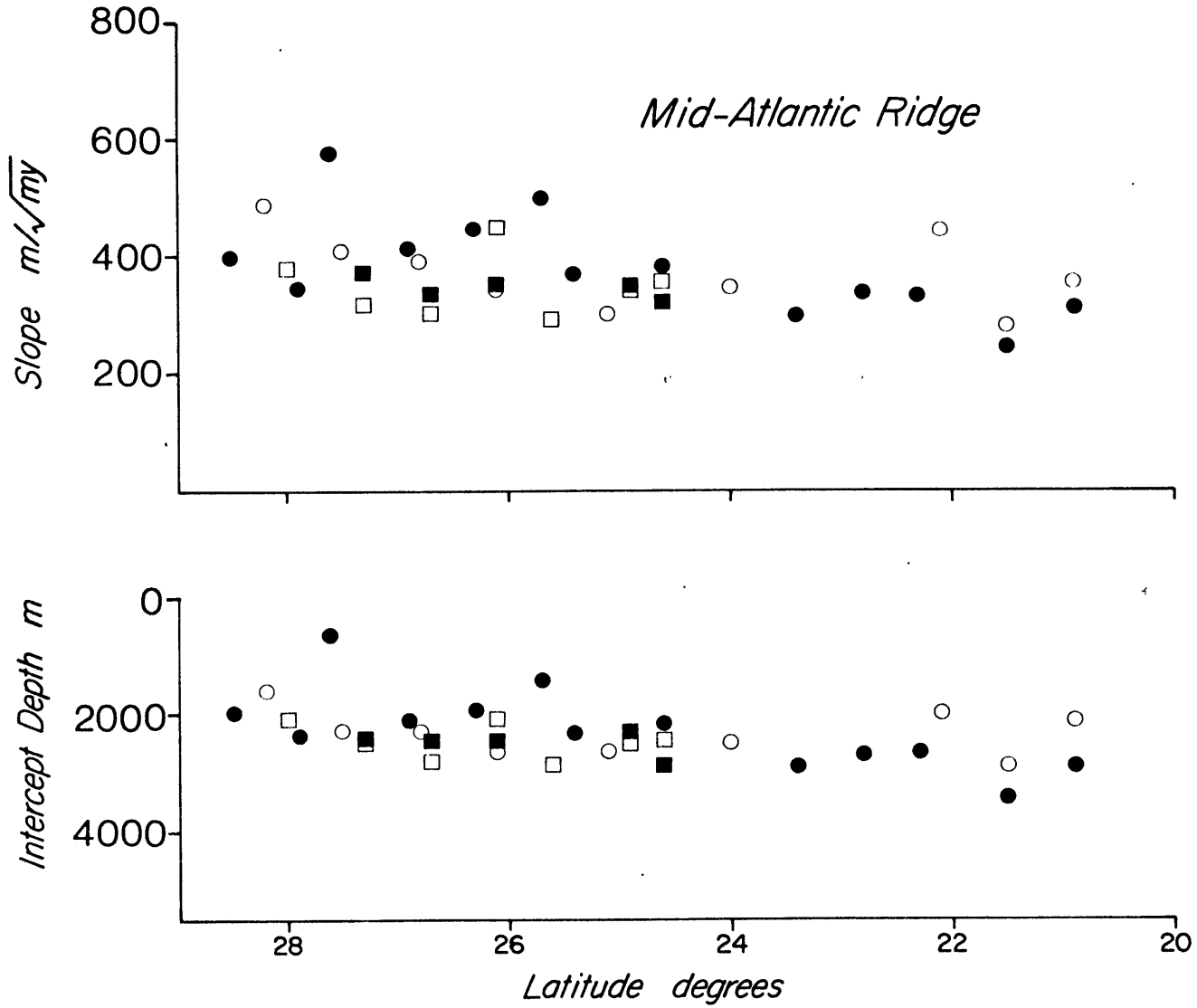


Table IV: Slope and y-Intercept of Best Fitting Depth Versus Square Root of Age Relationship Between 20° and 30°N Along the MAR

	Mean	Standard Deviation	Least Square Fit		Coefficient of Correlation
			y-Intercept	Slope	
Slope Navy Data	378 $\frac{\text{m}}{\text{sqrt}(\text{my})}$	78 $\frac{\text{m}}{\text{sqrt}(\text{my})}$	-63 $\frac{\text{m}}{\text{sqrt}(\text{my})}$	18 $\frac{\text{m}/\text{sqrt}(\text{my})}{\text{deg.lat.}}$	0.58
Slope Surface Ship	350	40	230	5	0.13
y-Intercept Navy Data	2258 m	580 m	5560 m	-133 $\frac{\text{m}}{\text{deg.lat.}}$	-0.58
y-Intercept Surface Ship	2479	252	3856	-53	-0.24

the sparse number of surface ship profiles assembled for this study.

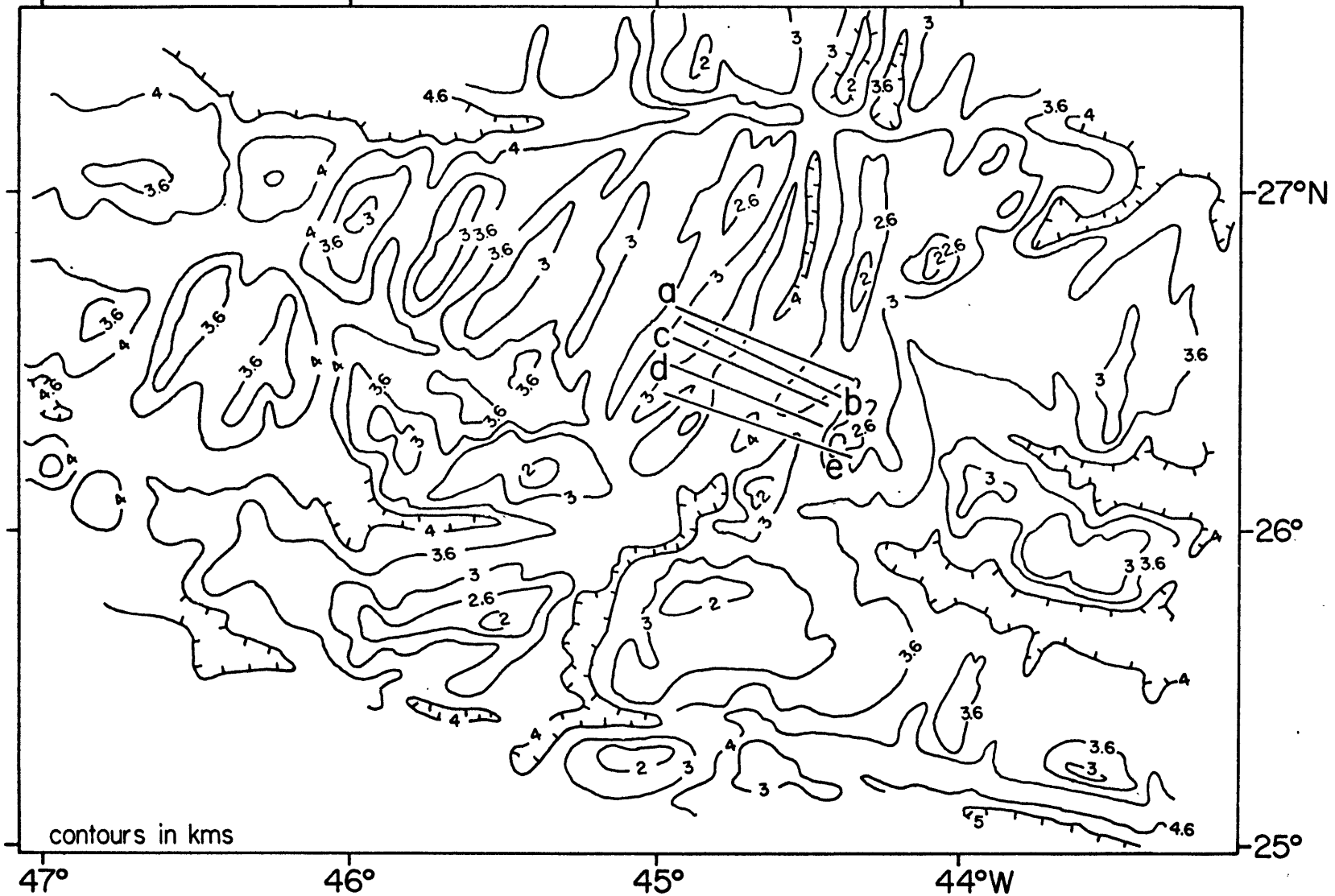
#### Detailed Surveys of the MAR Between 20° and 30°N

To provide some idea of how much the variability in the rift dimensions is independent of spreading rate, a search was made for detailed surveys of the MAR between 20° and 30°N which have profiles collected away from obvious transform faults. As the spreading rate cannot vary greatly over small regions, the variability in rift dimensions over small areas must be attributable to factors other than the spreading rate. Surveys close to transform faults were ignored because median rifts have been observed to deepen near transform faults and thus can contribute to variability to rift dimensions (Macdonald and Luyendyk, 1977; Macdonald et al, 1979b; Lonsdale and Shor, 1979). Figure 24 shows the locations of profiles from surveys reported by van Andel and Bowin (1968) and Rona et al (1976). The locations of the profiles are superimposed on detailed Navy bathymetric contour maps. There are some apparent fracture zone trends in the contour maps that come up to about 100 km from the spreading axis near 23°N and 50 km from the spreading axis near 26°N. However, the depth contours for the rift mountains next to the median rifts are quite continuous along extrapolations of those trends. If there are transform faults along extensions of those trends, the transform offset should be quite small. Ridge crest profiles away from transform faults have also been

Figure 24: Locations of bathymetric profiles from van Andel and Bowin (1968) and Rona et al (1976) superimposed on Navy bathymetric contour maps of the North Atlantic. The profiles are shown in Figure 26.



location of profiles from Rona et al (1976)





digitized from the Navy bathymetric contour maps and they are shown in Figure 25.

Best fit depth versus square root of age curves based on the Navy contour maps are superimposed on the bathymetric profiles in Figures 25 and 26. Figure 26 shows the curves to be well above the observed relief on the east flank of the ridge crest at  $26^{\circ}\text{N}$  but well below the relief on the west flank. Large mis-match between the bathymetry and the fitted subsidence curves are also evident in the profiles digitized from the Navy maps (Figure 25). The sometime extreme mis-match between the fitted subsidence curves and the observed ridge crest relief suggests the depth versus square root of age trends determined from the ridge flank bathymetry do not successfully approximate the regional isostatic level at the ridge crests. But more important, the rift volumes within the  $23^{\circ}$  and  $26^{\circ}\text{N}$  survey areas differ by almost a factor of three at each spreading center regardless of which reference level is used to define the rift dimensions.

It is possible that some of this variability in rift volumes is due to the proximity of transform faults. Navy contour maps consistently show a deepening of median rifts toward transform faults. However, it is not clear how far the effects of the transform fault intersections are felt by the rift relief maintenance processes. The large variability in median rift dimensions even within detailed survey areas suggests there are factors that affect median rift dimensions

Figure 25: Ridge crest profiles digitized from Navy bathymetric maps of the North Atlantic. Dotted lines show extrapolations of the best fitting depth versus square root of age curves also determined from the Navy bathymetric maps. Locations of the ridge crest profiles and the profiles used to calculate the square root of age curves are shown in Figure 22.

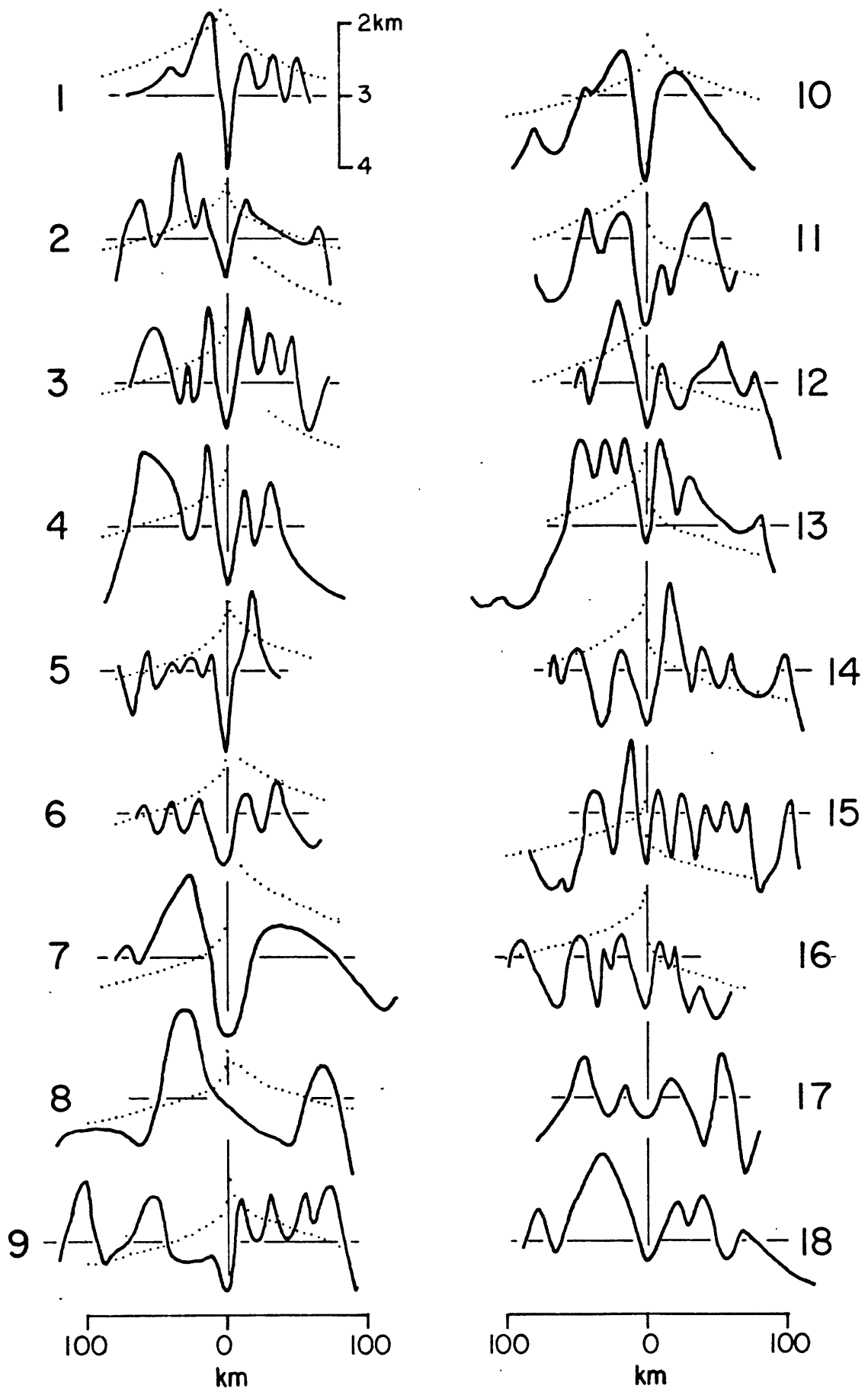
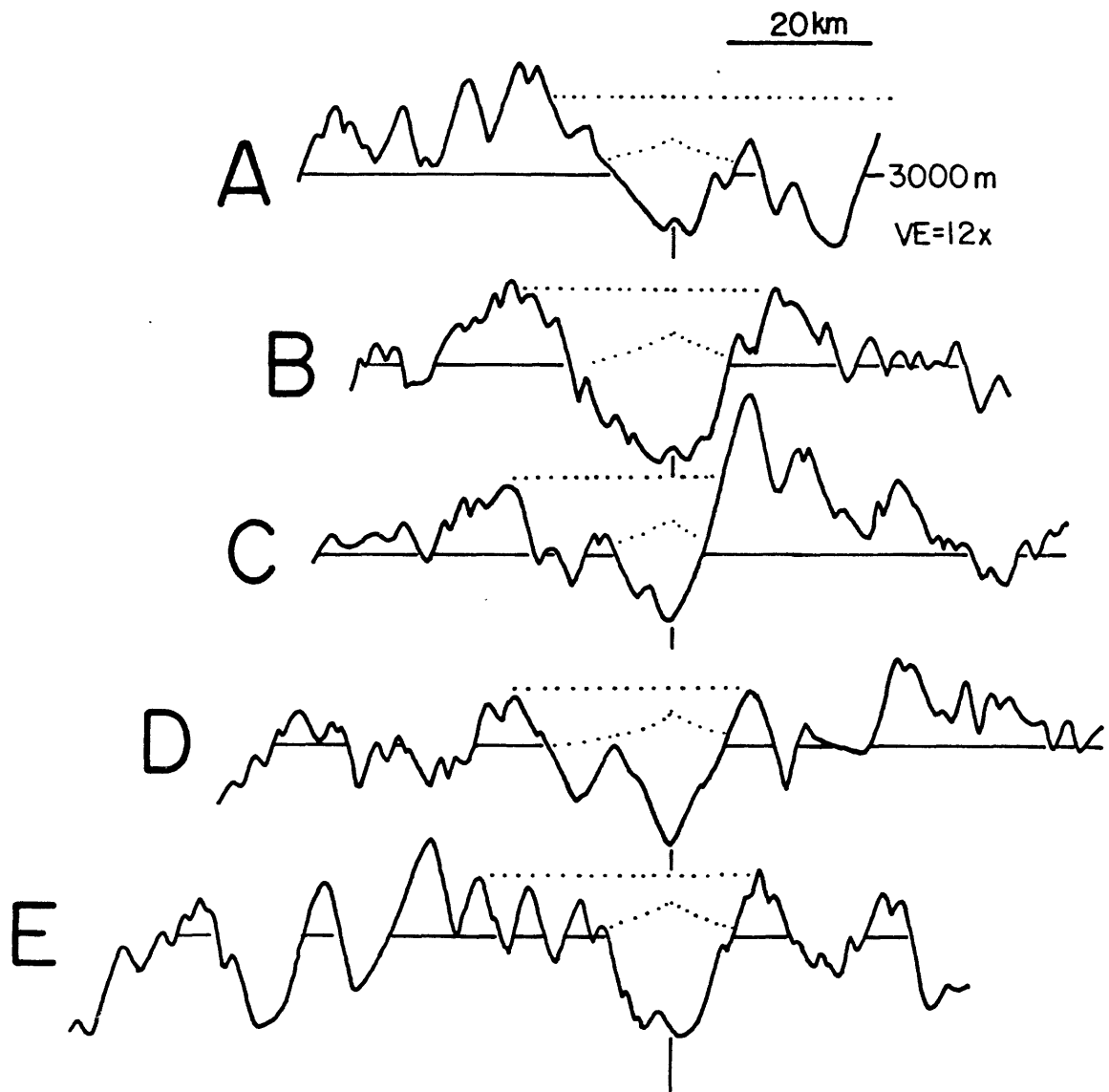
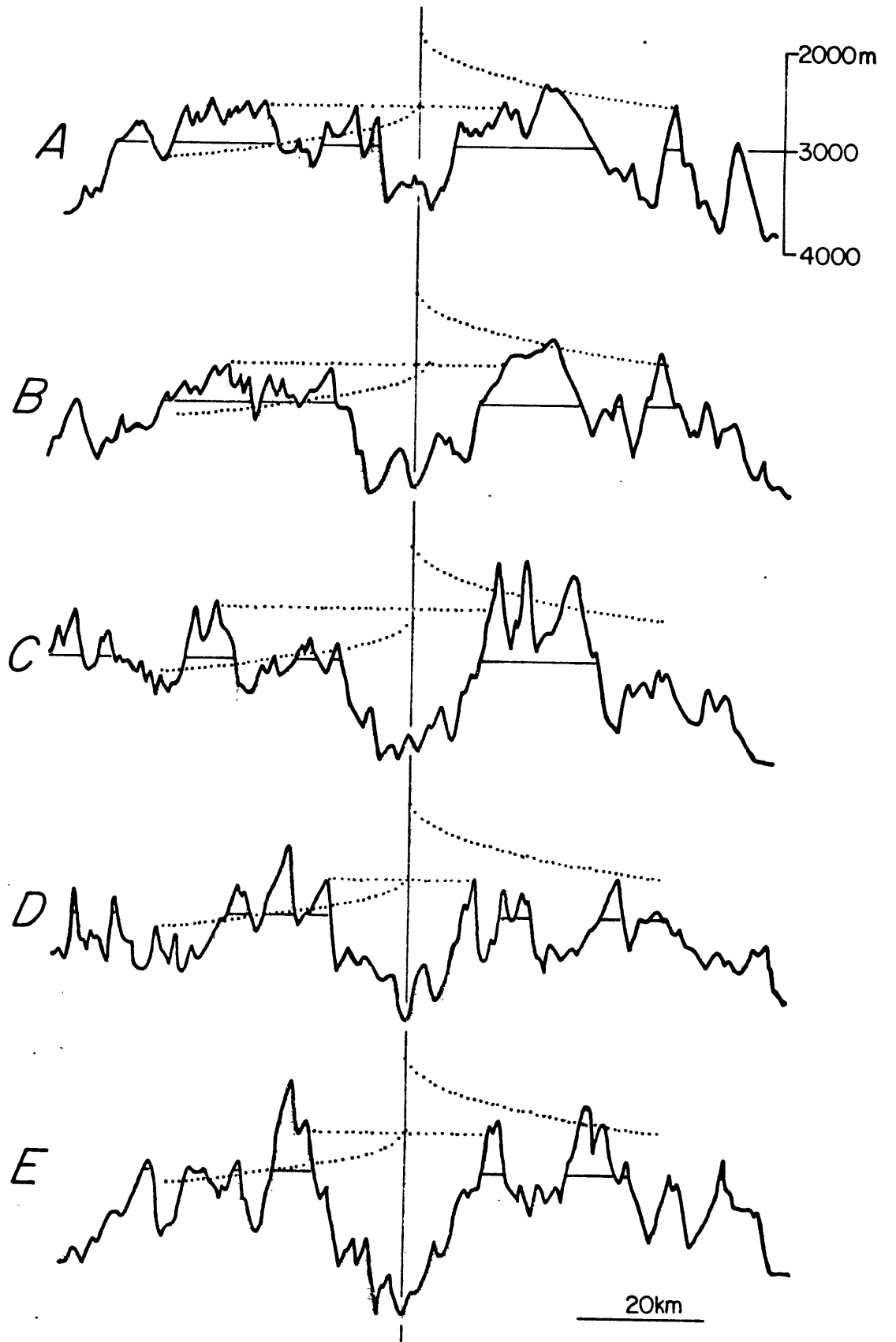


Figure 26: Ridge crest profiles of the Mid-Atlantic Ridge near  $23^{\circ}\text{N}$  and  $26^{\circ}\text{N}$  from van Andel and Bowin (1968) and Rona et al (1976) respectively. Curved dotted lines show the best fitting depth versus square root of age curves derived from Navy bathymetric maps. Horizontal dotted lines show upper estimates of rift volumes relative to the rift mountain peaks. Locations of the profiles shown in Figure 24.



profiles from van Andel & Bowin (1968)



profiles from Rona et al (1976)

other than spreading rate. The width of median valleys in the FAMOUS area vary by a factor of two to four (Macdonald and Luyendyk, 1977) and the variation has been postulated to represent different stages in the evolution of median rifts. Median rifts may widen with sea-floor spreading and then narrow through faulting episodically (Tapponnier and Francheteau, 1978). The possible episodic nature of rift evolution may contribute to the observed variability in rift dimensions.

## 2.7 Roughness of Sea-Floor Relief

### Definition of the Roughness of Sea-Floor Relief

The roughness of sea-floor relief can be defined as the vertical relief between evenly sampled depth points along projected bathymetric profiles divided by the sampling interval. This is the same definition of roughness used in Chapter I for deep tow profiles. Surface ship profiles compiled for this study were sampled at even 3.66 km (2 nautical mile) intervals and the absolute value of the difference in depth between successive points summed. Figure 16 shows the portions of the profiles used to estimate the sea-floor roughness. As in the calculation of the depth versus square root of age curves, data from closer than 37 km from the spreading axes in the Pacific and 146 km in the Atlantic were not used. Also, sea-floor older than about 5 my in the Pacific and further than 880 km from the spreading

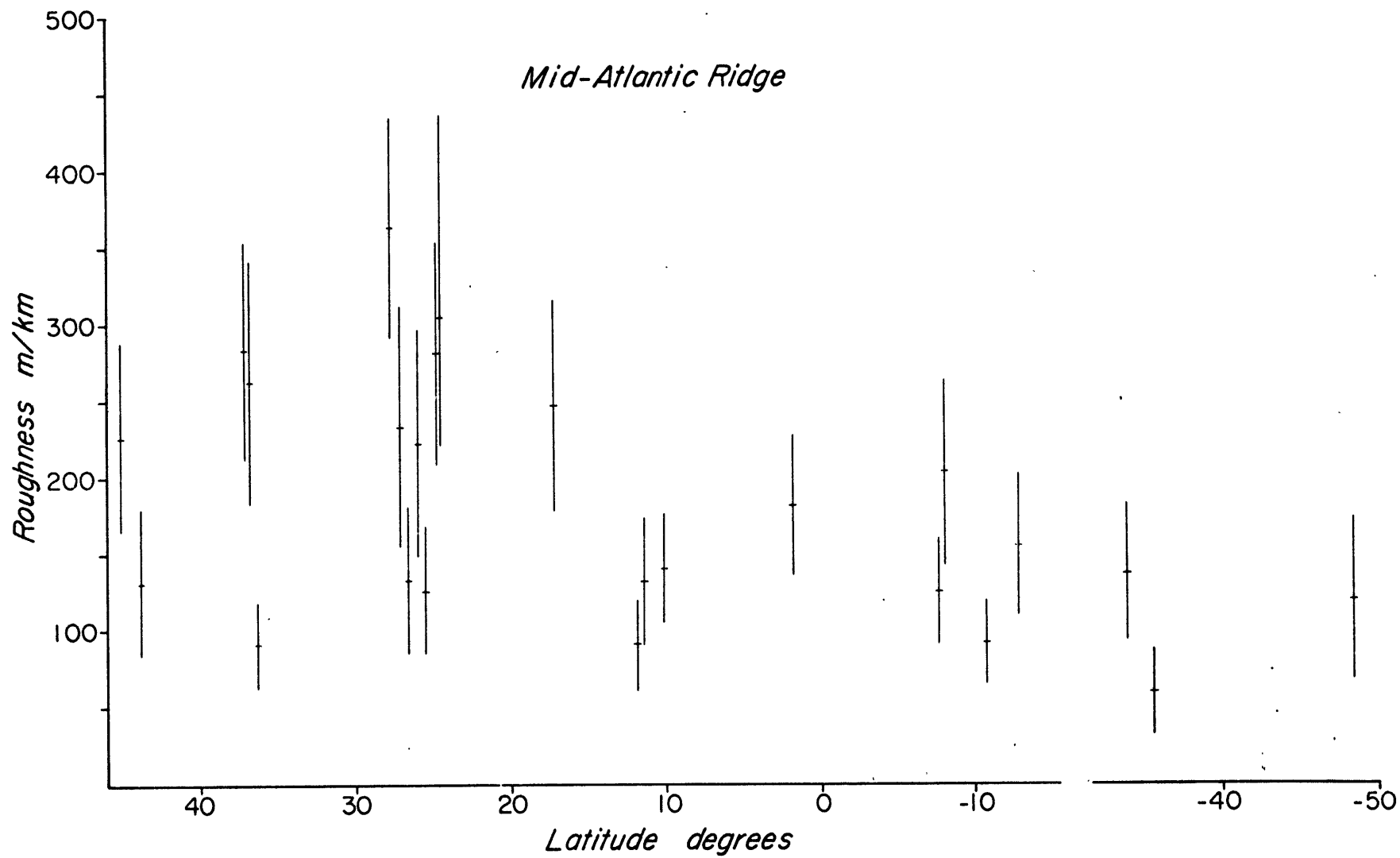
axes in the Atlantic was not considered. The mean and standard deviation of the roughness of the individual profiles are shown in Figure 27. Table V lists the mean, standard deviation, and parameters of the best fit linear relationship between roughness of the profiles and spreading rate for profiles from the Atlantic, the Pacific, and the two oceans together.

#### Roughness of Sea-Floor Relief Versus Spreading Rate

Figure 27 and Table V show there is a detectable correspondance between sea-floor roughness and spreading rate in the Atlantic. The roughness of sea-floor relief decreases with increasing spreading rate. Though the spreading rate ranges from 11 mm/yr to 20 mm/yr for the compiled profiles from the Atlantic today, much of the data used to calculate the roughness of relief is from sea-floor created at spreading rates different from today's. For example, using the Laughton et al (1975) spreading history of the Atlantic north of the Azores, about 69% of the profile length from that part of the Atlantic used in the roughness calculations was created at 10 mm/yr and about 31% at 25 mm/yr. This would give a weighted average spreading rate of 15 mm/yr, if such an average is meaningful. In spite of these changes, the inverse correlation of roughness with spreading rate is probably meaningful, since the South Atlantic also shows rate changes such that it has spread consistently faster than the North Atlantic in the past (Pitman and Talwani, 1972).



Figure 27: Roughness of sea-floor relief estimated in terms of the amount of vertical relief per unit of horizontal distance. The crosses show the mean of the vertical relief for each profile. The vertical bars span one standard deviation on either sides of the means.



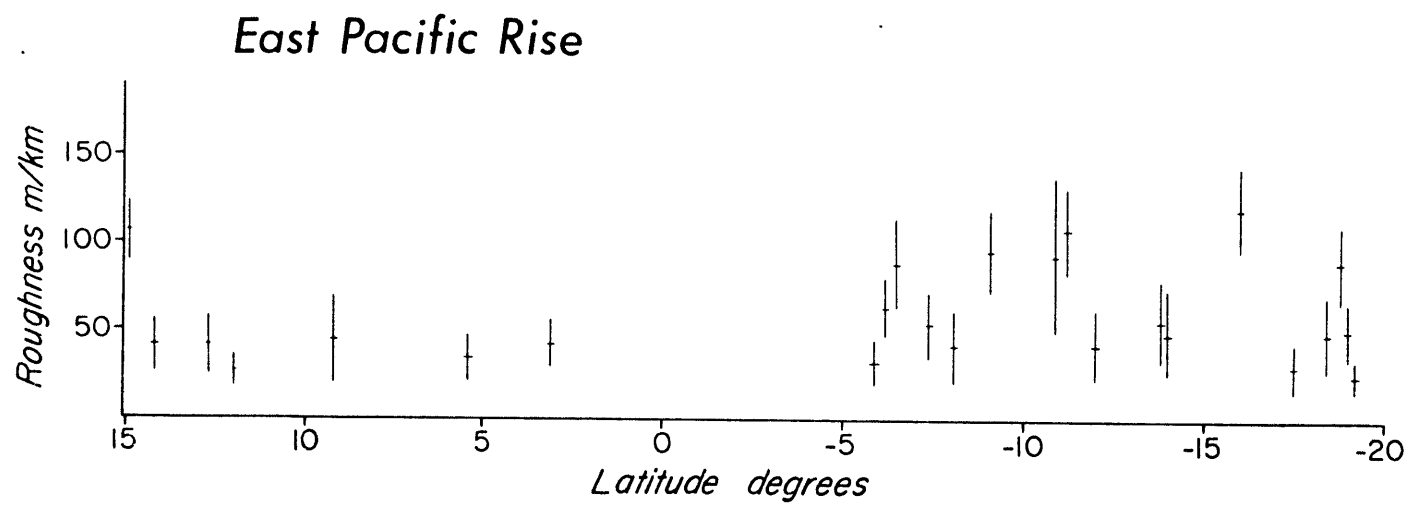


Table V: Roughness of Sea-Floor Relief and Its Relationship With Spreading Rate

	Mean	Standard Deviation	Least Square Fit		Coefficient of Correlation
			y-intercept	Slope	
Atlantic	182 m/km	80 m/km	393 m/km	$-14 \frac{\text{m/km}}{\text{mm/yr}}$	-0.51
Pacific	59	29	34	0.3	0.13
Pacific & Atlantic	121	86	208	-2	-0.71

In the Pacific, there is no clear trend in the roughness of sea-floor relief with spreading rate. The least square linear fit between roughness and spreading rate shows the roughness to be actually weakly correlated with spreading rate. The presence of numerous seamounts in the South Pacific may be the reason for the observed increase in sea-floor roughness there. The seamounts may actually obscure a trend toward lower sea-floor roughness with increasing rate for relief not due to seamounts. However, the roughness estimates for profiles from the South Pacific without seamounts (e.g. profiles 72110806, POL7302<sub>c</sub>, POL7302<sub>d</sub>, 72110803) show the roughness to be no less for sea-floor created at the faster spreading southern EPR than the slower spreading northern EPR. When the MAR and EPR roughness estimates are considered together, an inverse relationship between roughness of sea-floor relief and spreading rate becomes clear.

## 2.8 Summary

Surface ship bathymetric profiles of mid-ocean ridges have been compiled to look for relationships between the roughness of sea-floor relief, the dimensions of median rifts and central highs as a function of spreading rate. The roughness of sea-floor relief is definitely less for sea-floor created along the fast spreading EPR when compared to that created along the slow spreading MAR. An inverse relationship between roughness and spreading rate can also be

seen in the MAR data alone, where the spreading rate ranges from 11 to 20 mm/yr. However, no clear relationship between roughness and spreading rate can be seen in the Pacific where data for sea-floor created at between 50 and 85 mm/yr have been compiled.

There is only a very rough relationship between the dimensions of median rifts and central highs and spreading rate. Again, it is obvious that the slow spreading MAR tends to have median rifts and the fast spreading EPR has central highs. However, no clear correlation between ridge crest relief and spreading rate can be seen along the MAR and EPR individually. The depth and volume of median rifts were defined relative to both the adjacent rift mountain peaks and the best fitting depth versus square root of age curves. The best fitting depth versus square root of age curves were used to approximate the regional isostatic level. The height and volume of central highs were measured relative to the best fitting depth versus square root of age curves.

There is significant variability in the parameters of the depth versus square root of age curves fitted to the ridge crest profiles. To look for the source of the variability, best fit depth versus square root of age curves based on detailed bathymetric contour maps were compared with those derived from the compiled surface ship profiles between 20° and 30°N in the Atlantic. The results suggest a significant portion of the variability in the parameters of

the fitted depth versus square root of age curves is due to regional variations in the subsidence rate of the sea-floor not resolved by the sparse number of surface ship profiles compiled. However, the results from the surface ship profiles are consistent with those from the detailed bathymetric contour maps.

Examination of ridge crest profiles from two detailed surveys of the MAR found the rift volumes to vary by a factor of two to three, regardless of the way the rift dimensions are defined. This large variability in rift volumes over even small areas shows that spreading rate is not the only factor that influences ridge crest relief. Some of the variability may be related to the proximity of transform faults. However, spreading centers with highly asymmetrical ridge crest relief suggest there are important factors other than spreading rate and the proximity of transform faults. It is likely that while ridge crest relief is influenced by spreading rate, as evidenced by the contrast in ridge crest relief between the MAR and EPR, there are other processes which influence ridge crest relief and may be the source of the variability in ridge crest relief independent of spreading rate.

## Chapter III: The Formation of Fine-Scale Sea-Floor Relief at Mid-Ocean Ridges

### 3.1 Introduction

In Chapter I, analysis of deep tow data from spreading centers showed there are axial zones of low tectonic relief bordered by zones of increasing relief. The extent of tectonic activity was estimated by looking for the place where the relief matures to the scale of sea-floor relief well away from spreading centers. The extent of tectonism was measured in terms of the plate boundary width and the plate boundary width was appreciably wider only for the slow spreading MAR. When the extent of tectonic activity is expressed as the age of the sea-floor to which tectonism occurs, the age is considerably greater for the slow spreading MAR. Measurement of the roughness of sea-floor relief using deep tow data showed the relief created at fast spreading centers to be not significantly less than that created at slow spreading centers, contrary to the results from using surface ship data. The apparent contradiction was suggested to be due to the formation of more short wavelength/small amplitude relief at faster spreading centers.

Tapponnier and Francheteau (1978) suggested that the size of median rifts is limited by the strength of the lithosphere. When the buoyancy forces due to the relief of median rifts become sufficiently large to deform the



lithosphere, tectonic activity will occur to reduce the rift relief until the buoyancy forces become supportable by lithospheric strength. This idea of buoyancy forces limiting the size of sea-floor relief can be extended to faster spreading centers. Sea-floor relief, whether median rift relief or abyssal hill relief on the flanks of spreading centers, imposes buoyancy forces on the lithosphere. If this is so, then the nature of the roughness of sea-floor relief could be explainable by the strength of the lithosphere at the site where the relief is added to the sea-floor. Large scale sea-floor relief can be formed and supported in older and thus stronger lithosphere within the zone of tectonic activity at slow spreading centers such as the MAR. At faster spreading centers, tectonic activity is confined to younger and thus weaker lithosphere. Large scale sea-floor relief cannot be formed and preserved due to the weakness of the lithosphere there.

In this chapter, the lithospheric strength near spreading centers will be estimated following Tapponnier and Francheteau (1978) and Goetze and Evans (1979) based on laboratory measurements of rock strengths and models of the thermal field near ridge axes by Sleep (1975). The bathymetric profiles of ridge crests compiled in Chapter I will be used to constrain the buoyancy force attributable to sea-floor relief. The buoyancy forces will be compared to the calculated lithospheric strengths to see if they can

account for the scale of sea-floor relief.

It will become clear that there are considerable uncertainties in both the calculations of lithospheric strength and the estimations of buoyancy forces. However, the process of attempting to quantitatively match buoyancy forces to lithospheric strengths and develop a dynamic framework within which the formation of ridge crest and sea-floor relief can be explained will clarify the concepts of these processes and direct further work. Finally, though the scale of observed sea-floor relief at different spreading centers cannot be quantitatively related to estimates of lithospheric strength and tectonic forces, qualitatively the estimates of these forces can explain the variations in the roughness of sea-floor relief with spreading rate that were observed in Chapters I and II. These relationships suggest that the variations in sea-floor relief are due to variations in lithospheric strength and the extent of tectonic activity near spreading centers of different spreading rates.

### 3.2 The Strength of the Lithosphere Near Spreading Centers

#### Physical Properties of the Lithosphere

At low temperatures, the rocks that make up the lithosphere fail by brittle fracture and the strength of the rocks is determined primarily by the confining pressure and rock type (e.g. Robertson, 1972). When rocks fail by slip along previously fractured surfaces, the strength is primarily

determined only by the confining pressure (Byerlee, 1975). At high temperatures, rocks deform ductilely and they continue to support stresses after initial failure. The ductile behavior of rocks is described by flow laws where the strain rate is related to the stresses and temperatures. The ductile strength of rocks can be defined as the stress necessary to produce some give strain rate (Tapponnier and Francheteau, 1978; Goetze and Evans, 1979).

#### Calculation of Lithospheric Strengths

As it is likely that the upper oceanic crust is highly fractured, the strength of the lithosphere can be calculated by assuming the frictional strength of rocks is important for the brittle part of the lithosphere. The flow law is important for the ductile part of the lithosphere and the thermal model by Sleep (1975) can be used to estimate the temperature field for the lithosphere near spreading axes. Because the ductile strength of rocks is also sensitive to rock type, the lithosphere can be divided into an upper layer of basaltic composition 5 km thick and a lower layer of peridotitic composition. At mid-ocean ridges, the strain rate at which the lithosphere deforms can be very roughly estimated by dividing the spreading rate by the distance over which tectonic deformation of the lithosphere is expected. For the MAR where the total spreading rate is about 20 mm/yr and the straining of the lithosphere occurs over a 20-30 km wide zone (Chapter I), the gross strain rate can be

considered to be  $3.2 \times 10^{-14}$ /sec.

Tapponnier and Francheteau (1978) assumed the brittle part of the lithosphere to be composed of partially fractured rocks. In their model, the brittle strength increases at 1.5 times the effective confining pressure, lithostatic minus the hydrostatic, with depth. The effective confining pressure is assumed to increase at 200 bars/km. Following Tapponnier and Francheteau (1978), the brittle strength for the 5 km thick upper basaltic layer is given by:

$$\sigma = 500 \text{ bars} + 1.5 (z \times 200 \text{ bars/km}).$$

For the underlying peridotite layer, the brittle strength is given by:

$$\sigma = 2 \text{ kbars} + 1.5 (z \times 200 \text{ bars/km}).$$

In the above equations,

$\sigma$  is the differential stress, or strength, and

$z$  is the depth below the sea-floor.

The ductile strength of rocks for differential stresses less than 2-3 kbars can be described by equations of the form,

$$\dot{\epsilon} = A \sigma^3 \exp (-Q/RT)$$

where

$\dot{\epsilon}$  is the strain rate in 1/sec.

$\sigma$  is the differential stress, or strength in kbars,

A is a constant particular to the rock type in  
1/kbars<sup>3</sup>-sec.,

Q is the activation energy, particular to the rock type  
in kcal/mole,

R is the gas constant,

T is the temperature in °K.

There is little data available for the ductile behavior of basalt. Stress-strain curves from Tapponnier and Francheteau (1978) give the expression,

$$\dot{\epsilon} = 9.0 \times 10^7 / \text{kbars}^3\text{-sec} \times \sigma^3 \exp (-85 \text{ kcal/mole/RT})$$

This was based on unpublished work by Goetze on Maryland diabase. For lithosphere below 5 km from the sea-floor, the dominant mineralic phase is olivine. A large amount of data exist on the ductile behavior of olivine (Goetze, 1978). The flow law for dry dunite under stresses below 2-3 kbars used by Tapponnier and Francheteau (1978) is,

$$\dot{\epsilon} = 3.3 \times 10^{11} / \text{kbars}^3\text{-sec} \times \sigma^3 \exp (-125 \text{ kcal/mole/RT})$$

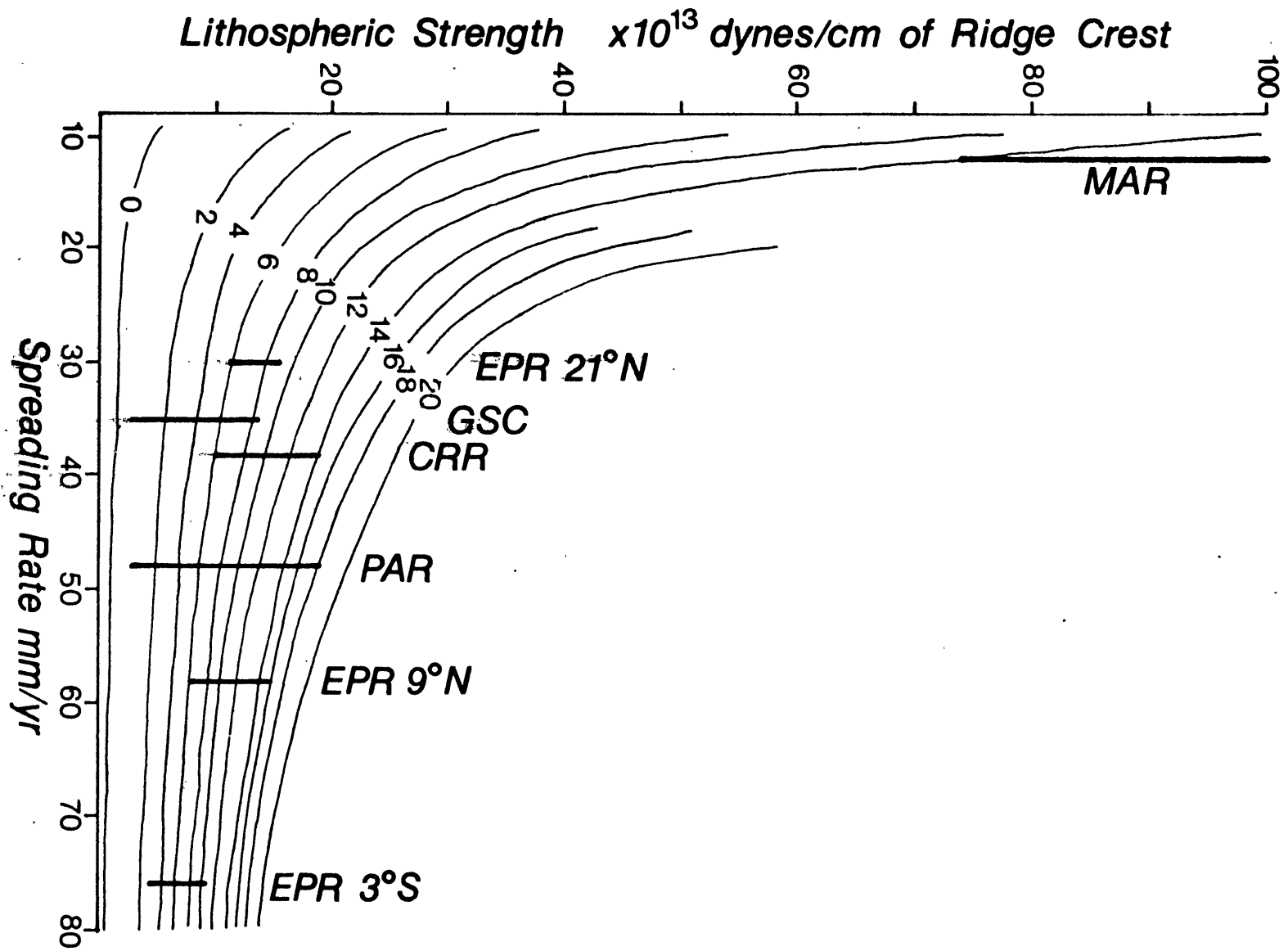
based on work by Kohlstedt and Goetze (1974). Compilation of data by other workers gives similar results (Goetze, 1978).

The relationships between temperature, pressure, and strength were used to estimate the strength of the lithosphere near spreading centers. The numerical calculation of the lithospheric strengths was done by dividing the crust and mantle in the vicinity of spreading centers into 0.1 km thick layers down to 20 km below the sea-floor. The temperature for each layer was calculated using a program by Sleep (1975) at two km intervals going away from the spreading axes. The total strength of the lithosphere was calculated by summing the strength for each layer down to the layer where the strength is less than 10 bars. Because little is known about the strength of rocks in the brittle-ductile transition zone (Logan, 1979), both the brittle and ductile strength for the lithosphere at 0.1 km depth increments were calculated and the lesser of the two used. Figure 28 shows the results with the plate boundary half-widths estimated from the deep tow data in Chapter I.

### 3.3 Estimates of the Buoyancy Forces

Buoyancy forces attributable to sea-floor relief can be estimated by integrating the volume of the sea-floor relief above or below the isostatic level times the density contrast between basalt and water and the gravitational acceleration. The shear stresses generated within the lithosphere can be

Figure 28: Lithospheric strengths calculated at 2 km intervals from the spreading axis. Vertical bars show the strength of the lithosphere within the zone of sea-floor relief formation for different spreading rate spreading centers based on the plate boundary half-widths estimated from deep tow profiles in Chapter I.





calculated by treating the lithosphere as a simply supported beam (Tapponnier and Francheteau, 1978). The differential force due to the buoyancy load, twice the shear stress times the thickness of the lithosphere, can be compared to the lithospheric strength. The thickness of the lithosphere is defined to be the depth below the sea-floor to where the lithospheric strength is less than 10 bars.

Ideally, the volume of relief that is used to calculate the buoyancy force should be measured relative to the regional isostatic level. Relief which stands above the isostatic level would impose a downward force on the lithosphere while relief which stands below the isostatic level would impose an upward force on the lithosphere. The maximum shear stress is generated at the locations where positive and negative loads are adjacent to each other. However, it is difficult to establish the isostatic level in the bathymetric profiles. As the true isostatic level is not likely to be entirely above or below the sea-floor relief, an upper limit on the magnitude of the buoyancy load can be established by assuming the isostatic level is entirely above the major relief features and using prominent negative relief features to calculate the buoyancy forces. The assumed isostatic level will be intentionally chosen to give the maximum likely buoyancy forces. The more prominent sea-floor relief features outside of the plate boundary zones in deep tow profiles from the MAR,

EPR 21°N, GSC, PAR, and EPR 3°S have been identified and the buoyancy forces attributable to these features calculated. Figure 29 shows the identified features and the average buoyancy forces attributable to these features are shown in Figure 30.

### 3.4 Relationships Between the Calculated Lithospheric Strengths and Buoyancy Forces

At all of the spreading centers analyzed, the upper limit of the buoyancy forces calculated from the observed mature sea-floor relief is about an order of magnitude less than the calculated lithospheric strengths within the plate boundary zone. The only feature that is produced within the plate boundary zone and generates buoyancy forces that approach or exceed the lithospheric strengths there is the median rift at MAR. The buoyancy force attributable to the median rift at MAR is about  $4.1 \times 10^{13}$  dynes/cm. However, the buoyancy force attributable to the mature relief outside of the median rifts is well below both this value and the lithospheric strength estimates within the plate boundary zone.

These observations present several problems. First, the observed buoyancy forces attributable to the observed relief is much too small compared to the expected strength of the lithosphere at the site of relief formation. Second, the results do suggest that median rifts can be supported by

Figure 29: The cross-sectional areas used to calculate the upper limit of the buoyancy forces attributable to sea-floor relief outside of the plate boundary zone are shown by the hashed areas. The magnitude of the buoyancy forces will be compared to the estimated lithospheric strengths to see if the scale of sea-floor relief formed at spreading centers is a function of the ability of the lithosphere to support relief within the zone of relief formation. The vertical exaggeration for all of the projected deep tow profiles is 4x.

# PAR

axis

east

2600  
3000

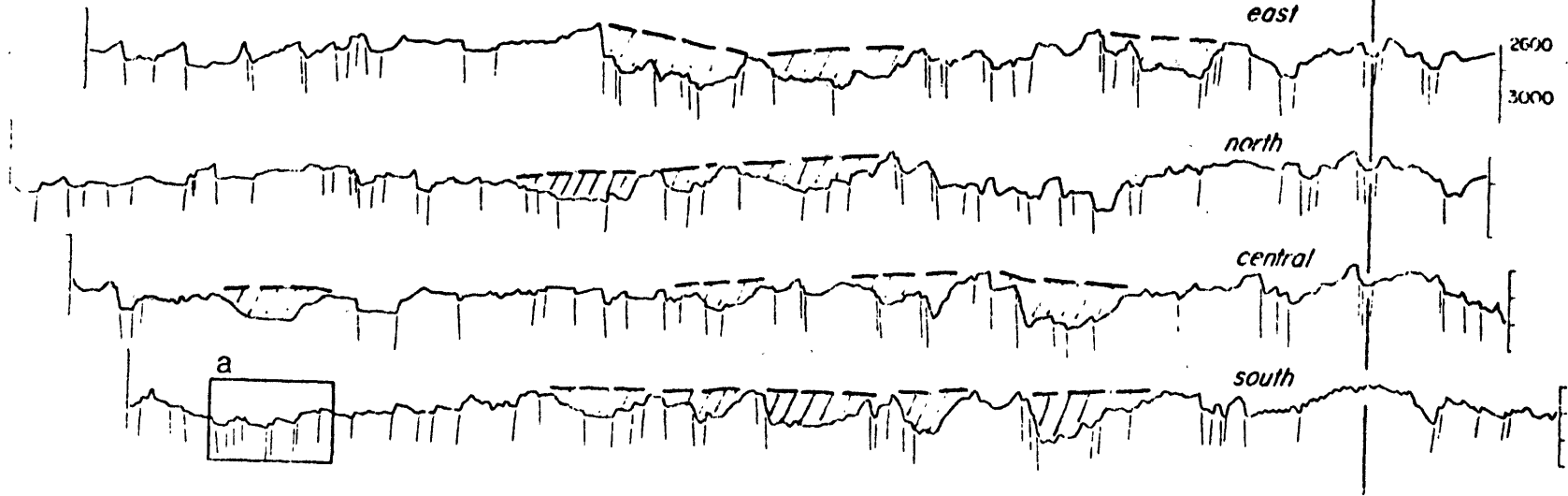
north

central

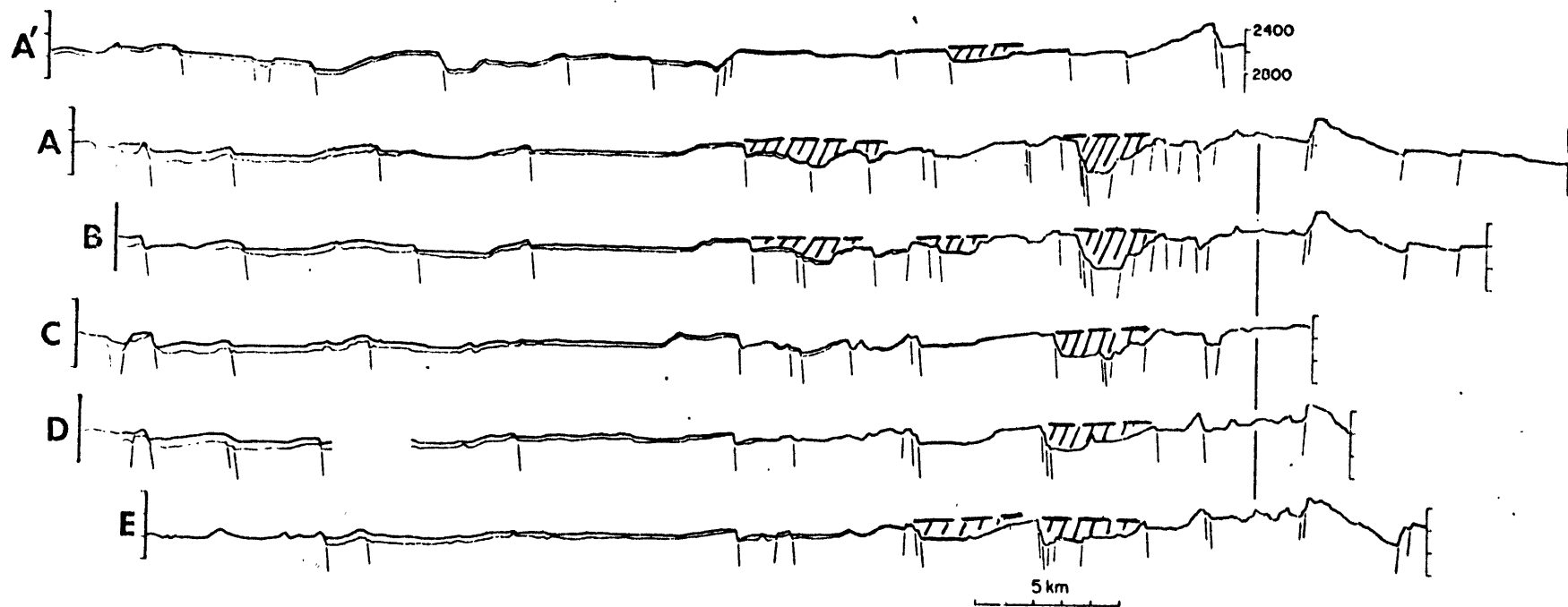
south

a

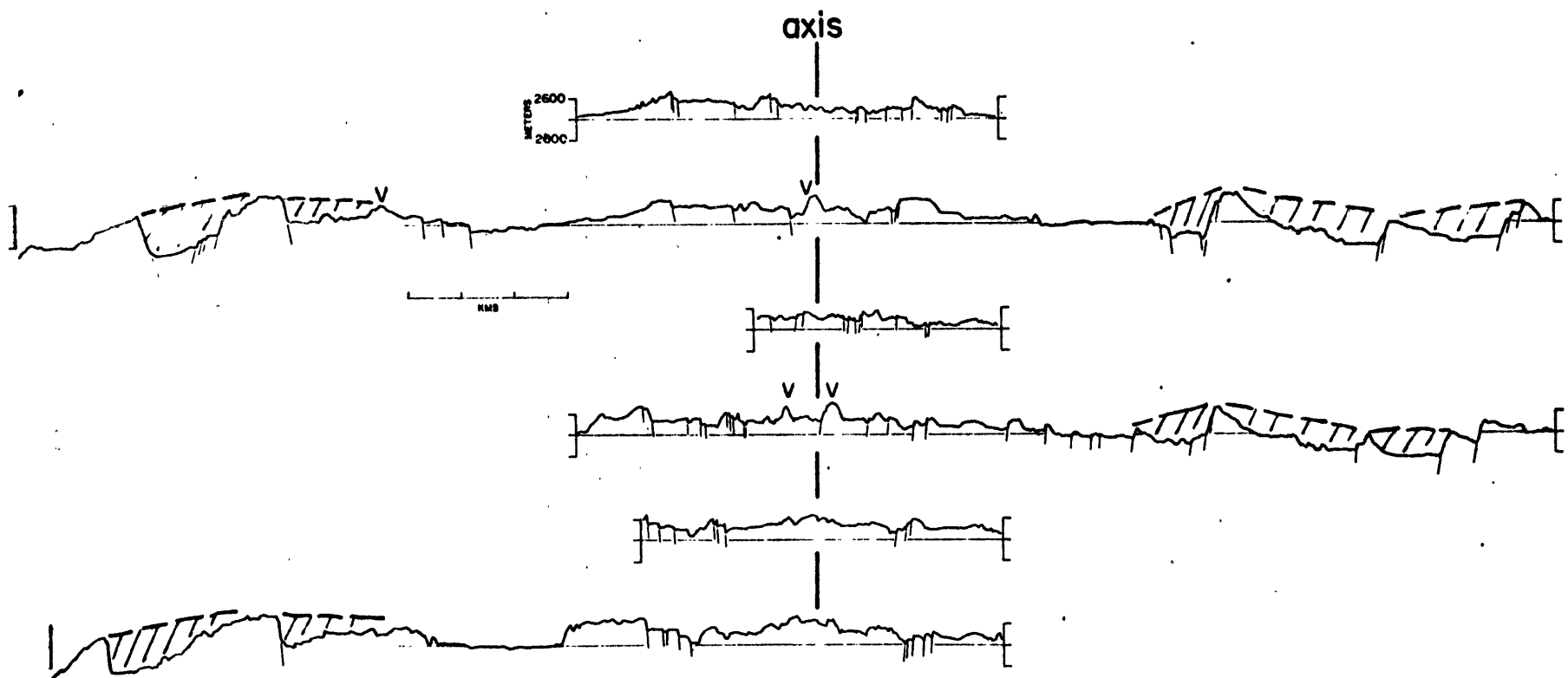
183



# GSC



# EPR 21°N



# MAR

186

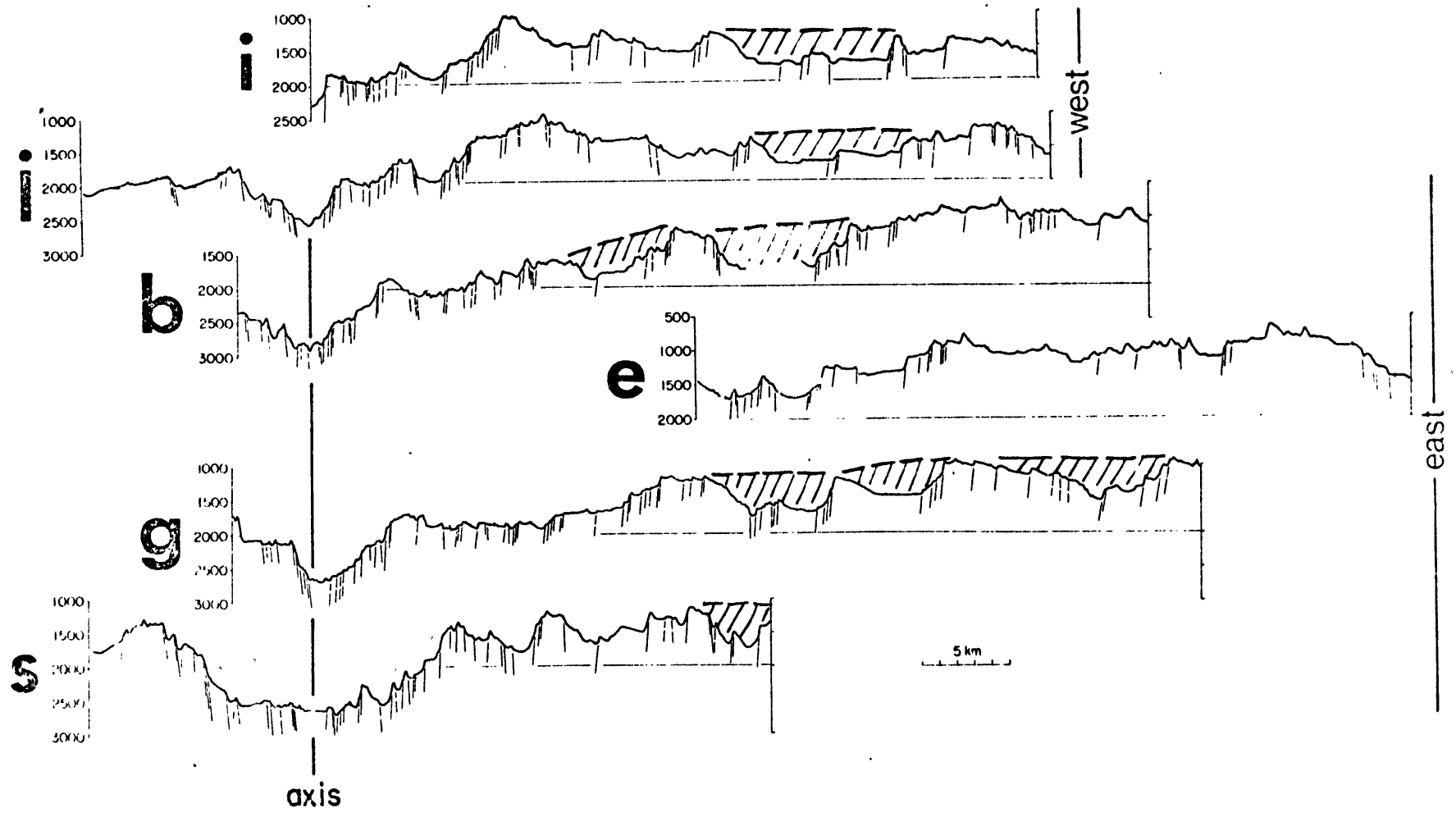
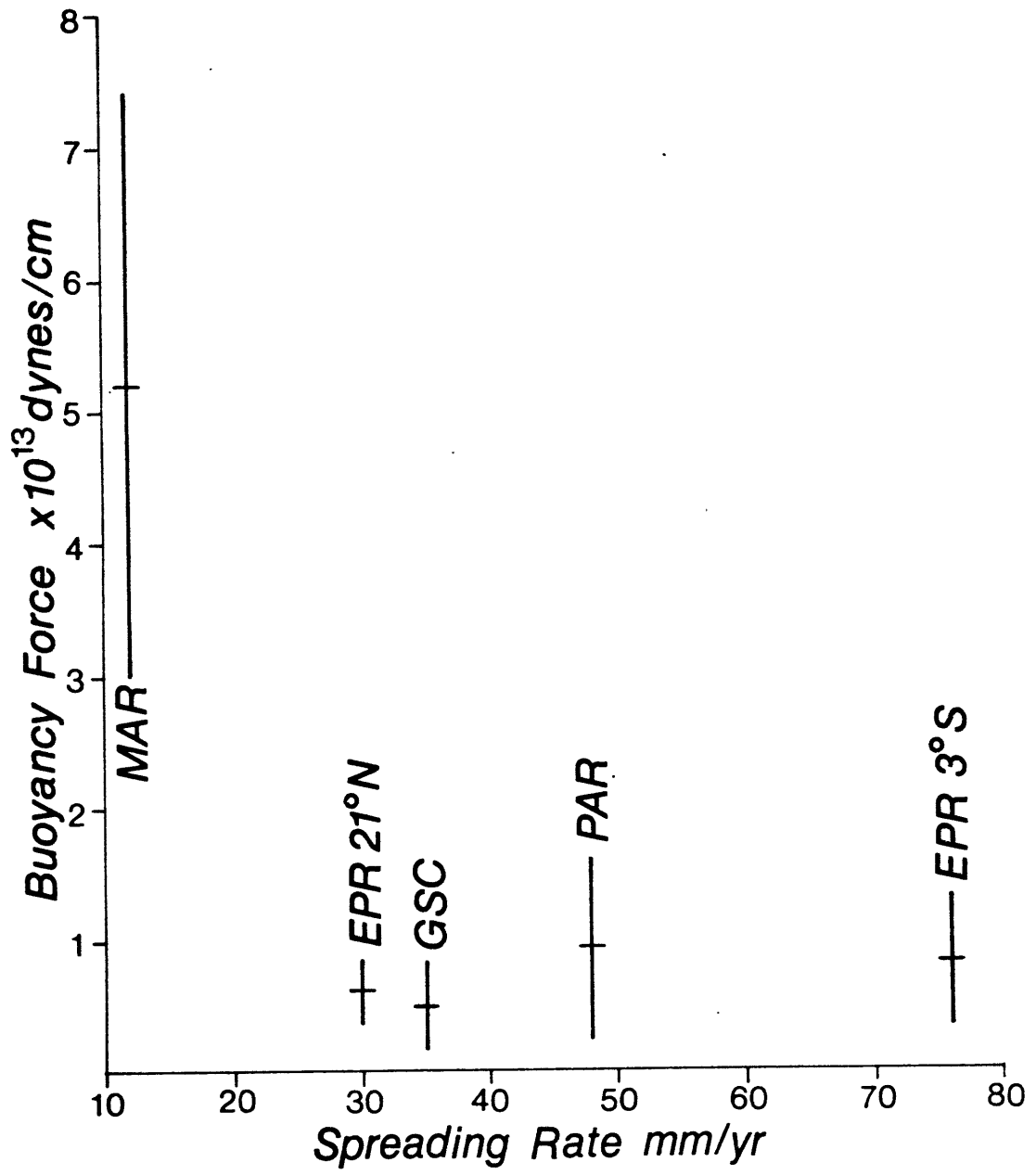


Figure 30: The buoyancy force attributable to mature sea-floor relief created at different spreading rates based on deep tow profiles. The vertical bars span one standard deviation about the means.





lithospheric strength as proposed by Tapponnier and Francheteau (1978). However, if the lithospheric strength is capable of supporting the very large median rift relief at the MAR, then there is the question of why the sea-floor relief outside of the median rift is so small. As the lithosphere should only increase in strength with distance from the spreading axes, the sea-floor relief further from the spreading axes should be as great or greater than the median rift. Two of the more obvious explanations for these problems are: 1) there are other forces at work at ridge crests, and 2) the lithospheric strengths have been over estimated.

#### Viscous Head Loss

Sleep (1969) suggested that there are viscous forces acting within the upwelling asthenosphere under spreading centers that prevent median rifts from rising to the isostatic level. He pointed out that the dynamic viscosity of fluids flowing through a pipe is inversely proportional to the cube of the pipe width. Thus if the dimensions of the conduit for the upwelling asthenosphere under spreading centers is related to spreading rate, there would be more viscous head loss at slower spreading centers in accordance with the observation that most slow spreading centers have median rifts. Relaxation of the viscous forces on the rift flanks causes the uplift of the sea-floor to form the rift mountains. Lachenbruch (1973) suggested that the long term

strength of the lithosphere is negligible and the median rift relief is defined essentially by the hydrodynamics of the upwelling asthenosphere within the conduit of the upwelling.

The work by Tapponnier and Francheteau (1978) and Goetze and Evans (1979) shows that the lithosphere at spreading centers does have strength. However, this does not preclude the possibility that viscous forces also contribute to the formation of ridge crest relief. The buoyancy force due to median rifts may be maintained by a combination of lithospheric strength and viscous head loss. On the rift flanks, relaxation of the viscous head loss may allow the buoyancy forces to exceed lithospheric strength, resulting in the uplift of the sea-floor to form the rift mountains.

Lachenbruch (1973) further suggested that the low density asthenospheric material in the conduit under spreading centers also contributes buoyancy forces to the system. Therefore, the viscous drag plus the lithospheric strength which act to hold down the sea-floor within the median rift can be envisaged to be balanced by the buoyancy forces due to the rift volume plus the extra buoyancy of the low density conduit fill which together act to uplift the sea-floor.

While the buoyancy force due to median rifts can be estimated from bathymetric profiles of ridge crests, little is known about the hydrodynamics of the upwelling asthenosphere and the geometry of the conduit region to allow calculations of the viscous forces. The magnitude of the

viscous forces has been estimated only from assuming they are balanced by the buoyancy forces and estimating the buoyancy forces from bathymetric data (Lachenbruch, 1973). Thus, little is actually known about the nature of the viscous forces. The best reason for postulating these forces may be the inadequacy of other forces to explain the formation of median rifts at most slow spreading centers.

The presence of viscous forces can explain the large difference in the scale of median rift relief and the relief of sea-floor away from spreading centers at the MAR. The scale of median rifts would reflect in part the viscous processes while the scale of relief away from median rifts would reflect the ability of the lithosphere to support relief by strength at the location where the relief is formed by tectonism. Though viscous forces can explain the difference in the scale of median rift and mature sea-floor relief at the MAR, the calculated lithospheric strength for the location of expected relief formation suggests the mature sea-floor relief should be much greater than that which is observed.

#### Uncertainties in the Calculated Lithospheric Strengths

In estimating the lithospheric strengths, the brittle part of the lithosphere was assumed to be composed of partially fractured rocks. Goetze and Evans (1979) suggested that it is only the frictional strength of rocks that is important. Byerlee (1975) found the frictional

strength of rocks to be 1.7 times the effective confining pressure for stresses less than 2 kbars. Lithospheric strengths calculated using the frictional strength for the brittle part of the lithosphere are about one-half of those using the strength for partially fractured rocks as given by Tapponnier and Francheteau (1978). However, the lower lithospheric strengths are still about five times larger than the buoyancy forces attributable to the observed mature sea-floor relief.

The brittle and ductile strengths of the lithosphere were calculated at 0.1 km depth intervals and the weaker of the two used. The brittle strength increases with depth as it is dependent on the effective confining pressure while the ductile strength decreases with depth due to the increasing temperature. Therefore, the strongest portion of the lithosphere is invariably at the ductile-brittle transition area. Unfortunately, it is the strength of rocks near the brittle-ductile transition zone that is the least well known (Logan, 1979). Because the rock strength in the brittle-ductile transition zone plays a dominant part in the calculated lithospheric strengths, any over-estimation of rock strengths in the brittle-ductile regime can greatly bias the calculated total lithospheric strengths.

If it is assumed that the calculated lithospheric strengths are too high due to uncertainties in the rock strengths in the brittle-ductile regime or even some other

unspecified mechanism, some limiting stress can be found which when assumed will give lithospheric strengths that match the buoyancy forces calculated from the observed bathymetric relief. In the above calculations, the maximum stresses found within the lithosphere were about 300 bars at the spreading axis and about 1100 bars at 10 km from the spreading axis for a 10 mm/yr spreading center. If a value of 100 bars is used as the limiting stress supportable by any part of the lithosphere, the lithospheric strength at 10 km from the spreading axis would be about  $9.7 \times 10^{13}$  dynes/cm for a 10 mm/yr spreading center and  $2.5 \times 10^{13}$  dynes/cm for a 80 mm/yr spreading center. These values are now about twice the lithospheric strengths implied by the observed sea-floor relief. If the hypothesis that mature sea-floor relief is limited by the strength of the lithosphere within the zone of tectonic activity at spreading centers is true, then the scale of sea-floor relief implies the lithosphere is capable of supporting stresses less than 100 bars in the zone of relief formation. Whether such small strengths are reasonable at all depends on better knowledge of the physical properties of rocks. Of course, there is also the possibility that the hypothesis is incorrect and that the scale of relief is determined by

          factors other than lithospheric strength and the extent of tectonic activity at spreading centers.

### 3.5 Relationships Between Spreading Rate and the Roughness of Sea-Floor Relief

Despite the large differences between the calculated lithospheric strengths and buoyancy forces, the relative magnitude of the lithospheric strengths and buoyancy forces for different spreading rates is quite similar (compare Figures 28 and 30). In fact, the two figures are almost identical except that the strengths are about an order of magnitude greater than the buoyancy forces. Strength calculations assuming there is some limiting stress supportable by the lithosphere would give qualitatively similar relationships for the strength at different spreading rates. This is due to the fact that the cooling of the lithosphere occurs much more rapidly near the spreading axes at slow spreading centers. Actually, almost any model in which the strength of the lithosphere is dependent on the thermal field will give similar relationships between lithospheric strength and spreading rate.

The rapid increase in lithospheric strength away from spreading axes and the greater extent of tectonic activity at slow spreading centers can qualitatively explain why larger amplitude/longer wavelength relief is created there. The strength of the lithosphere in which tectonism is active at slow spreading centers is much greater. Thus, once relief is formed, it can be maintained by strength. As discussed above, the size of median rifts probably is not determined solely

by the strength of the lithosphere. Instead, median rifts probably are maintained in part by viscous forces. At higher rate spreading centers, the lithosphere is not capable of maintaining large scale relief within the zone of tectonic activity. Only small amplitude/short wavelength relief can be preserved.

Figure 28 shows that the strength of the lithosphere near spreading axes decreases rapidly with increasing spreading rate at the slower spreading rates. The continued decrease in strength near spreading axes is slower at the higher spreading rates. The large change in lithospheric strength and thus the scale of relief created at the slow spreading rates can explain why the sea-floor roughness as seen by surface ship profiling systems can be correlated with spreading rate along the MAR. At the faster spreading EPR, the rather small expected decrease in the scale of relief with increasing spreading rate may be hidden in the noise of the data available (K.D. Klitgord, oral communication). Alternatively, the possible continued decrease in the scale of relief created at faster spreading rates is beyond the resolution of the profiling systems.

### 3.6 Extent of Tectonism at Spreading Centers

It is important to point out that the lithosphere created at any spreading rate will eventually become strong enough to support relief of equally large scale. Therefore,



there remains the question of how the extent of tectonic activity is limited at spreading centers and the variability in the roughness with spreading rate is achieved. One possibility is the presence of magma chambers under spreading axes. Magma chambers have been inferred from seismic data collected at fast and intermediate rate spreading centers (Orcutt et al, 1975; Rosendahl et al, 1976; Reid et al, 1977; Herron et al, 1978). Rosendahl (1976) and Lonsdale (1977a) suggested that the edge of the magma chambers coincides with the beginning of large scale relief at the fast spreading EPR 9°N and EPR 3°S. The edge of magma chambers may be a zone of stress concentration and thus the site of preferential lithospheric failure (Sleep and Rosendahl, 1979). It is also tempting to note that studies of caldera subsidence have shown that the lid over magma chambers tends to subside as an unit, creating ring dykes and normal faults around the edges of the caldera (Smith and Bailey, 1968; Simkin and Howard, 1970). The edge of magma chambers can thus determine the extent of major tectonic activity at faster spreading centers. It was noted in Chapter I that the location for the initiation of tectonic relief is quite well defined at many spreading centers. The width of the central low relief zone may well define the width of the magma chamber lid and the zone of tectonic relief formation associated with some zone rimming the magma chambers. It is easy to speculate that the penetration of sea water into the fault scarps associated

with the development of large scale tectonic relief helps limit the extent of magma chambers.

Magma chambers have also been postulated by petrologists and geochemists to explain the lateral variations in basalt composition at mid-ocean ridges and the petrologic layering found in ophiolites (e.g. Cann, 1974; Hekinian et al, 1976; Bryan and Moore, 1977; Nisbet and Fowler, 1978). Bryan and Moore (1977) suggested that the width of the inner valley floor along the MAR in the FAMOUS area equals the width of the underlying magma chamber. However, the lack of conclusive seismic evidence for significant magma chambers along the MAR suggests they cannot control the extent of tectonic activity which forms the continuous median rifts (Nisbet and Fowler, 1978). Furthermore, at deeply rifted mid-ocean ridges the need to remove the median rift relief at the rift margins dictates a zone of tectonic activity which must be wider than the possible magma chambers under the rift valley floors. It is not likely that magma chambers extend beyond the large normal faults present at the base of the median rift valley walls. It is probable that it is the geometry of the deeper seated viscous effects in the conduit for the upwelling asthenosphere that determines the zone of tectonic activity at deeply rifted mid-ocean ridges.

### 3.7 Summary

The suggestion that the scale of sea-floor relief formed

at spreading centers is limited by the buoyancy force supportable by the lithosphere within the zone of relief formation provides a qualitative means by which the contrast in the relief created at different spreading rates can be explained. Large scale relief created in older and thus stronger lithosphere at slow spreading centers can be preserved as the sea-floor continues to migrate away from spreading centers. Large scale relief cannot be supported by the younger and weaker lithosphere within the zone of relief formation at faster spreading centers.

Calculation of the lithospheric strength based on thermal models of the lithosphere at spreading centers and laboratory measurements of rock strengths give strengths which are about an order of magnitude greater than the buoyancy forces attributable to the observed mature sea-floor relief. Lithospheric strengths may have been over-estimated due to the assumption that the brittle portion of the lithosphere is only partially fractured and/or the strength of rocks in the brittle-ductile transitional regime can be estimated by extrapolating the brittle and ductile behavior of rocks. The scale of relief observed in deep tow profiles implies the stresses supportable by the lithosphere within the zone of relief formation are less than about 100 bars. Whether such low strengths are realistic remains uncertain. However, the qualitative similarity in the relative magnitude of the estimated strengths within the zone of tectonism and

the buoyancy forces calculated from observed sea-floor relief created at different spreading rates suggests that the scale of sea-floor relief is a function of lithospheric strength within the zone of tectonic activity at spreading centers. It was noted that if the roughness of sea-floor relief can be explained by the strength of the lithosphere at the site of relief formation, there remains the question of what factors limit the extent of tectonic activity at spreading centers. At faster spreading centers, it is possible that it is the size of magma chambers which controls the extent of tectonic activity. At deeply rifted mid-ocean ridges, the necessity of removing median rift relief extends the zone of tectonic activity to the top of the rift valley walls. If median rifts are maintained in part by viscous forces, then the extent of tectonic activity would be governed by the deeper seated viscous forces.

## Chapter IV: Summary and Conclusions

### 4.1 Deep Tow Results

Topographic profiles of mid-ocean ridges collected with the deep tow instrument package were quantitatively analyzed and compared. The examination of this data showed that the sea-floor is pervasively faulted and it is the tectonic relief that makes up most of the sea-floor relief. The presence of central low relief zones at spreading centers shows that the sea-floor is initially created with little relief and the tectonic relief is added as the sea-floor migrates away from the spreading axes.

The width of the zone over which the tectonic relief is created, or the plate boundary zone, was estimated by looking for the point at which the tectonic relief reached a density that is similar to mature sea-floor well away from the spreading centers. At deeply rifted mid-ocean ridges, the removal of the median rift relief is necessary before the sea-floor relief matures to that of relief well away from the spreading centers. Thus, the width of the plate boundary zone is defined by the distance to which the median rift relief is removed.

The plate boundary widths are not significantly different among the faster spreading mid-ocean ridges. The width of the slow spreading MAR is noticeably wider. Though the method used is far from being precise, it is clear that when the plate

boundary widths are expressed in terms of the age of sea-floor to which tectonism is active, the age is significantly greater for the slow spreading MAR.

The roughness of sea-floor relief was calculated by summing the absolute difference in depth points sampled at 50 m intervals along projected deep tow profiles. When calculated by this method, the roughness of relief turns out to have little correlation with spreading rate, contrary to the often noted inverse relationship between roughness and spreading rate noted in surface ship bathymetric profiles. This apparent contradiction can be explained by the fact that the amplitude and wavelength of relief created at faster spreading centers is less than that formed at slower spreading centers. Typical surface ship profiling systems are not capable of resolving the finer scale relief created at faster spreading centers. Thus, the relief created there appears to be smoother. Calculation of the roughness of relief that would be seen by wide beam surface ship profiling systems using deep tow data showed that the relief for faster spreading centers is indeed attenuated more than that of slow spreading centers. Spectral analysis of deep tow profiles also suggests this interpretation is correct.

#### 4.2 Surface Ship Results

Surface ship profiles of mid-ocean ridges were compiled to enlarge and complement the deep tow data set. The common

generalization that faster spreading centers have smaller median rifts or larger central highs and create smoother sea-floor relief was investigated. The depth and volume of median rifts have been defined relative to the adjacent rift mountain peaks as well as the regional isostatic level. The height and volume of central highs can also be defined relative to the isostatic level. Depth versus square root of age curves were fitted to projected ridge crest profiles in the attempt to define the isostatic level. The dimensions of median rifts along the MAR and central highs along the EPR defined in either manner had low coefficients of correlation with spreading rate. Only when the data sets from the MAR and EPR were compared does any sort of clear correlation become apparent.

There is large scatter in the dimensions of median rifts and central highs whether defined relative to the adjacent rift mountain peaks or the best fitting depth versus square root of age curves. The scatter in the ridge crest dimensions when defined relative to the best fit depth versus square root of age curves may be due to errors in the fitting of the depth versus square root of age curves. There is large variability in the parameters of the best fit depth versus square root of age curves both in the Atlantic and the Pacific. To look for the source of the variability in the fitted depth versus square root of age curves, numerous profiles were digitized from detailed bathymetric contour maps

of the MAR between  $20^{\circ}$  and  $30^{\circ}$ N. The parameters of the depth versus square root of age curves fitted to these profiles were compared to those fitted to the surface ship profiles compiled for this study. The comparison between the results showed that much of the variability in the depth versus square root of age curves fitted to the compiled surface ship profiles is due to regional variations in the subsidence rate of the sea-floor which were not resolved by the sparse number of surface ship profiles compiled.

The variability in median rift volumes independent of spreading rate was assessed by looking at ridge crest profiles gathered in detailed surveys of the MAR. Comparison of rift volumes determined from ridge crest profiles collected within small survey areas showed there is large variability not explainable by spreading rate differences. Other factors that have been postulated to influence median rift dimensions include the proximity of transform faults and the episodic nature of median rift evolution. It is clear that median rift and central high dimensions are not solely a function of spreading rate. Other processes are at work at mid-ocean ridges which influence ridge crest morphology and are responsible for the scatter in the imperfect relationship between ridge crest dimensions and spreading rate.

The roughness of sea-floor relief was calculated using projected surface ship profiles sampled at even 3.66 km intervals. An inverse correlation between roughness and



spreading rate can be detected in profiles from the Atlantic. A very slight positive correlation was found for profiles from the Pacific. The abundance of seamounts in the South Pacific may be the reason for the higher sea-floor roughness observed there. However, the roughness calculated for profiles from the South Pacific without seamounts shows the roughness of sea-floor relief not related to seamounts is not noticeably less than that in the North Pacific.

#### 4.3 Formation of Fine-Scale Sea-Floor Relief at Mid-Ocean Ridges

The deep tow and surface ship bathymetric data showed that large scale sea-floor relief is formed at slow spreading centers. The plate boundary width estimates suggested that tectonic activity occurs in older lithosphere at slow spreading centers. Tapponnier and Francheteau (1978) proposed that the size of median rift relief supportable by the lithosphere is determined by the strength of the lithosphere. It is proposed here that tectonic activity and formation of relief in older, stronger lithosphere can explain the larger scale relief created at slow spreading centers.

To test the above hypotheses, the buoyancy force attributable to mature sea-floor relief seen in deep tow profiles and the lithospheric strength within the zone of tectonic activity were estimated. The estimated strengths, if correct, suggest that the lithosphere within the zone of

relief formation is capable of supporting relief which is much larger than that observed. Only the buoyancy forces attributable to some of the median rifts at MAR equal or exceed the calculated lithospheric strengths. The large difference between the estimated lithospheric strengths and buoyancy forces may result from other forces which have not been accounted for and/or the over-estimation of the lithospheric strengths. Viscous forces can be postulated to maintain the large median rift relief while uncertainties in the strength of the rocks that make up the lithosphere may account for the high calculated lithospheric strengths. For the buoyancy forces attributable to the observed sea-floor relief to equal the lithospheric strengths, the stress which the lithosphere can support within the zone of relief formation needs to be less than 100 bars. Whether such low strengths are realistic is uncertain. However, the similarity in the relationship between the lithospheric strengths and the buoyancy forces attributable to observed sea-floor relief suggests that the roughness of relief created at different spreading rates is a result of the lithospheric strength at the point where the relief is created. Finally, it was speculated that it is the size of magma chambers at faster spreading centers and viscous forces at deeply rifted mid-ocean ridges that control the horizontal extent of the plate boundary zones and thus the age of lithosphere to which tectonism is active.

## REFERENCES

- Anderson, R.N., and H.C. Noltimier, A model for the horst and graben structure of mid-ocean ridge crests based upon spreading velocity and basalt delivery to the oceanic crust, *Geophys. J.R. astr. Soc.*, 34, 137-147, 1973.
- Anderson, R.N., D.A. Clague, K.D. Klitgord, M. Marshall, and R.K. Nishimori, Magnetic and petrological variations along the Galapagos melting anomaly, *Geol. Soc. Amer. Bull.*, 86, 683-694, 1975.
- Anderson, R.N., G.F. Moore, S.S. Schilt, R.C. Cardwell, A. Trehu, and V. Vacquier, Heat flow over a fossil ridge on the north flank of the Galapagos Spreading Center, *J. Geophys. Res.*, 81, 1828-1838, 1976.
- Atwater, T., and J.D. Mudie, Detailed near-bottom geophysical study of the Gorda Rise, *J. Geophys. Res.*, 78, 8665-8686, 1973.
- Atwater, T., R.D. Ballard, K. Crane, N. Gruver, C. Hopson, H.P. Johnson, B.P. Luyendyk, K.C. Macdonald, J. Peirce, J.S.F. Shih, L. Shure, D. Stakes, N. Walker, and T.H. van Andel, Expedition cruise report: AMAR 78- A coordinated submersible, photographic mapping, and dredging program in the Mid-Atlantic rift valley near 36.5° N, unpublished report, 191 pp., 1978.
- Ballard, R.D., and T.H. van Andel, Morphology and tectonics of the inner rift valley at lat. 36° 50' N on the Mid-Atlantic Ridge, *Geol. Soc. Amer. Bull.*, 88, 507-530, 1977.
- Bell, Jr., T.H., Statistical features of sea-floor topography, *Deep Sea Res.*, 22, 883-892, 1975.
- Bell, Jr., T.H., Mesoscale sea-floor roughness, *Deep Sea Res.*, 26A, 65-76, 1979.
- Bryan, W.B., and J.G. Moore, Compositional variations of young basalts in the Mid-Atlantic Ridge rift valley near lat. 36° 49' N, *Geol. Soc. Amer. Bull.*, 88, 556-570, 1977.
- Byerlee, J.D., The fracture strength and frictional strength of Weber sandstone, *Int. J. Rock Mech. Min. Sci. Geomech. Abstr.*, 12, 1-4, 1975.
- Cann, J.R., Geological processes at mid-ocean ridge crests, *Geophys. J.R. astr. Soc.*, 15, 331-341, 1968.

- Cann, J.R., A model for oceanic crustal structure developed, *Geophys. J.R. astr. Soc.*, 39, 169-187, 1974.
- Cochran, J.R., and M. Talwani, Gravity anomalies, regional elevation, and the deep structure of the North Atlantic, *J. Geophys. Res.*, 83, 4907-4924, 1978.
- Crane, K., The intersection of the Siqueiros Transform Fault and the East Pacific Rise, *Marine Geology*, 21, 25-46, 1976.
- Crane, K., and W.R. Normark, Hydrothermal activity and ridge crest structure of the East Pacific Rise at 21°N, *J. Geophys. Res.*, 82, 5336-5348, 1977.
- Davis, E.E., and C.R.B. Lister, Fundamentals of ridge crest topography, *Earth Planet. Sci. Lett.*, 21, 405-413, 1974.
- Goetze, C., The mechanism of creep in olivine, *Phil. Trans. Roy. Soc. Lon., Ser. A*, 288, 99-119, 1978.
- Goetze, C., and B. Evans, Stress and temperature in the bending lithosphere as constrained by experimental rock mechanics, *Geophys. J.R. astr. Soc.*, submitted, 1979.
- Grim, P.J., Connection of the Panama Fracture Zone with the Galapagos rift zone, eastern tropical Pacific, *Mar. Geophys. Res.*, 1, 85-90, 1970.
- Handschumacher, D.W., Post-Eocene plate tectonics of the Eastern Pacific, in The Geophysics of the Pacific Ocean Basin and Its Origin, edited by G.H. Sutton, M.N. Manghnani, and R. Moberly, pp. 177-202, AGU, Washington D.C., 1976.
- Harrison, C.G.A., Tectonics of mid-ocean ridges, *Tectonophysics*, 22, 301-310, 1974.
- Harrison, C.G.A., and L. Stieltjes, Faulting within the median valley, *Tectonophysics*, 38, 137-144, 1977.
- Hayes, D.E., and J.R. Conolly, Morphology of the Southeast Indian Ocean, in Antarctic Oceanology II; the Australian-New Zealand Sector, edited by D.H. Hayes, pp. 125-146, *Antarctic Res. Ser.*, 19, AGU, Washington D.C., 1972.
- Hayes, D.E., J.R. Heirtzler, E.M. Herron, and W.C. Pitman, III, Preliminary Report of Vol. 21, USNS ELTANIN, Cruises 22-27, January 1966-February 1967, Tech. Rept. 2-CU-2-69, Lamont-Doherty Geol. Observ., Palisades, N.Y., 1969.

Hayes, D.E., M. Talwani, R. Houtz, W.C. Pitman, III, and R.R. Meijer, II, Report of Vol. 22, USNS ELTANIN, Cruises 28-32, March, 1967-March 1968, Tech. Rept. CU-1-72, Lamont-Doherty Geol. Observ., Palisades, N.Y., 1972.

Hayes, D.E., R. Houtz, M. Talwani, A.B. Watts, J. Weissel, and T. Aitken, Preliminary Report of Vol. 23, USNS ELTANIN, Cruises 33-38, March 1968-May 1969, Tech. Rept. CU-1-75, Lamont-Doherty Geol. Observ., Palisades, N.Y., 1975.

Hayes, D.E., R. Houtz, M. Talwani, A.B. Watts, J. Weissel, and T. Aitken, Preliminary Report of Vol. 24, USNS ELTANIN, Cruises 39-45, June 1969-October 1970, Tech. Rept. CU-2-76, Lamont-Doherty Geol. Observ., Palisades, N.Y., 1976.

Hayes, D.E., J. Weissel, T. Aitken, R. Houtz, M. Talwani, and A.B. Watts, Preliminary Report of Vol. 25, USNS ELTANIN, Cruises 46-50, November 1970-January 1972, Tech. Rept. CU-1-77, Lamont-Doherty Geol. Observ., Palisades, N.Y., 1977.

Hayes, D.E., J. Weissel, T. Aitken, R. Houtz, M. Talwani, R.A. Shearer, and A.B. Watts, Preliminary Report of Vol. 26, USNS ELTANIN, Cruises 51-55A, January 1972-December 1972, Tech. Rept. CU-1-78, Lamont-Doherty Geol. Observ., Palisades, N.Y., 1978.

Heirtzler, J.R., D.E. Hayes, E.M. Herron, and W.C. Pitman, III, Preliminary Report of Vol. 20, USNS ELTANIN, Cruises 16-21, January 1965-January 1966, Tech. Rept. 3-CU-3-69, Lamont-Doherty Geol. Observ., Palisades, N.Y., 1969.

Hekinian, R., J.G. Moore, and W.B. Bryan, Volcanic rocks and processes of the Mid-Atlantic Ridge rift valley near 36°49'N, Contrib. Mineral. Petrol., 58, 83-110, 1976.

Herron, T.J., W.J. Ludwig, P.L. Stoffa, T.K. Kan, and P. Buhl, Structure of the East Pacific Rise crest from multichannel seismic reflection data, J. Geophys. Res., 83, 798-804, 1978.

Hey, R., G.L. Johnson, and A. Lowrie, Recent plate motions in the Galapagos area, Geol. Soc. Amer. Bull., 88, 1385-1403, 1977.

Ivers, W.D., and J.D. Mudie, Towing a long cable at slow speeds: A three-dimensional dynamic model, Mar. Tech. Soc. J., 7, 23-29, 1973.

Johnson, G.L., and P.R. Vogt, Mid-Atlantic Ridge from 47° to 51° North, Geol. Soc. Amer. Bull., 84, 3443-3462, 1973.

Johnson, G.L., P.R. Vogt, R. Hey, J. Campsie, and A. Lowrie, Morphology and structure of the Galapagos Rise, Marine Geology, 21, 81-120, 1976.

Klitgord, K.D., and J.D. Mudie, The Galapagos Spreading Center: A near-bottom geophysical survey, *Geophys. J.R. astr. Soc.*, 38, 563-586, 1974.

Klitgord, K.D., S.P. Heustis, R.L. Parker, and J.D. Mudie, An analysis of near-bottom magnetic anomalies: Sea-floor spreading, the magnetized layer, and the geomagnetic time scale, *Geophys. J.R. astr. Soc.*, 43, 387-424, 1975.

Kohlstedt, D.L., and C. Goetze, Low stress-high temperature creep in olivine single crystals, *J. Geophys. Res.*, 79, 2045-2051, 1974.

Krause, D.C., and H.W. Menard, Depth distribution and bathymetric classification of some sea-floor profiles, *Marine Geology*, 3, 169-193, 1965.

Lachenbruch, A.H., A simple mechanical model for oceanic spreading centers, *J. Geophys. Res.*, 78, 3395-3417, 1973.

Lachenbruch, A.H., Dynamics of a passive spreading center, *J. Geophys. Res.*, 81, 1883-1902, 1976.

Larson, R.L., Near-bottom geological studies of the East Pacific Rise crest, *Geol. Soc. Amer. Bull.*, 82, 823-842, 1971.

Larson, R.L., Bathymetry, magnetic anomalies, and plate tectonic history of the mouth of the Gulf of California, *Geol. Soc. Amer. Bull.*, 83, 3345-3360, 1972.

Laughton, A.S., D.G. Roberts, and R. Graves, Bathymetry of the northeast Atlantic: Mid-Atlantic Ridge to southwest Europe, *Deep Sea Res.*, 22, 791-810, 1975.

Laughton, A.S., R.C. Searle, and D.G. Roberts, The Reykjanes Ridge crest and the transition between its rifted and non-rifted regions, *Tectonophysics*, 55, 173-178, 1979.

Logan, L.M., Brittle phenomenon, *Rev. Geophys. Space Phys.*, 17, 1121-1132, 1969.

Lonsdale, P., Structural geomorphology of a fast-spreading rise crest: The East Pacific Rise near 3°25'S, *Mar. Geophys. Res.*, 3, 251-293, 1977a.

Lonsdale, P., Regional shape and tectonics of the equatorial East Pacific Rise, *Mar. Geophys. Res.*, 3, 295-315, 1977b.

Lonsdale, P., and A. Shor, The oblique intersection of the Mid-Atlantic Ridge with Charlie-Gibbs transform fault, *Tectonophysics*, 54, 195-210, 1979.

- Lonsdale, P., and F.N. Spiess, Deep tow observations at the East Pacific Rise, 8°45'N, and some interpretations, in Initial Reports of the Deep Sea Drilling Project, U.S. Government Printing Office, Washington D.C., in press, 1979.
- Luyendyk, B.P., and K.C. Macdonald, Spreading center terms and concepts, *Geology*, 4, 369-370, 1976.
- Luyendyk, B.P., and K.C. Macdonald, Physiography and structure of the inner floor of the FAMOUS rift valley: Observations with a deep tow instrument package, *Geol. Soc. Amer. Bull.*, 88, 648-663, 1977.
- Macdonald, K.C., Near-bottom magnetic anomalies, asymmetric spreading, oblique spreading, and tectonics of the accreting plate boundary on the Mid-Atlantic Ridge near 37°N, *Geol. Soc. Amer. Bull.*, 88, 541-555, 1977.
- Macdonald, K.C., and B.P. Luyendyk, Deep-tow studies of the structure of the Mid-Atlantic Ridge crest near latitude 37°N, *Geol. Soc. Amer. Bull.*, 88, 621-636, 1977.
- Macdonald, K.C., and T. Atwater, Evolution of rifted ocean ridges, *Earth Planet. Sci. Lett.*, 39, 319-327, 1978.
- Macdonald, K.C., S.P. Miller, S.P. Huestis and F.N. Spiess, Three-dimensional modelling of a magnetic reversal boundary from inversion of deep-tow measurement, submitted, 1979a.
- Macdonald, K.C., K. Kastens, F.N. Spiess, and S.P. Miller, Deep-tow studies of the Tamayo Transform Fault, *Marine Geophys. Res.*, 4, 37-70, 1979b.
- Mammerickx, J., S.M. Smith, I.L Taylor, and T.E. Chase, Bathymetry of the South Pacific, *Inst. Mar. Res. Tech. Rept.*, 47A, 48A, 52A, 53A, 1974.
- McKenzie, D., and J.G. Sclater, Evolution of the Indian Ocean since the Late Cretaceous, *Geophys. J.R. astr. Soc.*, 25, 437-528, 1971.
- Menard, H.W., Sea-floor spreading, topography, and the second layer, *Science*, 157, 923-924, 1967.
- Menard, H.W., and L.M. Dorman, Dependence of depth anomalies upon latitude and plate motions, *J. Geophys. Res.*, 82, 5329-5335, 1977.
- Minster, J.B., and T.H. Jordan, Present-day plate motions, *J. Geophys. Res.*, 83, 5331-5354, 1978.

- Minster, J.B., T.H. Jordan, P. Molnar, and E. Haines, Numerical modelling of instantaneous plate tectonics, *Geophys. J.R. astr. Soc.*, 36, 541-576, 1974.
- Molnar, P., T. Atwater, J. Mammerickx, and S.M. Smith, Magnetic anomalies, bathymetry, and the tectonic evolution of the South Pacific since the Late Cretaceous, *Geophys. J.R. astr. Soc.*, 40, 383-420, 1975.
- Mudie, J.D., J. Grow, K.D. Klitgord, and P. Larson, Shipboard cruise report on Leg 2 of Expedition SOUTHTOW: Studies in the southeast Pacific, Scripps Inst. Oceanography Ref. 72-66, La Jolla, Calif., 40 pp., 1972.
- NAVOCEANO, North Atlantic Ocean, World Relief Map, NA-6, NA-7, NA-9, NA-10, 1977.
- Nisbet, E.G., and C.M.R. Fowler, The Mid-Atlantic Ridge at 37° and 45°N: Some geophysical and petrological constraints, *Geophys. J.R. astr. Soc.*, 54, 631-660, 1978.
- Normark, W.R., Delineation of the main extrusive zone of the East Pacific Rise at lat. 21°N, *Geology*, 4, 681-685, 1976.
- Orcutt, J.A., B.L.N. Kennett, and L.M. Dorman, Structure of the East Pacific Rise from an ocean bottom seismic survey, *Geophys. J.R. astr. Soc.*, 45, 305-320, 1975.
- Osmaston, M.F., Genesis of ocean ridge median valleys and continental rift valleys, *Tectonophysics*, 11, 387-405, 1971.
- Parsons, B., and J.G. Sclater, An analysis of the variation of ocean floor bathymetry and heat flow with age, *J. Geophys. Res.*, 82, 803-827, 1977.
- Pitman, W.C., III, and M. Talwani, Sea-floor spreading in the North Atlantic, *Geol. Soc. Amer. Bull.*, 83, 619-646, 1972.
- Ramberg, I.B., D.F. Gray, and R.G.H. Reynolds, Tectonic evolution of the FAMOUS area of the Mid-Atlantic Ridge, lat. 35°50' to 37°20'N, *Geol. Soc. Amer. Bull.*, 88, 609-620, 1977.
- Reid, I., J.A. Orcutt, and W.A. Prothero, Seismic evidence for a narrow zone of partial melting underlying the East Pacific Rise at 21°N, *Geol. Soc. Amer. Bull.*, 88, 678-682, 1977.
- Robertson, E.C., Strength of metamorphosed graywacke and other rocks, in The Nature of the Solid Earth, edited by E.C. Robertson, pp. 631-659, McGraw-Hill, New York, 1972.



Rona, P.A., R.N. Harbison, B.G. Bassinger, R.B. Scott, and A.J. Nalwalk, Tectonic fabric and hydrothermal activity of Mid-Atlantic Ridge crest (lat. 26°N), Geol. Soc. Amer. Bull., 87, 661-674, 1976.

Rosendahl, B.R., Evolution of oceanic crust, 2, constraints, implications, and inferences, J. Geophys. Res., 81, 5305-5314, 1976.

Rosendahl, B.R., R.W. Raitt, L.M. Dorman, L.D. Bibee, D.M. Hussong, and G.H. Sutton, Evolution of oceanic crust, 1, A physical model of the East Pacific Rise crest derived from seismic data, J. Geophys. Res., 81, 5294-5304, 1976.

Sclater, J.G., and J. Francheteau, The implications of terrestrial heat flow observations on current tectonic and geochemical models of the crust and upper mantle of the earth, Geophys. J.R. astr. Soc., 20, 509-542, 1970.

Sclater, J.G., R.N. Anderson, and M.L. Bell, Elevation of ridges and evolution of the Central East Pacific, J. Geophys. Res., 76, 7888-7915, 1971.

Sclater, J.G., and K.D. Klitgord, A detailed heat flow, topographic, and magnetic survey across the Galapagos Spreading Center at 86°W, J. Geophys. Res., 78, 6951-6975, 1973.

Sclater, J.G., P.R. von Herzen, D.L. Williams, R.N. Anderson, and K.D. Klitgord, The Galapagos Spreading Center: Heat flow low on the north flank, Geophys. J.R. astr. Soc., 38, 609-625, 1974.

Sclater, J.G., C. Bowin, R. Hey, H. Hoskins, J. Peirce, J. Phillips, and C. Tapscott, The Bouvet Triple Junction, J. Geophys. Res., 81, 1857-1869, 1976.

Searle, R.C., and A.S. Laughton, Sonar studies of the Mid-Atlantic Ridge and Kurchatov Fracture Zone, J. Geophys. Res., 82, 5313-5329, 1977.

Shih, J.S.F., T. Atwater, and M. McNutt, A near-bottom geophysical traverse of the Reykjanes Ridge, Earth Planet. Sci. Lett., 39, 75-83, 1978.

Simkin, T., and K.A. Howard, Caldera collapse in the Galapagos Islands, 1968, Science, 169, 429-437, 1970.

Sleep, N.H., Sensitivity of heat flow and gravity to the mechanism of sea-floor spreading, J. Geophys. Res., 74, 542-549, 1969.

Sleep, N.H., Formation of oceanic crust: Some thermal constraints, *J. Geophys. Res.*, 80, 4037-4042, 1975.

Sleep, N.H., and S. Biehler, Topography and tectonics at the intersections of fracture zones with central rifts, *J. Geophys. Res.*, 75, 2748-2752, 1970.

Sleep, N.H., and B.R. Rosendahl, Topography and tectonics of mid-ocean ridge axes, *J. Geophys. Res.*, 84, 6831-6839, 1979.

Smith, R.L., and R.A. Bailey, Resurgent cauldrons, in Studies in Volcanology, edited by R.R. Coats, R.L. Hay, and C.A. Anderson, pp. 613-662, *Geol. Soc. Amer. Memoir*, 116, 1968.

Spieß, F.N., and R.C. Tyce, Deep-tow instrumentation system, Scripps Inst. Oceanography Ref. 73-4, La Jolla, Calif., 37 pp., 1973.

Talwani, M., D.E. Hayes, W. Pitman, III, and T. Aitken, Underway marine geophysical data in the North Atlantic, June, 1961-January, 1971, Tech. Rept. 9-CU-9-74 and 3-CU-3-74, Lamont-Doherty Geol. Observ., Palisades, N.Y., 1974.

Tapponnier, P., and J. Francheteau, Necking of the lithosphere and the mechanics of slowly accreting plate boundaries, *J. Geophys. Res.*, 83, 3955-3970, 1978.

Trehu, A.M., Depth versus  $(\text{age})^{\frac{1}{2}}$ , a perspective of mid-ocean rises, *Earth Planet. Sci. Lett.*, 27, 287-304, 1975.

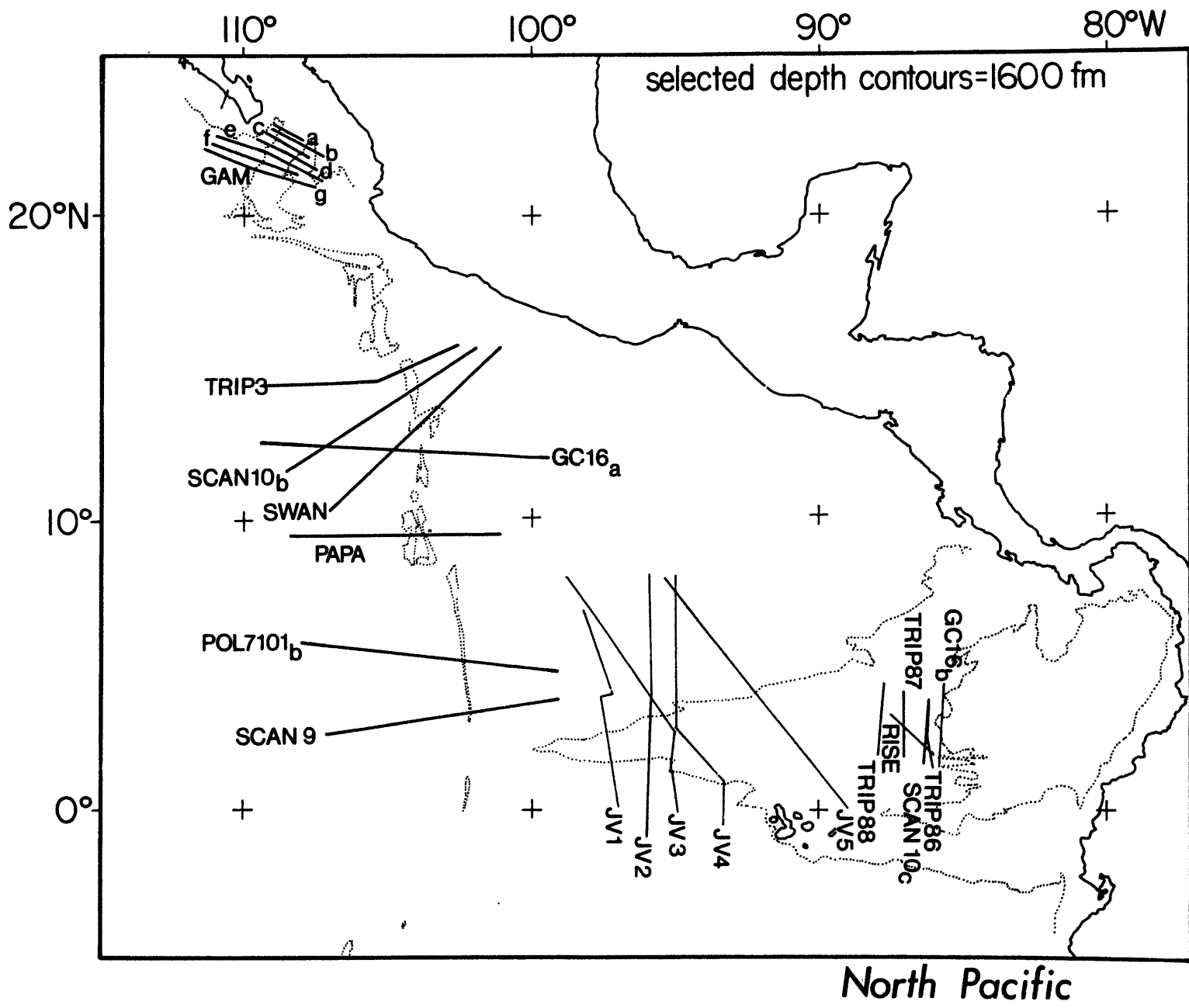
van Andel, T.J., and C.O. Bowin, Mid-Atlantic Ridge between 22° and 23° North latitude and the tectonics of mid-oceanic rises, *J. Geophys. Res.*, 73, 1279-1298, 1968.

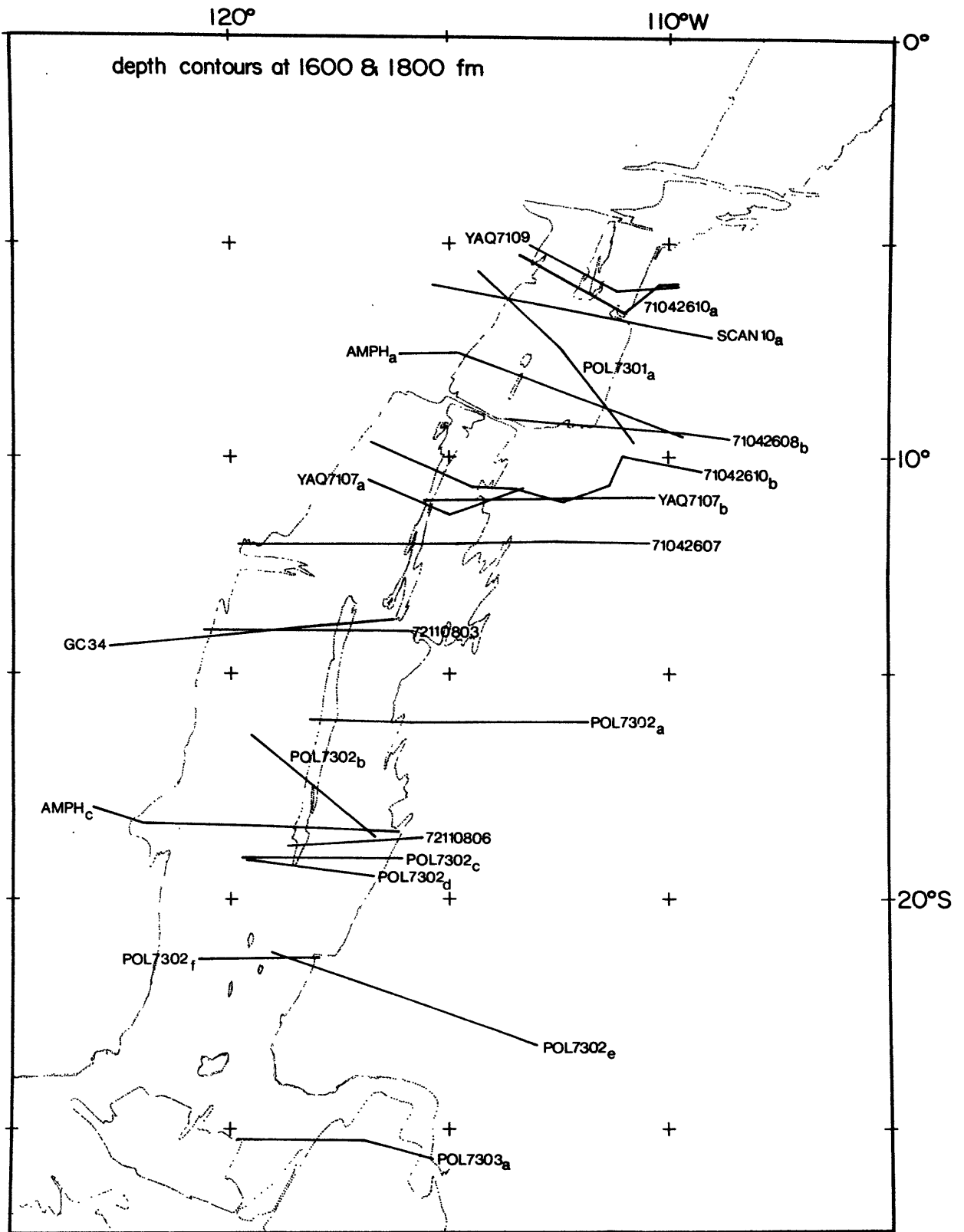
van Andel, T.J., R.P. von Herzen, and J.D. Phillips, The Vema Fracture Zone and the tectonics of transverse shear zones in oceanic crustal plates, *Mar. Geophys. Res.*, 1, 261-283, 1971.

Vogt, P.R., Asthenosphere motion recorded by the ocean floor south of Iceland, *Earth Planet. Sci. Lett.*, 13, 153-160, 1971.

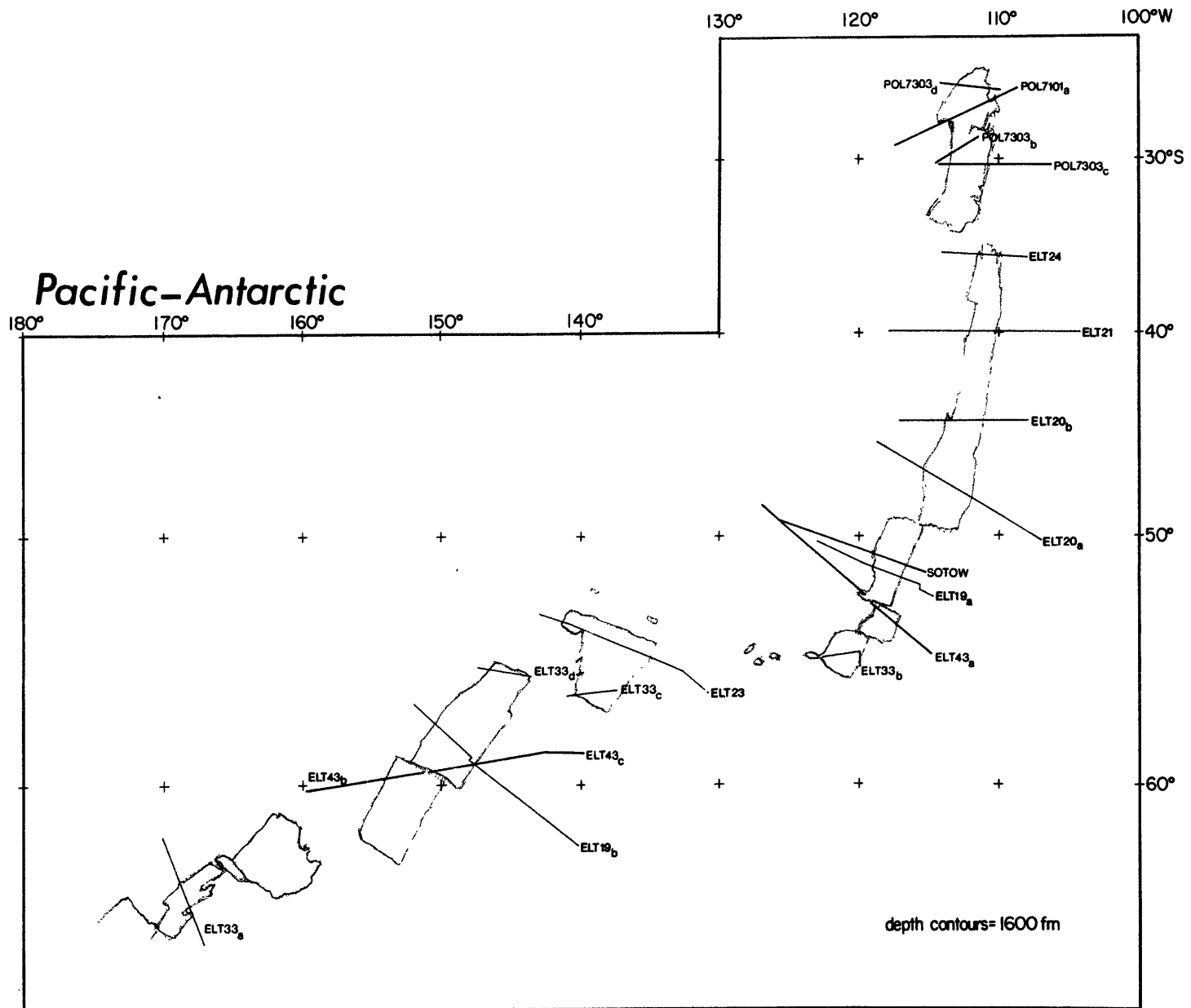
Weissel, J.K., and D.H. Hayes, The Australian-Antarctic discordance: New results and implications, *J. Geophys. Res.*, 79, 2579-2587, 1974.

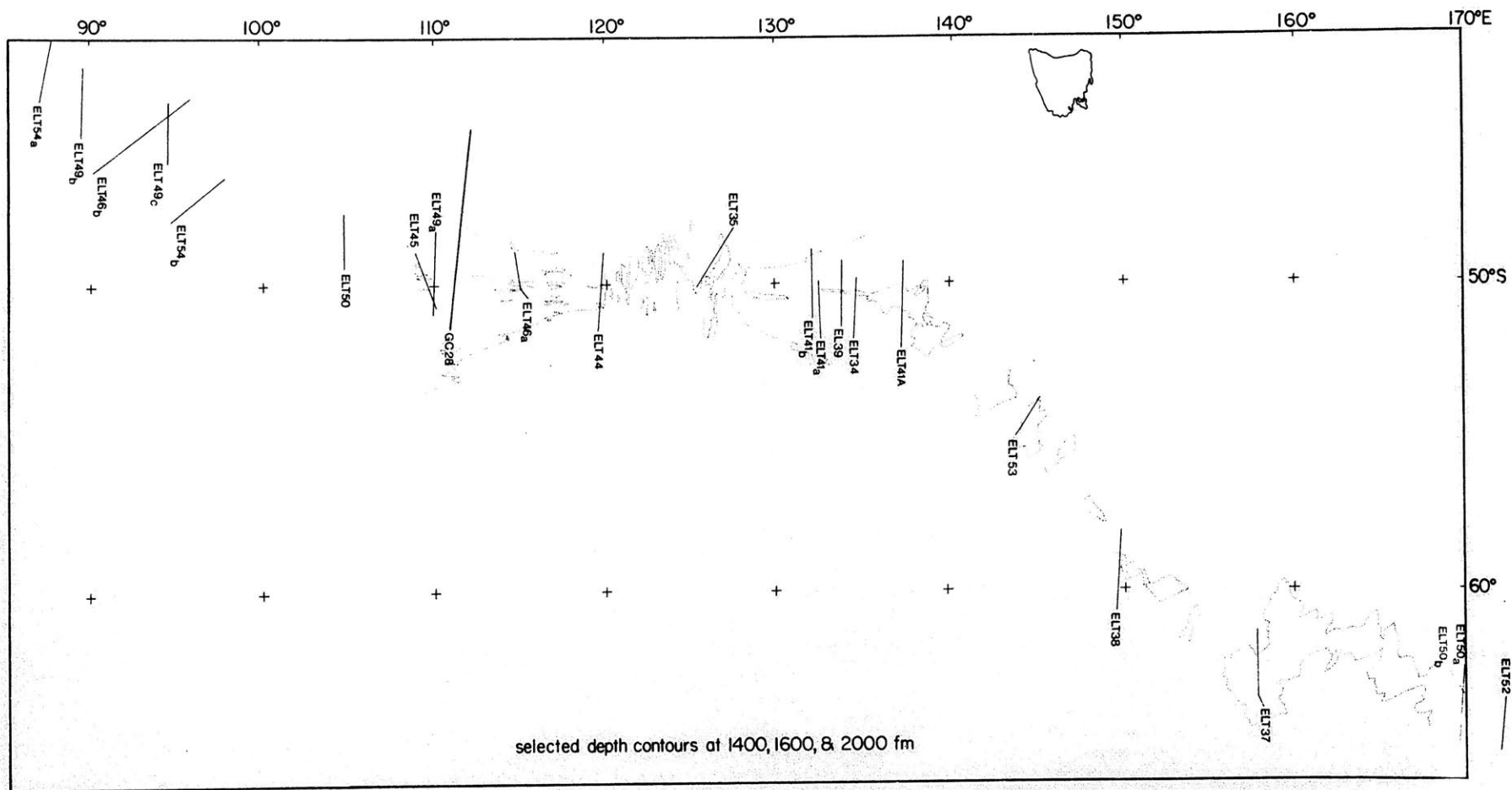
Appendix I: Location of surface ship profiles compiled in this study. Thicker lines indicate the location of profiles acquired in digital form. Bathymetric contours are from Mammerickx et al (1974), Molnar et al (1975), Hayes and Conolly (1972), Talwani et al (1974), and McKenzie and Sclater (1971). Ridge axes in the South Atlantic are from J.D. Phillips (personal communication).



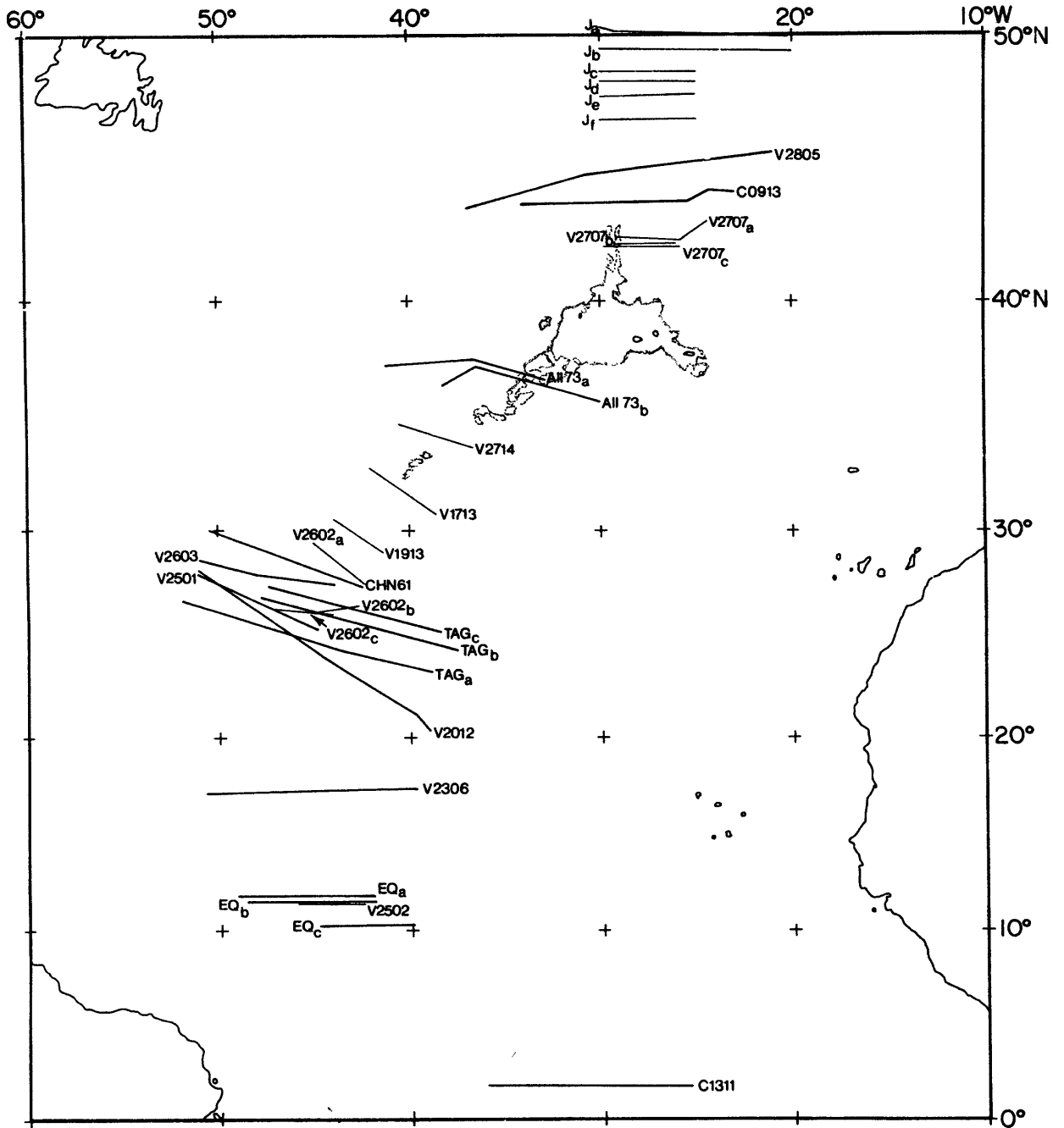


South Pacific



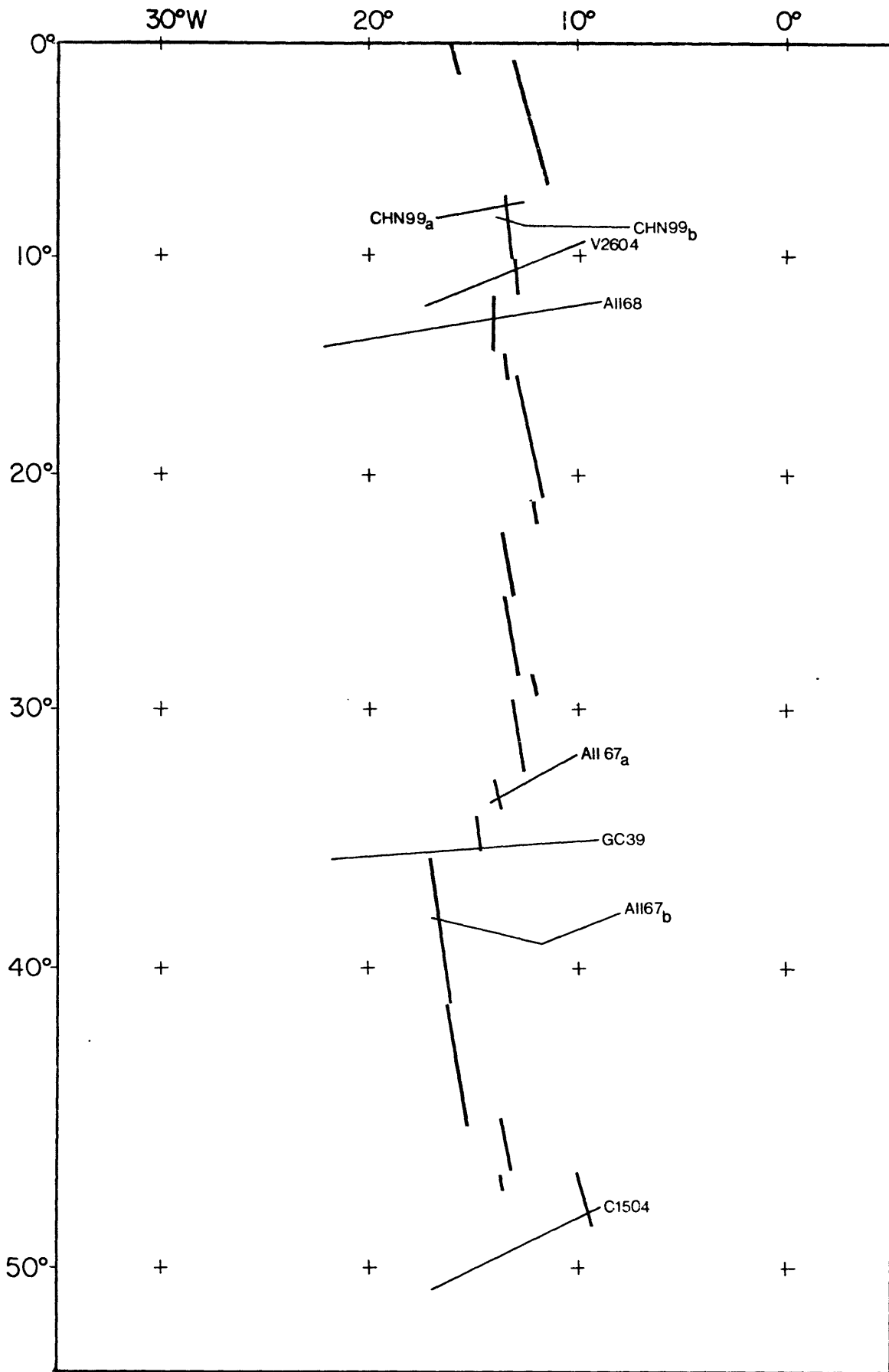


Southeast Indian

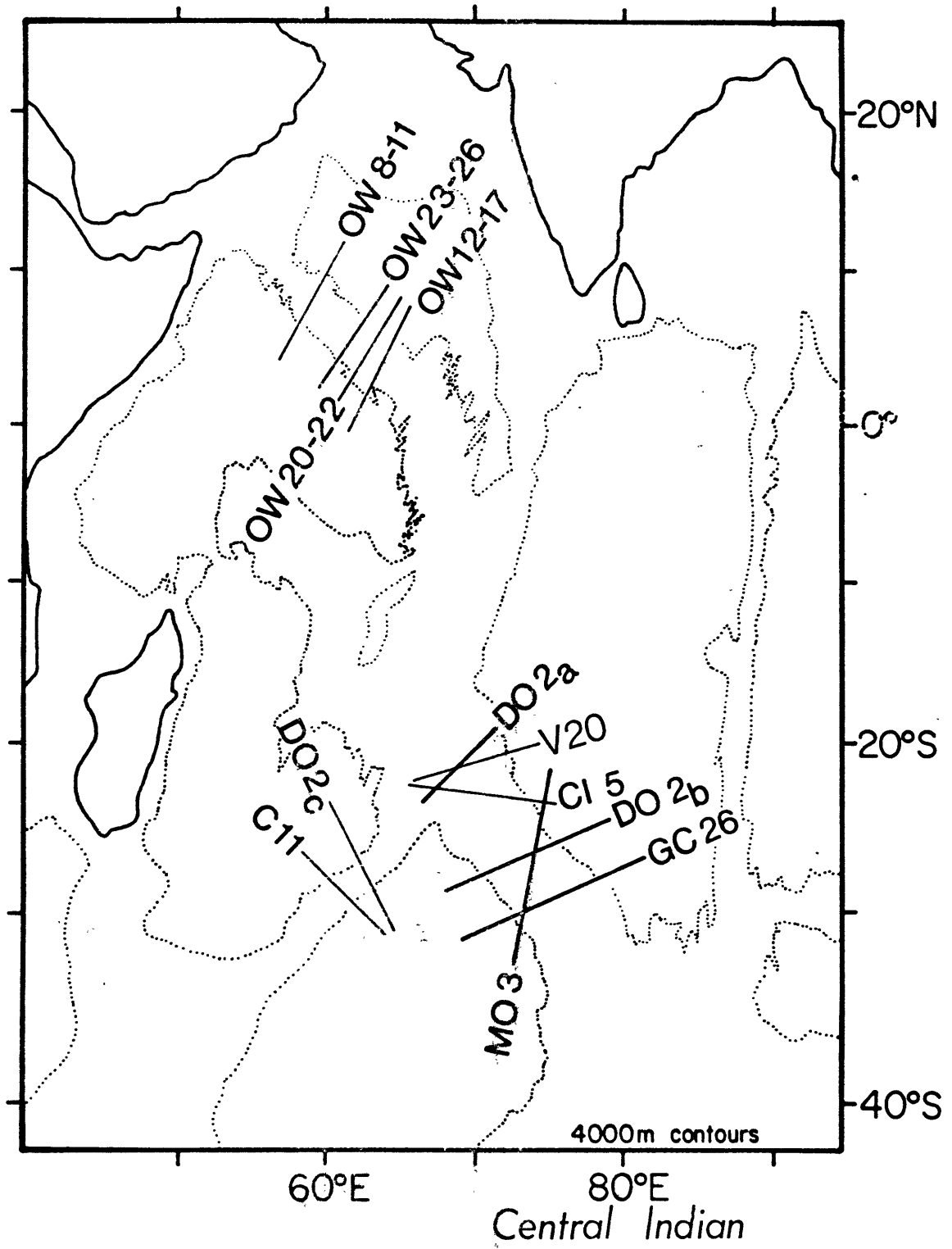


North Atlantic





South Atlantic



## BIOGRAPHICAL NOTE

Name: John Shai-Fu Shih

Birth Date: August 23, 1951

Birth Place: Taipei, Taiwan

Immigrated to U.S.A.: 1960

High School: West Seattle High School, Seattle, Washington.  
Graduated in June, 1970.

College: Columbia University, September 1970 to June 1971.

Stanford University, September 1971 to June 1974.  
Graduated with B.S. and M.S. in Geology.  
Phi Beta Kappa.  
Graduated with distinction.

Massachusetts Institute of Technology/Woods Hole  
Oceanographic Institution Joint Program in Oceanography,  
September 1974 to January 1980.  
Graduated with Ph.D. in Marine Geology and Geophysics.

Publications: J. Shih and P. Molnar, Analysis and implications of the sequence of ridge jumps that eliminated the Surveyor Transform Fault, J. Geophys. Res., 80, 4815-4822, 1975.

J.S.F. Shih, T. Atwater, and M. McNutt, A near-bottom geophysical traverse of the Reykjanes Ridge, Earth Planet. Sci. Lett., 39, 75-83, 1978.

P. Molnar, D. Freedman, and J.S.F. Shih, Lengths of intermediate and deep seismic zones and temperatures in downgoing slabs of lithosphere, Geophys. J.R. astr. Soc., 56, 41-54, 1979.